Short and long term behaviour of reinforced, prestressed and composite prestressed concrete beams.

Elbeih, F K

To my wife and my daughter, Salwa

SHORT AND LONG TERM BEHAVIOUR OF REINFORCED, PRESTRESSED AND COMPOSITE PRESTRESSED CONCRETE BEAMS

BY

FAROUK KHALIL ELBEIH, B.Sc. (Eng.)

A THESIS SUBMITTED FOR THE DEGREE OF

DOCTOR OF PHILOSOPHY

IN THE FACULTY OF ENGINEERING

OF THE UNIVERSITY OF LONDON

KING'S COLLEGE

LONDON

MAY, 1981

ABSTRACT

This thesis presents a comparison between the observed time-dependent behaviour of three types of two-span continuous concrete beams of approximately the same ultimate moment carrying capacity. Reinforced, prestressed and composite prestressed beams were tested and recordings were made of strains, deflected shape and support reactions. All beams were tested at laboratory temperature and the duration of the experiments was approximately 9 months. Control experiments were conducted to determine the basic concrete properties, e.g. creep, shrinkage and elastic modulus, for use later in predictive analysis.

The results indicate that the long-term deformational behaviour of the three types of beams is different and that alteration to the support reaction occurred only in the case of the composite prestressed beam. Ultimate load tests at the end of the experiments confirmed that all beams were of approximately the same strength and that sustained loading and creep during the main experiments had not influenced this strength.

A numerical calculation procedure is presented for the prediction of time-dependent stress and strain behaviour of the beams. For this the length of the beam is divided into elements longitudinally and in depth. Cracking takes place in regions of high tensile stress and allowance is made for the restraining effects of the concrete between adjacent cracks in reinforced members. Creep has been included in the analysis through the effective modulus approach.

Comparison of the theoretical predictions and experimental results was made for the deformational behaviour of all beam types. The theory is then extended to cover structures in which beams are subjected to thermal gradients. Theoretical comparisons are then made between the same three types of beam construction for similar states of temperatures and between similar beams maintained at uniform temperature and subjected to sustained temperature crossfalls through their depth. It is concluded that creep gives rise to increased deflections in all cases at uniform temperature (the deformations being greatest for reinforced beams and least for composite and prestressed beams) and to considerable additional increases when temperature crossfalls exist. For a crossfall of 60^{o}C to 30^{o}C (top to bottom) the predicted mid-span deflection of reinforced concrete beam was 1.43 times that for the corresponding uniform temperature case at an age of 32 days and 2.34 times the initial elastic deflection.

ACKNOWLEDGEMENTS

The work presented in this thesis was carried out under the continuous supervision of Dr. G. L. England, Reader in Engineering Mechanics to whom the author is deeply grateful for his help, valuable guidance and constructive criticism throughout the research program.

The author acknowledges the help of the retired Chief Technician, Mr. A. W. Blake, and his successor, Mr. R. Earl. Sincere thanks are extended to all the workshop staff and laboratory technicians for their help with the experimental part of this investigation and in particular to Mr. M. Collins and Mr. R. Hunt who prepared the photographs for the thesis.

Last, but certainly not least, the author is grateful to his wife for her encouragement and assistance, and also to his daughter, Salwa.

TABLE OF CONTENTS

INTRODUCTION

Creep and shrinkage of concrete result in a continuous variation with time of stresses and strains in the concrete and steel components of reinforced and prestressed concrete structures. The long-term behaviour of these structures will be affected by the inelastic properties of concrete which will then change the redundant moments and forces in these structures whenever they are subjected to a thermal gradient. Some of the modern methods of design require the use of different concrete properties in a single member, as in composite prestressed construction where a member has concrete parts of different ages bonded together so as to act as a monolithic unit. Each concrete part may have steel reinforcement contained in it. The consideration of time-dependent effects in the design has therefore become increasingly important to avoid serviceability problems such as excessive deformations and cracks.

Numerous papers and reports have been published on the time-dependent inelastic properties, creep and shrinkage of concrete at atmospheric and elevated temperatures. Their effects on structures have also been reported. Concrete tests of elevated temperature in the range 20 - 100°C show that both creep and shrinkage at 100°C may be four times as much as those at 20°C.

In order to understand fully the effect of creep and shrinkage in concrete structures of various types it is necessary to develop methods of analysis which are capable of taking into account the geometry of the particular type of structure, its loading and environmental conditions. Temperature is an important parameter to be considered since it is frequently responsible for severe time-dependent redistribution of the stresses in addition to causing increased deformations.

The objectives of this present work are:

1. To compare experimentally and theoretically the short and long-term behaviour at laboratory temperature of three types of two span continuous concrete beams of the same size and virtually the same ultimate capacity while carrying a constant sustained load.

2. To provide an analytical numerical approach for the prediction of the short and long-term behaviour of the three types of concrete beams taking into consideration the effects of concrete tension between cracks developed in the beams.

3. To extend the above mentioned numerical approach to take into account the influence of temperature gradients on the short and long-term behaviour of the three types of concrete beams.

CHAPTER 1

Review of Literature relating to Material Properties of Concrete at normal and elevated temperature. Methods of creep analysis and the behaviour of concrete beams carrying working loads.

1.1 MATERIAL PROPERTIES OF CONCRETE

1.1.1 Elastic Modulus

Modulus of elasticity of a particular concrete mix is obtained by loading a concrete specimen in a testing machine to approximately one third of its ultimate compressive strength. Graph 1.1 shows a typical stress-strain diagram for a concrete specimen loaded in compression or tension, in which the strain measurements are made at intervals of stress.

It can be seen that Young's modulus of elasticity can strictly be applied only to the straight part of the stress-strain curve or when no straight portion is present to the tangent to the curve at the origin. The magnitude of the observed strains and the curvature of the stress-strain relation depend at least in part on the rate of application of stress. The curvature increases if the rate of loading is reduced and if the rate of loading is increased the curvature becomes less and the stress-strain relationship will approach the straight line oA.

The increase in strain while the load, or part of it, is acting is due to creep of concrete. The slower is the rate of loading, the greater are the creep strains obtained. In sustained load tests, the elastic strain is usually taken as the first strain measurement recorded after loading. The elastic modulus in tension is slightly lower than in compression, but they are normally assumed to be equal[1].

Immediate increase in strain is obtained when a concrete specimen is loaded at raised temperature than when loaded at atmospheric

temperatures. Part of this increase is caused by increased creep at the higher temperature, and part of it is caused by a reduction in the elastic modulus. It is difficult to exclude the former effect, except in a dynamic modulus test where the stresses induced are small and transient and will cause negligible creep. Tests by Philleo[3] have shown a reduction in the dynamic modulus when the temperature was raised from 75 to 200°F (24 to 93°C). The decrease was 12 and 14% for a concrete with water-cement ratio 0.4 when tested at 28 and 90 days. The decrease was similar for 0.6 and 0.8 water-cement ratio. He observed little difference in the percentage decrease of specimens air-cured at 50% relative humidity from 3 days and those continuously moist-cured, although the values themselves were higher for the moist-cured concrete.

Graph 1.2 shows the values of the secant modulus obtained by Saemann & Washa[4] at $\frac{1}{3}$ ultimate strength at temperatures varying from 0 to 450°F (-18 to 232°C) it shows that for a concrete heated to 200-250°F (93-121°C) from room temperature (70°F or 24°C) there was a drop in the static modulus of 10% for a strong concrete (curve 1C, 0.4 w/c ratio) and 20% for weaker concretes (curve 2C, 0.8 w/c ratio, curve 3C, light aggregates).

Theuer[5] obtained, for a saturated specimen of 0.4 water/cement ratio tested at 28 days, a drop in the static modulus from 4.66×10^6 lb/in^2 (3.213×10^4 MN/m^2) at 34°F (6°C) to 4.40×10^6 lb/in^2 (3.033×10^4 MN/m^2) at 125°F (52°C). Similar reductions were obtained for specimens previously heated for one week at 100°C and 40°C.

England[6] loaded some specimens sealed against moisture loss and also unsealed specimens to 1000 lb/ln^2 (6.895 MN/m^2) at various temperatures in the range 20 to 140°C. After 80 days of sustained loading, the loads were removed and the variation of the modulus of elasticity obtained on unloading showed a general reduction of 20-25% from 20 to 100°C for sealed and unsealed specimens.

'Serafim & Guerriro[7] observed a reduction of 10% in the modulus at 45°C from that at room temperature, for young concretes of 3 to 8 days old. The increase in modulus with age was correspondingly greater for the concrete kept at room temperature. Glucklich & Ishai[8] also found that the modulus at 45°C were 10% less than the value at room temperature for cement paste beams tested at 28 days.

The pattern of influence of temperature on the modulus of elasticity is also shown in Graph 1.3. For mass-cured concrete there is no difference in modulus in the range 21 to 96°C (70 to 205°F)[9], however, when water can be expelled from concrete, there is a progressive decrease in the modulus of elasticity between 50 and 400°C (120 and 750°F) (see Graph 1.3)[10]. The decrease in the modulus depends on the aggregate used.

These results from different sources indicate that there is a reduction in the modulus of elasticity on increasing temperature from room temperature.

1.1.2 Creep and Shrinkage

Withdrawal of water from concrete stored in unsaturated air causes drying shrinkage. Although it is a volume change, shrinkage is

normally measured as a linear strain. Like all other materials, concrete also exhibits thermal strains, it expands on heating and contracts on cooling. So in a sustained load test on concrete subjected to varying temperature the total strain measured will be a combination of four different effects:

Total strain = Elastic strain + creep + shrinkage + Thermal strain

..... (1.1)

Shrinkage and thermal strains can be measured from a companion non-loaded specimen kept under the same conditions as the loaded specimen. Graph 1.4 shows a deformation versus time curve after shrinkage and thermal strain have been deducted. Shrinkage-time curves have roughly the same shape as creep-time curves and the magnitude of shrinkage in ordinary environment is of the same order as creep for specimens loaded to their working stresses.

The relation between stress and strain for concrete is a function of time. The gradual increase in strain with time is due to creep. Creep can thus be defined as an increase in strain under a sustained stress. Creep is rapid at first, but the rate decreases as time goes on, and since the increase in strain can be several times as large as the strain on loading, creep is of considerable importance in structural mechanics. Creep has been noticed on concrete specimens even after 30 years of sustained loading[2] but the shape of the curves shows that it tends towards a finite limit. Graph 1.4 shows the strain movements when a specimen is unloaded.

Creep occurs in compression, in tension, in bending and in shear.

Compressive stresses are normally used to obtain creep data and

nearly all creep tests have been on concrete in compression because of the high compressive strength of concrete and of its greater use in compression. In determining the various factors affecting creep, the results are invariably from compression tests.

There are many factors influencing the magnitudes of creep and shrinkage in the same way. These factors related to the physical properties of concrete and to the environment in which it is stored. Creep and shrinkage increase as the water-cement ratio increases, as aggregate to cement ratio decreases, as the elastic modulus of the aggregate decreases, as the surface volume ratio of the specimen increases, as the relative humidity decreases, as the temperature of the specimen increases. Creep is also affected by the loads and the loading conditions. Alternating wetting and drying increases the magnitude of creep so that results of laboratory tests may underestimate the creep under normal weather conditions.

In many tests a direct proportionality between creep and the applied stress has been found to exist[11] with a possible exception of specimens loaded at an early age and it appears safe to conclude that within the range of working stresses the proportionality between creep and stress holds good.

Fineness of cement influences creep of concrete as creep tests were done at a relative humidity of 55 percent using ultra high early strength Portland cement whose fineness is above 700 m^2/kg all mixes having the water/cement ratio and the same stress/strength ratio of 0.5. The age at loading was chosen so that all the concretes had the same strength. Graph 1.5 shows that although the creep with the finest cement was at first greatest,

it became least after 1,000 days. This is probably due to the high gain of strength of the finest cement with a resultant rapid drop in the actual stress/strength ratio[12].

Creep has been found to increase in many but not all cases[14],[15] due to the water-reducing and set retarding admixtures, see Graph 1.6.

The effect of elevated temperature on creep was first published to investigate cracking in mass concrete. Kelley[16] found that cracking occurred after 79 days when the temperature was still 14°F above the initial. Lee[17] found that gradual cooling as in a dam would not cause cracking, although tensile stresses developed by using a slightly different temperature. However, an earlier accelerated cooling caused cracking when the temperature of the concrete was above the initial. These effects can be explained by the large creep rate which greatly reduced compressive stresses in the initial period of rising temperature. When the temperature began to fall these compressive stresses were soon reduced to zero, and with further cooling tensile stresses developed. Theuer[5] conducted creep tests between 26 and 125°F (-3 and 52°C) on concrete of 0.4 water/cement ratio with 3 different water contents. One series was saturated, another was heated for one week at 40°C reducing the water content by 15 to 24% (referred to as semi-dry), the other was heated for one week at 100°C reducing its water content by 65 to 70% (dry). The specimens were sealed in rubber tubing and tested after 28 days at about 20% of the ultimate strength for 3 days followed by 3 days of recovery. Graph 1.7 gives the specific creep versus temperature curves after 3 days for the various concretes. The residual strains after 3 days recovery were

also greater the higher the temperature.

Lee[17] reported some sustained load tests on concrete under water. He found that creep and creep recovery both increased with temperature between 20 and 40°C the increase between 20 and 30°C being greater than that between 30 and 40°C. The period in which observations were made was up to 9 days.

Serafim & Guerriro[7] tested sealed concrete at an age of 3 and 8 days, they found only slight differences between creep values at 45°C and at room temperature (17 to 27°C). The slight increase at the higher temperature was only felt in the first 5 to 7 days after loading.

England & Ross[21] tested sealed and unsealed cylinders 12" (304 mm) long and 4.45" (113 mm) in diameter of a concrete of 1:2:4 mix with 0.45 water/cement ratio both by weight, at 14 days after casting for periods of 80 and 60 days. Graphs 1.8 and 1.9 show their results for variation of specific creep with temperature after different periods of loading. The applied stress was approximately 20% of the compressive strength and the temperature range was 20 to 140°C. The results were more consistent for the sealed than the unsealed specimens. The unsealed specimens showed greater specific creep in the early days, but after 60 days it was approximately equal for sealed and unsealed specimens.

Their curves show that creep is approximately proportional to temperature for all ages after loading between 20 and 80°C, at higher temperature the rate of increase in specific creep with temperature falls off.

The influence of temperature on creep has become of increased

interest in connection with the use of concrete in the construction of prestressed concrete nuclear pressure vessels but the problem is of significance also in other types of structures e.g. bridges. The rate of creep increases with temperature up to about 70°C (160°F), when at least for a 1:7 mix with a water/cement ratio of 0.6, it is approximately 3.5 times higher than at 21°C (70°F). Between 70°C (160°F) and 96°C (205°F) the rate drops off to 1.7 times the rate at 21°C (70°F)[9]. These differences in rate persist at least for 15 months under load. Graph 1.10 show the behaviour over a wide range of temperature. Freezing produces a higher initial rate of creep but it quickly drops to zero[24].

The effect of elevated temperature on shrinkage was observed by Saemann, Warren & Washa[25]. They observed an increase in the water loss and also in the rate of water loss in the first day of drying, Graph 1.11. After one day's drying at 240°F (116°C), water loss amounted to 4.5%, compared with an initial water content of 6.2%.

Graph 1.12 shows England and Ross[21] curves for shrinkage at different times for a concrete heated to various constant temperatures. The concrete was a 1:2:4 mix with a water cement ratio of 0.45 and tested at 14 days.

A series of tests carried out by Hannant[74] on reinforced and unreinforced concrete cylinders 9" (228 mm) long and 4.5" (114 mm) in diameter. Graph 1.13 shows the results at room temperature. The temperatures reached in the test cycles, duration of each cycle and the age at the start of each cycle are listed in Table 1.1.

Test No.	Temperature ^{o}C	Duration Hrs.	Age at start of test, days
1.	75	72	37
2	75	144	45
3	77	600	97
4	77	120	123
5	95	120	129
6	95	300	136
7	95	300	150
8	132	300	164
9	132	300	170
10	132	150	192
11	132	150	202
12	155	150	209

Table 1.1

Zero readings were taken after 8 days curing in water. In the initial 37 days, the specimens were kept in laboratory temperature at 20^{o}C and 40% relative humidity and 20^{o}C. Graph 1.13 shows the effect of reinforcement in restraining shrinkage, and the effect of high temperature in increasing the rate of shrinkage and after 60 days at 100^{o}C it may be 4 or 5 times the value at ordinary room temperatures.

Restraint in the form of reinforcing bars on a gradient of stress increases extensibility in that it allows concrete to develop strain well beyond that corresponding to maximum stress.

A high extensibility of concrete is generally desirable because it permits concrete to withstand greater volume changes. The Bureau of Reclamation[26] made some thermal cycle tests on concrete at a constant strain and found that tension developed on cooling to the original temperature.

1.1.3 The Coefficient of Expansion of Concrete

Concrete has a positive coefficient of expansion, but its value depends both on the composition of the mix and on its hygral state at the time of the temperature change.

The influence of the mix proportions arises from the fact that the two main constituents of the concrete, cement paste and aggregate have dissimilar thermal coefficients, and the coefficient of concrete is a resultant of the two values. The coefficient of thermal expansion of cement paste varies between about 11 x 10^{-6} and 20 x 10^{-6} per ^{o}C (6 x 10^{-6} and 11 x 10^{-6} per ^{o}F)[27], and is higher than the coefficient of aggregate. Table 1.2 shows that the coefficient of concrete is a function of the quantity of aggregate in the mix and of the coefficient of the aggregate by itself[28].

Cement/Sand ratio	Linear coefficient of thermal expansion at the age of 2 years	
	10^{-6} per ^{o}C	10^{-6} per ^{o}F
neat cement	18.5	10.3
1:1	13.5	7.5
1:3	11.2	6.2
1:6	10.1	5.6

Table 1.2 Influence of aggregate content on the coefficient of thermal expansion[33]

Graph 1.14 shows the influence of the aggregate on the coefficient of thermal expansion of 1:6 concretes made with different aggregates[32].

Meyers[31] said that the coefficient decreases for an increase in age of cement paste, but Bonnell[32] states that the age of concrete from 2 weeks to 1 year had only a minor effect on the coefficient. Relative humidity of concrete has an effect on the coefficient which was found higher at intermediate humidities. For a quartz concrete, Meyers[31] obtained the following values:

Relative humidity (%)	30	70	100
Coefficient of expansion	10.1	10.8	$9.4 \times 10^{-6}/^{o}C$

Bonnell & Harper[32] obtained the following values for their gravel concrete:

Relative humidity (%)	32	52	65	76	93	100
Coefficient of expansion	14.0	14.6	13.1	12.4	13.5	$12.2 \times 10^{-6}/^{o}C$

They also found that saturating gravel concrete (after air storage at 65% R.H. for 3 months) reduced the coefficient of expansion from 13.1 to $11.7 \times 10^{-6}/^{o}C$. Meyers[33] reported a change of coefficient from 14.6 to $8.8 \times 10^{-6}/^{o}C$ on wetting a flint concrete which had been stored in a sealed condition for 9 months.

One report[32] states that drying saturated concrete over anhydrous calcium chloride had no effect on the coefficient which again did not change on resaturation. Meyers[33] reported values for the coefficient 10.0, 7.7, 7.9 $\times 10^{-6}/^{o}C$ respectively for 9 months sealed storage, saturated for 1 week, dried over

anhydrous calcium chloride for 1 week. Value changed from 16.9 to 10.8 x $10^{-6}/^{o}C$ for a cement paste with 9 months sealed storage when dried for 1 week at 100°C.

These results show that coefficient of expansion changes when moisture change takes place in a concrete.

Bonnell & Harper[32] reported the following values for the coefficient of expansion for a gravel concrete of 1:6 cement to aggregate ratio and 2" (50.8 mm) slump:

13.1 x $10^{-6}/^{o}C$ for a specimen at 65% R.H. and

12.2 x $10^{-6}/^{o}C$ for a saturated specimen.

The water cement ratio was not reported.

Temperature of concrete affects the coefficient of expansion Bonnell & Harper[32] found a linear relation between expansion and temperature over the range tested of 32 to 104°F (0 to 40°C). Philleo[3] found that below about 500°F (260°C) the coefficient of expansion for concrete was the same as the room temperature but above about 320°C (600°F) the coefficient of thermal expansion increases probably owing to dehydration of the cement paste as shown in Graph 1.15. At these high temperatures shrinkage becomes a very important factor.

Berwanger Carl & Sarkar, A. F.[38] determined the thermal coefficient of expansion of concrete and reinforced concrete under short-term steady state temperatures -100 to 150°F (-73 to 66°C). Specimens were cured both saturated and air-dried in laboratory and tested at 7, 28 and 84 days and at 1 year. One hundred and twenty five reinforced concrete prisms were tested for thermal coefficient of expansion. They found that

the coefficient decreased with increase in water cement ratio, increased with age, and was smaller below the freezing point of the concrete. The saturated concrete had lower coefficients than the air dried concrete. Steel reinforcement ranged from 0 to about 5 percent: the coefficient for symmetrically reinforced concrete increased with the steel percentage. For unsymmetrically reinforced concrete, the coefficient for the face at the steel increased and the coefficient for the opposite face decreased with increased steel.

1.2 METHODS OF CREEP ANALYSIS

When an applied stress is sustained in a structural member it produces instantaneous and creep strains. Creep starts to develop at the time of stress application and increases as time progresses. It is widely accepted that, for stresses within service limits, both the instantaneous and the creep strains are linearly proportional to the applied stress. Therefore, it is possible to express creep as a strain per unit stress usually referred to as specific creep or in terms of a creep coefficient, C, which may be defined as the ratio of the creep strain to the instantaneous strain. When test values are established for either the specific creep or the creep coefficient, they can be used to evaluate the long-term strain for any value of a constant sustained stress in a direct manner.. Moreover, several methods have been established to analyse structures subjected to variable loading conditions, which are more common in engineering problems using the creep-time relations derived from constant stress tests. These methods are briefly reviewed and their limitations and the approximations involved are discussed.

1.2.1 Creep under constant sustained stress

Let a direct stress, f, be applied on a concrete specimen at age, t_1 and sustained until t_2. Instantaneous strain occurs at t_1 and creep strain develops with time. The constitutive relation between the total strain $\varepsilon(t_2)$ and the stress $f(t_1)$ is governed by the equation.

$$\varepsilon(t_2) = \frac{f(t_1)}{Ec(t_1)} (1 + c(t_2 , t_1)) , \qquad (1.2)$$

where $Ec(t_1)$ is the modulus of elasticity of concrete at time t_1, $c(t_2,t_1)$ is a creep coefficient depending on t_1, $(t_2 - t_1)$, the composition of concrete and the environment in which it is kept.

Numerous papers on the mechanism of creep and the evaluation of C have been published (see Neville and Dilger[40] for list of references). The most significant of these for structural design purposes are given by the CEB-FIP Committee[41] and by the ACI Committee 209[42] based on Branson and Christiason[43]. In the absence of test data on the particular concrete used, the designer may resort to these methods for creep prediction.

In equation 1.2, it is obvious that the instantaneous strain at t_1 as well as the creep strain at t_2 are assumed to be linearly proportional to the applied stress. This is known to be acceptable for stresses below about 0.4 to 0.5 of the strength.

1.2.2 The Principle of superposition

McHenry[44] generalised the above assumption of linearity to variable stress. His findings are summarised in the following statement.

Strains produced in concrete at any time by a stress increment

are independent of the effects of any stress applied either earlier or later. The stress increment may be either positive or negative, but stresses which approach the ultimate strength are excluded. The principle takes into account the entire stress history, and also the changes in the properties of concrete due to ageing. McHenry found this to hold for sealed concrete specimens loaded at 28 days and unloaded at 90 days.

Tests by Davies[45] and Ross[46] have shown that creep recovery upon the removal of stress is less than creep of virgin concrete loaded at the same age at which the recovery specimen is unloaded. It has also been noticed by Ross[46] and England and Illston[47] that even under increasing stress the actual strain is overestimated by superposition of strains in virgin specimens. Therefore, the dependence of the creep coefficient on the stress history which is ignored in the principle of superposition by McHenry[44], causes deviations from measured values. Gamble[48] and Kountouris[49] suggested that, the linear creep law being retained, a reduction factor be applied to the creep coefficient only for recovery under stress decrements. The reduction factor was derived from tests in which the specimens were fully unloaded at different ages after loading.

1.2.3 Methods of Analysis for variable stress conditions

A. The Effective Modulus Method

The Effective Modulus Method is the oldest and simplest one. The instantaneous elastic modulus is reduced to take into account elastic and creep strains. If e is the elastic strain due to a stress of 1 N/mm^2, c is the creep strain due to a stress of $1N/mm^2$ Then the instantaneous modulus $E_c = \frac{1}{e}$

and the Effective Modulus $E_c' = \frac{1}{e + c}$

The strain at any instant is the stress at that instant divided by the effective modulus at that instant. Thus it neglects the stress history and predicts complete recovery of creep after removal of stress. When there are significant variations of stress, this method, obviously, gives erroneous results.

B. The Rate of Creep Method

In this method the time variation of stress is accounted for. The rate of creep at any time 't' under unit stress is the slope of the specific creep curve $\frac{dc}{dt}$ at that time. If the stress at that time is f, then creep during an element of time is $f.\frac{dc}{dt}.dt$.

Therefore, total creep is $\int_0^t f \frac{dc}{dt}.dt$.

This takes some account of the stress history but the rate of creep is assumed to be constant at that time, whether the concrete was assumed previously stressed severely or negligibly when the stress is removed at any instant, f = 0, the method predicts no recovery of creep. The rate of creep method is based on an approximate creep-time function in order to produce analytically solvable differential equations. Contrary to the effective modulus method, it underestimates creep strain due to stress increments and vice versa. The two methods, therefore, give two bounds to the actual solution but only when stress variation with time is monotonous. The rate of creep method usually gives better results but at the expense of greater arithmetic burden.

1.2.4 Approach adopted in the thesis

In the present study the effective modulus approach is used in the analysis to predict the long-term behaviour of the different types of continuous concrete beams as the effect of concrete tension between cracks developed in reinforced and composite beams could be easily taken into consideration by using the above mentioned approach in connection with theory[18] for cracked prestressed beams.

1.3 SHORT AND LONG-TERM BEHAVIOUR OF CONCRETE BEAMS CARRYING WORKING LOADS

1.3.1 Reinforced Concrete Beams

A. Short-term behaviour

Application of external load on a beam creates a moment at a cross section which is resisted by an internal couple in the beam caused by compressive stresses in the upper fibre and tensile stresses in the lower fibre. The neutral axis is the unstressed plane between the compressive and tensile zones. Cracks occur in some parts in the beam even at working loads when the extreme fibre stress exceeds the modulus of rupture of concrete, and some of the tensile force is transferred to the steel. At this stage the flexural rigidity decreases and the deflection increases at a faster rate.

Graph 1.19(a) shows the load-deflection curve for a simply supported beam up to working load.

The deflection of the beam up to its cracking load at A can be predicted with reasonable accuracy by simple elastic theory, the moment of inertia being based on the uncracked transformed section, or simply on the gross concrete section (line (i) in

Graph 1.19(a) . It is clear from Graph 1.19(a) that once a beam has cracked the use of the uncracked moment of inertia, I_o, considerably underestimates the deflection.

At a load greater than the cracking load Graph 1.19(b) shows the stress distribution in the concrete at various cross sections along the span. If the fully cracked, transformed moment of inertia, I_{cr}, is now used in conjunction with elastic analysis, thereby ignoring the concrete in tension along the whole length of the beam, the computed deflection is greater than the true deflection, line (ii) in Graph 1.19(a). This is generally believed to be due to the following three reasons:

(a) In the uncracked regions of beam where the applied bending moment is less than the cracking moment the concrete is completely effective in tension and the moment of inertia is I_o not the assumed I_{cr}.

(b) At a cracked section the crack does not penetrate right up to the neutral axis as usually assumed in determining I_{cr}. The extent of the wedge of effective concrete between the neutral axis and the tip of the crack depends on the ratio of the applied moment to the cracking moment, the smaller the ratio the greater the wedge, and also on the percentage of reinforcement in the beam.

(c) In the cracked regions of the beam the concrete between the cracks still carries some tension, as a result of which the tensile stress in the steel at a crack is greater than the corresponding stress between cracks. This is generally referred to as the tension-stiffening effect of the concrete.

A number of methods of calculating the short-term deflection of a cracked beam are available. Most of these methods allow for the three effects mentioned above empirically.

The existing methods fall broadly under two categories:

(a) The use of an effective moment of inertia.

(b) The idealisation of the moment-deflection curve.

Yu and Winter[76] and Branson[77], for example, proposed the use of an effective or average moment of inertia. The basic principle is to modify the cracked moment of inertia by an empirically adjusted factor which depends on the ratio of cracking moment to maximum applied moment. The unified code, CP110[78], method also falls under this category, although the principle is somewhat different, in this case the stress of the concrete in tension in the cracked region is directly taken into consideration.

The proposal to use the idealised form of the moment deflection curve first came from the CEB[79]. The approach here is to idealise the experimental moment-deflection curve of a cracked beam into a simple bilinear relationship. The total deflection is then calculated by the summation of two parts: A portion corresponding to the cracking moment, and a second portion corresponding to the moment in excess of the cracking moment.

Beeby[80] proposed a method very similar to the CEB approach, but using an idealised moment curvature relationship instead of a moment-deflection one.

The method which appeared in the 1969 draft of the unified code[81] is very similar to the CEB method, except that the moment curvature relationship instead of the moment-deflection one is used. A number of authors[82,80,83] have compared the accuracy of the various methods. The general conclusion is that most methods predict deflections reasonably well, with the calculated values differing from the measured values by not more than 20% in almost all cases.

TEXT CUT OFF IN ORIGINAL

Mohamedbhai[83] proposed a method whereby the curvature at various points along the beam is calculated and the deflection then computed by double integration of the curvature. The curvature at an uncracked section is easily determined by the use of the uncracked moment of inertia. At a cracked section the concrete in tension is considered between the neutral axis and the top of the crack. The method entirely ignores the tension-stiffening effect of concrete between cracks.

Stevens[88] tested a series of simple beams consisting of 24 pairs. These tests investigated the effects of strength of reinforcement used, cover, proportions of reinforcement and environment. A further six pairs of beams were tested to investigate additional variables: type of concrete, effect of compression reinforcement and specimen size. These tests have shown the following behaviour: The average tensile force in the concrete diminishes with time at a reducing rate. The maximum compressive strain in the concrete, the maximum tensile strain in the steel and the maximum central deflection increase with time at a reducing rate. Concrete beams exposed to natural environment display about three-quarters of the deflections of companion beams in the controlled environment of the laboratory. The addition of compression steel equal in amount to that in the tension zone approximately halves the amount of creep.

Illston and Stevens[89] studied the progress of cracking in reinforced concrete beams kept under load for over two years. The influence of major variables such as concrete cover, type of steel and conditions of storage was investigated. The main series of test beams comprised 24 pairs of beams.

Clark and Speirs[90] tested fourteen reinforced concrete simple beams with various depths and steel areas and nine slabs with various steel areas and bar arrangements. These tests were designed to provide information on the tension stiffening phenomenon. It is concluded that the tension stiffening can be calculated on the basis of an average tensile stress equal to fraction of the tensile strength of concrete acting over an effective area of concrete surrounding the bars in the tension zone. A value of the average tensile stress and the effective areas appropriate to beams and slabs was recommended.

Srinivasa Rao and Subrahmanyam[91] proposed a semi-empirical method for the calculation of trisegmental moment-curvature relations for reinforced concrete members taking into consideration the contribution to stiffness by the concrete in the tensile zone in between cracks. Predictions of the method are compared with tests and are found to be good.

B. Long-term behaviour

Long-term tests on simply supported reinforced concrete beams carried out by some investigators have shown the following behaviour:

1. The deflection increases at a gradually declining rate to several times the initial deflection after a few years. Hajnal-Konyi[35] found that the deflection of beams tested at 4 to 7 weeks old were 3.28 times the initial deflection after 2 years sustained loading and 3.53 times after 5 years.

2. The strain distribution at any section of the beam is approximately linear even in the cracked tension zone.

3. The concrete strain in the compressive fibre of the beam increases several times after a few years of sustained loading. Washa & Fluck[36] found that for 30 beams the strain readings at the level of the compressive steel were 2.34 times and 5.66 times the initial after 2½ years but the strain at the tensile steel level only increased by 1.14 and 1.41 times the initial. Therefore, the increase in the tensile steel stresses was comparatively small.

4. Washa & Fluck[36] found from strain measurements a gradual lowering of the neutral axis with time causes changes in the concrete stress diagram. Even in a non-shrinking beam, if creep is considered to occur in tension, the neutral axis for stress and strain do not coincide as in short-term behaviour[37].

5. Washa & Fluck[36] found that compressive steel reduces the total deflection after sustained loading, but using equal areas of tensile and compressive reinforcement they found the increase in deflection over two and a half years was only

46% of the increase in beams without compressive reinforcement. Using half the above amount of compressive steel the increase in deflection was 62%.

6. Compressive reinforcement reduces the total strain in the extreme compressive fibres.

7. Sustained load does not affect the ultimate load.

Glanville & Thomas[37] found no difference in the ultimate load of beams tested after 6 to 9 months sustained working load and theircompanion non-loaded shrinkage beams.

Long-term tests on two-span continuous reinforced concrete beams carried out by Washa, G. and Fluck, P. G.[39] have shown the following behaviour:

1. Inclusion of arbitrary amounts of compressive steel in positive moment regions is effective in reducing creep deflection.

2. Ratio of 2½ year creep deflection to the immediate elastic deflection varied between 1.03 and 1.62.

3. Mid length reactions increased during the sustained loading periods. The increase was about 5 percent for beams without compressive steel in the positive moment region and about 2 percent for beams with compressive steel. The increase in reaction was accompanied by a corresponding increase in mid length bending moment.

4. Inclusion of full compressive steel in the positive moment region reduced compressive creep strains in that region by about one half.

5. Tensile creep strains in the positive moment region were small but were greatest for beams with full compressive steel.

6. Compressive creep strains in the negative moment regions were found to be nearly the same for all beams of a given type despite the difference in compressive reinforcement in the positive moment region.

7. Tensile creep strains in negative moment region were found relatively large, but inclusion of full compressive steel in the positive moment region decreased these strains by more than one half.

1.3.2 Prestressed Concrete Beams

A. Short-term behaviour

In general, prestress involves the imposition of stress opposite in sign to those which are caused by the subsequent application of service loads. Prestressing wires placed eccentrically in a simple beam produce an axial compression as well as a bending moment, and the beam cambers up due to the eccentricity of the cable. The camber increases as time goes on. The application of live loads let the beam deflect downwards and may or may not continue to camber under sustained loads depending on the amount of loading. There are two systems of forces and the deflection and stresses can be calculated by superposing the two effects. Graph 1.17 shows the superposition of stresses for a prestressed concrete beam.

The uncertain effects of concrete in tension and cracking do not arise in fully prestressed beams because under working loads, concrete remains uncracked.

B. Long-term behaviour

Superposition by direct addition is usually assumed to hold because creep is proportional to stress in the working range of stresses. But Davis[45] pointed out that the superposition is only exact if McHenry's[44] Principle holds. Creep is very important in prestressed concrete because at all stages after prestressing the concrete beam will be subjected to working stresses whether the live load is acting or not.

There are two main factors which reduce the prestressing force in the tendons with time:

a. Creep and shrinkage

b. relaxation of stress will occur at constant strain due to the high stresses in the tendons ACI Committee 435[52] suggests that the long-term deflection due to transverse load should be separated from those due to shrinkage, prestress and loss of prestress. The deflection at any time is the algebraic sum of these effects. Long term deflection due to transverse loads is increased by the creep factor defined as $\frac{\text{creep strain}}{\text{instantaneous strain}}$. For the other effects, creep occurs under varying stresses because the prestressing force is gradually reduced. Shrinkage strains are added to the creep strains and these resulting strains, together with a knowledge of the relaxation properties of steel, enable the calculation of deflection due to causes other than transverse loads.
Corley, Cozen & Siess[53] measured the deflection of 4 long term tests on prestressed concrete beams and compared these with calculated values. Good agreement was obtained between measured and computed curves by either the rate of creep

or superposition method. Branson & Ozell[54] observed the increase in camber in prestressed concrete beam without transverse loads.

Branson, D. E., Meyers, B. L. and Kripanarayanan[55], used sand lightweight concrete in prestressed laboratory beams and bridge girders, they studied the behaviour of 5 non-composite prestressed beams and field measurement of camber of prestressed girders. The computed initial camber agreed well in most cases with the measured initial camber. All of the bridge girder data indicated an increase in camber of about 0.4" (10.16 mm) between 300 to 370 days. This appears to be due to higher temperature and is consistent with the observations of Delarue[56]. The computed prestress loss for the laboratory non-composite beams was slightly higher than the experimental results. The direct application of laboratory creep data for uniformly loaded specimens to beams with non-uniform stress distribution appears to slightly over-estimate the creep effect relative to loss of prestress of non-composite beams. The same over-prediction was not found in the case of camber, apparently because the stress component F/A which is a dominant factor in loss of prestress results does not contribute directly to camber. In tests of prestressed concrete beams reported by Cottingham, Fluck & Washa[57] the deflection and strain readings were commenced after loading, so in the bottom fibres the initial strains were tensile. In fact, the concrete was generally under compression in those fibres due to prestressing force and would creep in compression. With the passing of time the strains might change from tensile to compressive. The same applies to creep strains of tests

carried out by Cernica and Charignon[58]. They also reported the following observations:

1. The ratio of the 7 year creep deflection to the immediate elastic deflection varied between 1.23 and 1.73.

2. The creep reflections and the compressive creep strains near the top of the beam increased at a decreasing rate as the period of sustained loading increased.

3. About 75 percent of the 7 year creep deflection was obtained in the first year of loading.

4. Beams subjected to sustained loads that did not produce cracking during the 7 year creep tests showed essentially the same elastic behaviour on unloading that they had during original loading.

5. The loads required to cause failure of the beams which had been loaded to $\frac{1}{2}$, $\frac{3}{4}$ and full design load for 7 years were not significantly different.

6. The beams which sustained full design load developed tension cracks and changed their elastic properties.

1.3.3 Composite Prestressed Concrete Beams

A. Short-term behaviour

Composite construction is an attempt to economise over normal prestressed concrete design and yet retain the advantages of that type of construction. The precast and cast in place portions thus act together (with stirrups if necessary) and form a composite section.

Graph 1.18 shows a composite section at the midspan of a simply supported beam, whose lower stem is precast and lifted into position with the top slab cast in place resting directly on the stem. If no temporary intermediate support is furnished, the weight of both the slab and the stem will be carried by the stem acting alone. After the slab concrete has hardened, the composite section will carry any live or dead load that may be added onto it.

In the same figure, stress distributions are shown for various stages of loading. These are discussed as follows:

(a) Owing to the initial prestress and the weight of the stem, there will be heavy compression in the lower fibres and possibly some small tension in the top fibres. The tensile force, T, in the steel and the compressive force C in the concrete form a resisting couple with a small lever arm between them.

(b) After losses have taken place in the prestress, the effective prestress, together with the weight of the stem, will result in a slightly lower compression in the bottom fibre and some small tension or compression in the top fibre. The C-T couple will act with a slightly greater lever arm.

(c) Owing to the addition of the slab, its weight produces additional moment and stresses as shown.

(d) Owing to effective prestress plus the weight of the stem and slab, we can add (b) to (c) and a somewhat smaller compression is found to exist at the bottom fibres and some

compression at the top fibres. The lever arm for the C-T couple further increases.

(e) Stresses resulting from live load moment are shown, the moment being resisted by the composite section.

(f) Adding (d) to (e) we have stress block as in (f) with slight tension or compression in the bottom fibres, but with high compressive stresses in the top fibres of the stem and the slab. The couple T and C now acts with an appreciable arm.

The above shows the stress distribution under working load condition.

Evans, R. H. and Parker, A. S.[59] tested three types of composite prestressed beams, they found the following:

(a) Good bond between prestressed and in-situ concretes can be obtained if the jointing surface is sufficiently roughened. Bond may be assisted by leaving stirrups protruding from the prestressed concrete.

(b) Composite construction does not affect the extensibility of either prestressed or in-situ concrete.

(c) The relative qualities of concrete in a composite design do not affect bond. If the relative strengths are taken into consideration in the normal way, then the only additional effect peculiar to this type of construction is that of differential shrinkage.

(d) Any of the plastic theories of failure may be applied to composite beams in the same way as they are applied to the normal prestressed beams.

(e) The differential shrinkage between the two elements may affect cracking loads either to advantage or adversely and the magnitude of the effect may be as much as 20% in normal design.

Ozell[60] tested to failure four groups of composite simple beams which were made of prestressed beams 8" (203 mm) wide and 10" (254 mm) deep. These were later topped with a cast in place portion also 8" (203 mm) wide and 10" (254 mm) deep making a composite beam 8" (203 mm) wide and 20" (508 mm) deep. His results lead to the following conclusions:

1. The friction and natural bond between the cast in place and the precast concretes is sufficient to resist all horizontal shearing forces up to cracking load. To ensure monolithic action beyond the cracking load the contact surface should be roughened to provide mechanical bond.

2. Although there seems to be almost no distinction in the behaviour of beams with roughened contact surfaces but having no shear ties and those with stirrups extending into the cast-in-place concrete, use of long stirrups to serve as shear ties seems advisable to ensure a more positive composite action.

3. Flexural strain distribution of the beams gave further evidence of complete bonding of the two concretes and of monolithic and elastic behaviour.

4. Deflections may be predicted accurately using the theoretical moment of inertia.

An experimental investigation of the flexural properties of composite prestressed concrete beams was carried out by Bryson, J.O., Skoda, L.F. and Watstein, D.[61]. The composite beams were made by separately forming the tensile and compressive sections of the beams. The tensile section was cast first and prestressed and the compressive section was formed with plain concrete bonded to the prestressed element. Three sets of composite beams were tested and the results compared with those from conventionally prestressed beams. They concluded that the flexural behaviour of the composite beams and the reference prestressed beams were similar up to the cracking load, but beyond the cracking load the reference prestressed beams exhibited a greater degree of stiffness than the composite beams. The procedure used for combining the two elements of composite beams proved to be adequate for the development of sufficient bond for monolithic beam action throughout the tests. They found also for the same working load capacity, the prestressing force required for composite beams is considerably less than that required for a conventionally prestressed beam, and consequently a significant reduction in the amount of reinforcing steel can be achieved by this method of construction.

B. Long-term Behaviour

Mattock[62] reported results of an extensive laboratory investigation of a type of bridge involving precast, prestressed I-shaped girders with a continuous, situ-cast deck slab. His investigation is concerned with the influence of creep and shrinkage of the concrete on the long-term behaviour of this type of composite continuous construction. It is found that creep and shrinkage will not affect

the ultimate load carrying capacity of the girders, the influence of creep and shrinkage is restricted to deformations and possibility of cracking at service load level. In view of the qualitative agreement between experiment and theory presented in the investigation, it is concluded that if a statically indeterminate concrete structure is made from several precast elements, which are made continuous with one another after being subjected to permanent loads as separate elements, then the distribution of moments and forces within the structure will progressively change during the subsequent life of the structure.

Branson and Ozell[63] studied both experimentally and analytically the effects of shrinkage and creep in composite construction consisting of a prestressed concrete beam and cast-in-place slab, they found that the most important variables influencing the effect of shrinkage and creep in composite prestressed concrete beams are the following:

(a) relative casting dates

(b) surrounding moisture conditions

(c) whether slab is reinforced or not

(d) relative quality of the two concrete mixes

(e) magnitude of prestress.

Evans and Chung[64] reported a simple method of analysing the effects of differential shrinkage in composite members. Their study leads to the following recommendations, insofar as differential shrinkage is concerned.

1. Concrete mixes having similar moduli of elasticity should be used for the precast component and the cast-insitu component.

2. A rectangular composite beam should be proportioned in such a way that the depth of the cast-insitu component is two to three times the depth of the precast component.

3. A section with a relatively small flange, both in thickness and depth should be adopted for a composite T-beam.

Dilger and Neville[65,40] have reported a method of analysis for the time-dependent behaviour of these beams which considers changes of stresses as unknowns and involves a large number of equations for analysis.

Rao and Dilger[66] developed the varying stiffness method of analysis for the time dependent behaviour of composite prestressed concrete beams and compare the analyticial results with experimental values and a fairly good agreement is found between the two.

Tadros, Ghali and Dilger[67] present a general approach for the analysis of the effects of creep and shrinkage of concrete and relaxation of prestressing steel in composite beam on plane frame statically indeterminate or not. The method assumes that concrete creep is proportional to stress and thus superposition of stresses and strains is assumed valid.

1.3.4 Effect of thermal gradient on the elastic and long-term behaviour of concrete beams

Simply supported homogeneous beam subjected to a constant thermal gradient will give rise to no stresses over the cross section and the beam bends. Some stresses will be produced if the beam is made of reinforced concrete or composite prestressed concrete because of the differing coefficients of thermal expansion of

the two composite materials, steel and concrete in reinforced concrete and steel and different concrete mixes in composite beams. If the temperature distribution is not linear, additional stresses will be set up because the strain distribution at a cross section must remain linear. If we allow each small longitudinal element of the beam to undergo thermal expansion without restraint, thus producing a free strain diagram as shown by line DD in Graph 1.16. These strains are compatible with the assumptions of plane sections and give rise to no stresses over the cross section when the temperature distribution is linear. When the free strains do not conform to compatibility, then compatibility and equilibrium can be achieved by introducing the straight line AA which represents the actual strains in the element. Thus the strains represented between lines AA and DD are associated with stresses which themselves satisfy the equilibrium conditions of the longitudinal element. These stresses can be calculated once the distribution of temperature is known by applying two equations of equilibrium:

1. Total forces in the longitudinal direction must be zero.
2. The moment of these forces about any horizontal axis in the plane of the cross section is equal to the external applied moment, M.

Davis[68] has given values of end restraint moments for rectangular parabolic and triangular distributions of temperature gradient along the beam, and Fischer[69] has given the values for a general distribution. If the tensile stresses caused by the restraints exceed the modulus of rupture for concrete, then the steel reinforcement will be required. In biological shields for nuclear reactors, preliminary elastic design assumes that the

the walls are restrained from bending. Bonsall[70] has calculated that for permissible stresses in concrete and steel of 1000 and 18,000 lb/m^2 (6895 and 1.24 x 10^2 MN/m^2) and neglecting concrete in tension, then if the temperature difference in the wall exceeded 87^{o}C either the concrete or the steel would be stressed beyond their permissible values, but if the temperature difference was 50^{o}C, only nominal reinforcement would be required. Davidson[71] also obtained the same kind of values. Davis[68] calculated that only 0.2% of steel was required if the temperature difference was 69^{o}C and 1.6% required for a difference of 97^{o}C.

In continuous structures subjected to temperature changes, we can first consider each member to be fixed in position. Moments and axial forces are set up in each member and these are distributed to obtain the final values of moments and forces[69,72].

It is seen that thermal stresses will be produced if free expansion is restrained either by non-linear temperature distribution or by externally applied restraints. These stresses will be modified by creep which is much increased under elevated temperature conditions. Shrinkage will accompany creep effects if moisture loss can occur.

Hannah[73] has tested unreinforced gravel concrete beam 10" x 6" x 10' (254 mm x 152.4 mm x 3.048 m) subjected to a temperature crossfall of 90^{o}F (50^{o}C) with a mean temperature of 178^{o}F (81^{o}C). The beam was simply supported over 9 ft. (2.74 m) span and was initially free from external loads. Rapid shrinkage took place on heating since it was unsealed. After 17 days equal loads were applied at the third points producing deflections in opposition to the thermal gradient deflections.

His results are given in Graph 1.20 which shows a plot against time of the central deflection with respect to the third points. The curve depicts the initial upward deflection due to the thermal gradient and rapid reduction of this with time by shrinkage which was greater at the hot face than the cold. Then the beam deflected downwards on applying the loads and continued to do so under the combined influence of creep and shrinkage. Also shown in the figure are the thermal gradient curve and the deflection curve of a non-heated companion beam subjected to the same loads. Two calculated deflection curves for the heated beam are also shown, one neglecting creep and the other including creep obtained from speciments kept at a laboratory temperature of 70°F. It shows the inadequacy of these methods in predicting such deflections.

England and Ross[21] have tested reinforced concrete beams of 5" x 4" x 24" (127 mm x 101 mm x 609 mm) which were flexurally restrained. The beams were subjected to a thermal gradient and did not carry the live loads. Two beams were cast back to back with large stirrups near their ends to prevent bending. They were reinforced in tension with 0.61% of steel: Graph 1.21 shows the variation in steel stress with time. Heating was commenced at 80 days after casting so that some compressive stresses were induced in the steel by shrinkage before heating. After heating the steel stress initially became tensile, but the direction soon changed back to compressive. The elastic theory solution is also given and shows a large discrepancy between it and the experimental curve. They analysed the stress and strain situations incorporating the effects of creep and shrinkage at the various elevated temperatures and also the effect of cracking using a

step-by-step method taking small time increments. The curve for their predictions is also given in Graph 1.21. Good agreement was obtained between predicted and experimental curves bearing in mind the uncertainties of cracking and the creep and shrinkage data.

England and Ross tested a similar specimen but this time moisture loss was initially prevented by sealing it in a copper jacket. The measured steel stress on heating was only 25% less than the elastic value and little variation was obtained for 50 days. After this period, the copper jacket was removed and a sharp reduction in steel stress to nearly zero after 30 days was recorded. This brings out clearly the effect of shrinkage of concrete on the steel stress.

In one set of unsealed beams, compressive steel equal in area to the tensile steel was used. Large increase in the compressive steel stress was measured.

Hannant[74] tested concrete slabs reinforced in tension also cast back to back and restrained from bending. He obtained large reductions in tensile steel stresses after heating. Sometimes the steel stresses changed into compression even while the thermal gradient was considerable. On cooling large compressive stresses were always induced in the steel with tensile stresses in the concrete which was originally in compression.

These tests demonstrate the important effect of creep and shrinkage under elevated temperature conditions on concrete beams subjected to a thermal gradient. In plain concrete beams[73] the deflections were much increased and after long periods of

loading the elastic theory predicted the wrong direction of deflection in flexurally restrained reinforced concrete members. The elastic theory predicted the wrong sign of tensile steel stress when they had been heated for a long time and particularly on cooling. In concrete, tensile stresses were induced in regions which, according to the elastic theory, were under compression.

Ross, England and Suan[19] tested heated simply supported and continuous prestressed beams. The simply supported beams were 5" x 8" x 10' (127 mm x 203 mm x 3.048 m). The continuous beams had the same section and total length but were divided into two spans each of 5 ft. (1.52 m). Certain principles and assumptions were presented and an iterative numerical method was introduced to allow for creep in the calculation of the variation with time of stresses, strains and displacements. The results of the tests are compared with the predictions of the theory. Finally it is concluded that in most cases, the stresses of prestressed beams which are subjected to a sustained temperature crossfall exhibit severe variations with time and there are substantial changes in the reactions due to sustained temperature crossfall. It was found also that cooling after a period of sustained heating is likely to create tension in some beams and may lead to cracking despite the prestress. It is also demonstrated in general terms that under a prolonged temperature crossfall, a prestressed concrete beam will in general reach a stable stress distribution.

Suan[20] tested two span continuous beams as well as simply supported beams. The beams were subjected to a crossfall of about 35 - 45°C between the hot and cold faces with max temperature of about 85 - 100°C. The long-term deflections of two

reinforced concrete and four prestressed concrete simply supported beams showed severe deviations from elastic theory. Four pre-stressed concrete continuous beams were tested, two with level supports and two with the central support raised. A marked change with time in the reactions caused by the thermal gradient was observed and this was due to creep and shrinkage at the elevated temperature as shown in Graph 1.22.

Arthanari[22] carried out experiments to study the behaviour of a long prestressed concrete ring structure under a combination of temperature gradient and internal pressure loads. As a simple structural member for these tests, a flexurally restrained beam sealed on five sides, representing a ring structure of infinite radius with the desired moisture movement was chosen. Two sets of 4 ft. (1.21 m) long twin beams 12 x 16¾ in. (304 x 425 mm) in section subjected to a temperature gradient of 36.5°C but under different prestress were used in these tests. His experiments lead to the following conclusions:

1. Differential creep together with differential shrinkage causes a redistribution of stresses in ring structures subjected to temperature gradient. The elastic thermal stresses may even be nullified by sustained heating.

2. The initial cracking may close in course of time owing to creep and shrinkage.

3. The iterative analysis based upon the rate of creep method has been quite successful in predicting the behaviour of flexurally restrained beams.

England[29] described numerical procedure for uniaxially pre-stressed member subjected to a linear temperature crossfall. The example corresponds to that of a flexurally restrained beam in order to discuss the influence of creep and temperature with reference to the calculation of stresses in prestressed concrete structures. His analysis shows that under conditions of non-uniform temperature and stress, stress distribution takes place and this is accompanied by changes of redundant forces and moments which thus become time-dependent quantities. The procedure shows that under conditions of sustained temperature and loads, moments and reactions will eventually stabilise and that these steady-state quantities which result from creep may be calculated directly and without reference to the elastic modulus or coefficient of thermal expansion of concrete.

England[87] discussed the effects of creep and temperature on the behaviour of concrete structures by three methods of analyses based on a specific thermal creep concept. Stresses become time variables in structures which are subject to thermal gradients, because creep, which is temperature-dependent, causes redistribution of stress to take place.

He concluded that some saving of computational time can result by using the rate of creep and relaxation methods.

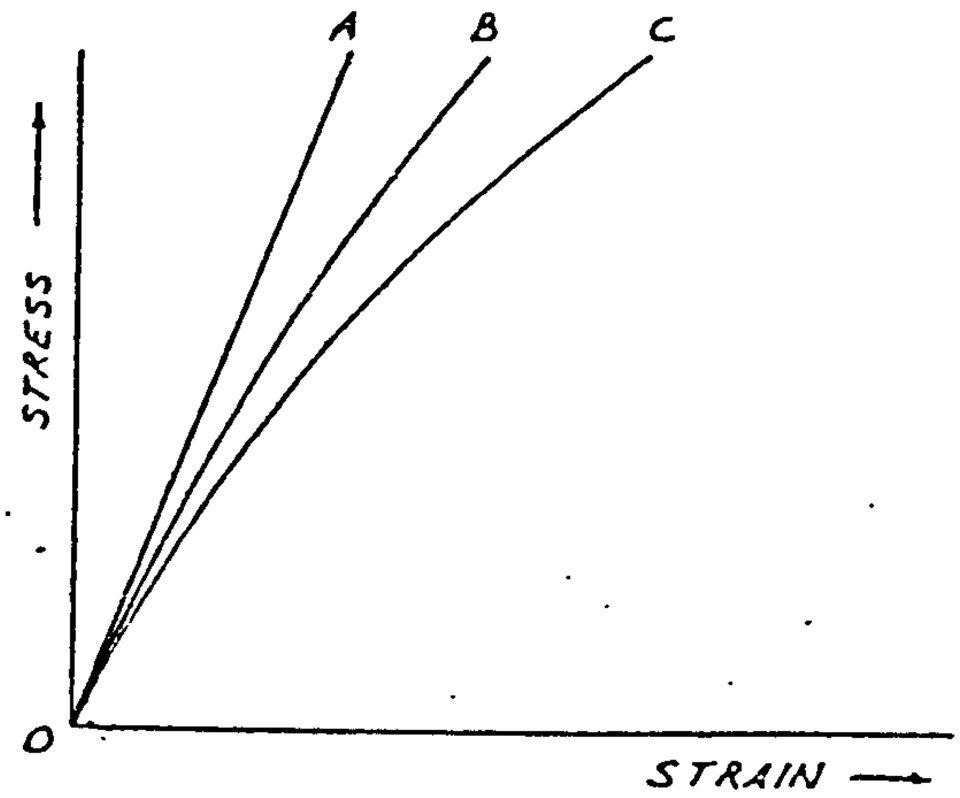

Graph 1.1 Stress-Strain Curves for Concrete On Loading.

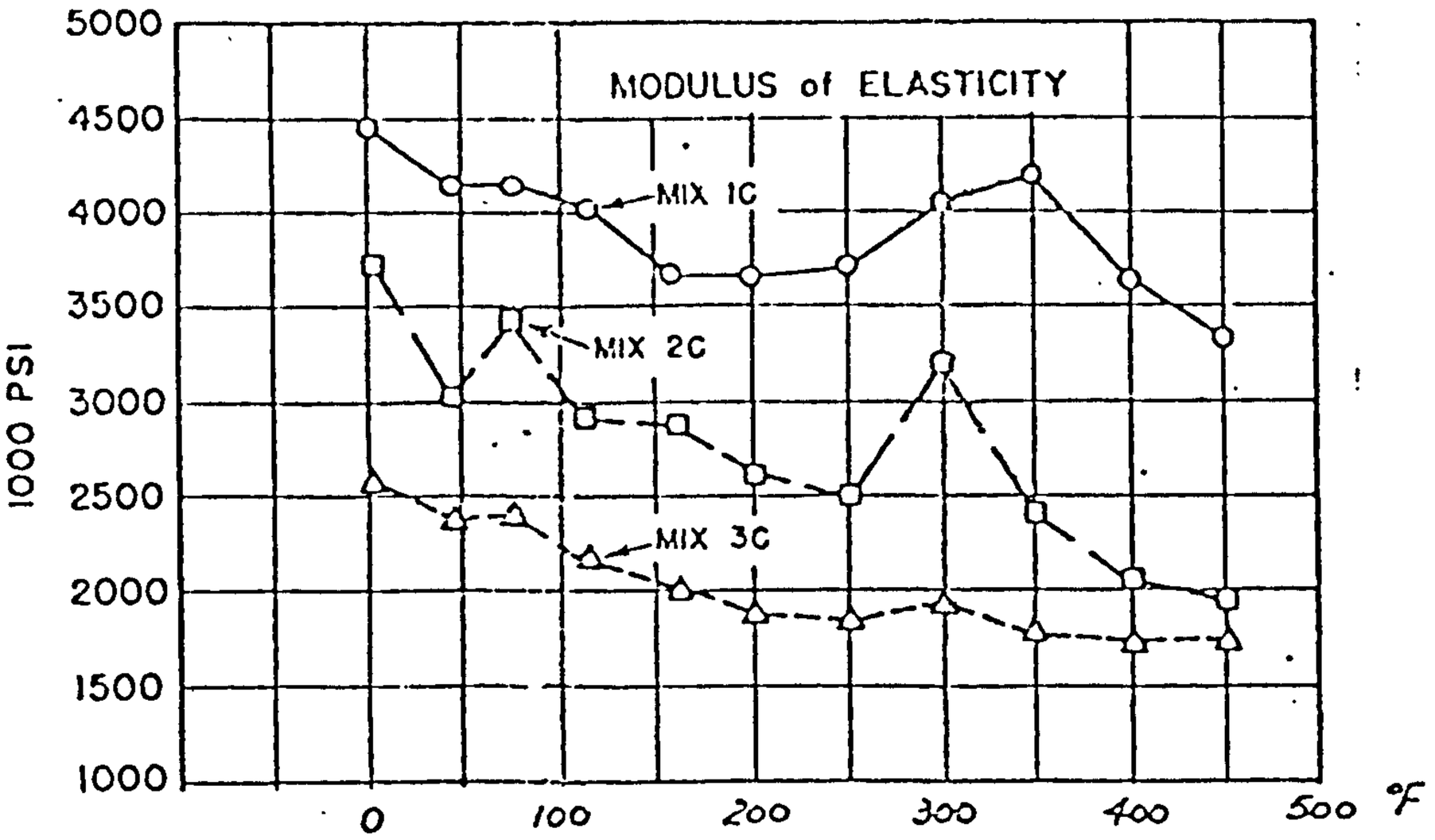

Graph 1.2 Variation of Modulus of Elasticity with Temperature.(4)

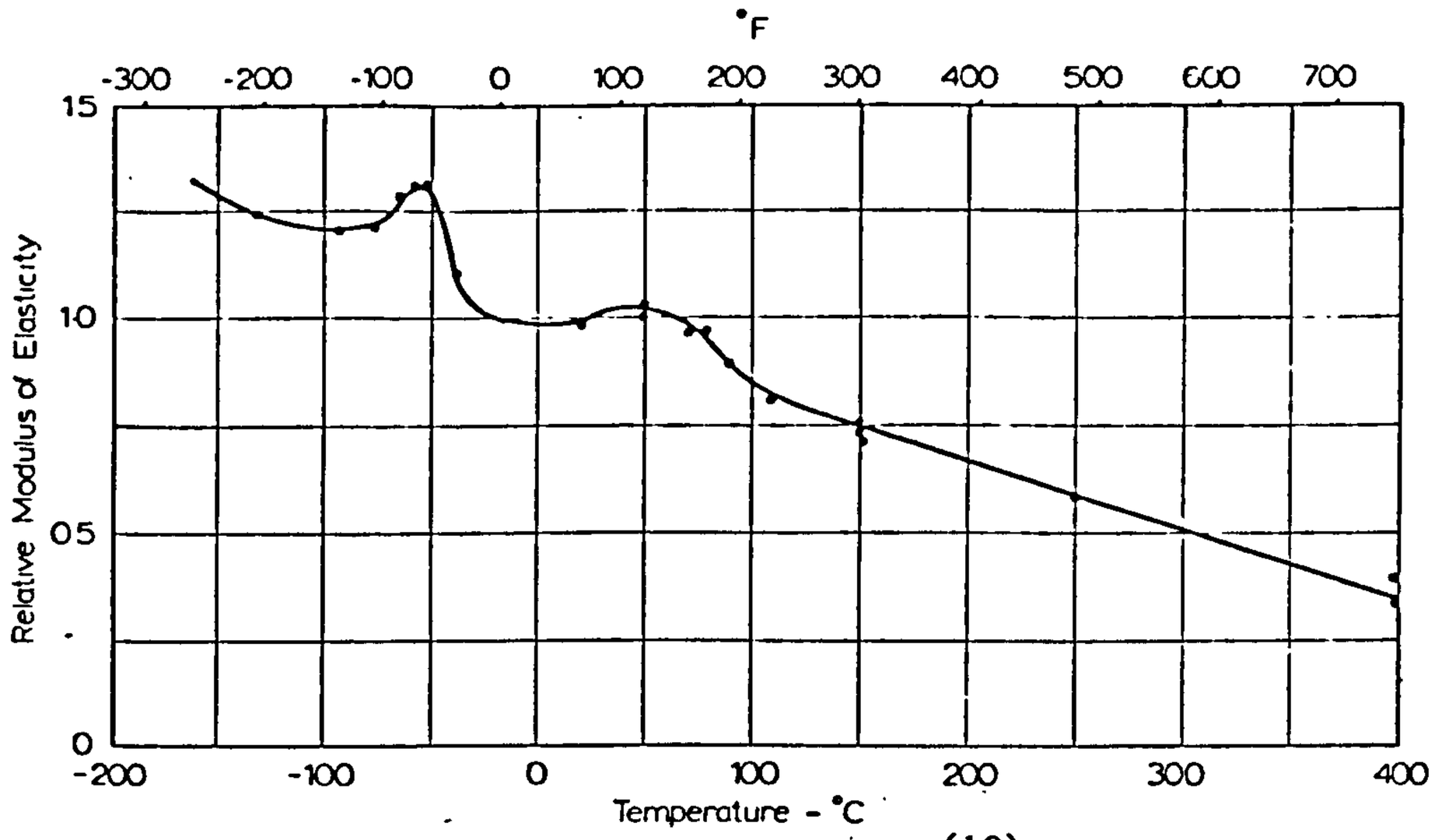

Graph 1.3 *Influence of temperature on modulus of elasticity of concrete*(10)

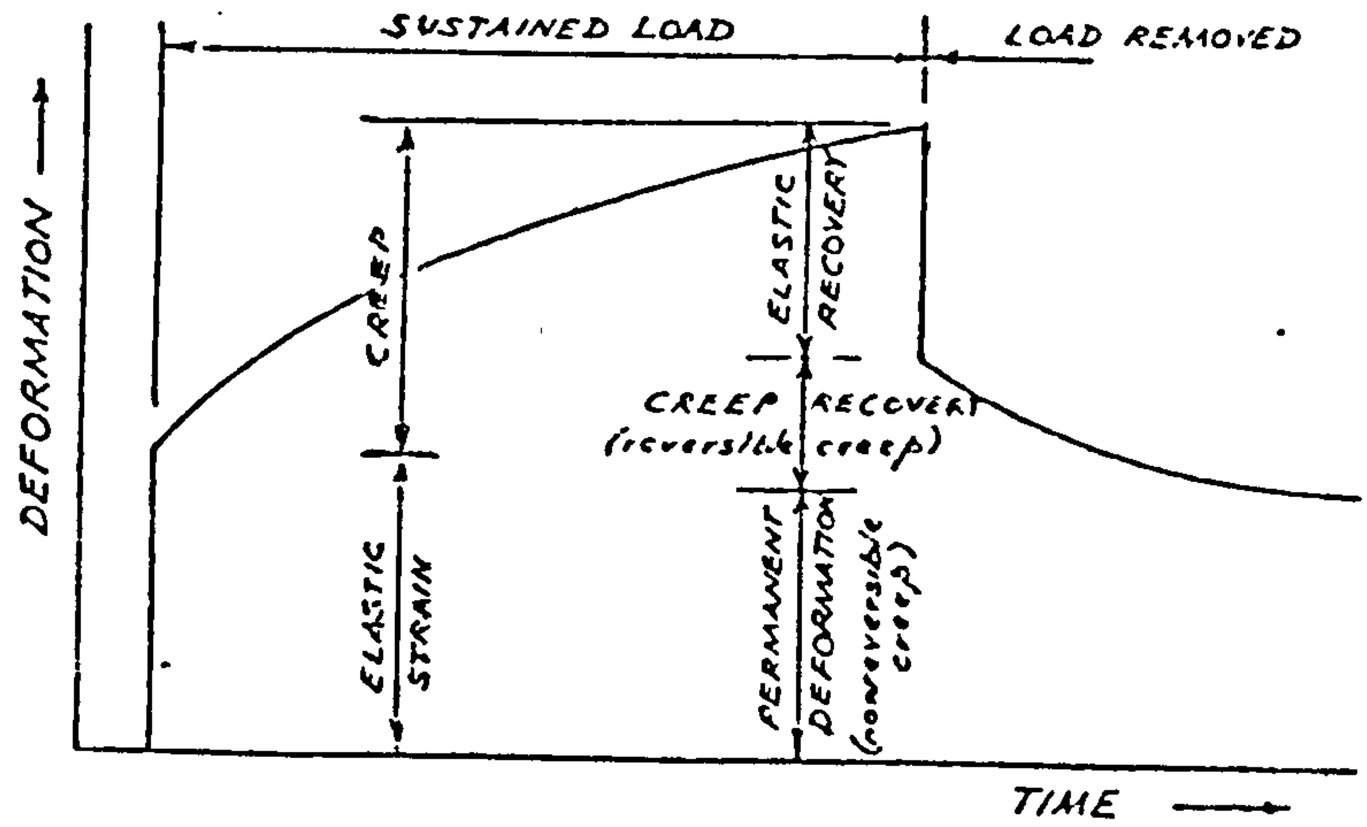

Graph 1.4 Deformation-Time Curve for a Concrete Specimen Subjected to a Constant Sustained Load and Then Unloaded Completely.

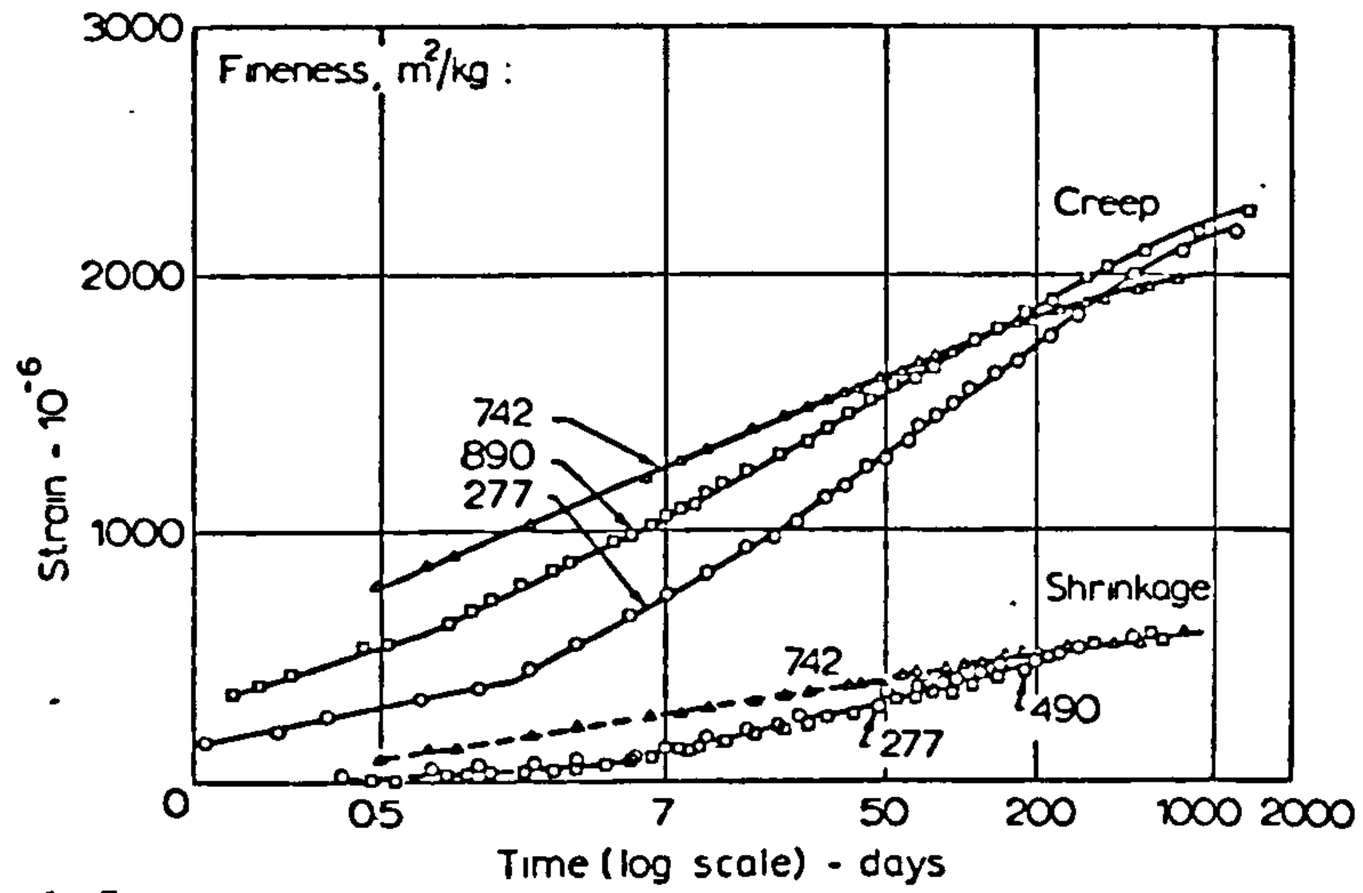

Graph 1.5 *Creep and shrinkage of concretes made with cements of different fineness. (All concretes had the same mix proportions; in the case of creep specimens, the age was chosen so that the stress-strength ratio was 0·5 for all the concretes)* (13)

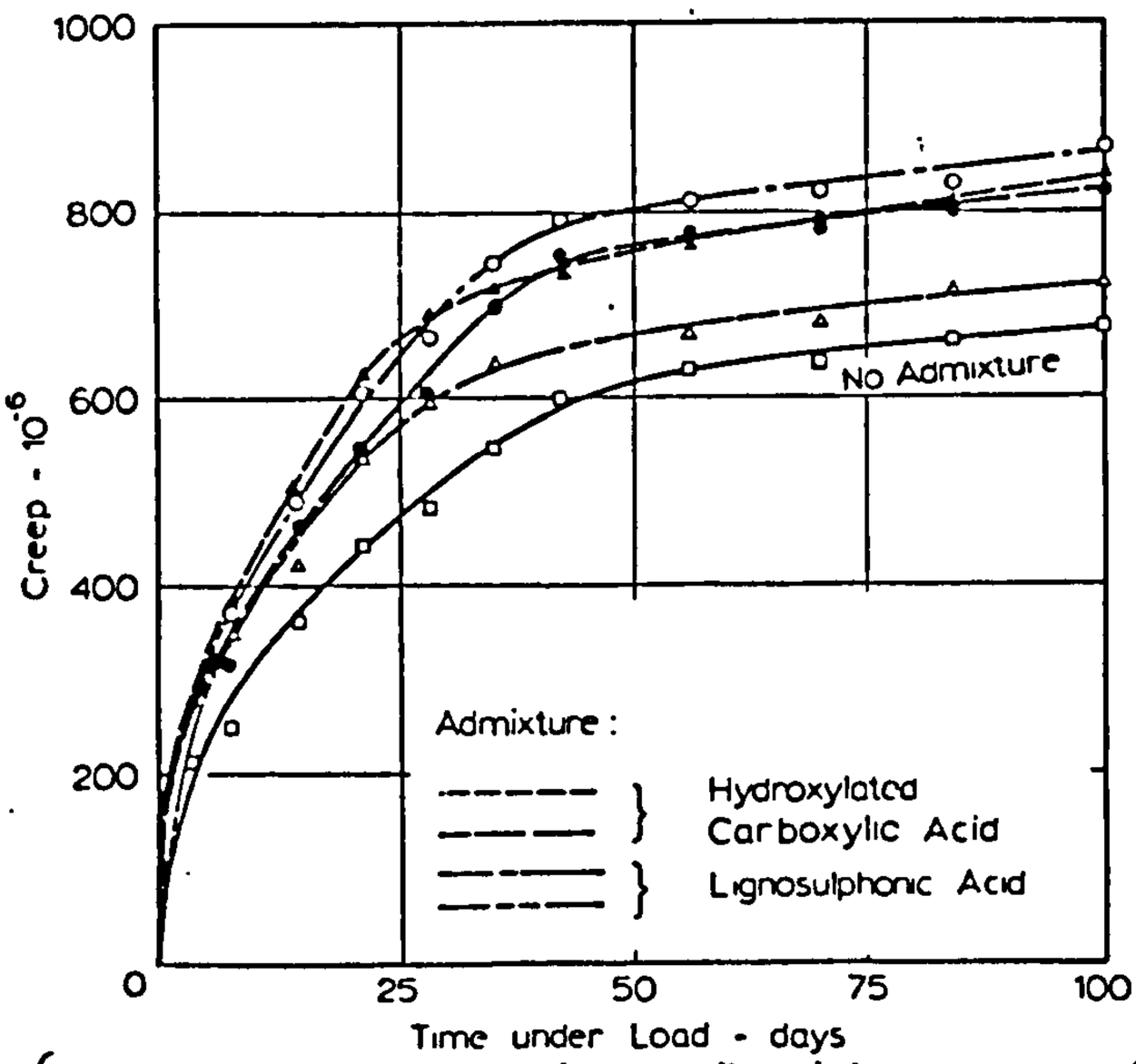

Graph 1.6 *Influence of water-reducing and set-retarding admixtures on creep of concrete (water/cement ratio = 0·65; age at loading = 28 days; relative humidity of storage = 94 per cent)* (14)

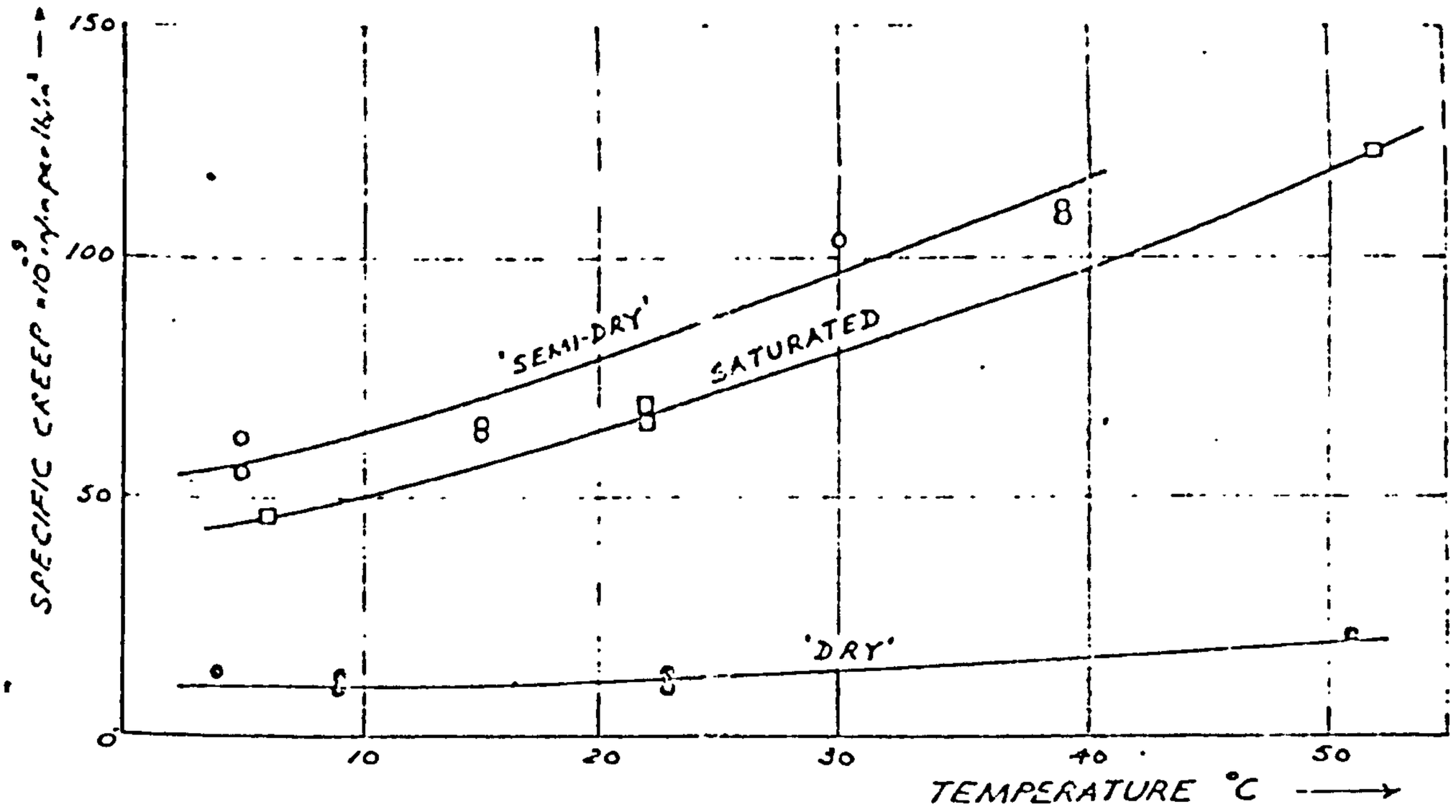

Graph 1.7 Specific creep versus temperature curves(5)

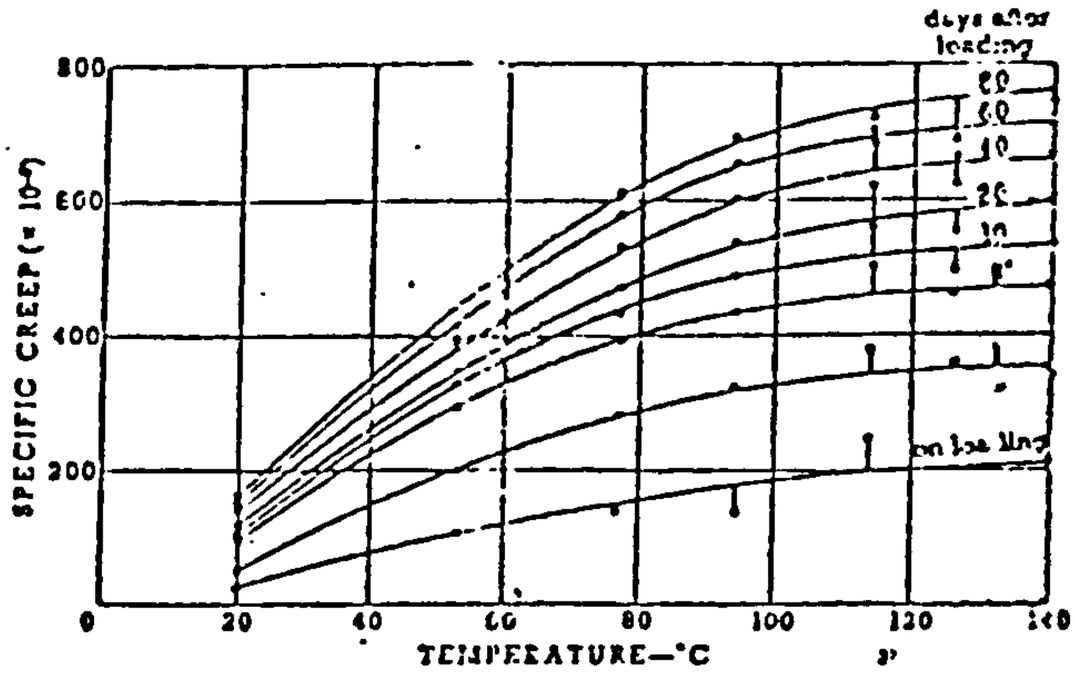

Graph 1.8 Graph showing variation of specific creep with time and temperature for sealed concrete specimens.(21)

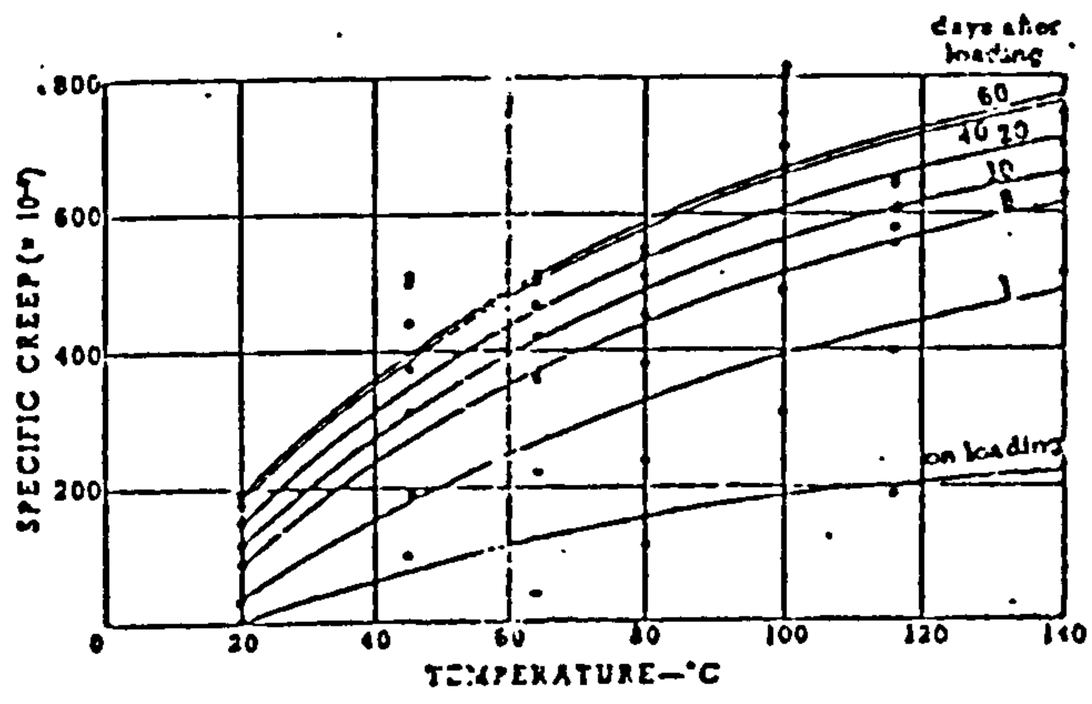

Graph 1.9 Graph showing variation of specific creep with time and temperature for unsealed concrete specimens.(21)

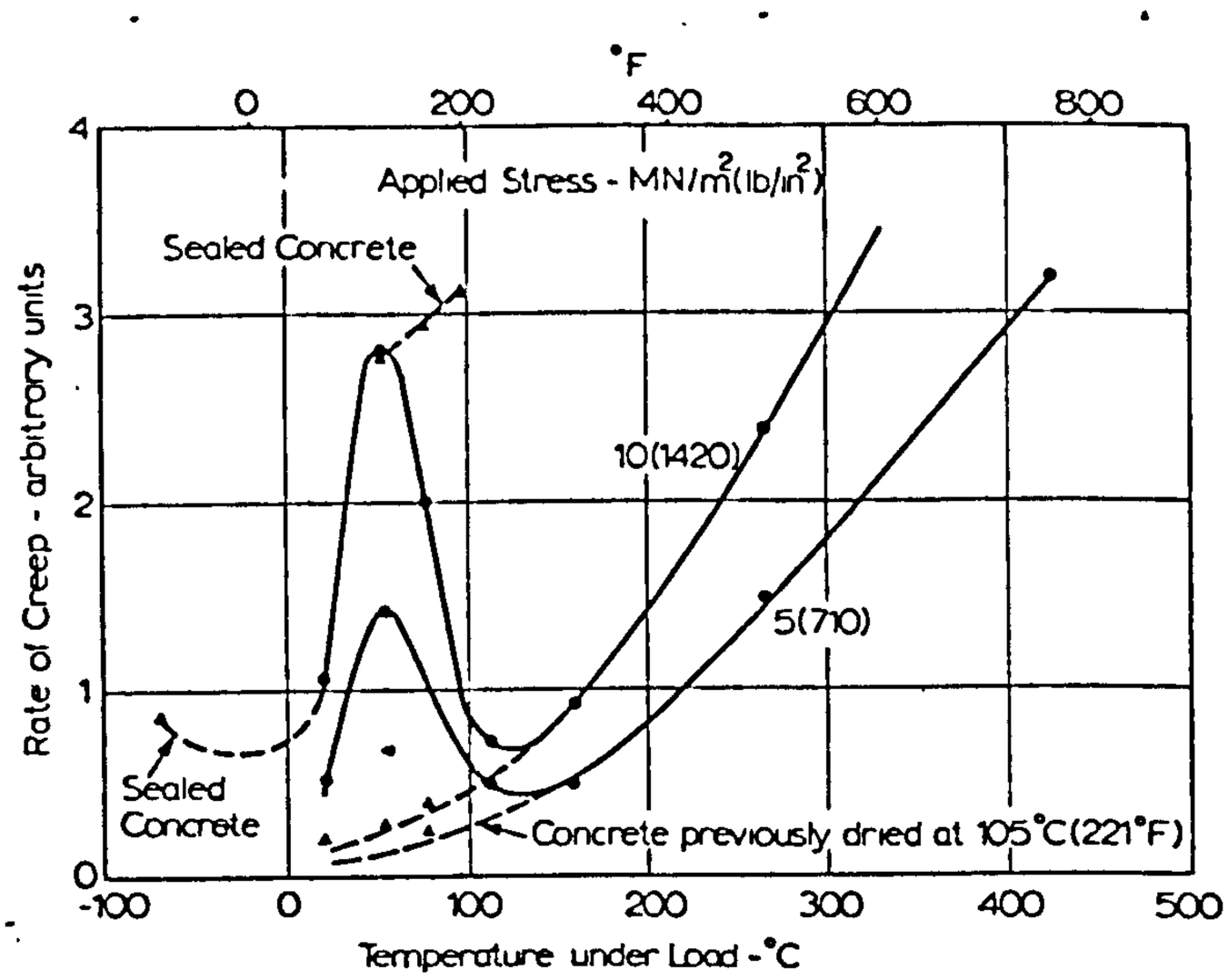

Graph 1.10 *Influence of temperature on rate of creep* (23)

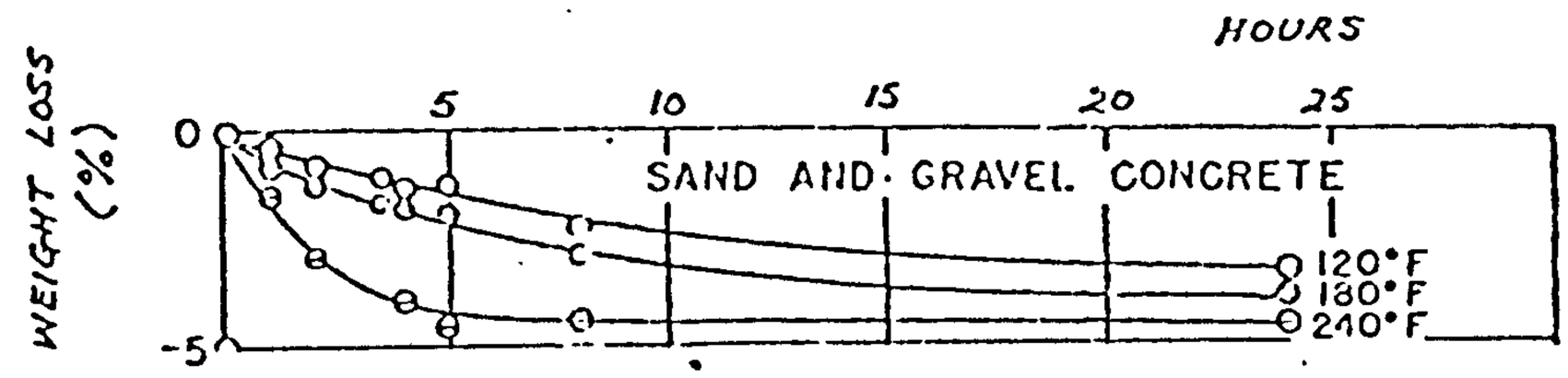

Graph 1.11 Percentage loss in weight of concrete specimens heated to various temperatures after various times. Mixing water content was 6.2%.(25)

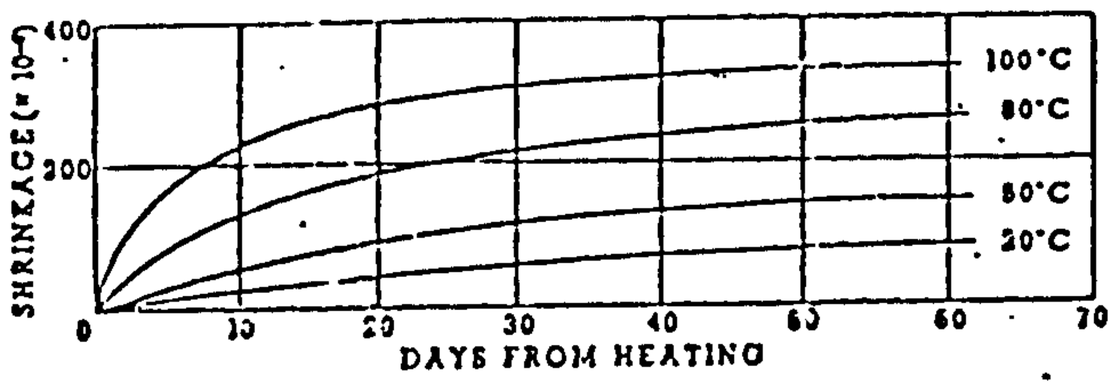

Graph 1.12 Graph showing variation of shrinkage with time for unsealed concrete specimens maintained at various constant temperatures.(21)

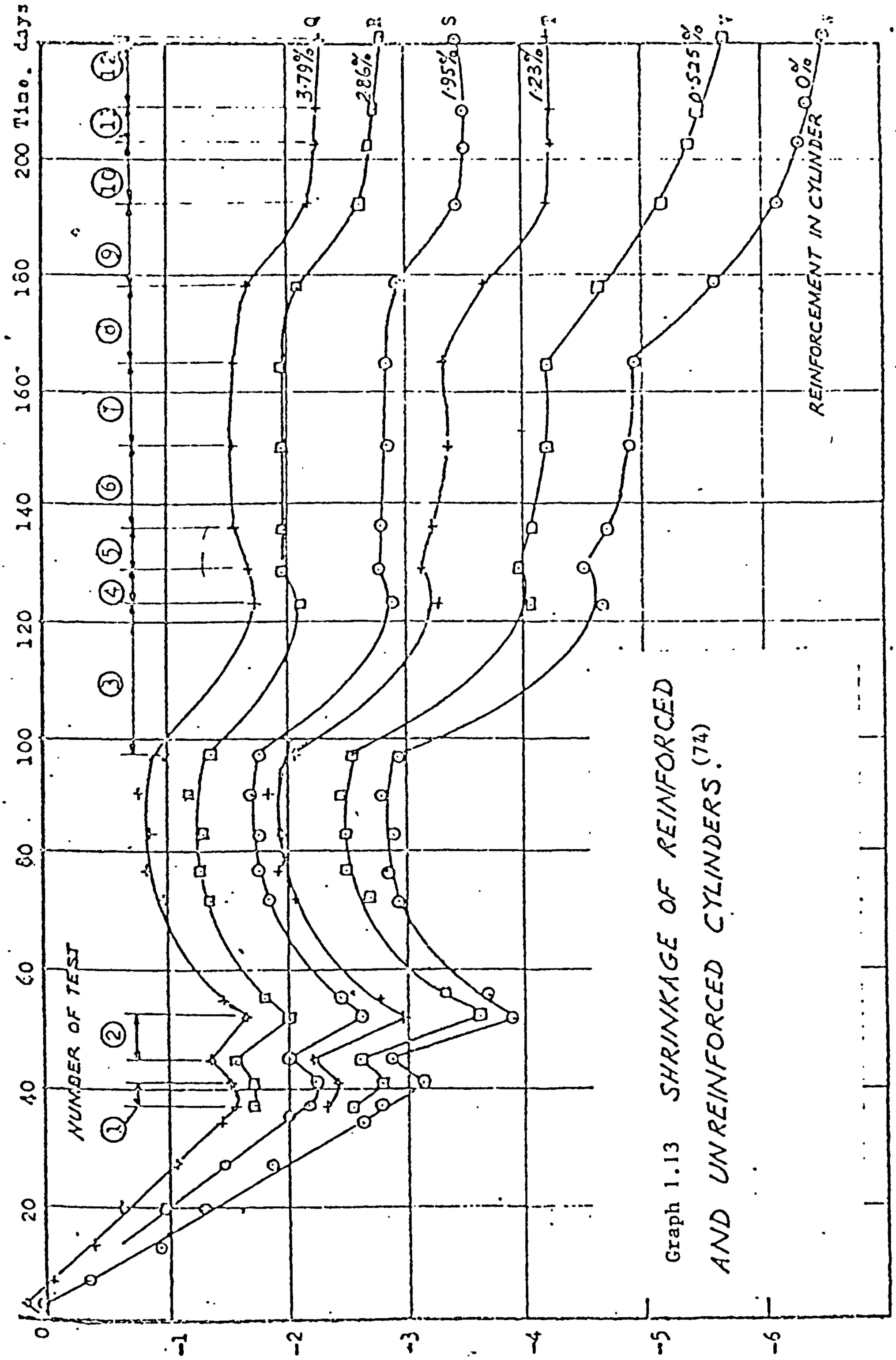

Graph 1.13 SHRINKAGE OF REINFORCED AND UNREINFORCED CYLINDERS.(74)

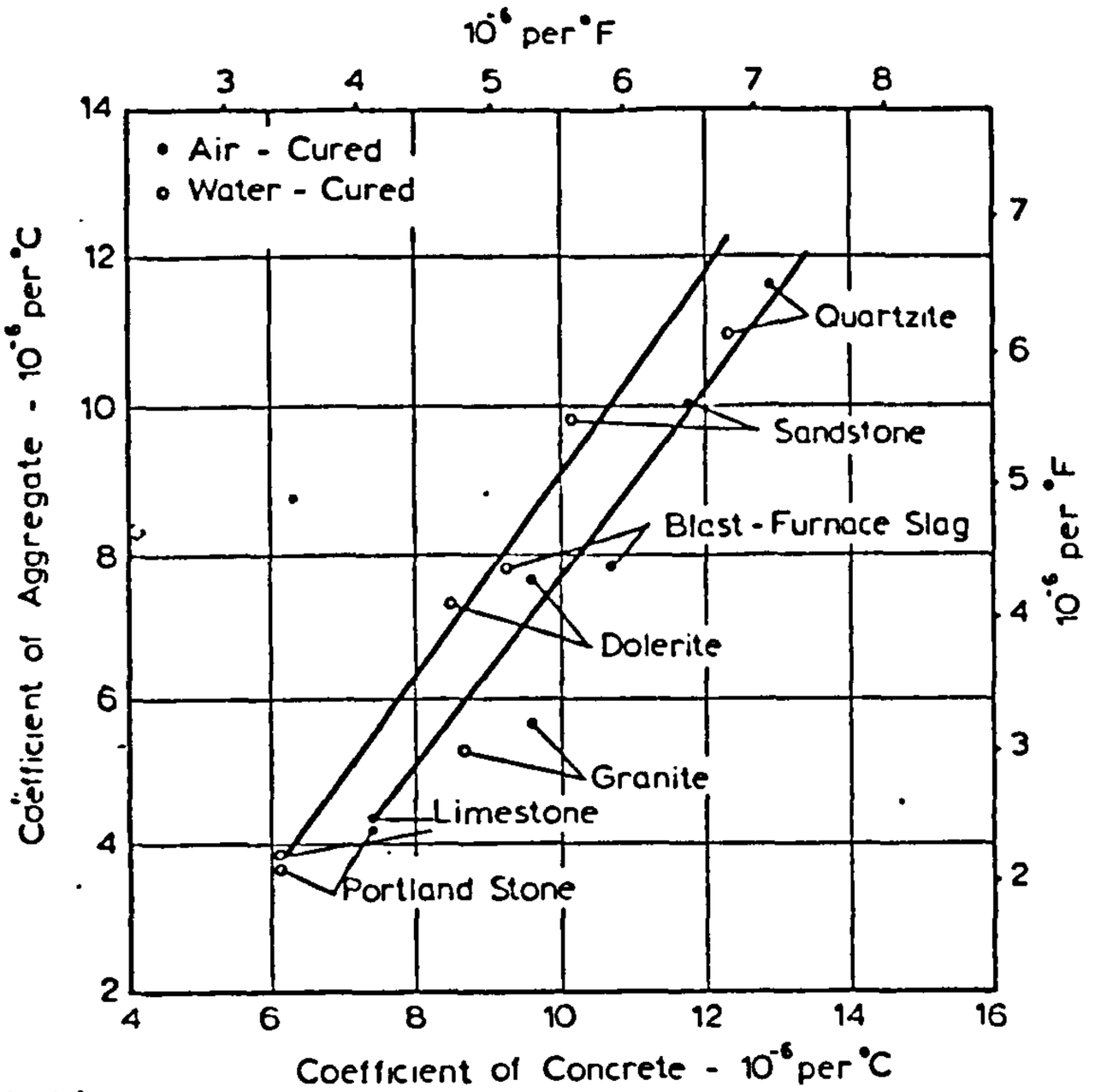

Graph 1.14 *Influence of the linear coefficient of thermal expansion of aggregate on the coefficient of thermal expansion of a 1:6 concrete* (32)

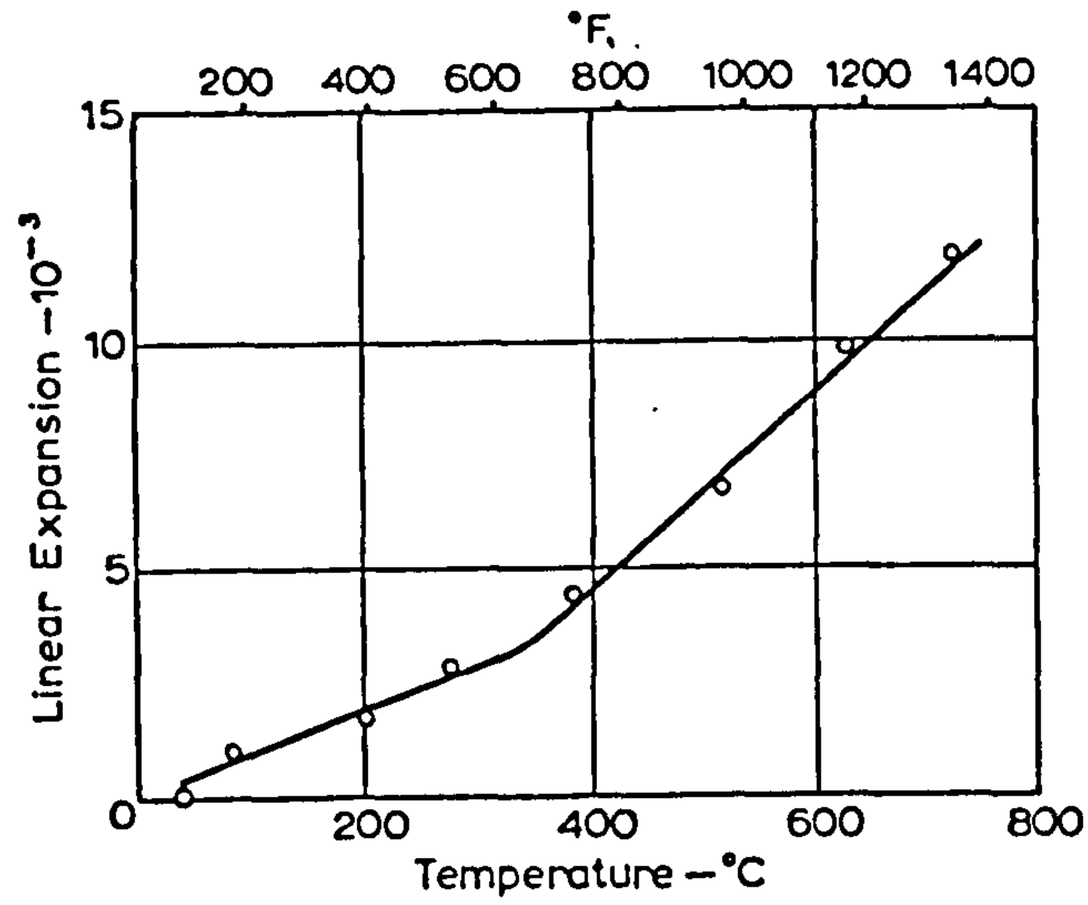

Graph 1.15 *Linear expansion of concrete on heating (calcareous aggregate; water/cement ratio = 0·4)* (3)

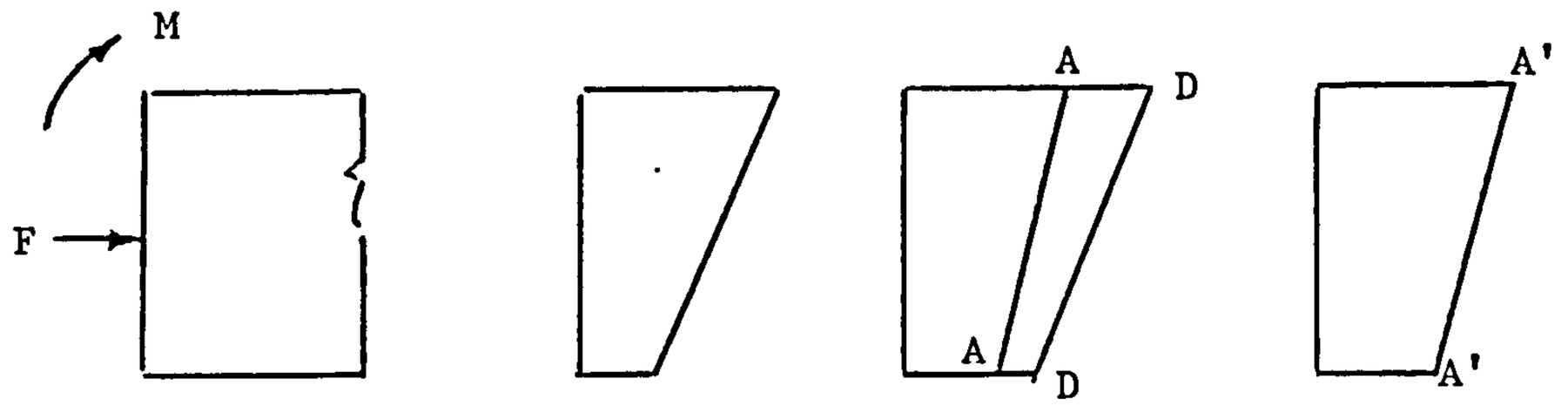

Longitudinal Element	Temperature Distribution	Initial Strains	Strains with creep

Graph 1.16 Strains by the Effective Modulus Method

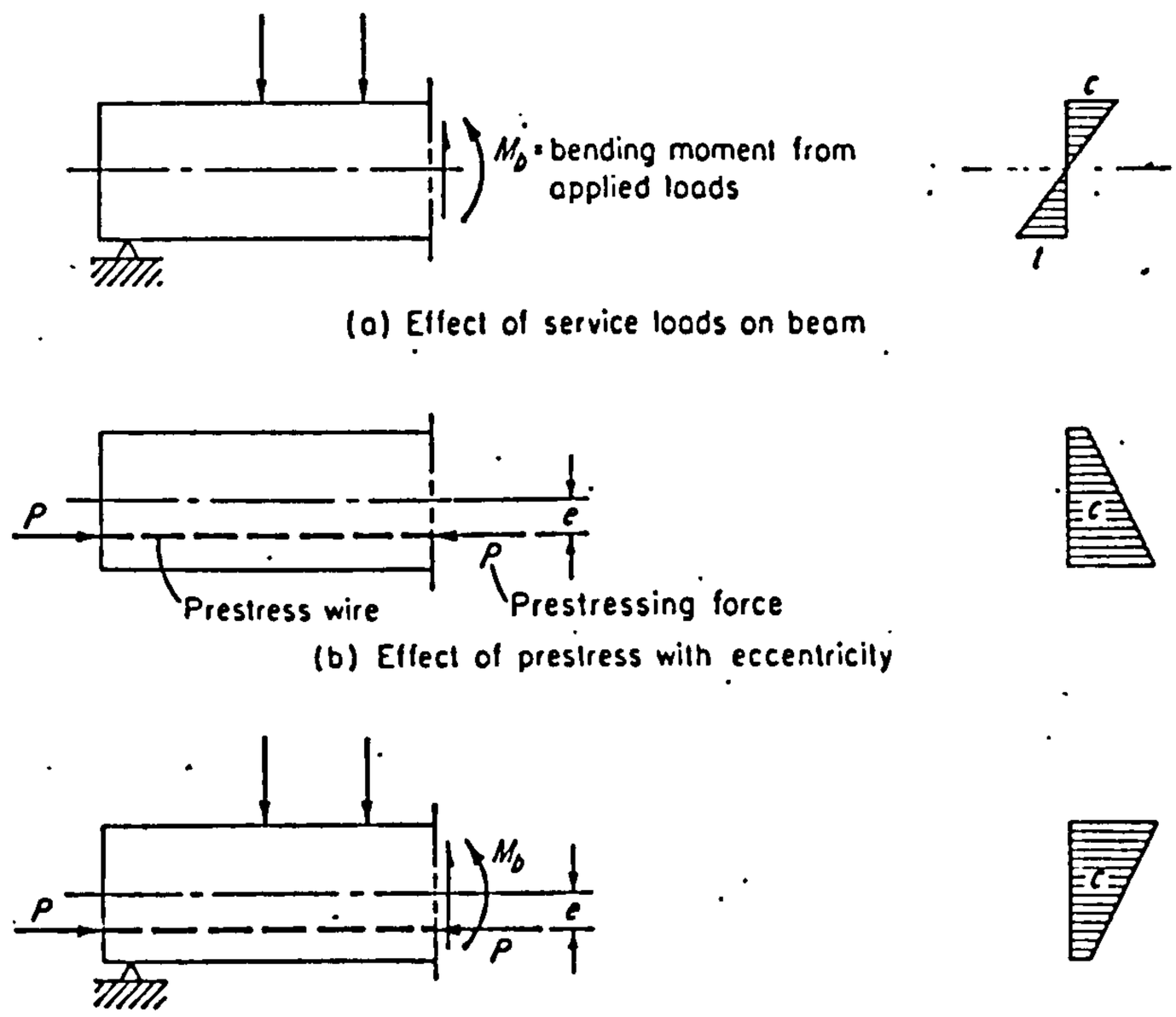

Graph 1.17 Opposite effects of service load and prestress on simple beam.

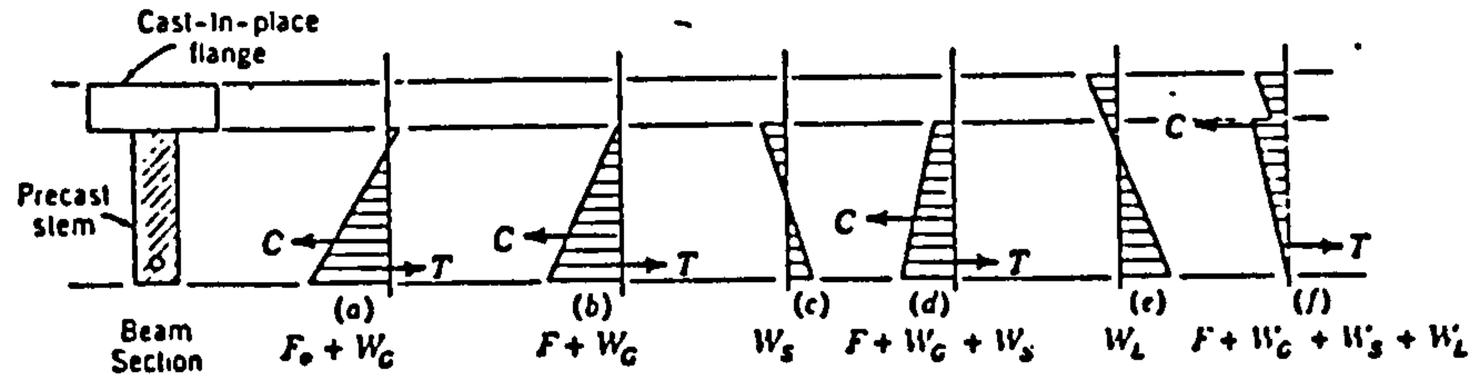

Graph 1.18 Stress distribution for a composite section.

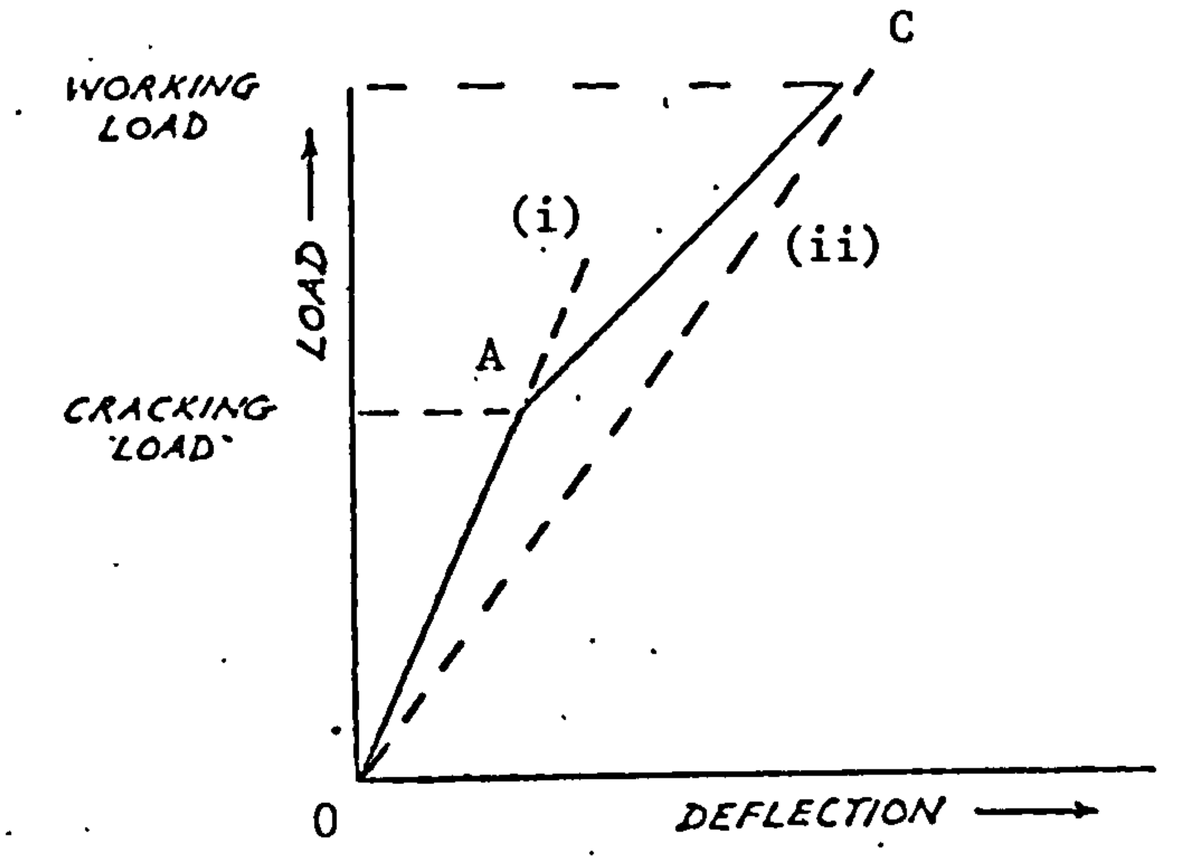

Graph 1.19(a) Load-deflection curve for a simply supported beam up to working load.

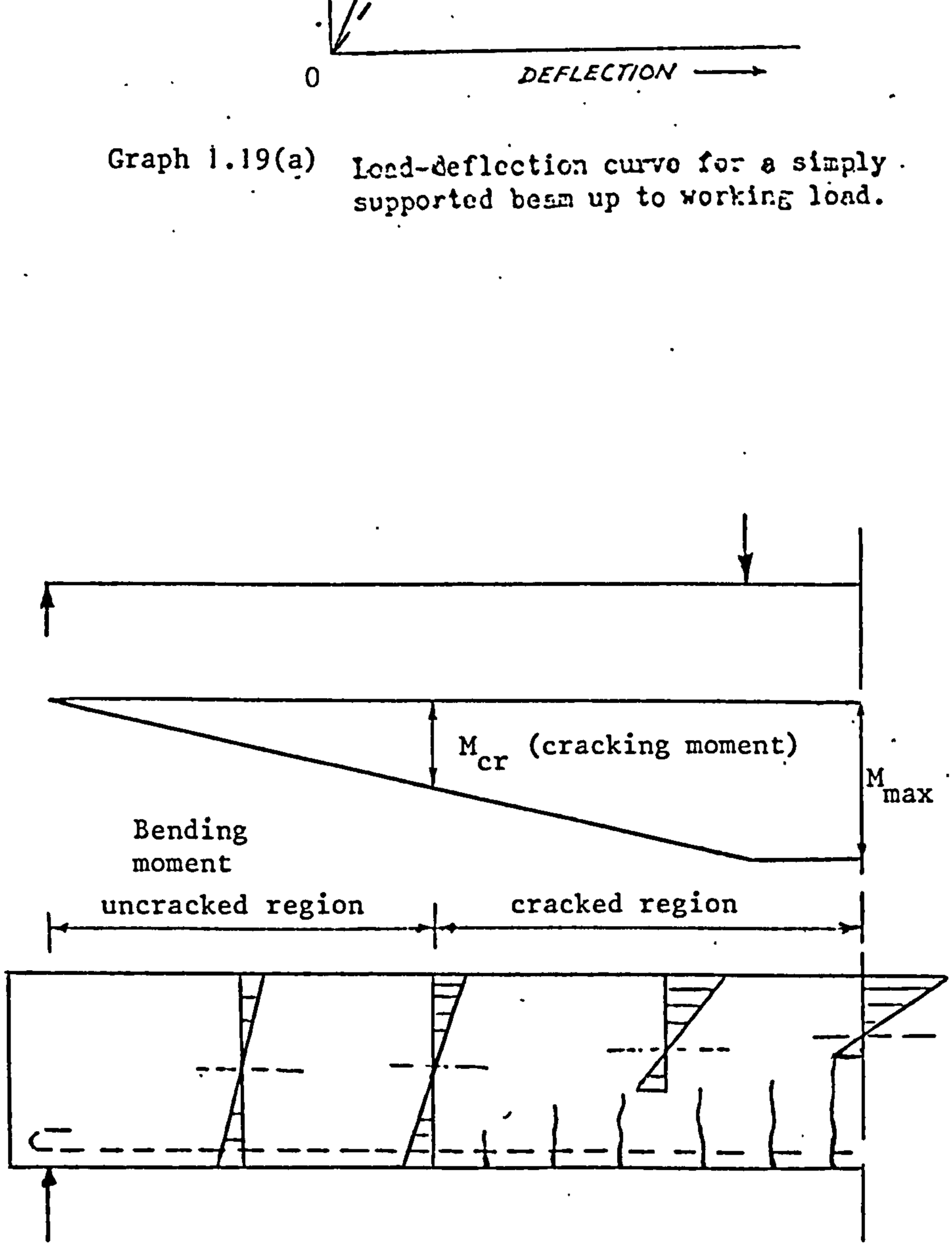

Graph 1.19(b) Stress distribution at various sections along the span

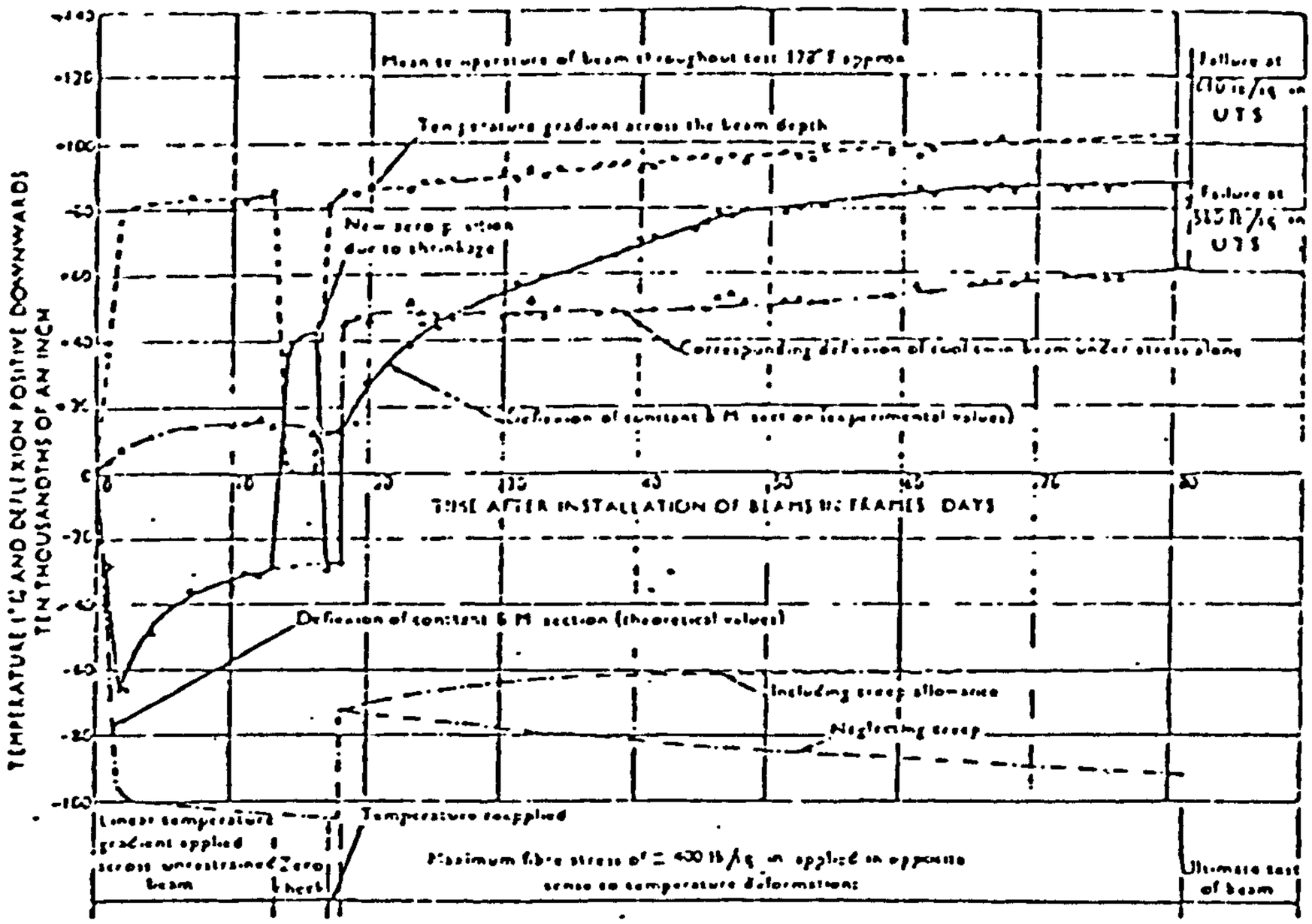

Graph 1.20 Graph showing variation of long-term deflections and thermal gradient for gravel concrete beams.(75)

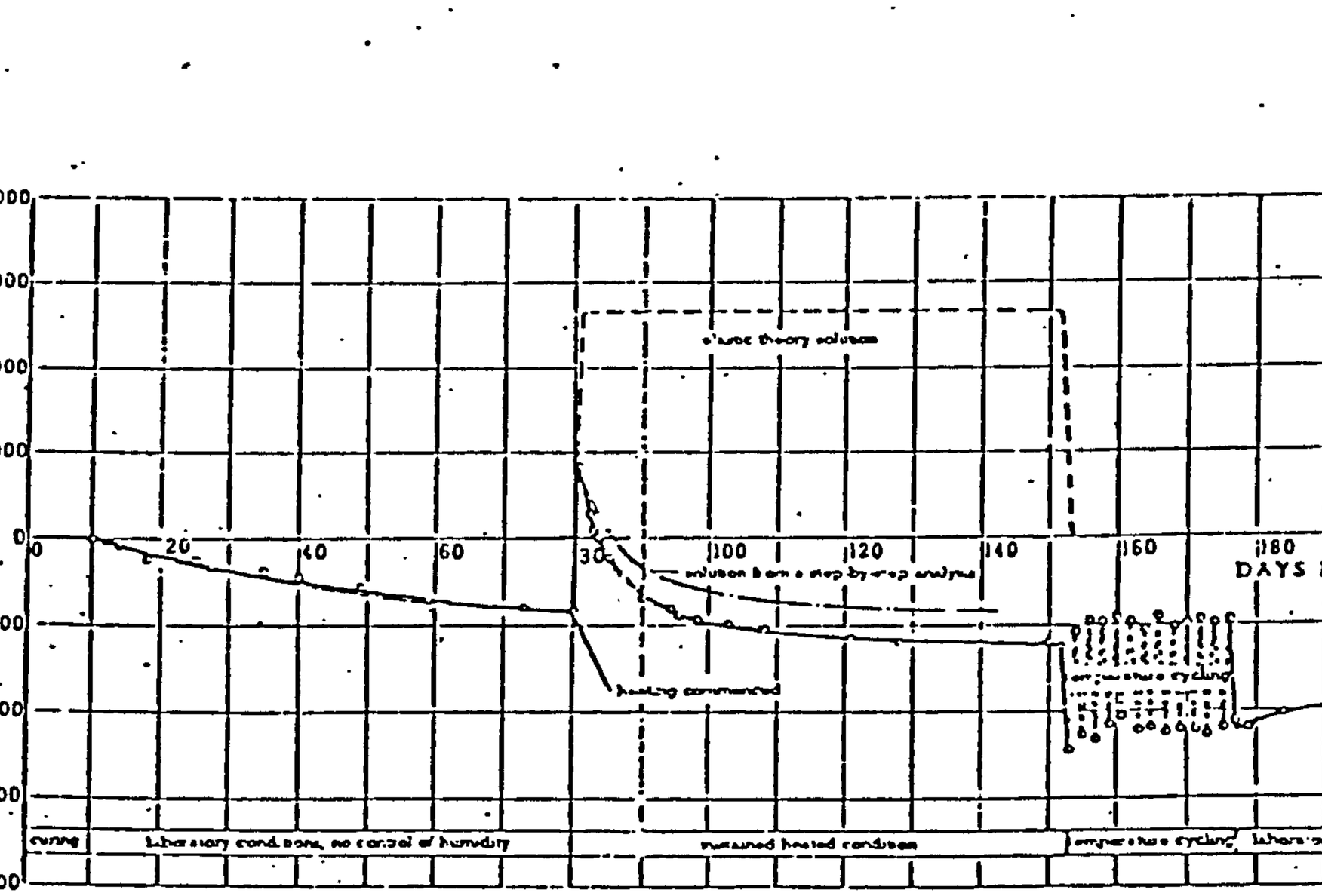

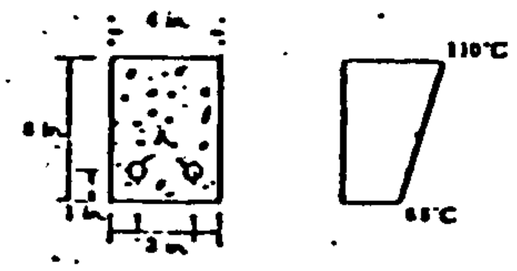

Concrete section and temperature distribution diagram

Graph 1.21 Graph showing variation of steel stress with time for flexurally restrained reinforced concrete beam subjected to a thermal gradient.(21)

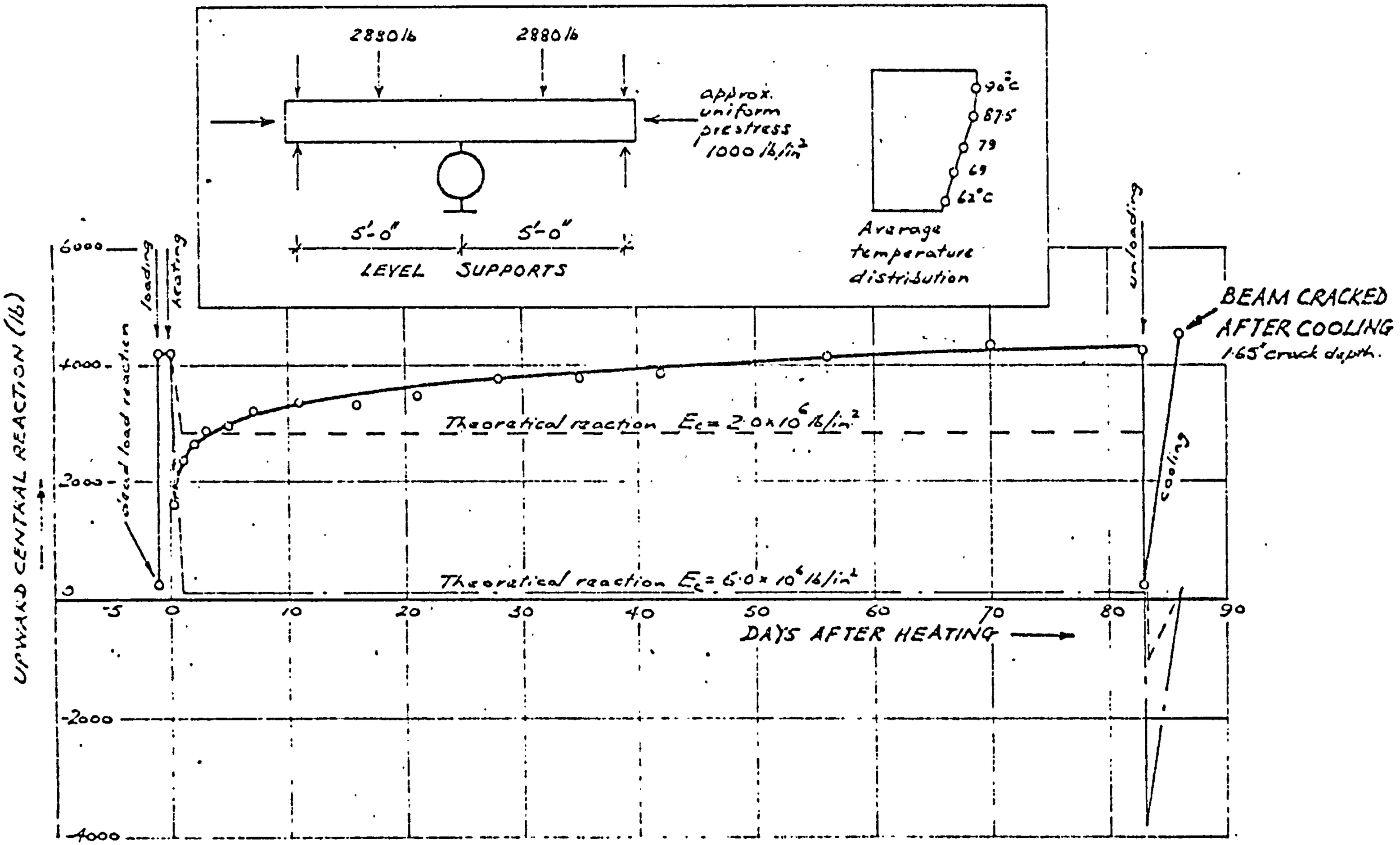

GRAPH 1.22 CHANGE OF CENTRAL REACTION WITH TIME FOR BEAM 13.

(PRESTRESSED, LOADED & HEATED CONTINUOUS BEAM WITH LEVEL SUPPORTS) (20)

CHAPTER 2

Part 1

Experimental work - short-term (elastic) behaviour and ultimate strength of reinforced, prestressed and composite prestressed concrete simple beams.

2.1 SIMPLE BEAMS

2.1.1 Synopsis

Experimental studies on elastic behaviour and ultimate strength of reinforced, prestressed and composite prestressed concrete simple beams of the same size and virtually the same ultimate capacity are reported.

Test results of three rectangular simple beams are presented.

All'the beams failed in flexure either by crushing of concrete after excessive elongation of reinforcement or by crushing of concrete while steel was in the elastic range.

The ultimate load tests on reinforced and prestressed concrete beams were carried out at an age of 28 days, and after 28 days from casting the reinforced concrete portion of the composite beam.

Whitney's method[30] was used in designing beams sections: the experimental results show that the assumptions of the above-mentioned method are satisfactory.

2.1.2 Introduction

The principle object of the investigation was to provide a direct and quantitative comparison of the elastic and ultimate behaviour of simple concrete beams with three types of straight tension reinforcement:

1. Deformed bar reinforcement;
2. Pretensioned reinforcement;
3. Composite prestressed plank reinforcement.

Tests were conducted to determine the longitudinal strain distributions, vertical deflections, cracking loads and ultimate loads.

The experimental ultimate moments were in good agreement with the designed values for all three types of concrete beams.

Three simple beams 127 x 204 mm in cross section and 1.67 m overall length were tested with equal loads at the third points of a 1.52 metre span.

2.1.3 Experimental beams and details of concrete mixes A and B

2.1.3.1 Dimensions and reinforcement

The reinforcement of the three types of beams are presented in Table 2.1.1. The reinforcement and position of the stirrups are shown in Figs. 2.1.1, 2.1.2 and 2.1.3.

The dimensions of all the beams were 127 x 204 mm in cross section and 1.67 m overall length and they were designed to have the same ultimate moment capacity. The prestressing wires used in prestressed and composite prestressed concrete beams were 5 mm in diameter and each wire was initially tensioned to 1132 MN/m^2

The properties of reinforcing steel used are given in Table 2.1.2.

Beam Type	Top Reinforcement	Bottom Reinforcement	Stirrups
R.C.	1 No. 8 mm Ø deformed bar	3 No. 8 mm Ø deformed bars	1 No. 8 mm Ø deformed bar @ 127 mm
P.C.	-	2 No. 5 mm Ø H.T.S. bars	1 No. 8 mm Ø deformed bar @ 127 mm
C.P.C.	-	Prestressed pre-tensioned concrete plank reinforced with 2 No. 5 mm Ø H.T.S. bars	1 No. 8 mm Ø deformed bar @ 127 mm

Table 2.1.1 Reinforcement in reinforced, prestressed and composite prestressed concrete beams

Size	Yield Point MN/m^2	Ultimate tensile strength MN/m^2	Young's Modulus GN/m^2
8 mm Ø deformed bars	427.490	503.500	179.27
5 mm Ø H.T.S. bars	-	1652.590	197.88

Table 2.1.2 Properties of Reinforcing Steel

2.1.3.2 Mix

Table 2.1.3 presents proportions by weight of concrete mix types A and B used in concrete beams.

Table 2.1.4 presents the beam type and concrete mix used.

The coarse aggregate was a flint gravel and contained equal portions of those of size between $\frac{3}{16}$" and $\frac{3}{8}$" (4.7 mm and 9.5 mm) and those between $\frac{3}{8}$" and $\frac{3}{4}$" (9.5 mm and 19 mm). The properties of concrete mixes used are given in Table 2.1.5.

Beam Type	Mix Type used
R.C.	A
P.C.	B
C.P.C.	
a. Cast in place portion	A
b. Prestressed portion	B

Table 2.1.4 Type of Concrete Beams and Mix Used

Mix Type	Cement	Sand	Aggre-gate	W/C
A	1	2	4	0.50
B	1	1.9	2.8	0.45

Table 2.1.3 Concrete mix types used in Concrete Beams

Concrete Mix Type	Average compressive strength MN/m^2		Average tensile strength MN/m^2	Young's Modulus GN/m^2
	100 mm cube	113 mm Ø x 304 mm Long Cylinder	Split Test	
	28 day	28 day	28 day	28 day
A	42.628	30.710	2.620	34.475
B	50.202	35.095	2.800	37.922

Table 2.1.5 Properties of Concrete Mixes

2.1.3.3 Mould

Beam rigid steel mould used is shown in Photo 2.1.1.

2.1.3.4 Casting Procedure

(a) Reinforced and prestressed concrete beams. One beam 127 x 204 mm in cross section and 1.67 m overall length. Four 100 mm cubes and four 113 mm diameter x 304 mm long cylinders were cast together. The ingredients were put into a pan mixer for three minutes. The beam was vibrated with a Kango electric hammer and the cubes and cylinders were made on a vibrating table.

After the last layer the beam was finally smoothed off with a trowel.

(b) Composite prestressed concrete beam

Prestressed Portion:

One plank 51 x 127 mm in cross section and 1.67 metres long, four 100 mm cubes and four 113 mm diameter x 304 mm long cylinders were cast together. The ingredients were put into a pan mixer for three minutes. The plank, cubes and cylinders were made on a vibrating table.

Photo 2.1.2 shows the plank rigid steel mould and the pump operating the hydraulic jack to stress the wires just before casting.

Cast in place portion:

When the plank was 14 days old cast in place portion, four 100 mm cubes and four 113 mm diameter x 304 mm long cylinders were cast together. The casting procedure was the same as the one used in reinforced and prestressed concrete beams.

2.1.3.5 Curing prior to testing

The beams were covered with wet sacks on the day after casting. Table 2.1.6 presents all the operations undertaken from casting till testing.

2.1.4 Testing Apparatus

Photos 2.1.3, 2.1.4 and 2.1.5 show reinforced, prestressed and composite prestressed concrete simple beams on the testing rig after failure.

2.1.4.1 End supports

The end supports were so made of H.T.S. bars that the beam rested on two steel plates which in turn rested on two knife edges spaced at 1.52 metres apart(see Photo 2.1.3). When the beam was seated on the supports some wet plaster was placed between the concrete and steel plate to offset any irregularities in the concrete surface and any displacement between the two surfaces.

2.1.4.2 Loading apparatus

Static loads were applied to the centre of each beam by 20 tons hydraulic jack connected to hydraulic testing machine.

2.1.4.3 Strain gauges for deflections

Three dial gauges, each reading 0.01 mm per dial division were used. They measured rigid holly movements at the ends of the beam and the mid span displacement during the loading operation.

2.1.4.4 Strain measurement

Strain measurements, using the 8" (203 mm) Demec gauge, (each dial

TABLE 2.1.6

Beam Type	Casting	Days after casting						
		1	7	14	21	28	35	42
R.C.	a.Beam b.4 cubes c.4 cylinders	1.Wet sack curing 2.Demoulding cubes and cylinders	1.Demoulding the beam 2.Placing the beam on two stools		Placing the beam on testing rig	1.Testing the beam 2.Testing cubes and cylinders		
P.C.	a.Beam b.4 cubes c.4 cylinders	1.Wet sack curing 2.Demoulding cubes and cylinders	1.Applying Prestressing force 2.Demoulding the beam 3.Placing the beam on two stools		Placing the beam on testing rig	Testing the beam, cubes and cylinders		
C.P.C.		Days after casting P.C. plank						
	a.One P.C. Plank b.4 cubes c.4 cylinders	1.Wet sack curing 2.Demoulding cubes and cylinders	1.Applying Prestressing force 2.Demoulding the plank	1.Casting Cast in place portion 2.Casting cubes and cylinders	1.Demoulding the beam 2.Placing the beam on two stools		Placing the beam on testing rig	Testing the beam, cubes and cylinders

division corresponding to 0.78×10^{-4}in. (19.8×10^{-4}mm)) were made at the mid span at the following locations

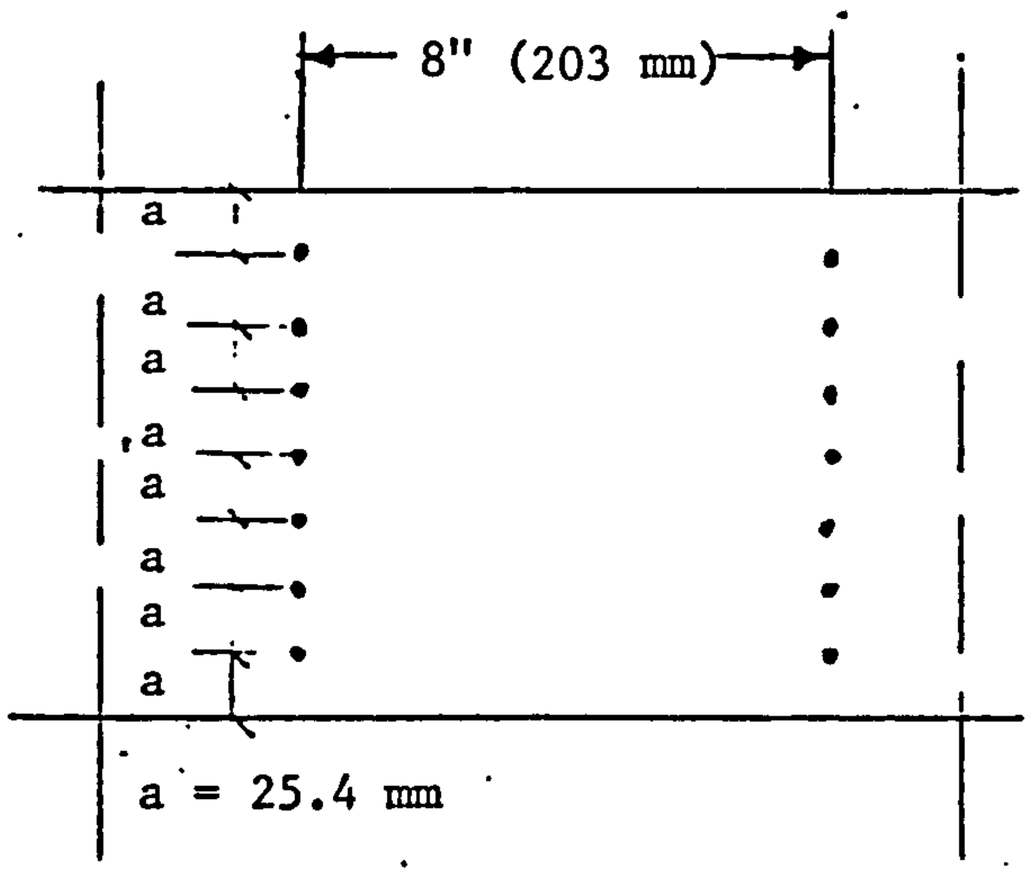

2.1.5 Testing Procedure

Load was applied in increments of 1000 lbs.(4448 N)while readings were taken of deflection and strains at each increment of load up to cracking. The dial gauges were removed soon after cracking so that they would not be damaged at failure and the load is increased up to failure of the beams.

Photo 2.1.6 shows the mechanical instruments used in measuring strains and displacements.

2.1.6 Results and Discussions

2.1.6.1 Cracking and ultimate loads

Table 2.1.6 compares the measured and computed values of the cracking and ultimate loads of the three types of concrete beams. The cracking load was determined by a combination of three methods. The first by observation of the beam for any visible cracks, the second was by detecting an appreciable increase in the strains and

the third was by observing a sharp break in the load deflection curve.

Beam Type	Cracking Load kN		Ultimate load kN	
	Measured	Computed	Measured	Computed
R.C.	7.5	9.1	42.25	39.50
P.C.	17	14.8	37.80	41.59
C.P.C.	28.00	30.01	37.80	43.00

Table 2.1.6 Cracking and ultimate loads measured versus computed values - simple beams

2.1.6.2 Strain gauge readings

Measured strain distribution at mid span gauge lengths corresponding to the tested beams are plotted in Graphs 2.1.1, 2.1.2 and 2.1.3.

Upon further increase in bending moment, the strain increases and its distribution greatly deviated from a straight line and the neutral axis moves further towards the compression side as failure is approached.

2.1.6.3 Deflections

Mid span load deflection curves for the beams tested to failure deviated from a straight line soon after cracking as shown in graphs 2.1.4, 2.1.5 and 2.1.6.

2.1.7 Conclusions

1. The behaviour of all the beams followed the elastic theory predictions very closely until cracking. The elastic deflection can be computed by elastic theory using a modulus of elasticity recorded

from control tests to within an accuracy of approximately 10 per cent. For the prediction of the onset of cracking the elastic theory gave excellent predictions of cracking load.

2. Observed and calculated cracking and ultimate loads for the three types of beams are listed in Table 2.1.6. The table shows that the measured ultimate strengths were in close agreement with values computed by using Whitney's method[30].

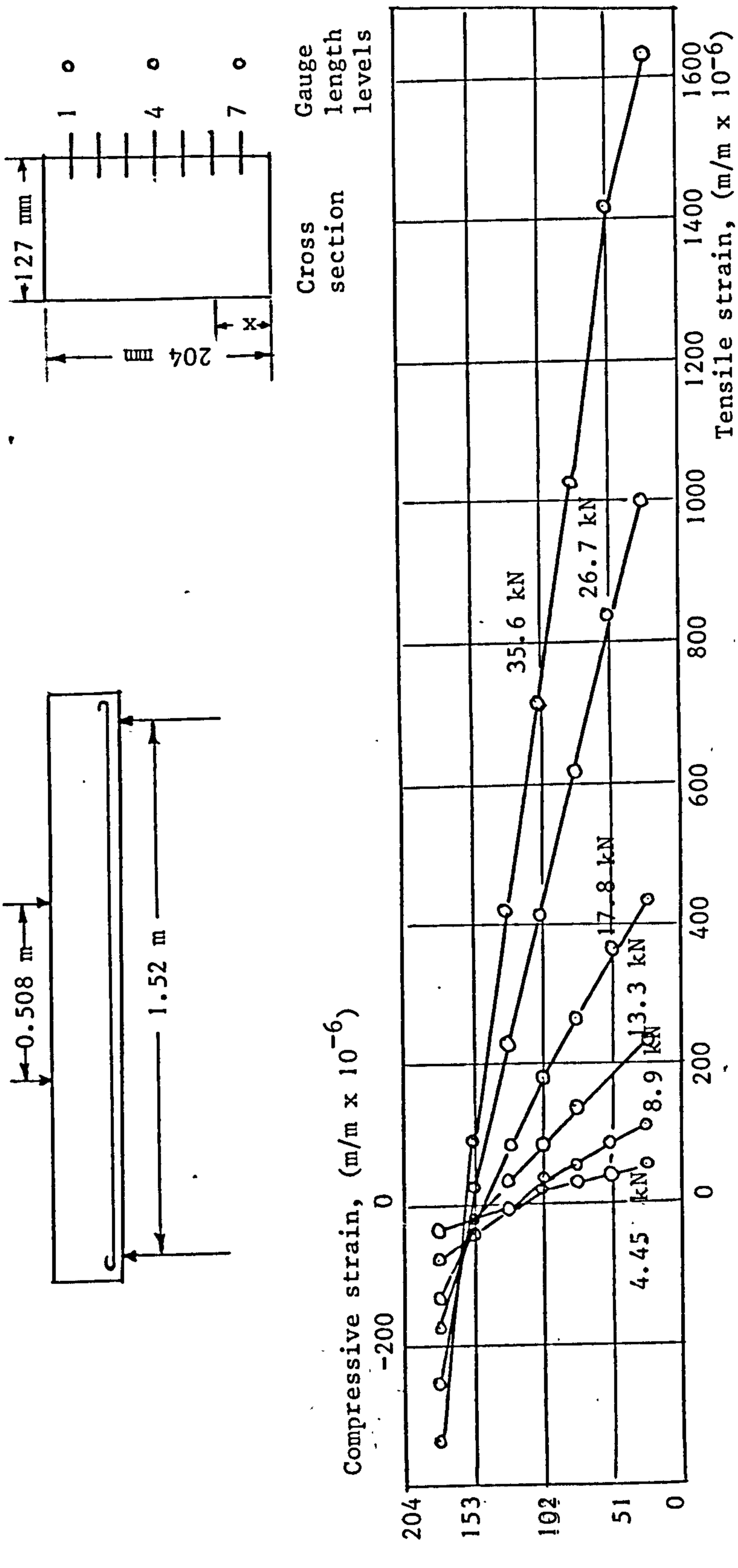

Graph 2.1.1 Measured strain distributions at mid span gauge lengths of reinforced concrete simple beam tested to failure

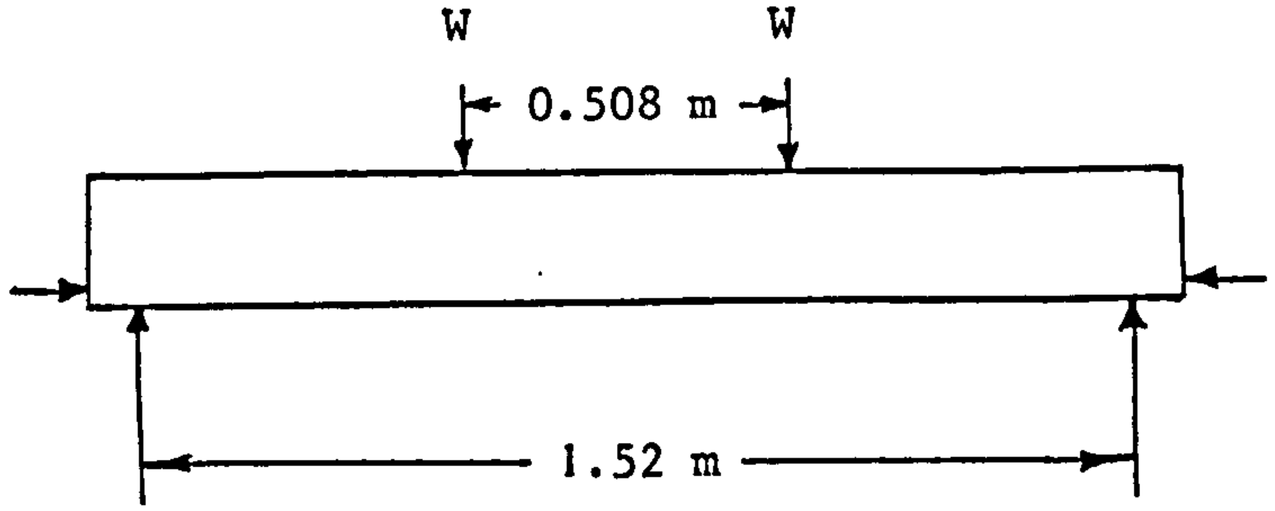

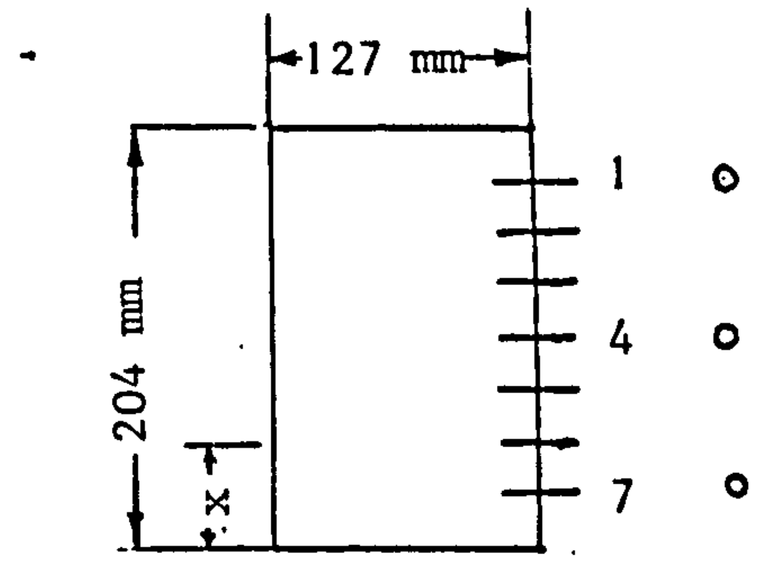

Cross section

Gauge length levels

(See art. 2.1.4.4)

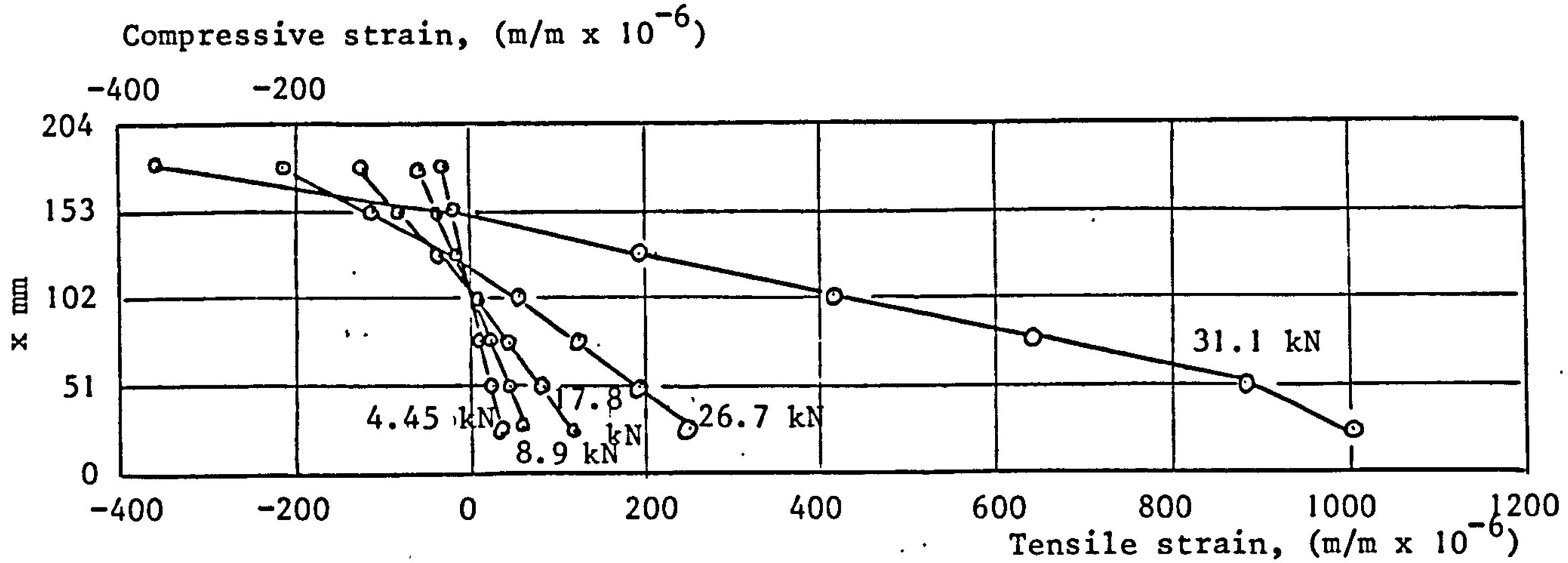

Graph 2.1.2 Measured strain distributions at midspan gauge lengths of prestressed concrete simple beam tested to failure

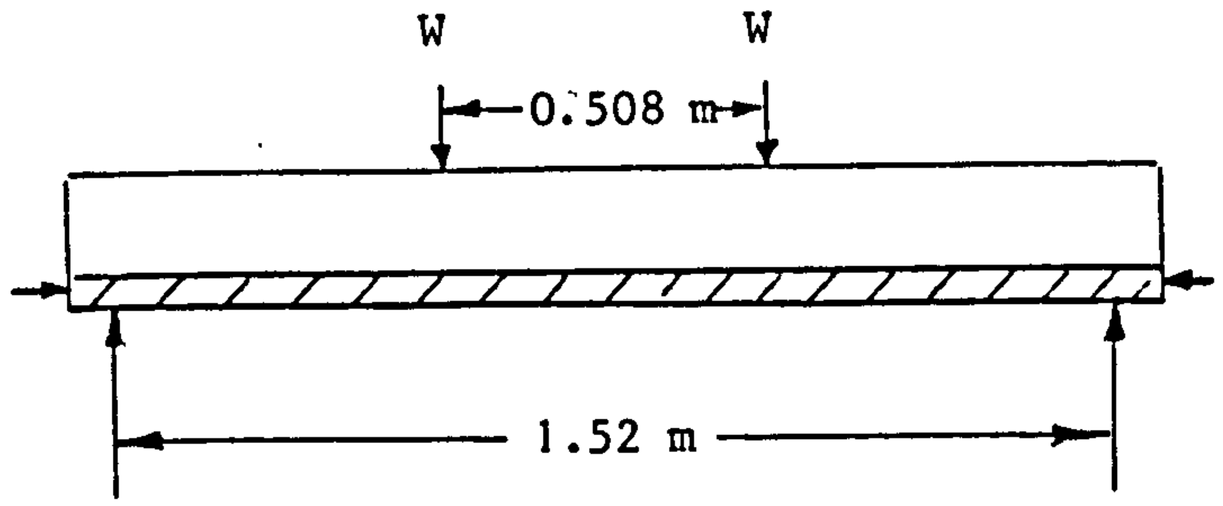

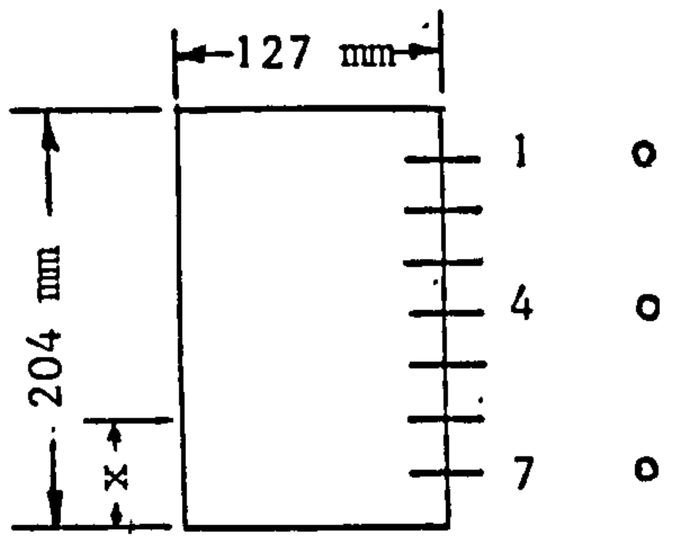

Cross section

Gauge length levels

Graph 2.1.3 Measured strain distributions at mid span gauge lengths of composite prestressed concrete simple beam tested to failure

(See art. 2.1.4.4)

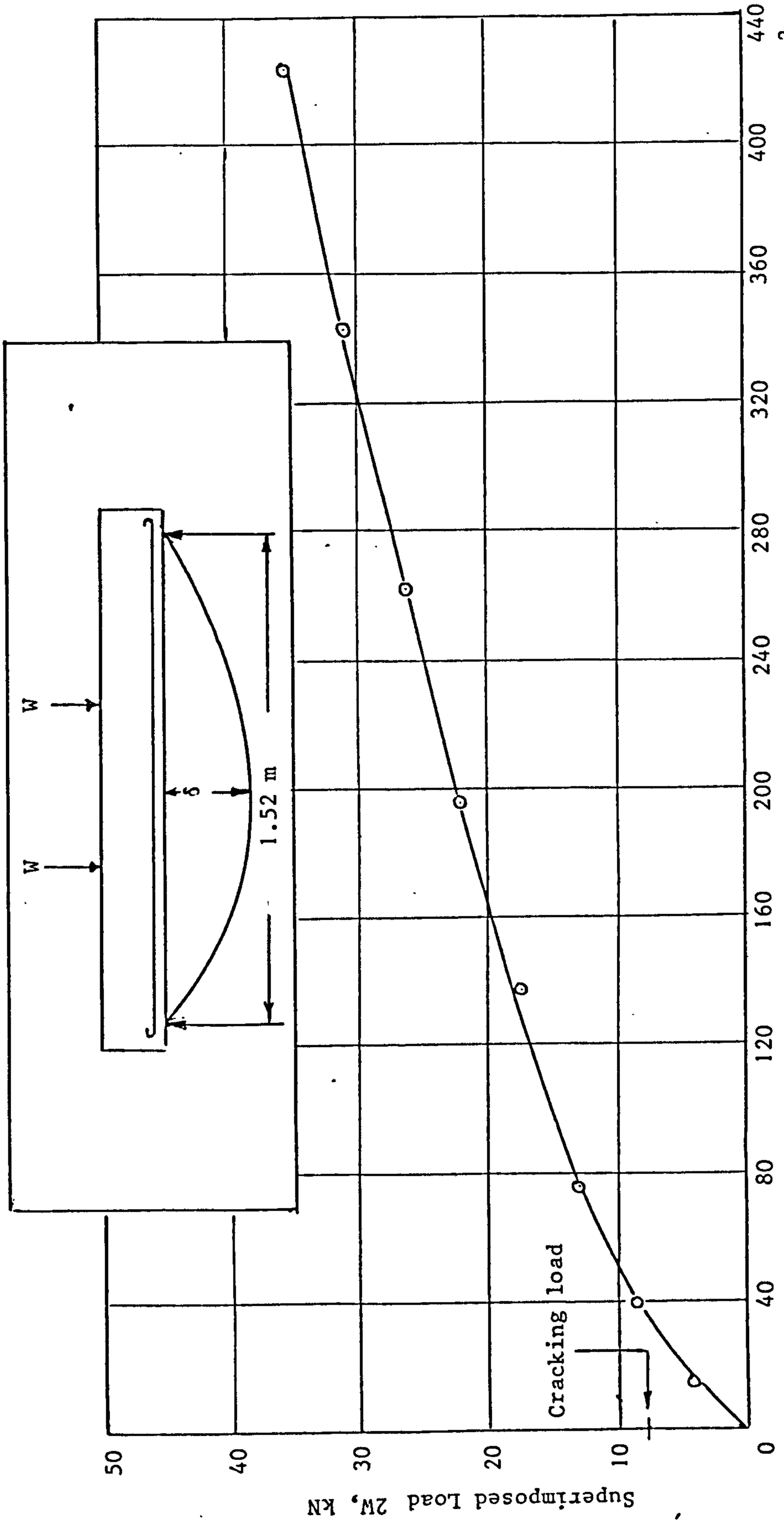

Graph 2.1.4 Load deflection behaviour of reinforced concrete simple beam at midspan

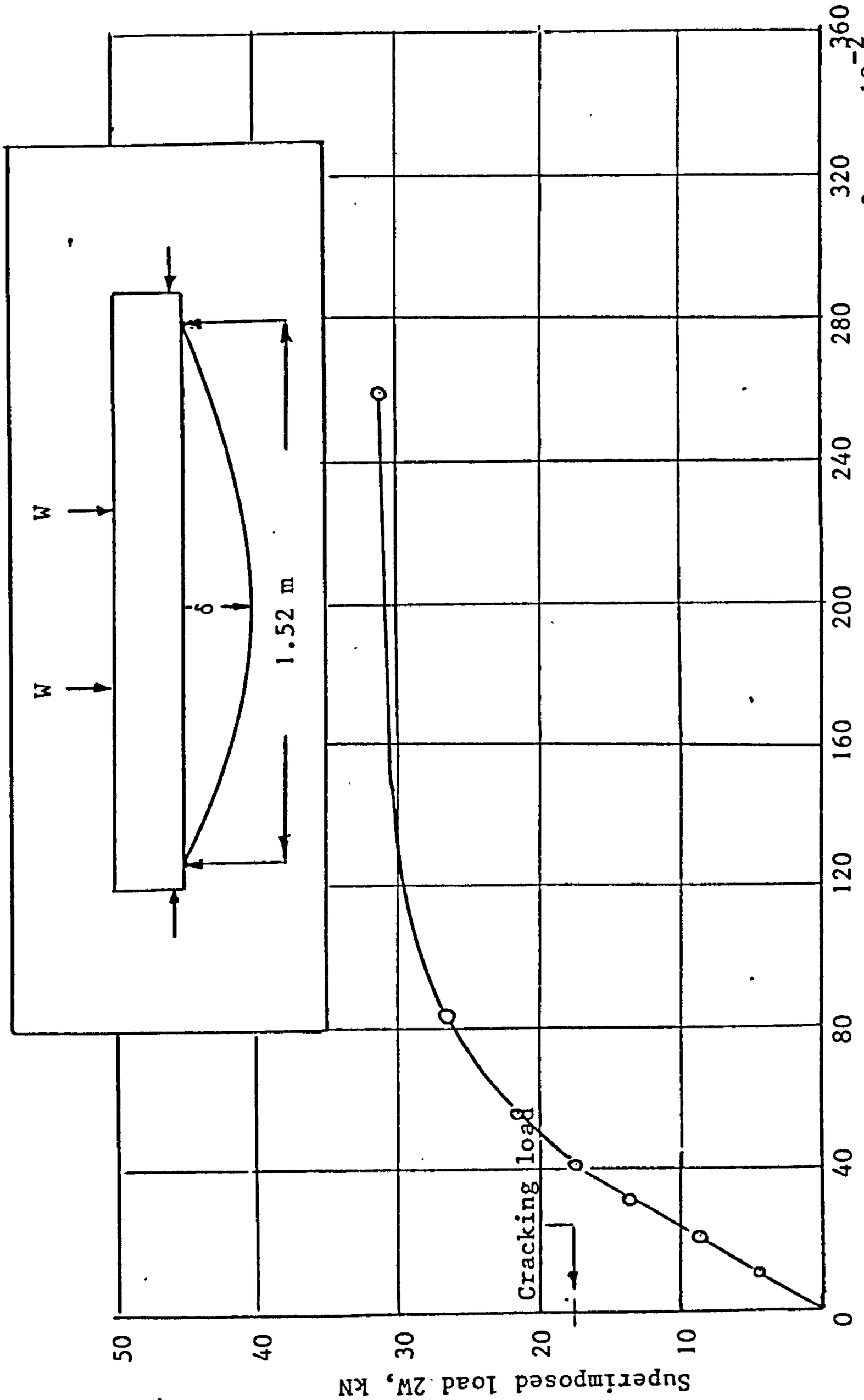

Graph 2.1.5 Load deflection behaviour of prestressed concrete simple beam at midspan

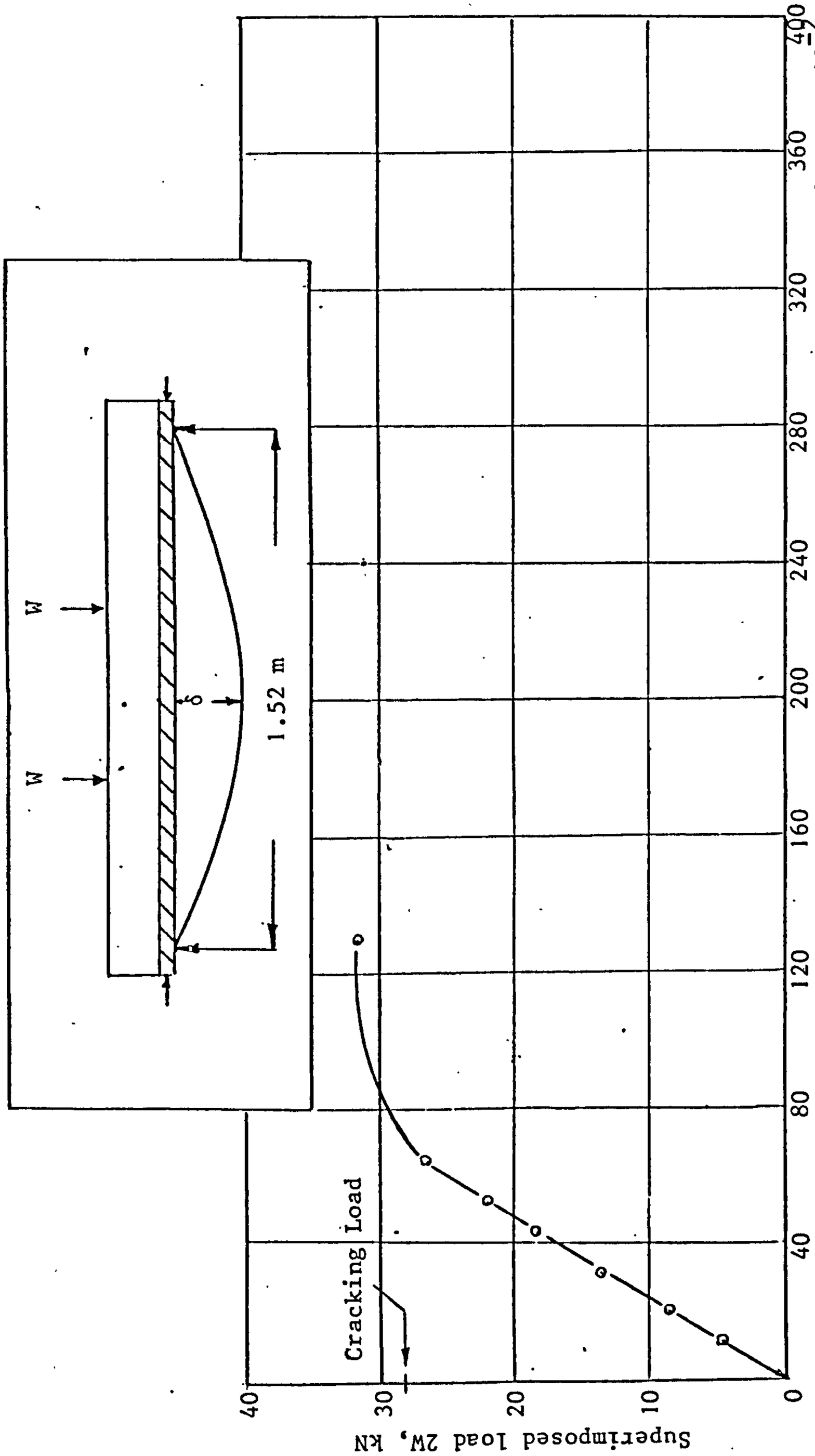

Graph 2.1.6 Load deflection behaviour of composite prestressed concrete simple beam at midspan

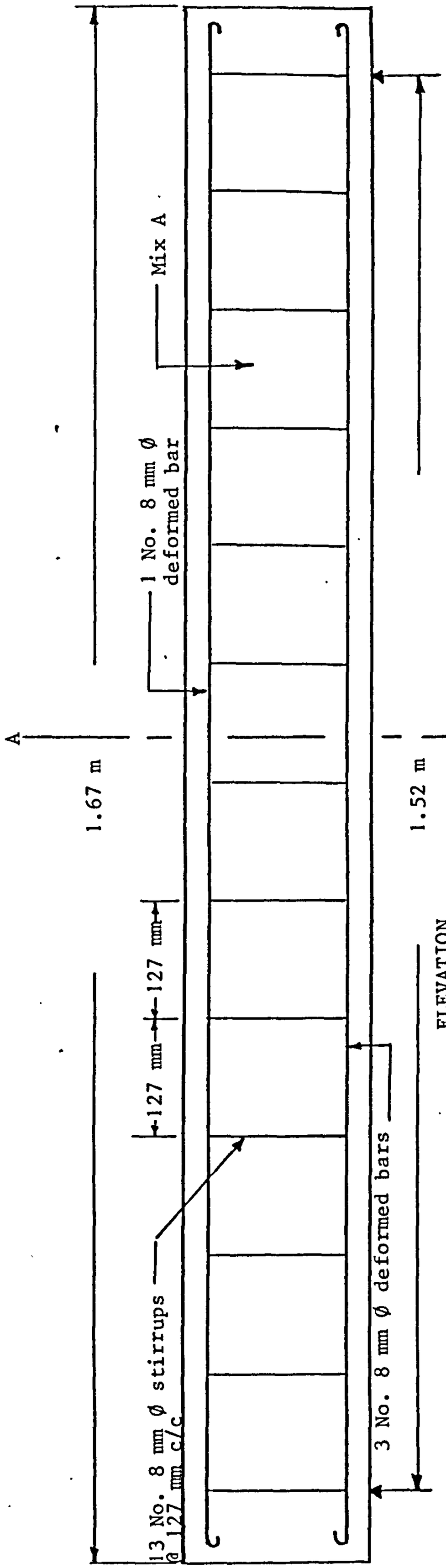

Fig. 2.1.1 Diagram showing reinforcement in reinforced concrete simple beam

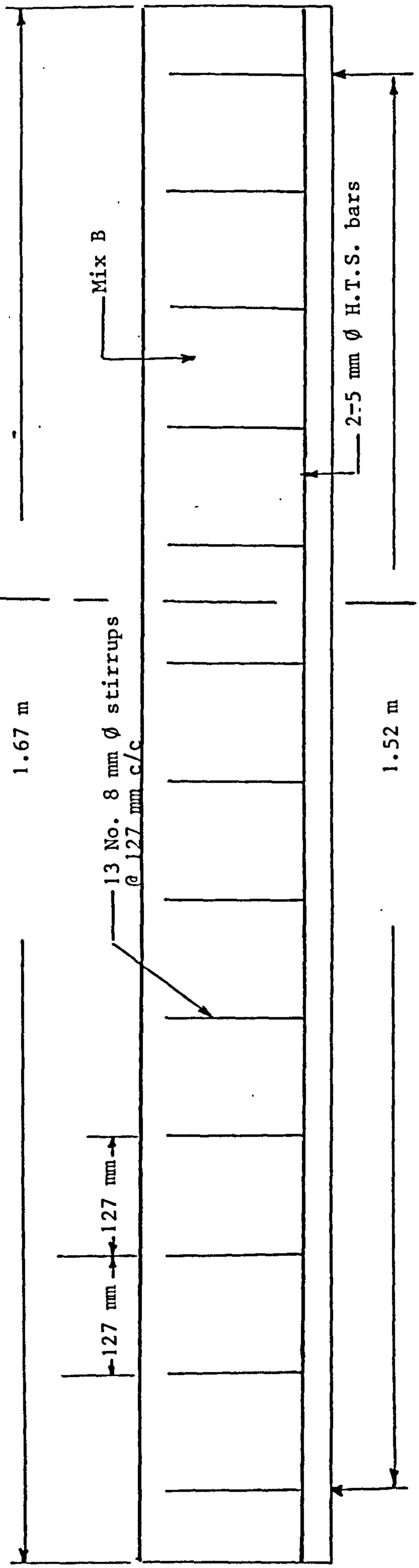

Fig. 2.1.2 Diagram showing reinforcement in prestressed concrete simple beam.

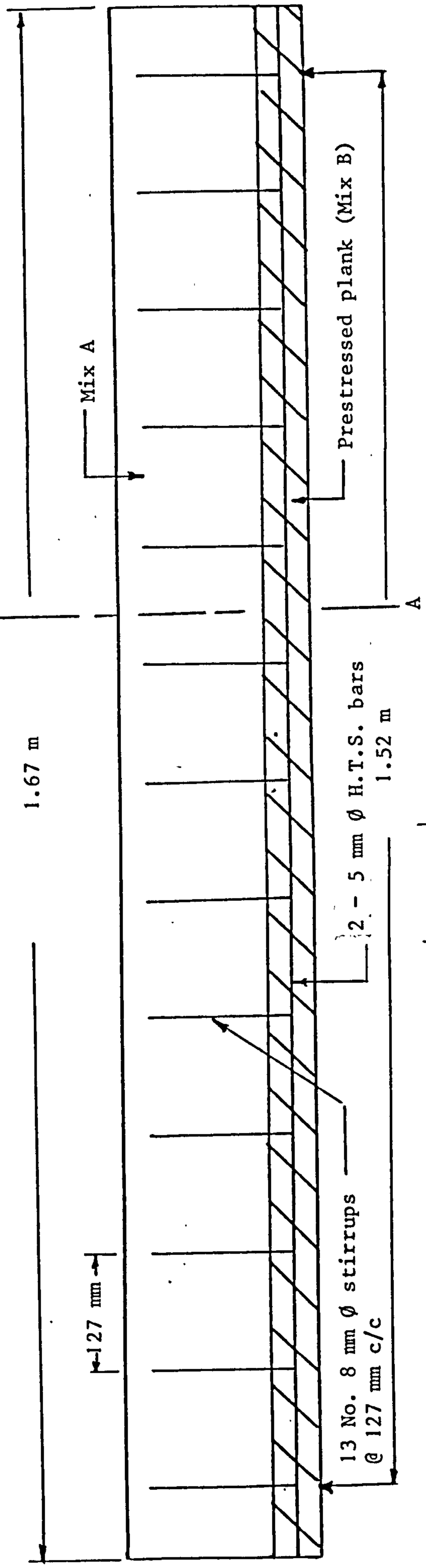

Fig. 2.1.3 Diagram showing reinforcement in composite prestressed concrete simple beam

Photo 2.1.1 Beam Rigid Steel Mould

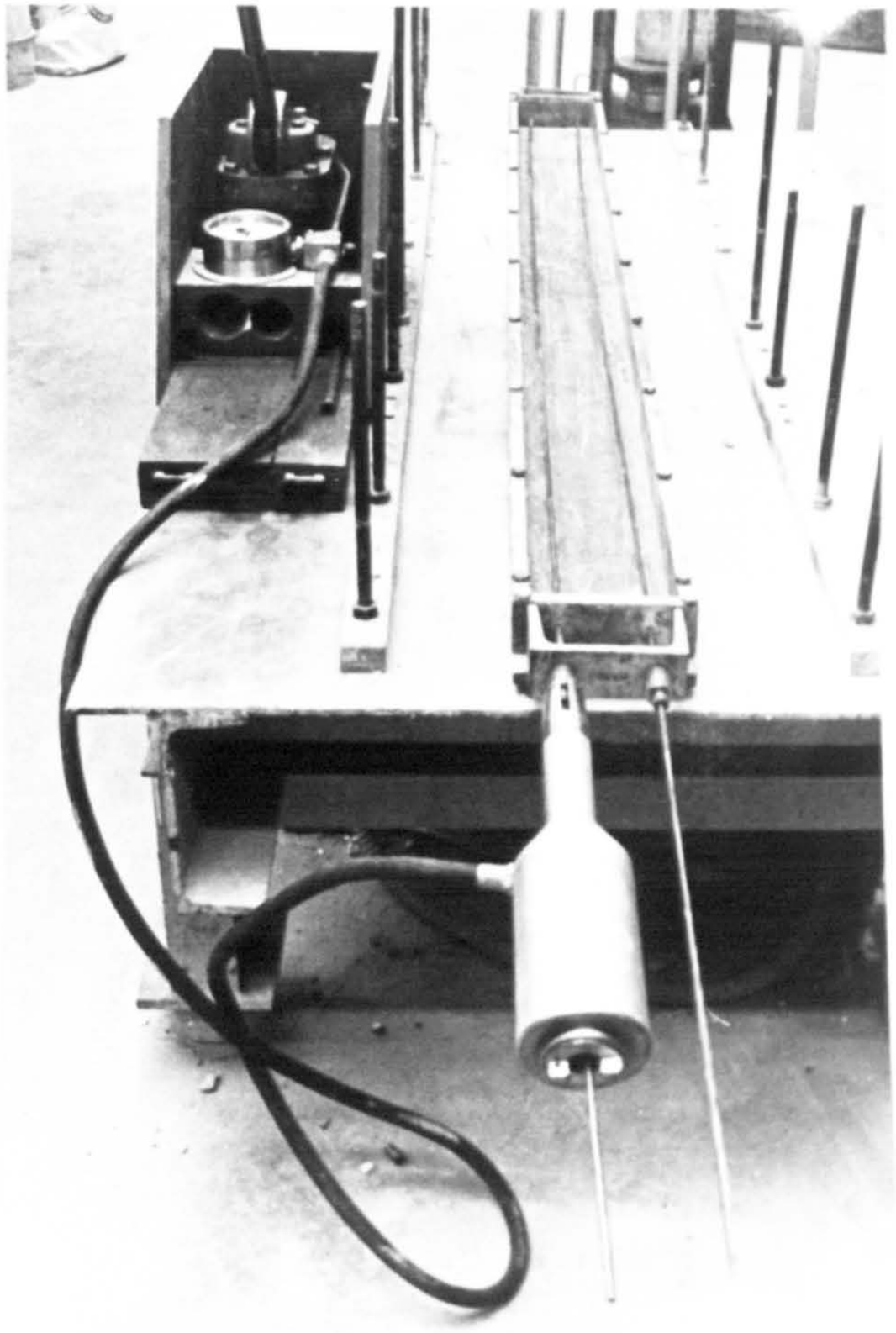

Photo 2.1.2 Plank rigid steel mould and the pump operating the hydraulic jack

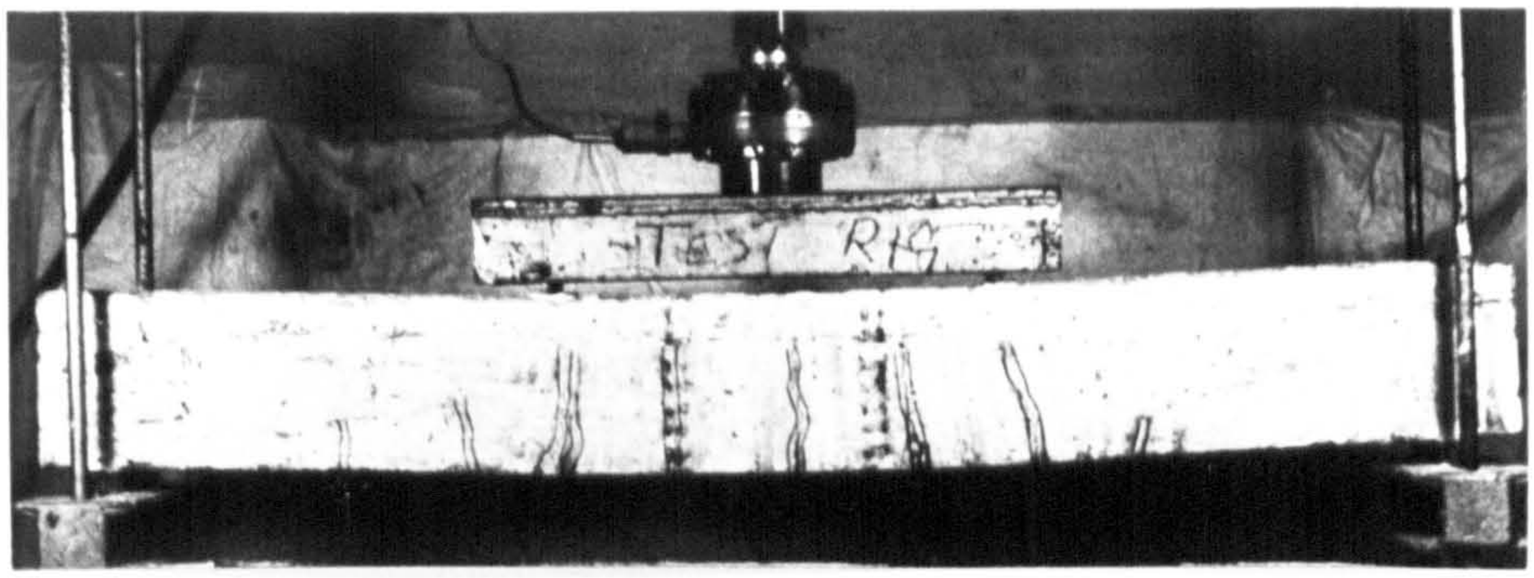

Photo 2.1.3 Reinforced concrete simple beam on testing rig after failure

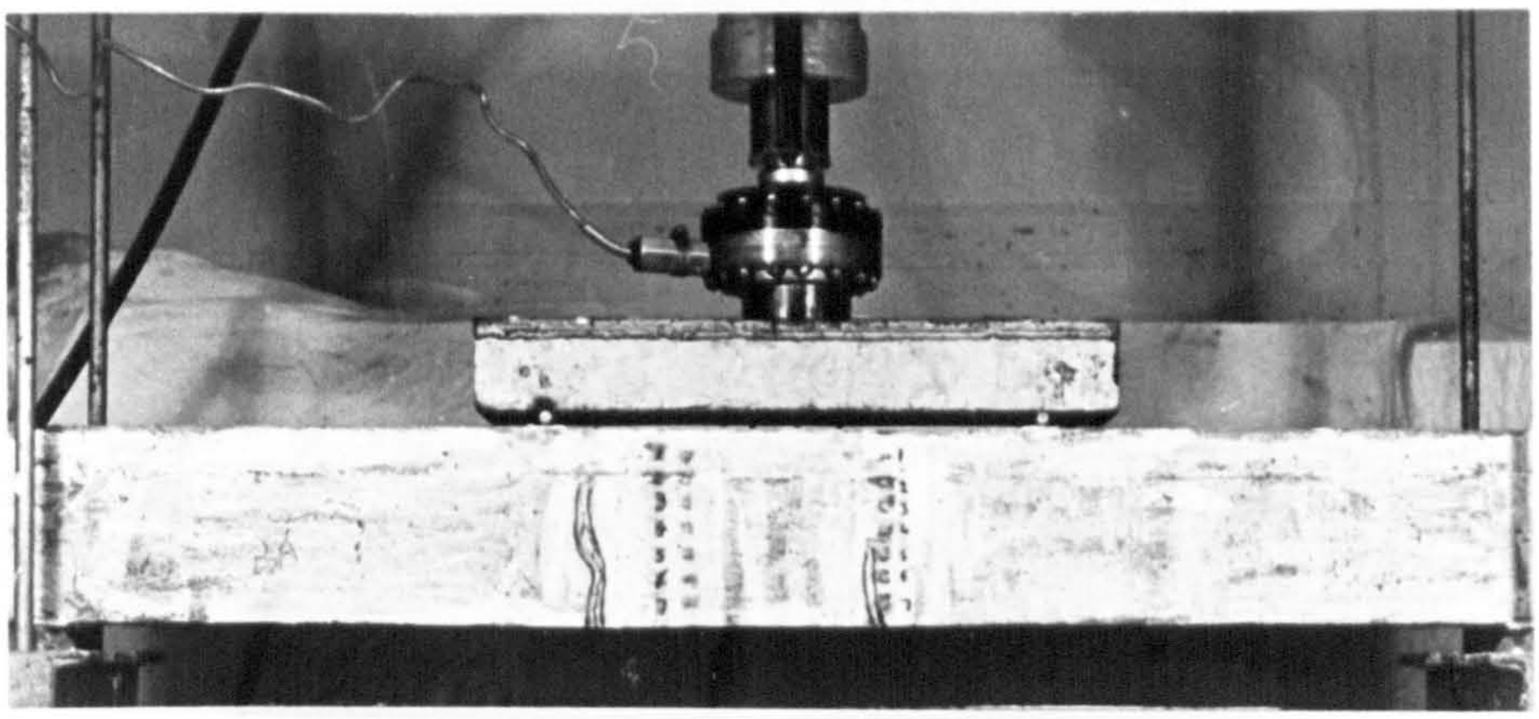

Photo 2.1.4 Prestressed concrete simple beam on testing rig after failure

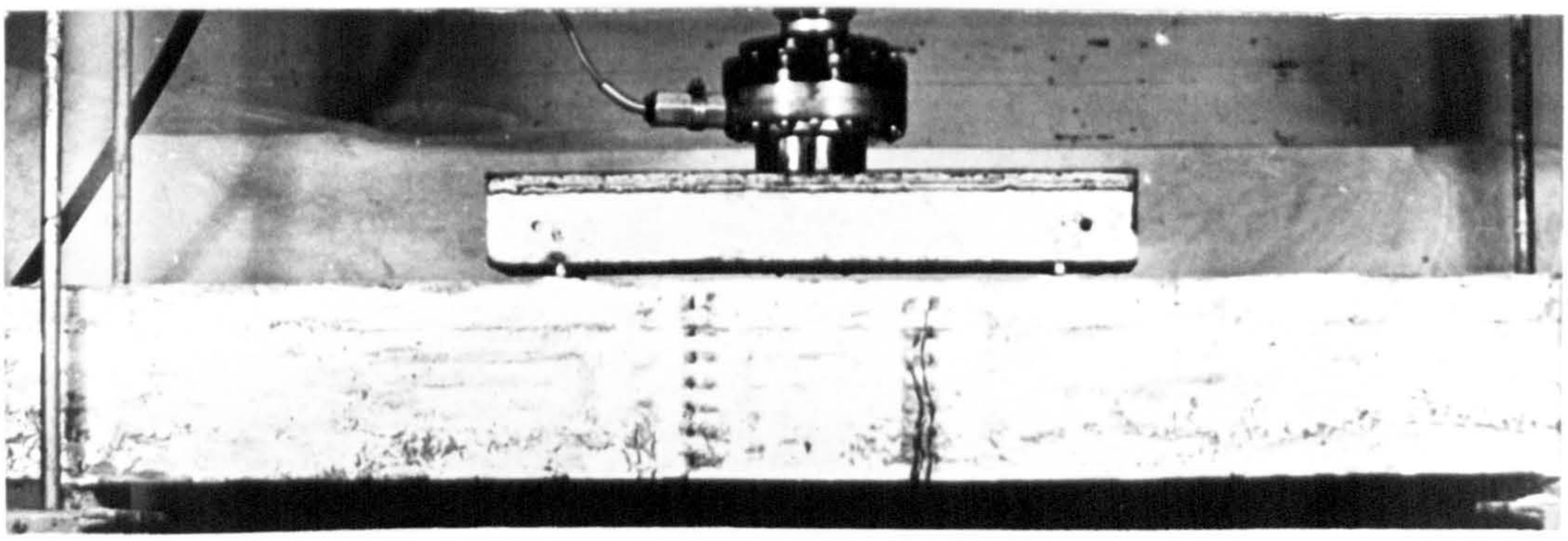

Photo 2.1.5 Composite prestressed concrete simple beam on testing rig after failure

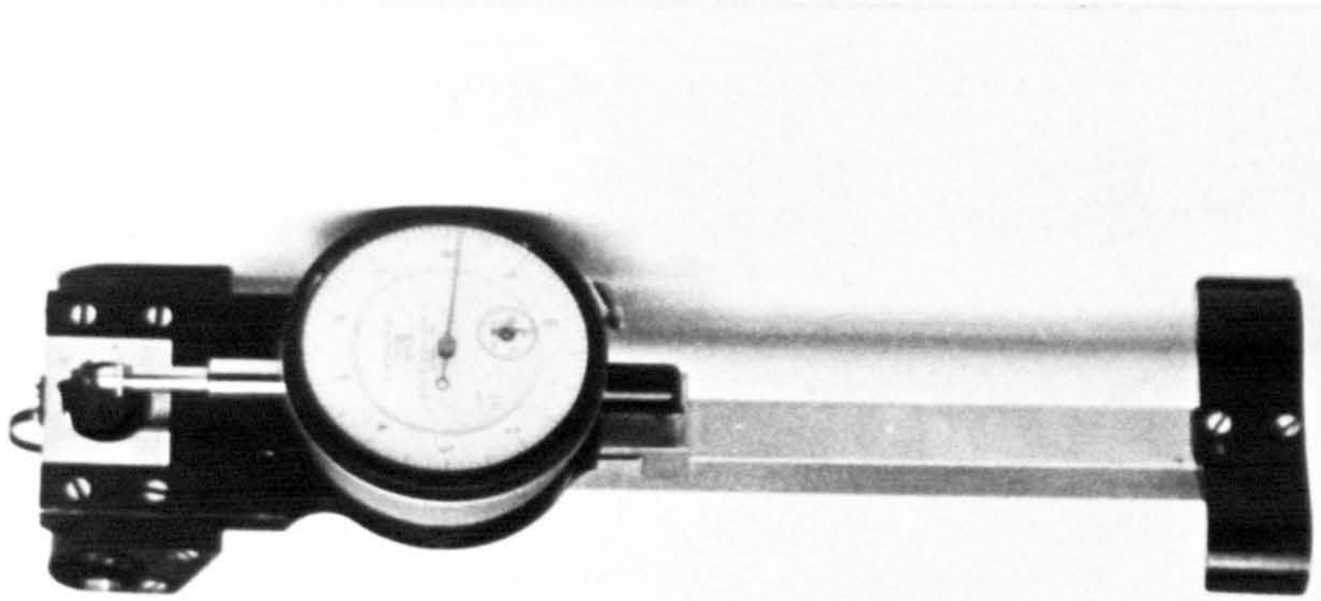

Demec Gauge

Dial Gauge

Photo 2.1.6 Mechanical instruments

Part 2

Experimental work - short-term (elastic) behaviour and ultimate strength of reinforced, prestressed and composite prestressed concrete two span continuous beams

2.2 CONTINUOUS BEAMS

2.2.1 Synopsis

Experimental studies on elastic behaviour and ultimate strength of reinforced, prestressed and composite prestressed concrete two span continuous beams of the same size and virtually the same ultimate capacity are reported. Test results of three beams are presented after long-term tests. Ultimate strength of three shrinkage control beams are also reported for comparison. The three types of concrete beams failed in flexure either by crushing of concrete after excessive elongation of reinforcement or by crushing of concrete while steel was in the elastic range or by bond failure. Ultimate load tests were carried out after long-term tests of up to 9 months of sustained loading for all beam types. The theoretical prediction for the behaviour of the three types of concrete beams from the numerical analysis reported in Chapter 6 which takes into account the effect of concrete tension between cracks developed in reinforced and composite prestressed concrete beams was in good agreement with the experimental results.

In order to show the significant effect that tension-stiffening of concrete between cracks has on deflections, the deflection behaviour of reinforced concrete beam had also been predicted by the above-mentioned numerical analyses but ignoring the effect of concrete tension between cracks for comparison (see curve (b) in Graph 2.2.4).

2.2.2 Introduction

The principle object of the investigation was to provide a direct and quantitative comparison of the elastic and ultimate behaviour of two span continuous concrete beams with three types of straight tension reinforcement similar to the previous simply supported beams of Part 1 and to show the effect of sustained loading and creep on the ultimate strength.

Tests were conducted to determine the longitudinal strain distributions, vertical deflections, cracking loads and ultimate loads. Experimental results were in good agreement with the theoretical predicted values.

Six two span continuous concrete beams 127 x 204 mm in cross section and 3.20 metres overall length were tested with equal loads at the third points of each span of length 1.52 metres (see figures in graphs 2.2.1, 2.2.2, and 2.2.3.)

2.2.3 Experimental Beams

2.2.3.1 Dimensions and reinforcement

The reinforcement of the three types of continuous concrete beams at two cross sections of each beam are presented in Table 2.2.1. The reinforcement and position of the stirrups are shown in figures 2.2.1, 2.2.2 and 2.2.3.

The dimensions of the beams were 127 x 204 mm in cross section and 3.20 metres overall length and they were designed according to the theory of ultimate design to have all approximately the same ultimate capacity. The prestressing wires used in prestressed and composite prestressed concrete beams were 5 mm diameter and each wire was initially tensioned to 22240 N. The properties of reinforcing steel used were the same as those used in simple beams of Part 1 (see Table 2.1.2).

2.2.3.2 Mix

The mix proportions A and B used in the three types of continuous concrete beams were essentially similar to the mix proportions used in simple concrete beams of Part 1 (see table 2.1.3).

Beam Type	Beam Sections	Top Reinforcement	Bottom Reinforcement	Stirrups
R.C.	I-I	1 No. 8 mm Ø deformed bar	3 No. 8 mm Ø deformed bars	1 No. 8 mm Ø deformed bar @ 127 mm
	II-II	3 No. 8 mm Ø deformed bars	3 No. 8 mm Ø deformed bars	
P.C.	I-I	2 No. 5 mm Ø H.T.S. bars	2 No. 5 mm Ø H.T.S bars	1 No. 8 mm Ø deformed bar @ 127 mm
	II-II	2 No. 5 mm Ø H.T.S. bars	2 No. 5 mm Ø H.T.S. bars	
C.P.C.	I-I	1 No. 8 mm Ø deformed bar	Prestressed pretensioned concrete plank reinforced with 2 No. 5 mm Ø H.T.S. bars	1 No. 8 mm Ø deformed bar @ 127 mm
	II-II	3 No. 8 mm Ø deformed bars	-	

TABLE 2.2.1Reinforcement in reinforced,prestressed and composite prestressed two span continuous beams

2.2.3.3 Mould

The rigid steel mould used is shown in photo 2.1.1.

2.2.3.4 Casting Procedure

Casting procedure was similar to the one used in simple concrete beams of Part 1 art.2.1.3.4.

2.2.3.5 Curing prior to testing

Curing procedure was similar to the one used in simple concrete beams of Part 1 art.2.1.3.5.

2.2.4 Testing Apparatus

Photos 2.2.1, 2.2.2 and 2.2.3 show reinforced, prestressed and composite concrete two span continuous beams on the testing rig after failure.

2.2.4.1 Centre and end supports

The centre and end supports were so made the same as the end supports of simple concrete beams of Part 1. The two end supports spaced at 3.04 metres apart. (See Photo 2.2.1)

2.2.4.2 Loading Apparatus

The loading apparatus is the same as the one used in loading the simple beams in Part 1 (see art. 2.1.4.2).

2.2.4.3 Strain gauges for deflections

Five dial gauges, each reading to 0.01 mm per dial division, were used for each beam. One was placed at the middle of each end support, one was placed at the top side of the centre support, and one was placed at the third point from the end support of each span

for measuring deflections. Graphs 2.2.1, 2.2.2 and 2.2.3 show the load deflection behaviour at Sec. I-I for the three types of beams.

2.2.4.4 Strain measurements

Strain measurements, using 8" (203 mm) Demec gauge were made at the third point of each span and at the centre support at the following locations.

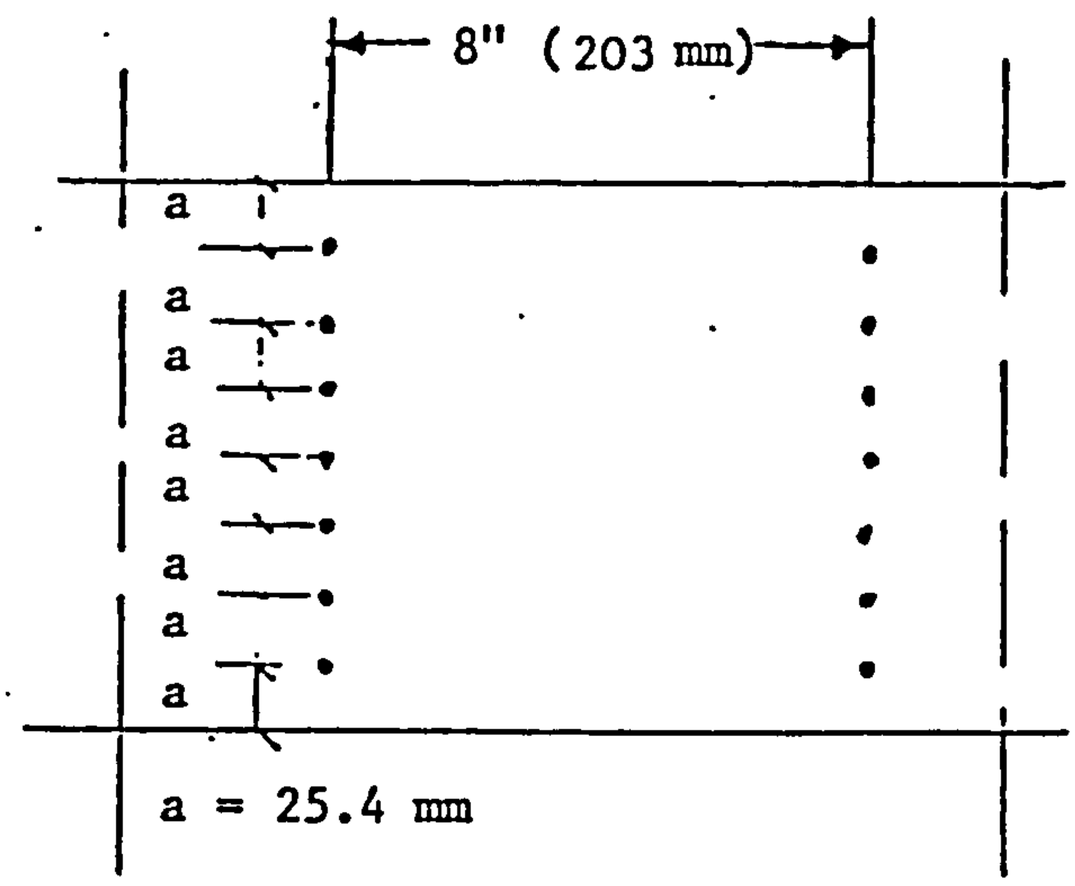

2.2.5 Testing Procedure

The load is applied in increments of 2000 lbs (8896 N) using the same procedure used in testing simple beams in Part 1 art. 2.1.5.

2.2.6 Results and Discussions

2.2.6.1 Cracking and ultimate loads

Table 2.2.2 compares the measured and computed values of the cracking and ultimate loads of the three types of two span continuous concrete beams tested to failure after 9 months of sustained loading. Ultimate strength at 9 months of shrinkage control beams is also reported.

Beam Type	Shrinkage Control beams	Beams tested after 9 months of sustained loading			
	Ultimate Load kN	Cracking Load kN		Ultimate Load kN	
	Measured	Measured	Computed	Measured	Computed
R.C.	122	20	18.2	128	105.35
P.C.	86	38	39.7	80	110.92
C.P.C.	110	-	18.2	105	105.35

Table2.2.2 Cracking and ultimate loads measured versus computed values - continuous beams

2.2.6.2 Strain gauge readings at span Section I-I

Curves for strain gauge readings at Sec. I-I gauge lengths corresponding to the tested beams are plotted in graphs 2.2.1, 2.2.2 and 2.2.3. Upon further increase in bending moment, the strain increases and the neutral axis moves further towards the compression side as failure is approached.

2.2.6.3 Deflections at Span Section I-I

Deflection curves at Sec. I-I corresponding to the beams tested to failure are plotted in figures 2.2.4, 2.2.5 and 2.2.6. It is obvious that the curves deviated from a straight line soon after cracking. Deflections were measured up to nearly the ultimate load as the dials were removed soon after cracking so that they would not be damaged at failure.

Theoretical deflection curves (a) and (b) in Graph 2.2.4 show the significant effect of tension stiffening of concrete between cracks had on deflection of reinforced concrete beam.

2.2.7 Conclusions

1. The behaviour of all the beams followed the elastic theory predictions very closely until cracking.

2. Observed and calculated ultimate loads listed in Table 2.2.2 for the three types of continuous concrete beams show that measured and calculated ultimate loads for reinforced and composite prestressed beams were in close agreement with values calculated by using Whitney's method[30] except the prestressed beam which had bond failure.

3. The assumptions of the analytical numerical approach reported in Chapter 6 permitted prediction of measured deflections with satisfactory accuracy for the three types of continuous concrete beams.

4. Calculated deflection behaviour of reinforced concrete continuous beam is over-estimated by ignoring the effect of concrete tension between cracks in the above mentioned numerical approach (see curves (a) and (b) in Graph 2.2.4).

5. Sustained loading and creep during the main experiments had not influenced the ultimate strength of the beams.

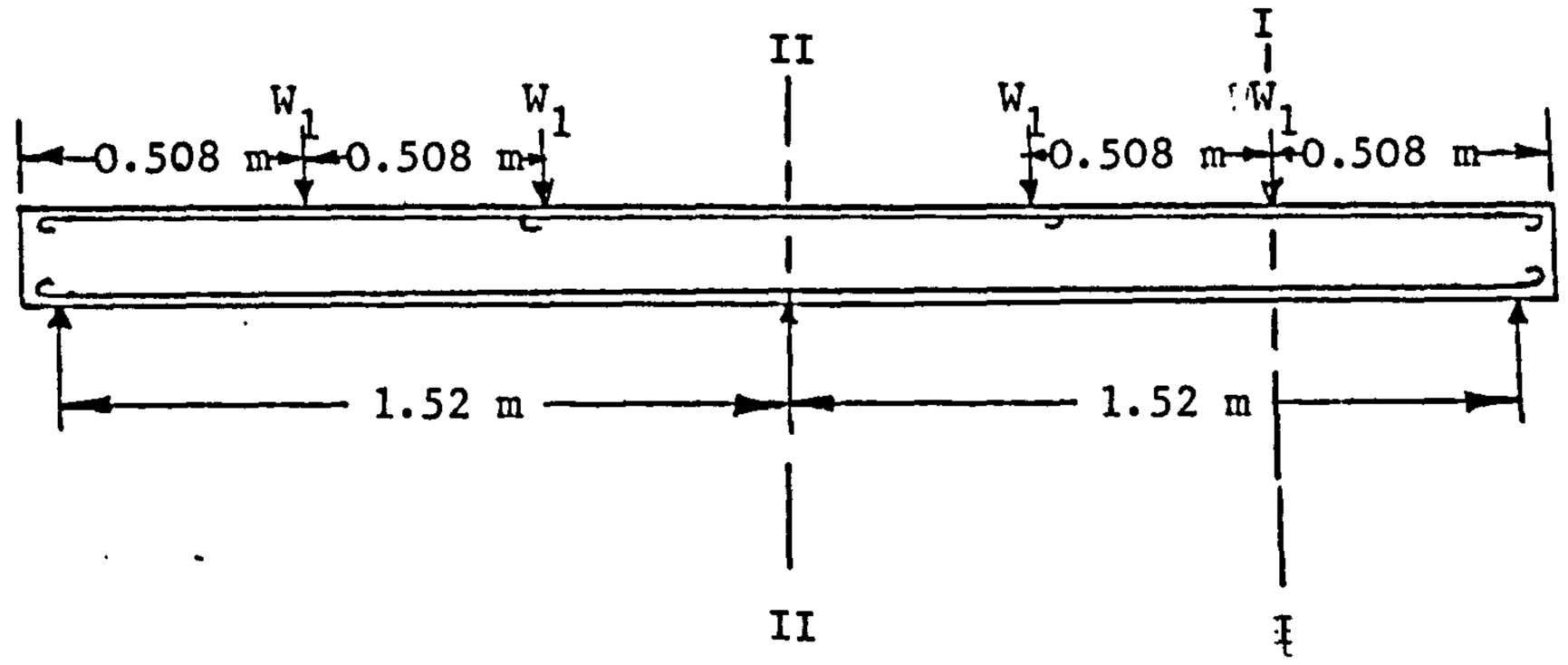

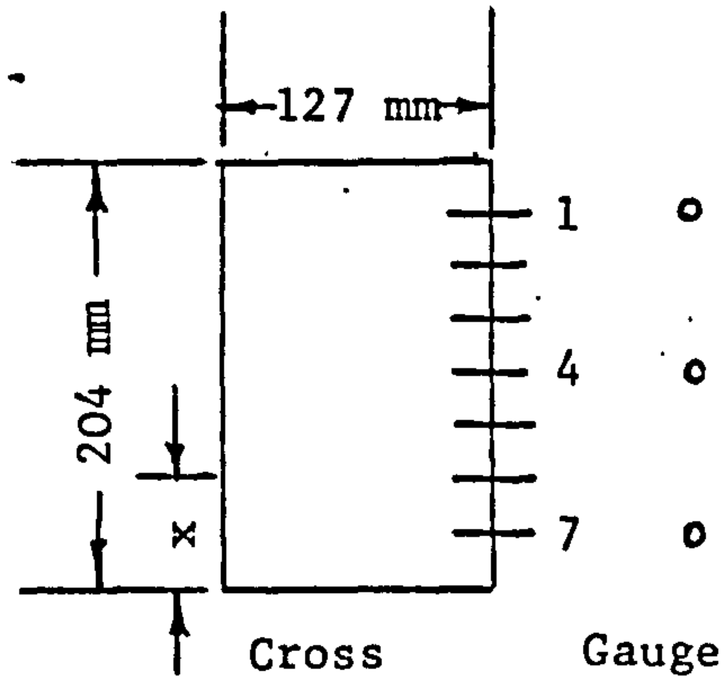

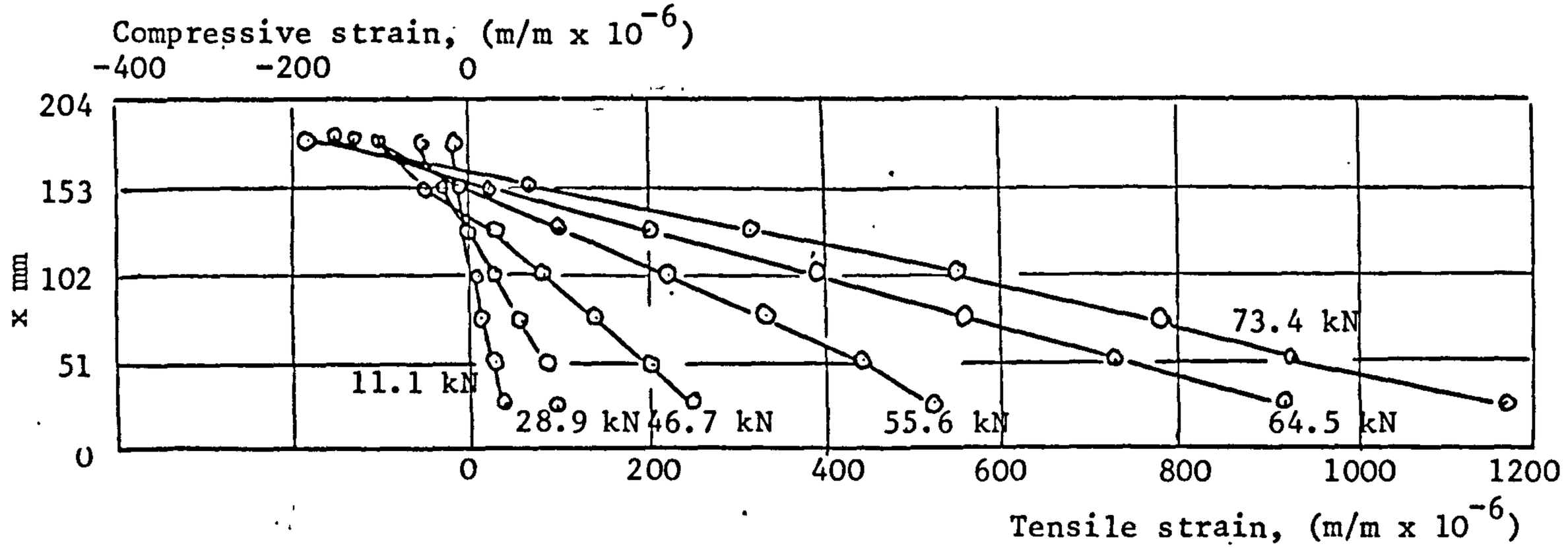

Graph 2.2.1 Measured strain distributions at Sec. I-I gauge lengths of reinforced concrete continuous beam tested to failure

(See art. 2.2.4.4)

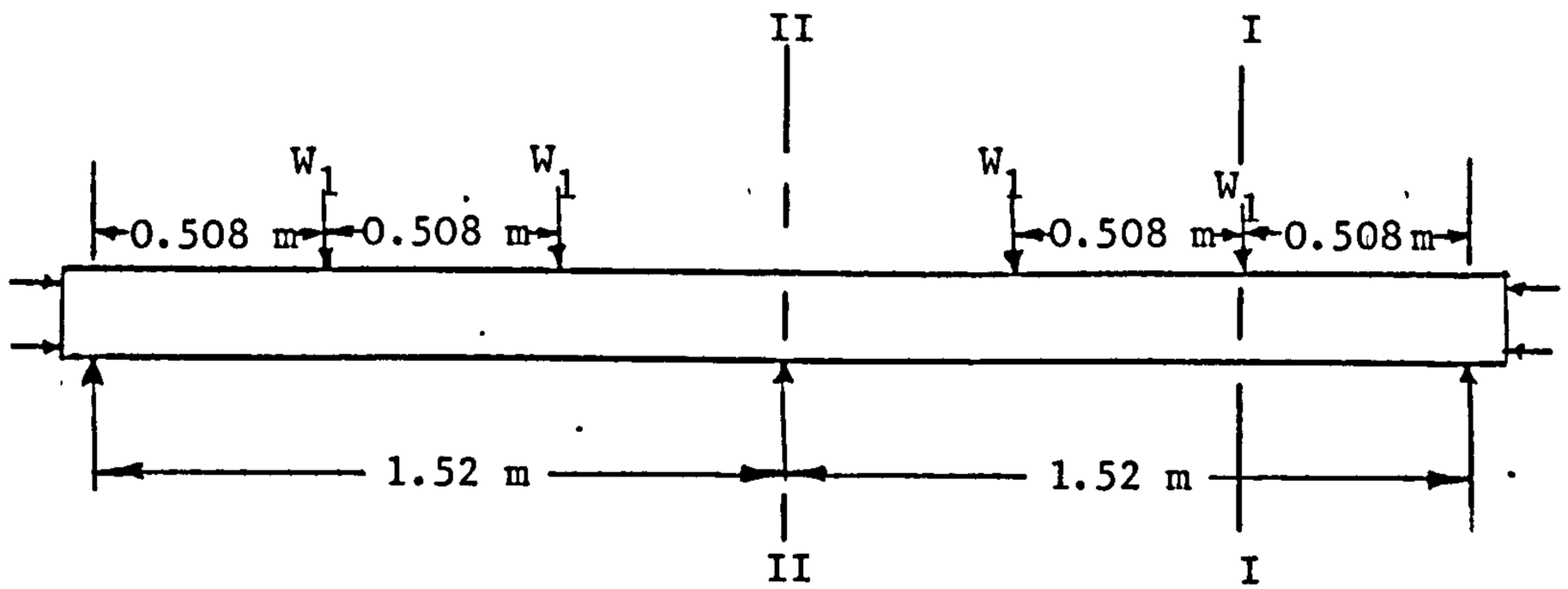

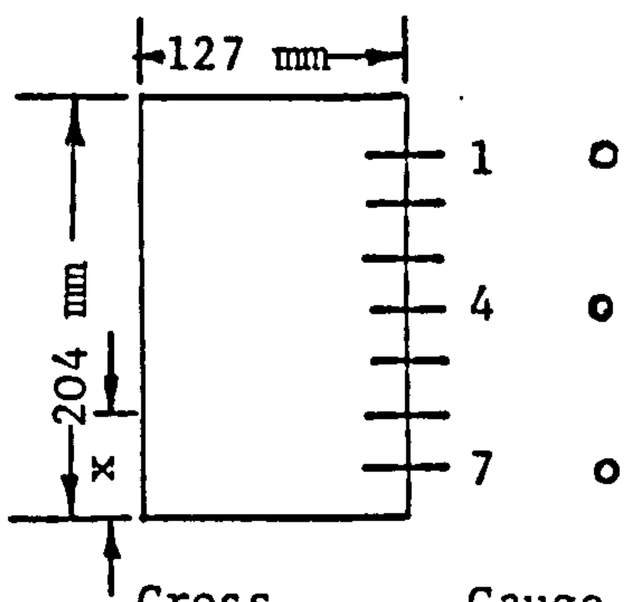

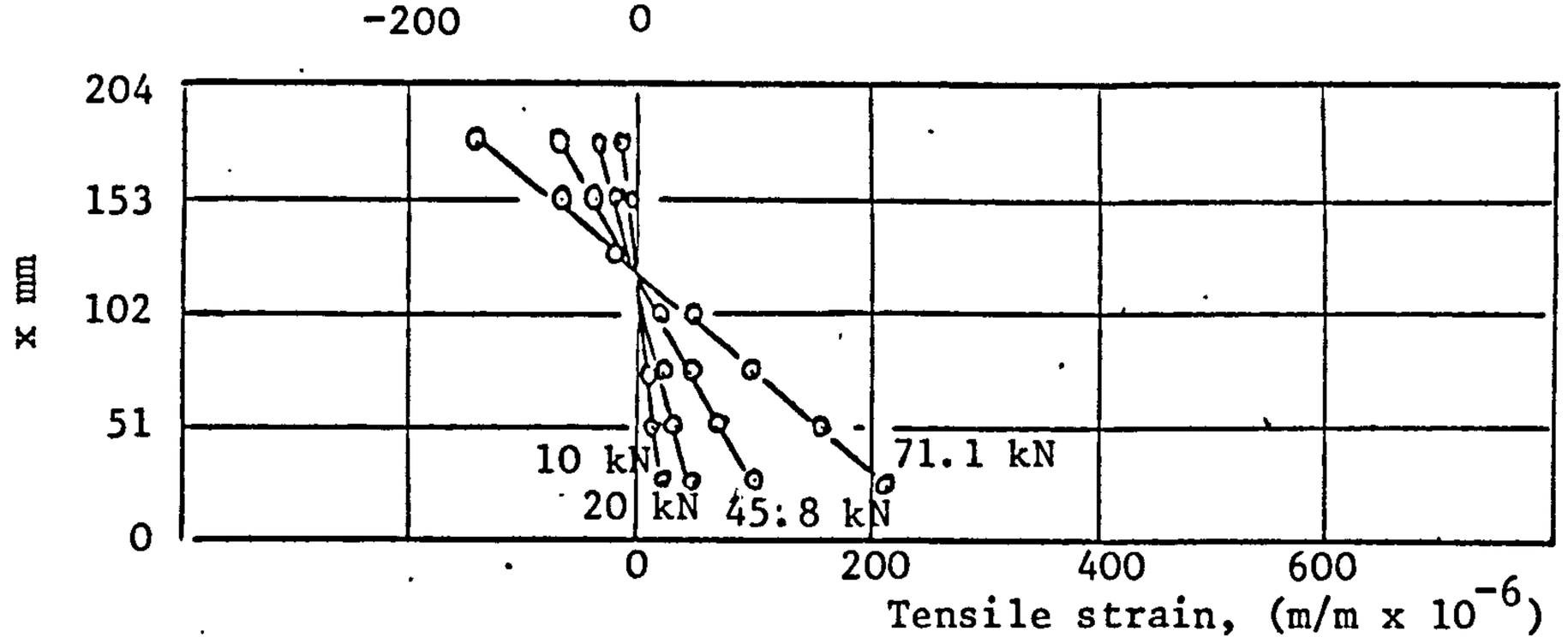

Graph 2.2.2 Measured strain distribution at Sec. I-I gauge lengths of prestressed concrete continuous beam tested to failure

(See art. 2.2.4.4)

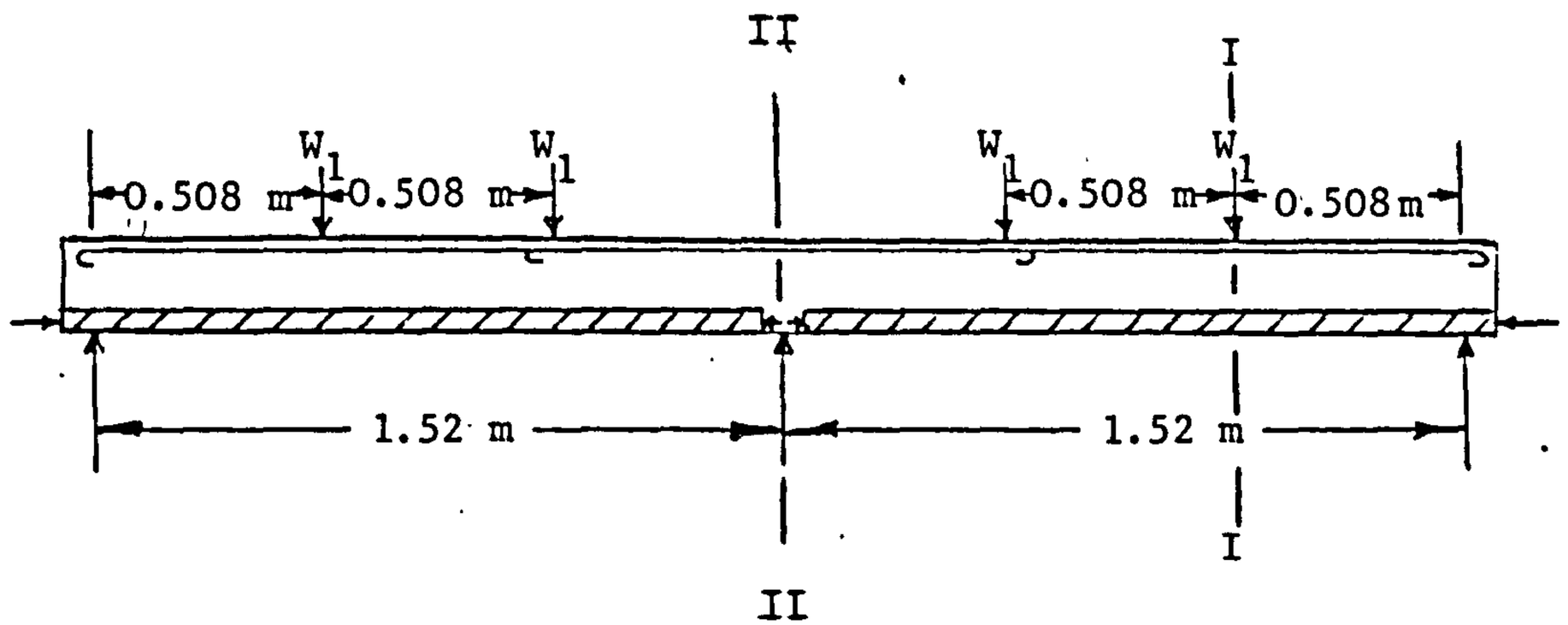

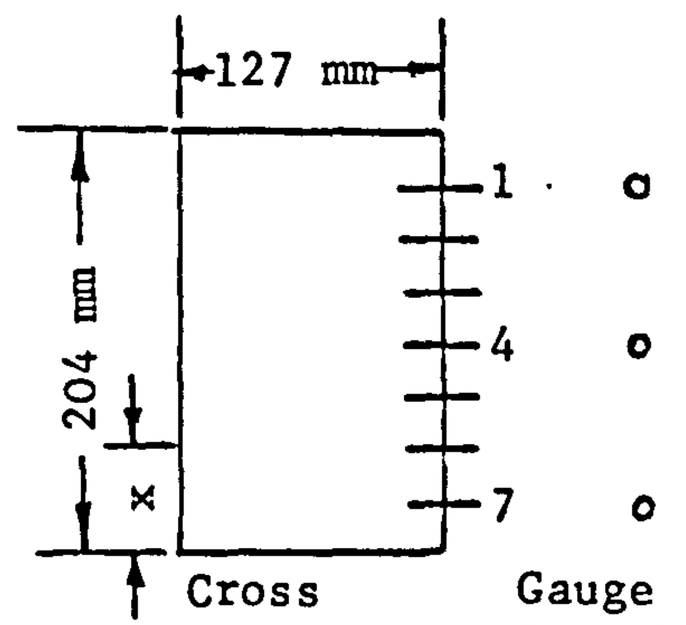

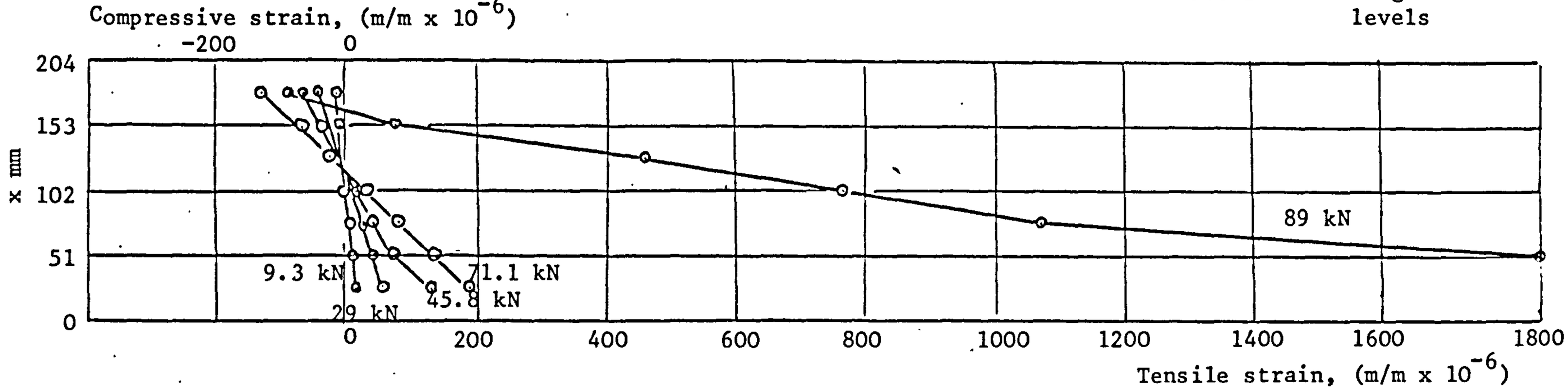

Graph 2.2.3 Measured strain distribution at Sec. I-I gauge lengths of composite prestressed concrete continuous beam tested to failure

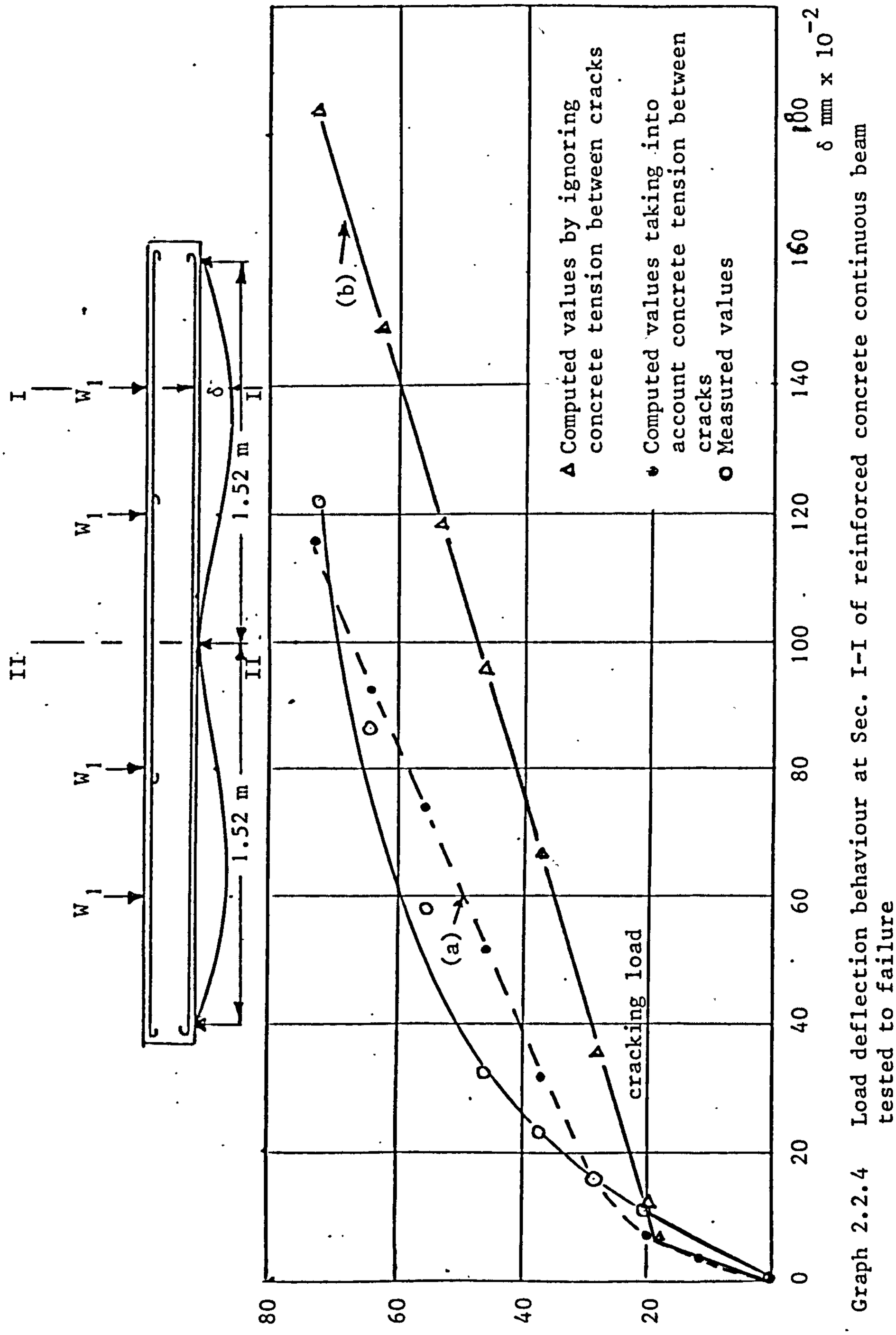

Graph 2.2.4 Load deflection behaviour at Sec. I-I of reinforced concrete continuous beam tested to failure

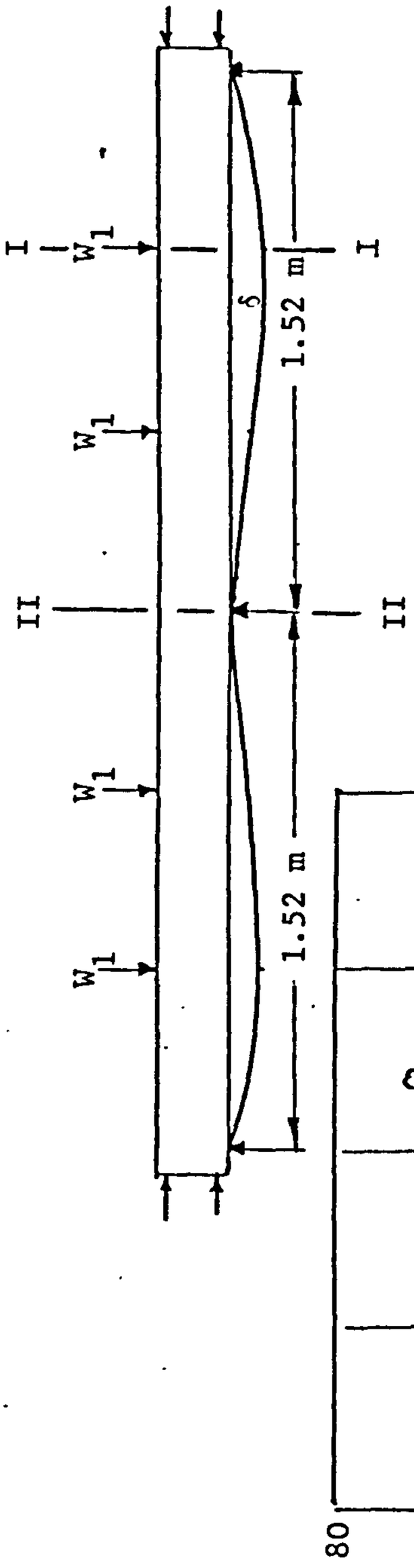

Graph 2.2.5 Load deflection behaviour at Sec. I-I of prestressed concrete continuous beam tested to failure

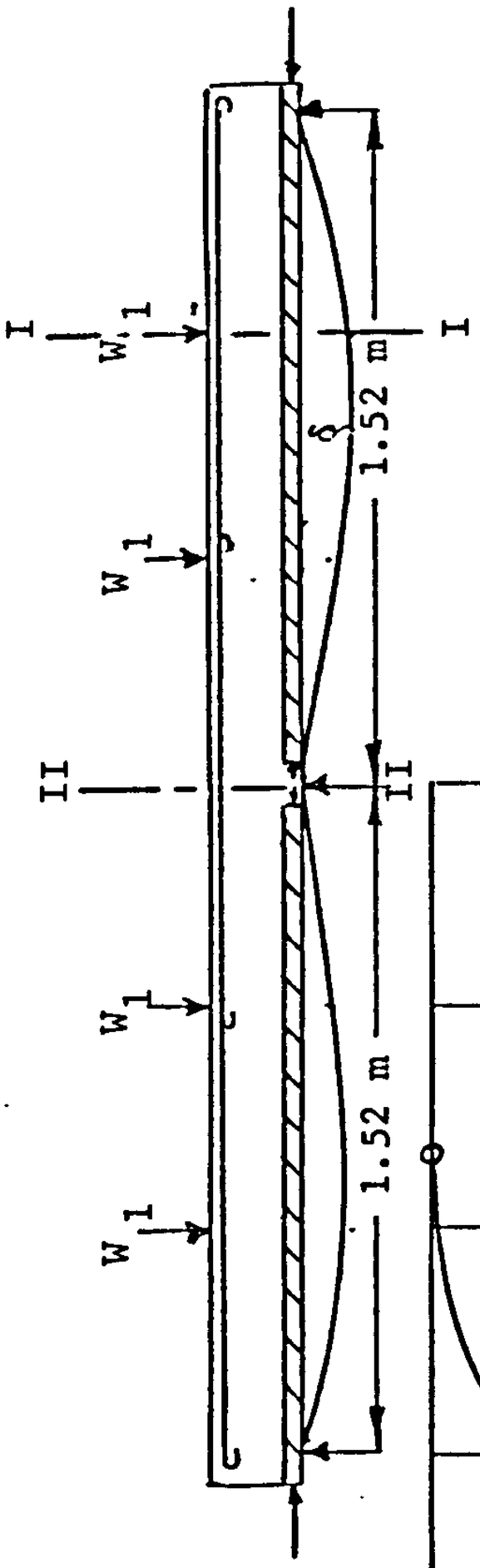

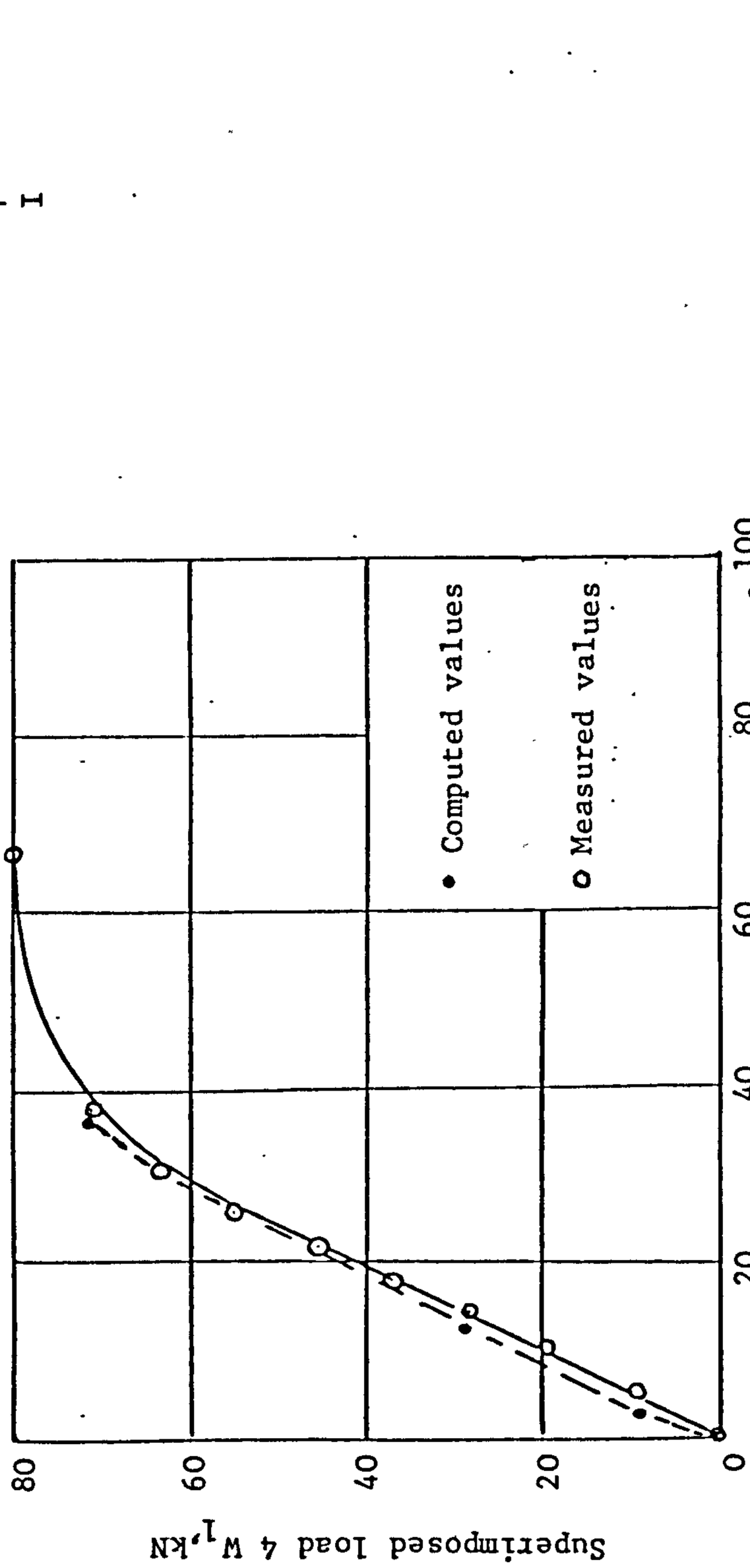

Graph 2.2.6 Load deflection behaviour at Sec. I-I of composite prestressed concrete continuous beam tested to failure

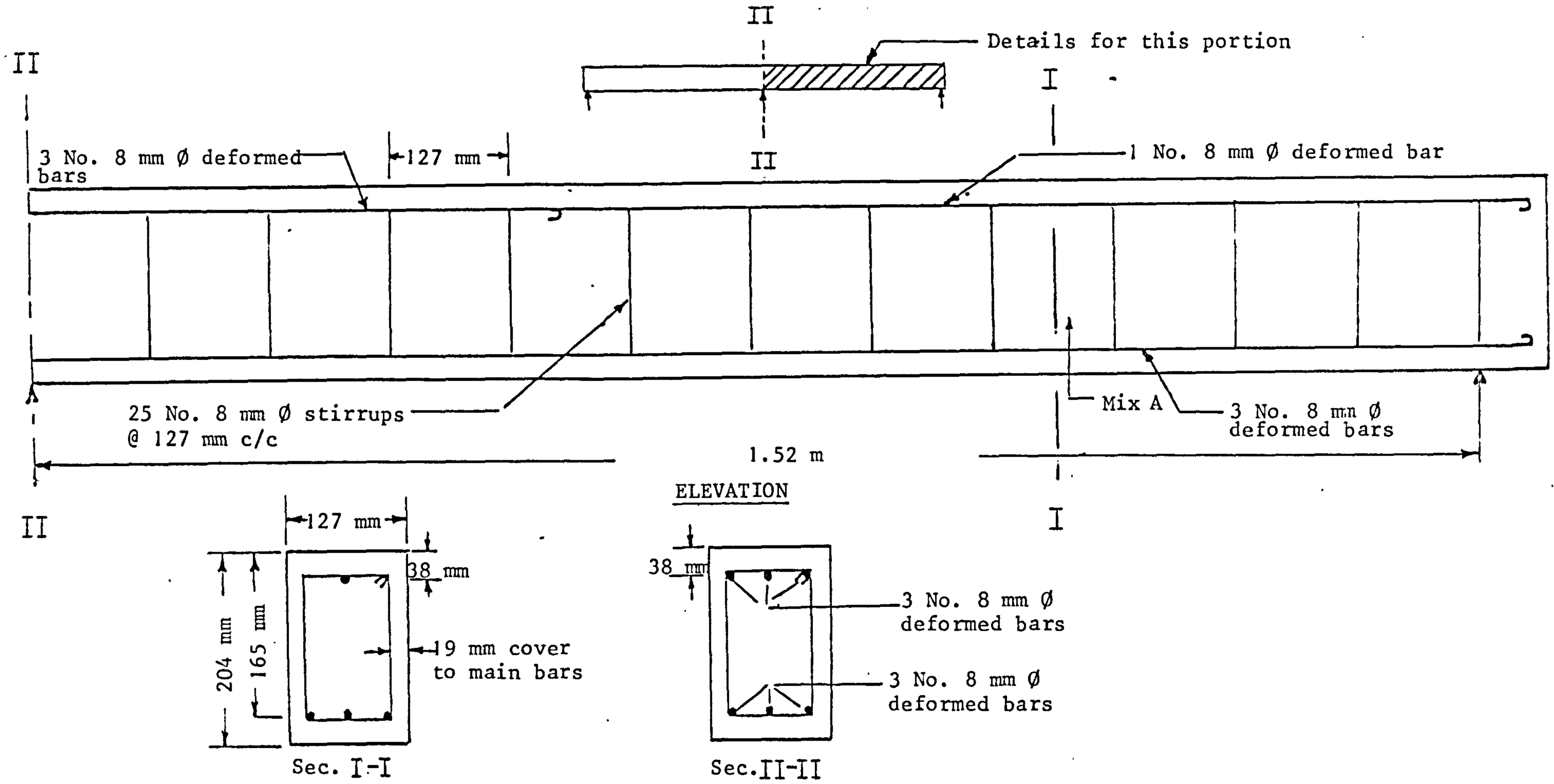

Fig.2.2.1 Diagram showing reinforcement in reinforced concrete continuous beam

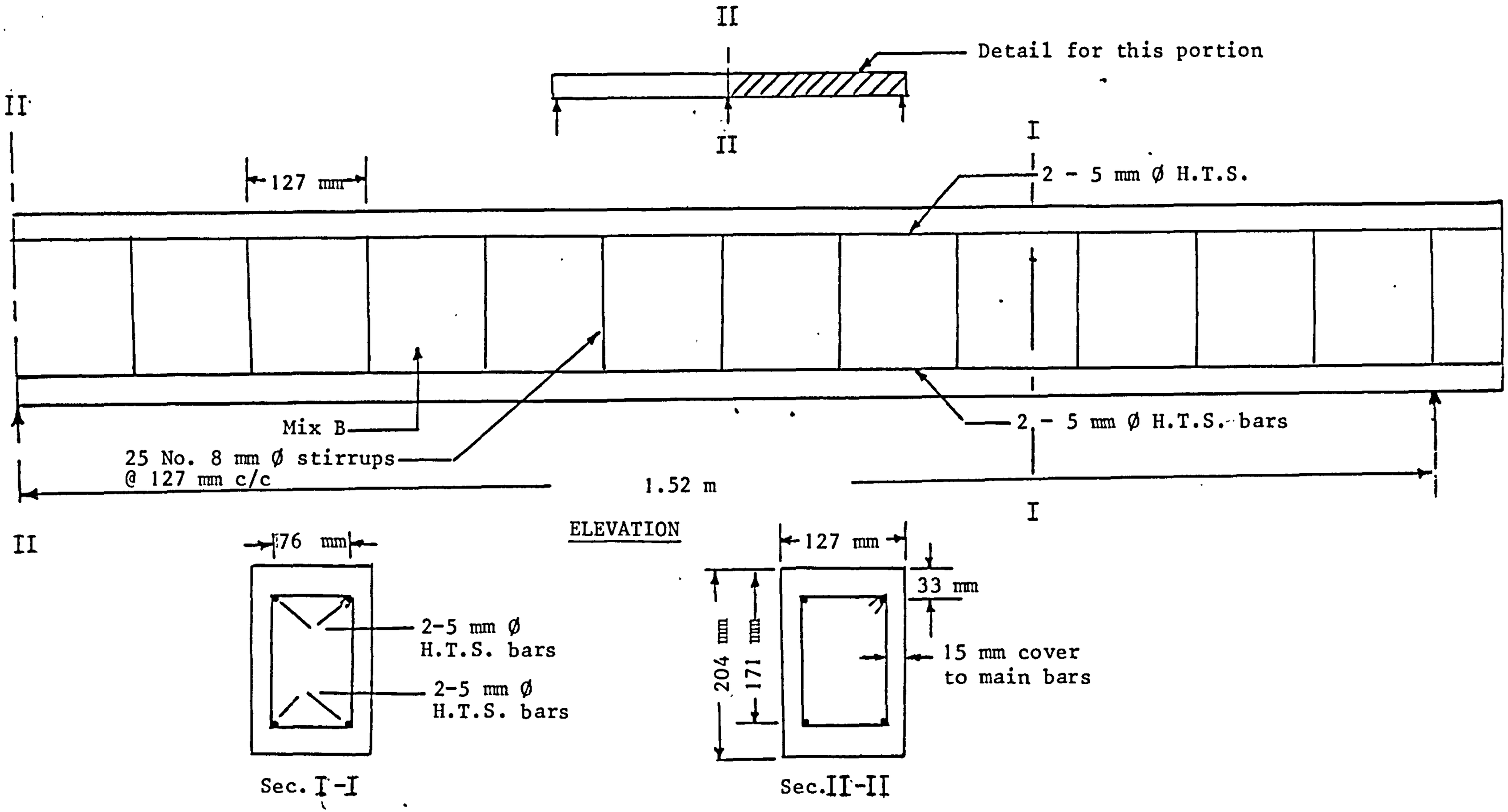

Fig. 2.2.2 Diagram showing reinforcement in prestressed concrete continuous beam

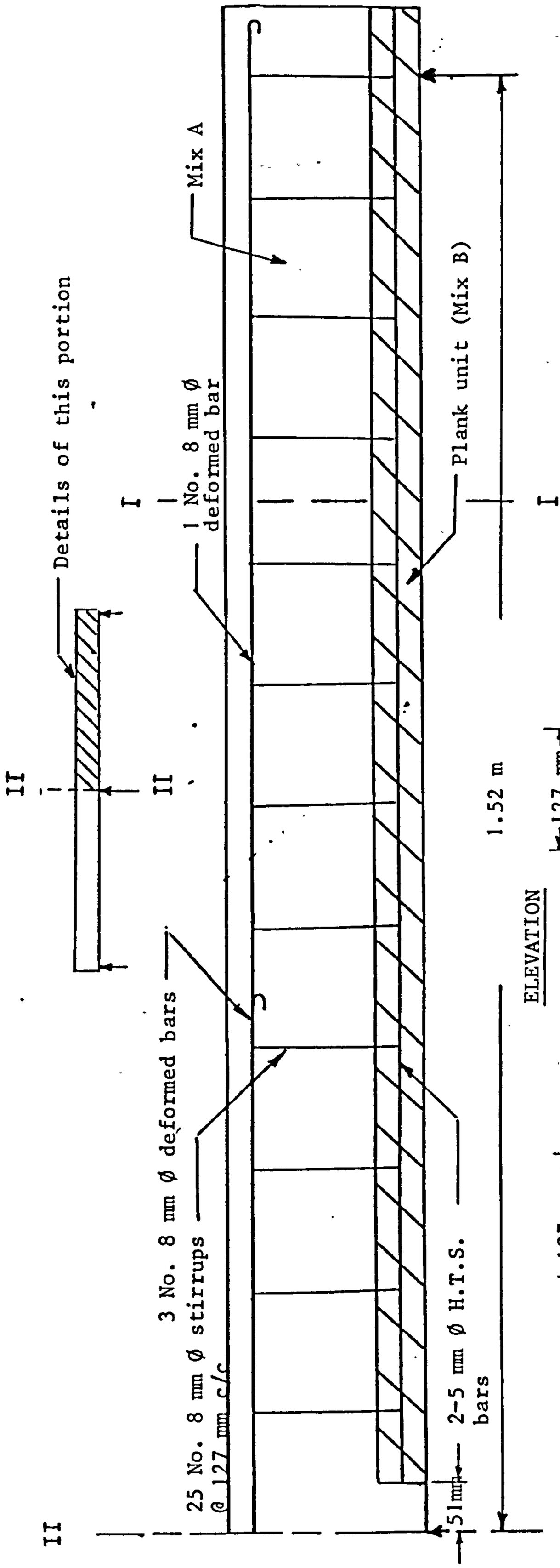

Fig. 2.2.3 Diagram showing reinforcement in composite prestressed concrete continuous beam

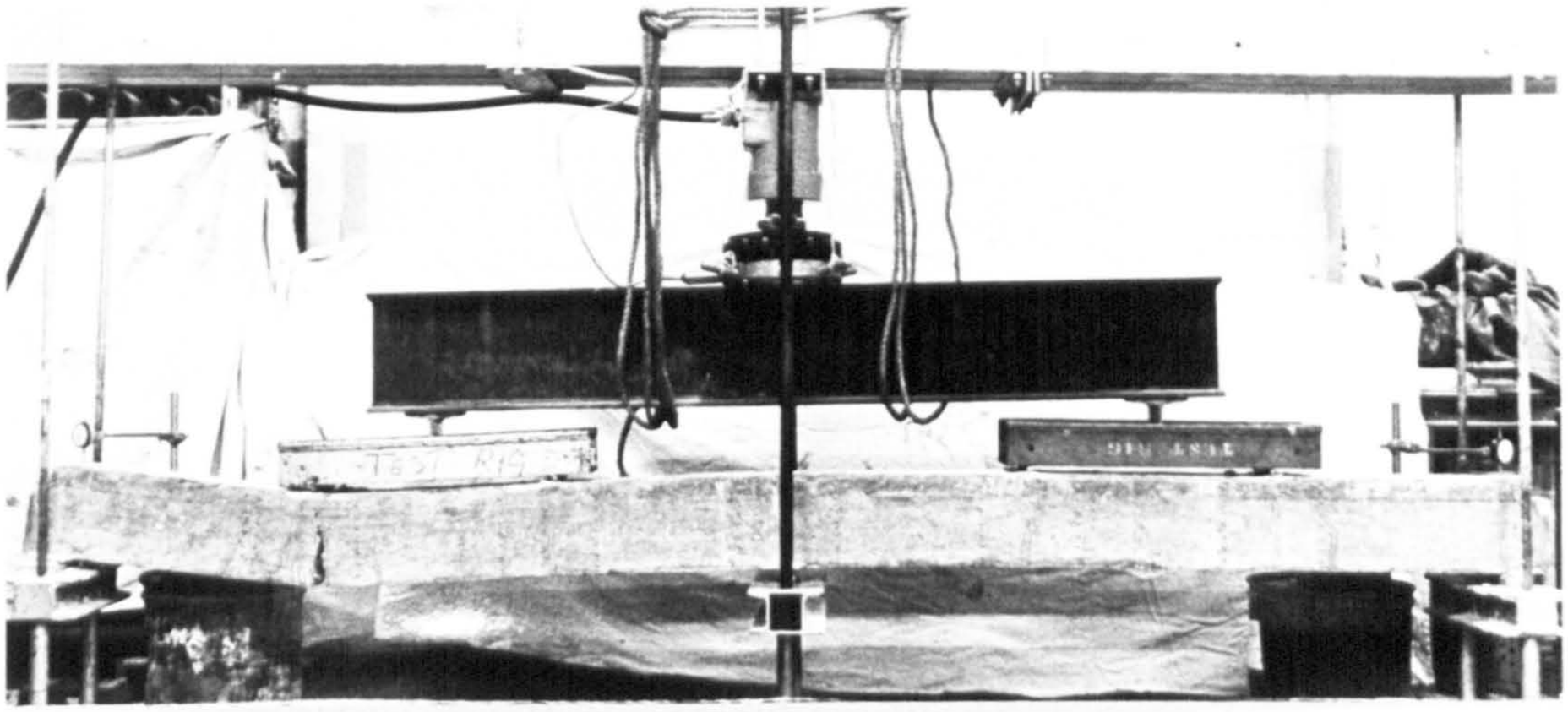

Photo 2.2.1 Reinforced concrete continuous beam on testing rig after failure

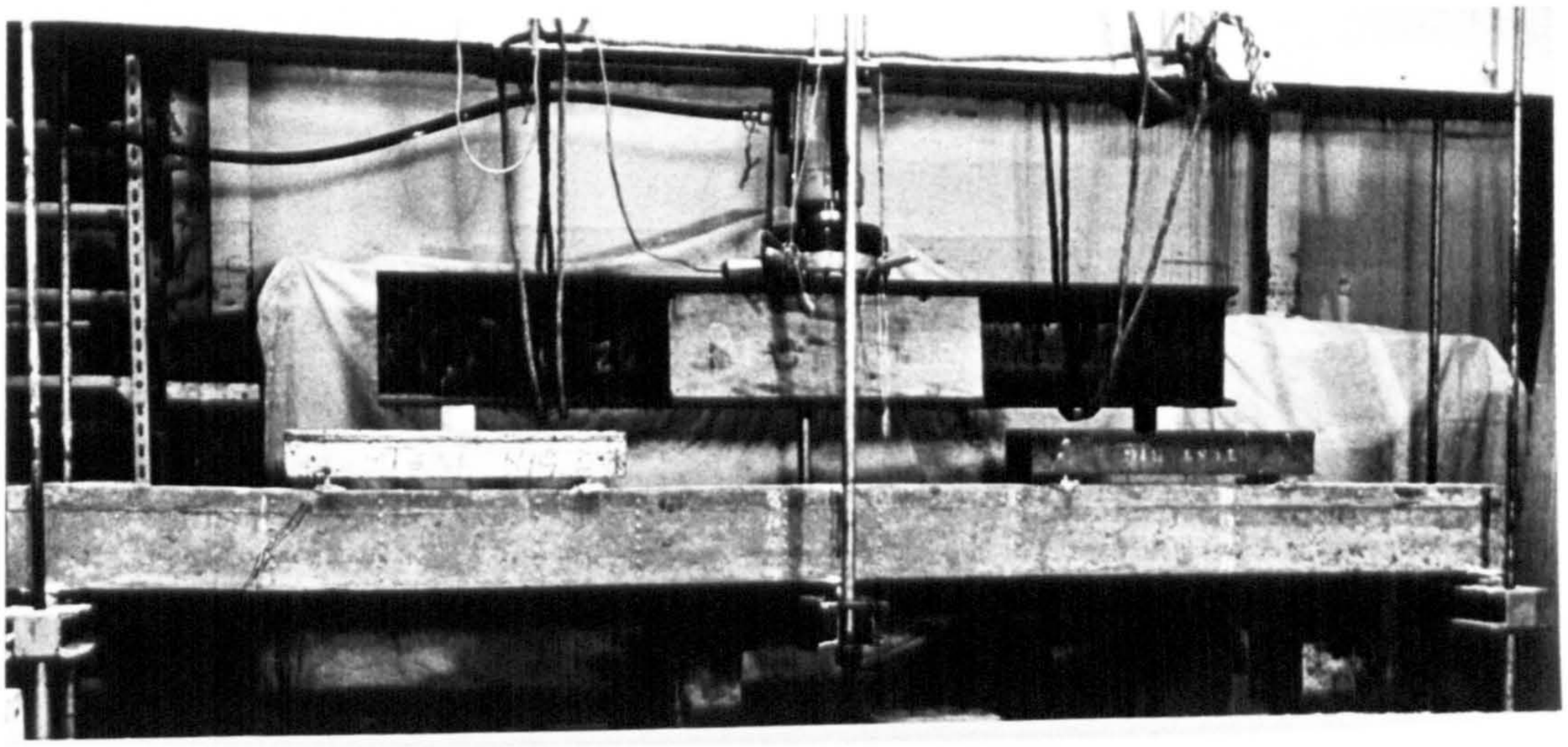

Photo 2.2.2 Prestressed concrete continuous beam on testing rig after failure

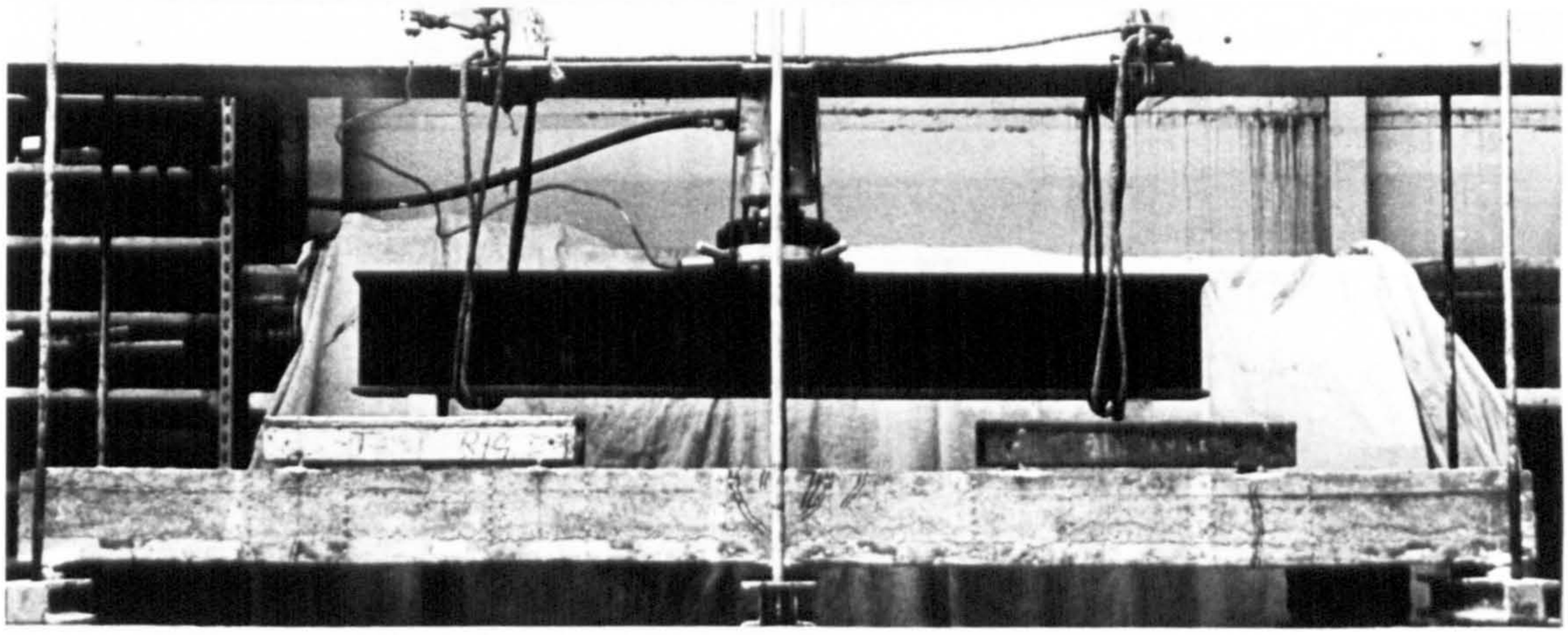

Photo 2.2.3 Composite prestressed concrete continuous beam on testing rig after failure

CHAPTER 3

Experimental work - Long-Term Behaviour of reinforced, prestressed and composite prestressed concrete two span continuous beams at laboratory temperature

3.1 SYNOPSIS

Experimental studies on Long-term Behaviour at laboratory temperature of the three types of two span continuous concrete beams reported in Chapter 2 Part 2 are reported in this Chapter.

Long term tests on rectangular two span reinforced and pre-stressed concrete continuous beams were carried out at an age of 35 days after casting and after 35 days of casting reinforced concrete portion of the composite concrete beam and up to 9 months of sustained loading for all types of beams. The analytical numerical approach reported in Chapter 6 was used to predict the elastic and long-term behaviour of the three types of concrete beams, see Photo 3.6.

3.2 INTRODUCTION

The principal object of the investigation was to compare the long-term behaviour of the three types of two span continuous concrete beams at laboratory temperature while carrying a constant sustained working load of 7472 N* at the third points of each span of length 1.52 metres.

Tests were conducted to measure the long-term longitudinal strain distributions, vertical deflections, and variation of reactions.

The experimental results were in good agreement with the theoretical predicted values from the numerical analysis.

3.3 TESTING APPARATUS

The beams were tested in two equal spans of 1.52 m. The centre support reaction was treated as the redundancy. It was measured

* Imperial equivalent $\frac{3}{4}$ ton.

by a high tensile steel proving ring (see Photos 3.3 and 3.4).

Fig. 3.1 shows reinforced concrete continuous beam on the testing rig. The beam was loaded against two 5" x 2½" (127 x 63 mm) steel channels by means of heavy springs and tension rods.

3.3.1 End Supports

The end supports were so made that the beam rested on two steel plates which in turn rested on two steel rods 19 mm diameter spaced at 3.04 m apart, (see Fig. 3.1). When the beam was seated on the supports, some wet plaster was placed between the concrete and steel plate to offset any irregularities in the concrete surface and any displacement between the two surfaces. Two dial gauges, each reading to 0.01 mm per dial division were placed directly at the supports on top surface of the beam.

3.3.2 Centre Support

The centre of the beam was supported on a high tensile steel proving ring which in turn was supported on a 19 mm B.S.F. high tensile bolt. The bolt passed through a 12 mm steel plate resting on the main channels. Thus the centre support reaction was transferred to the main channels. The bolt could be turned by a spanner and enabled the beam to be moved up or down at the centre to maintain level supports (see Photo 3.5).

A 50 kN proving ring was used to support the centre of each beam. Each dial division on the gauge attached to the proving ring corresponds to approximately 44 N. One dial gauge, each reading to 0.01 mm per dial division, was placed directly at the middle of the beam. Level supports could be maintained by observing the relative movements of the three dial gauges on the beam in order

to move the beam up or down at centre support by the proving ring. Photo 3.1 shows the proving ring.

3.3.3 Loading Apparatus

Because of the large load, 7472 N, required at each loading point, a proportionately smaller load was given to the springs compared to the stronger tension rods. The springs were given 0.3 metre lever arm and the tension rods 0.15 m, so that the total load was three times the spring load. The loading channels were 127 x 63 mm and 0.5 m long. See Fig. 3.1.

3.3.4 Datum Bar for Deflections

Three dial gauges, each reading to 0.01 mm per dial division, were used for each beam. They measured the vertical movements at the ends of the beams and the centre support displacements during the loading operation and during the whole period of sustained loading.

To obtain the deflection profile of the beam at all stages of test a Datum Bar 25 x 25 mm x 3 m long with ends resting on 19 mm rods placed below the beam supports shown in Fig. 1 was used. A dial gauge for measuring deflections shown in Photo 3.2 was attached to the Datum Bar at points spaced 127 mm starting from the end support where deflection is required.

3.3.5 Strain Measurement

Strain measurements using the 8" (203 mm) Demec Gauge were made at the third point of each span and at the centre support at the following locations.

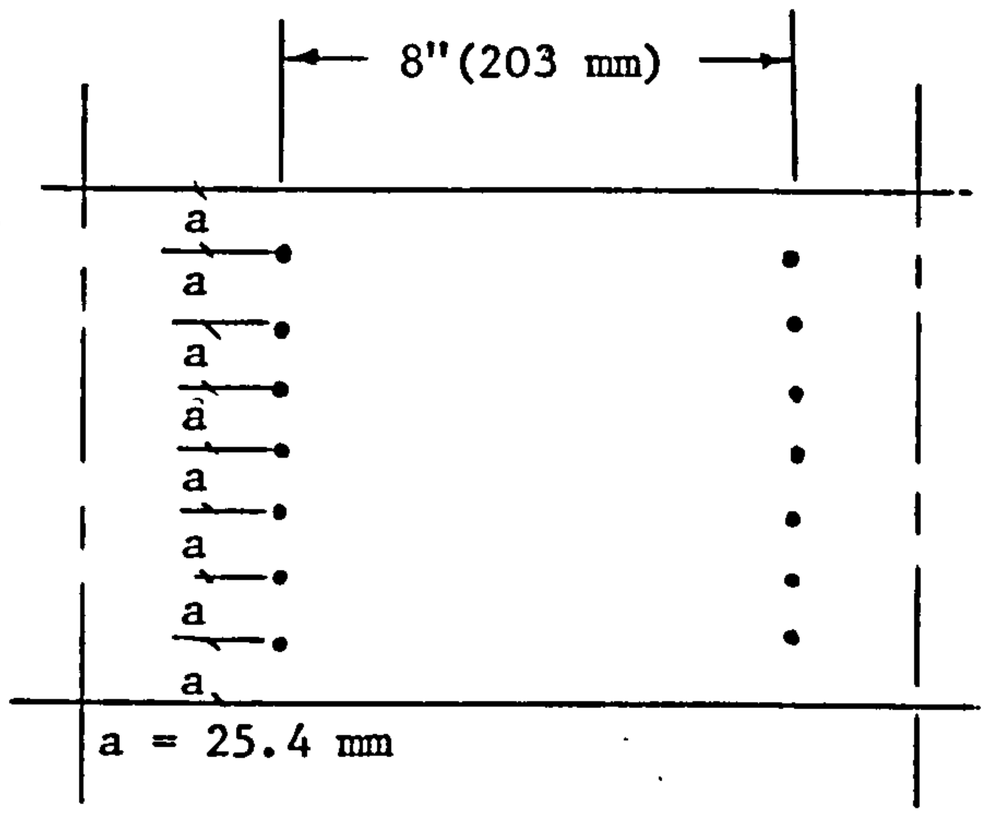

3.4 TESTING PROCEDURE

Two weeks after casting, each beam was moved to the testing apparatus and placed on the end supports. The centre support was applied and adjusted so that the proving ring was loaded to the elastic value of centre support reaction under dead load for level supports. The three supports were fixed at this same relative level throughout the testing period from dial gauges. Working loads of 7472 N were applied at the third Pts of each span, 35 days after casting reinforced and prestressed concrete beams and at 35 days after casting reinforced concrete portion for the composite prestressed beam. This load was maintained for 9 months while the strains and displacement behaviour of the beams were observed. After removing the loads the beams were finally tested to failure in short term tests. These are reported in Chapter 2 Part 2.

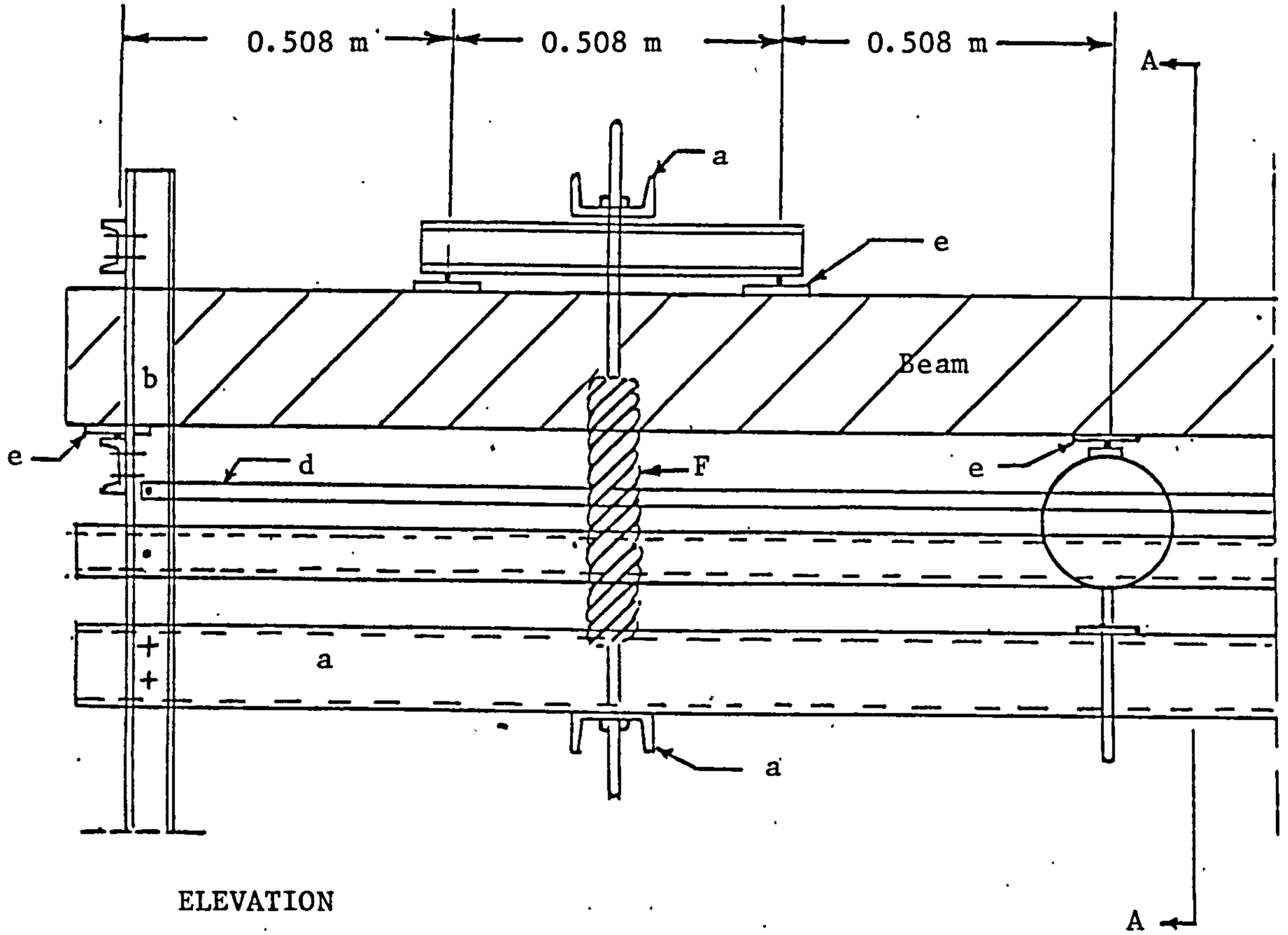

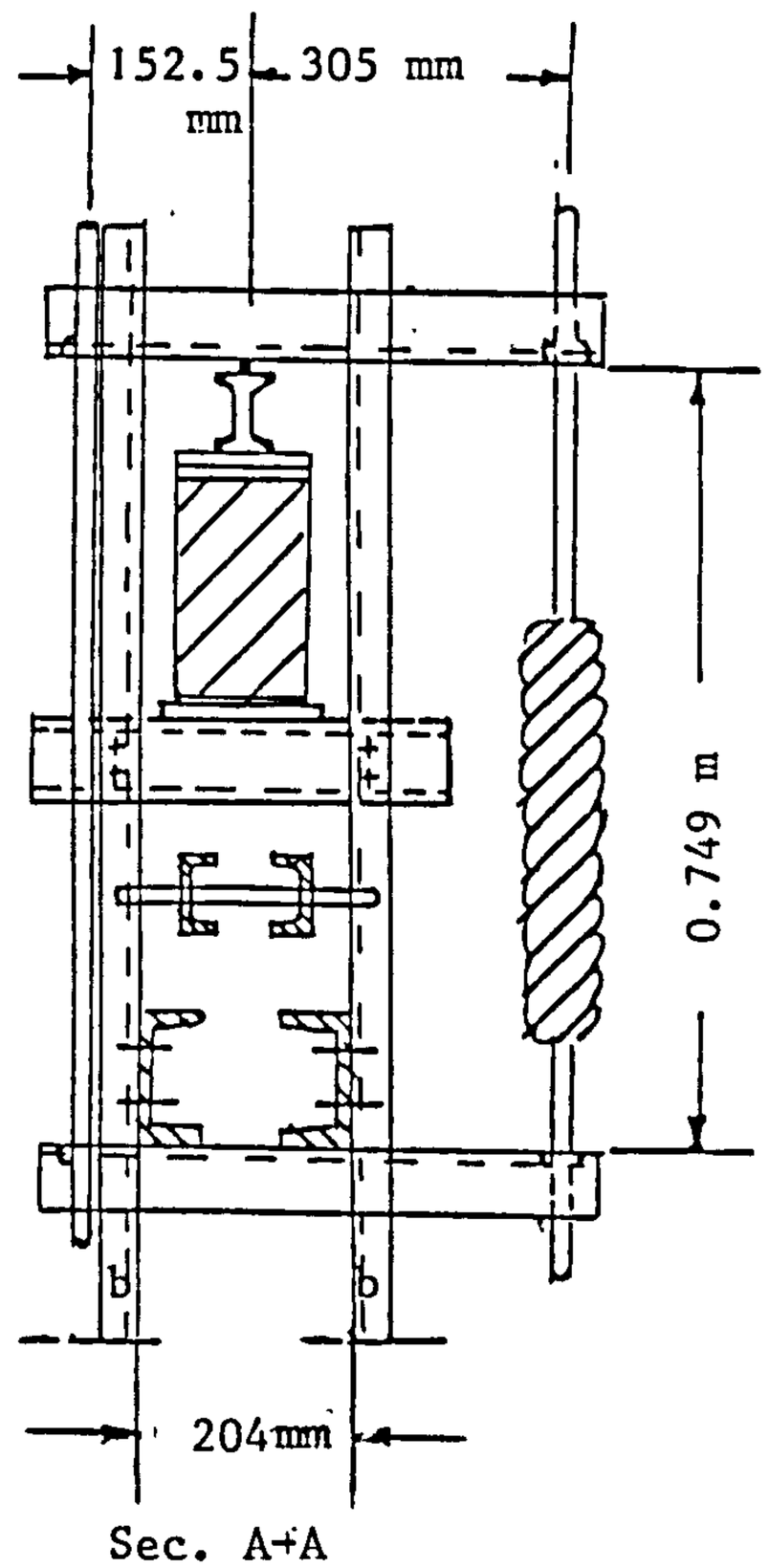

ELEVATION

a channel section 127 x 63 x 6.4 mm
b channel section 76 x 38 x 6.4 mm
d steel datum bar section 25 x 25 mm
e steel bearing plate 127 x 102 x 13 mm
F heavy spring

Fig. 3.1 General design of the mounting frame

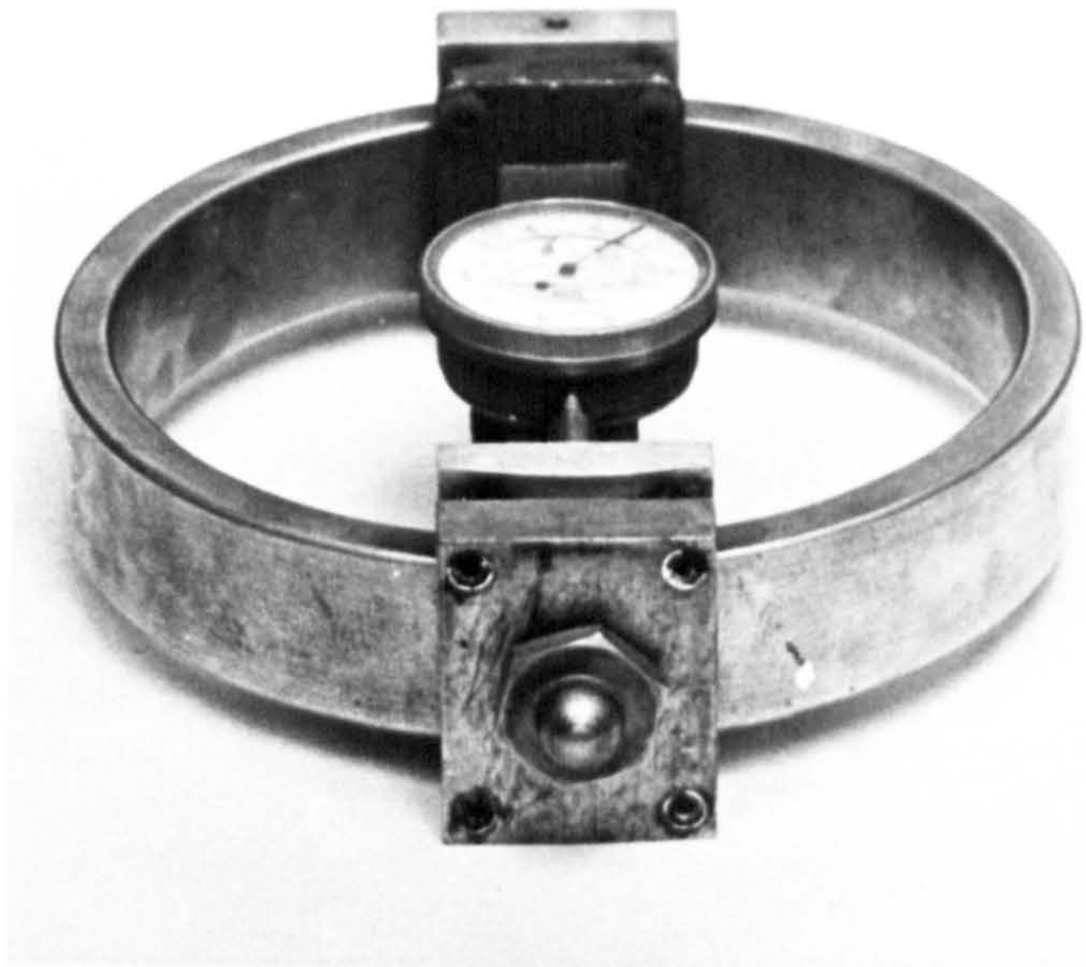

Photo 3.1 Proving ring for supporting the centre of the beam

Photo 3.2 Deflection gauge

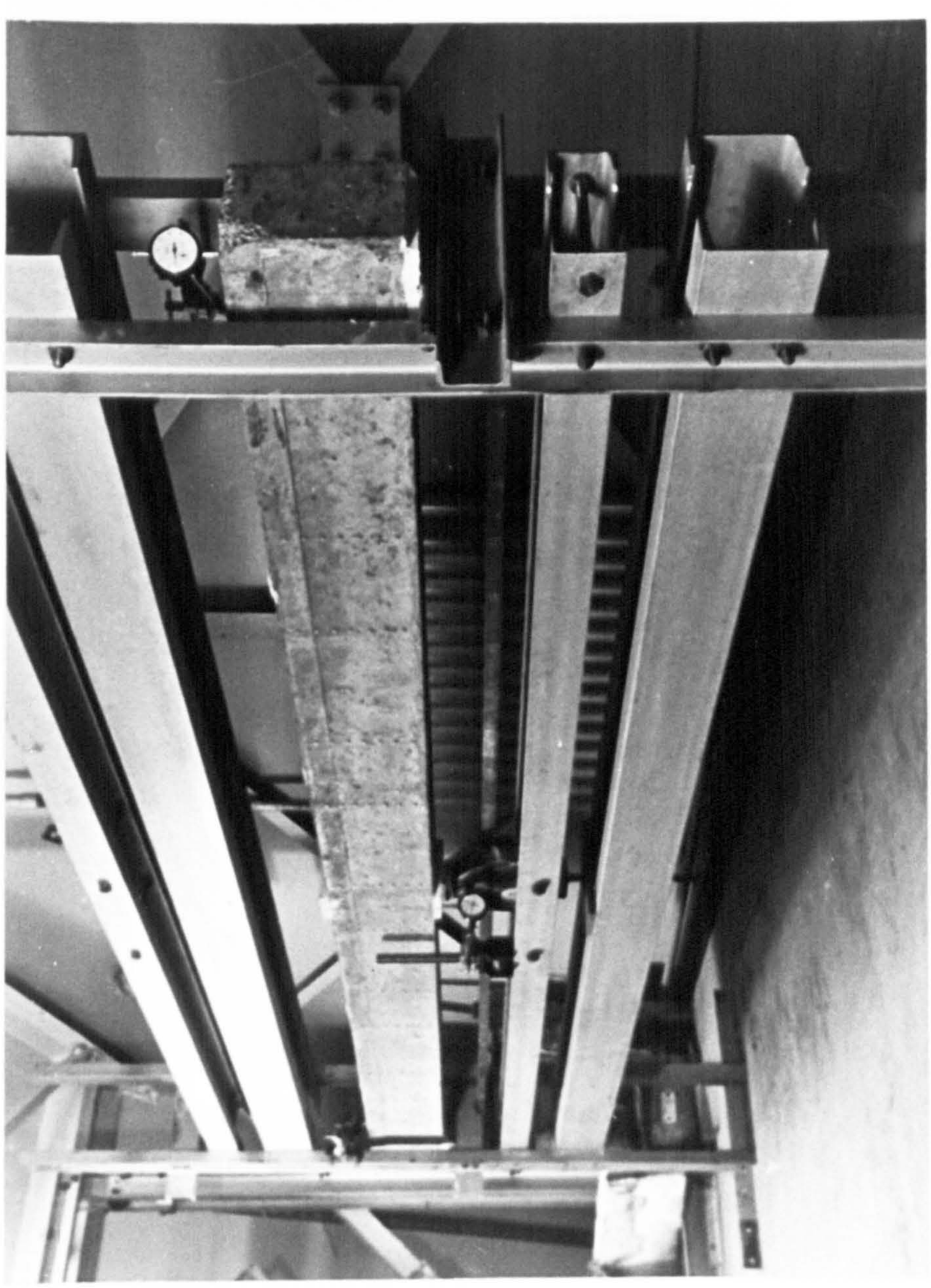

Photo 3.3 General view of the testing rig showing the beam before loading

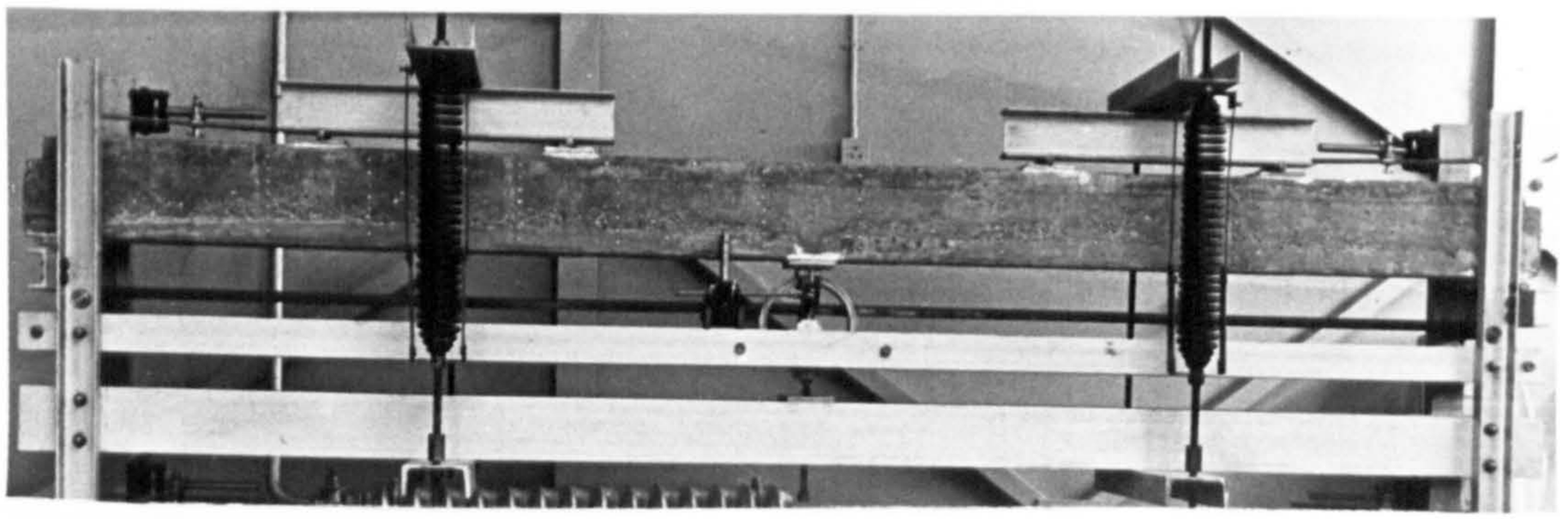

Photo 3.4 General view of the testing rig showing the beam after loading

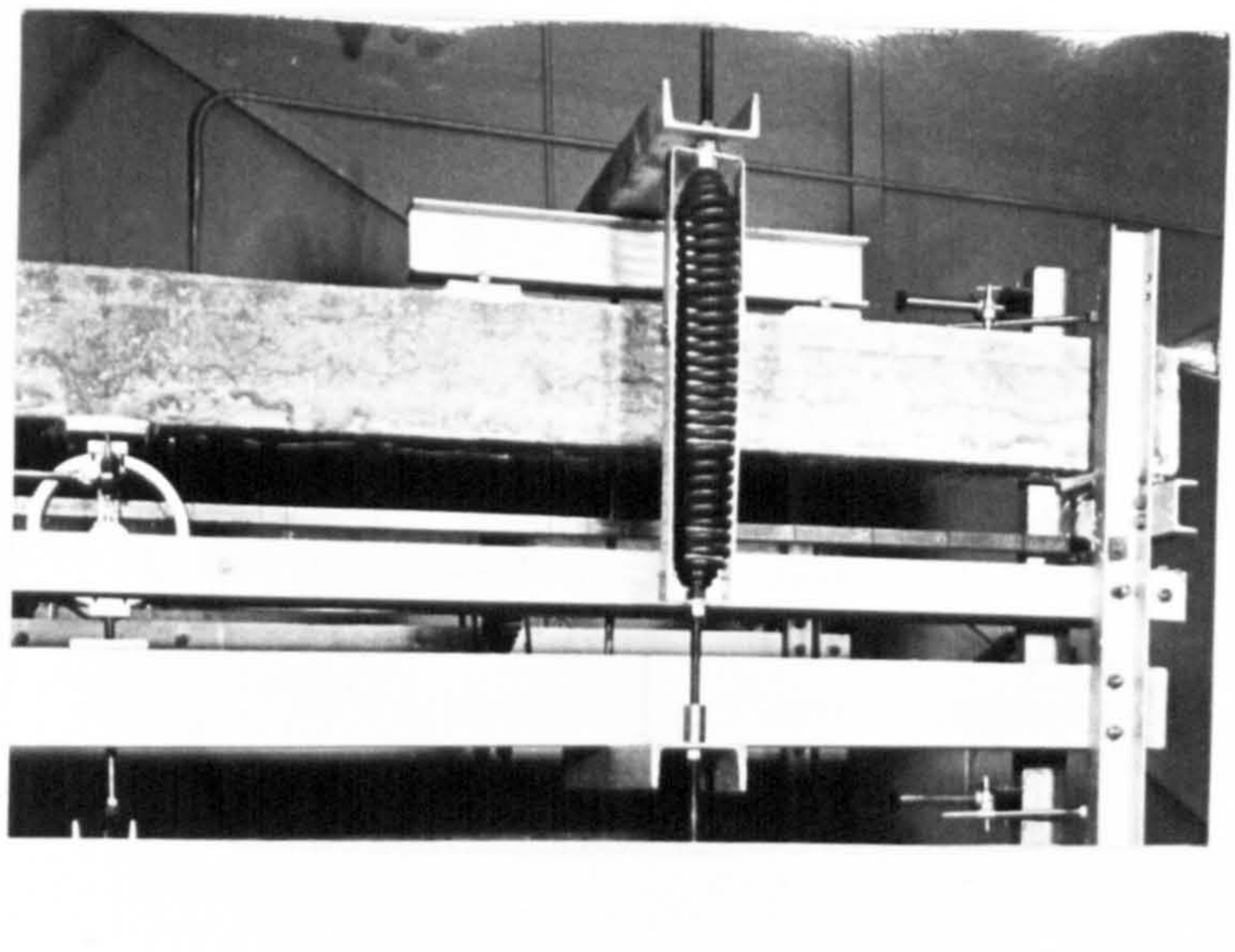

Photo 3.5 General view showing centre support and details of loading apparatus

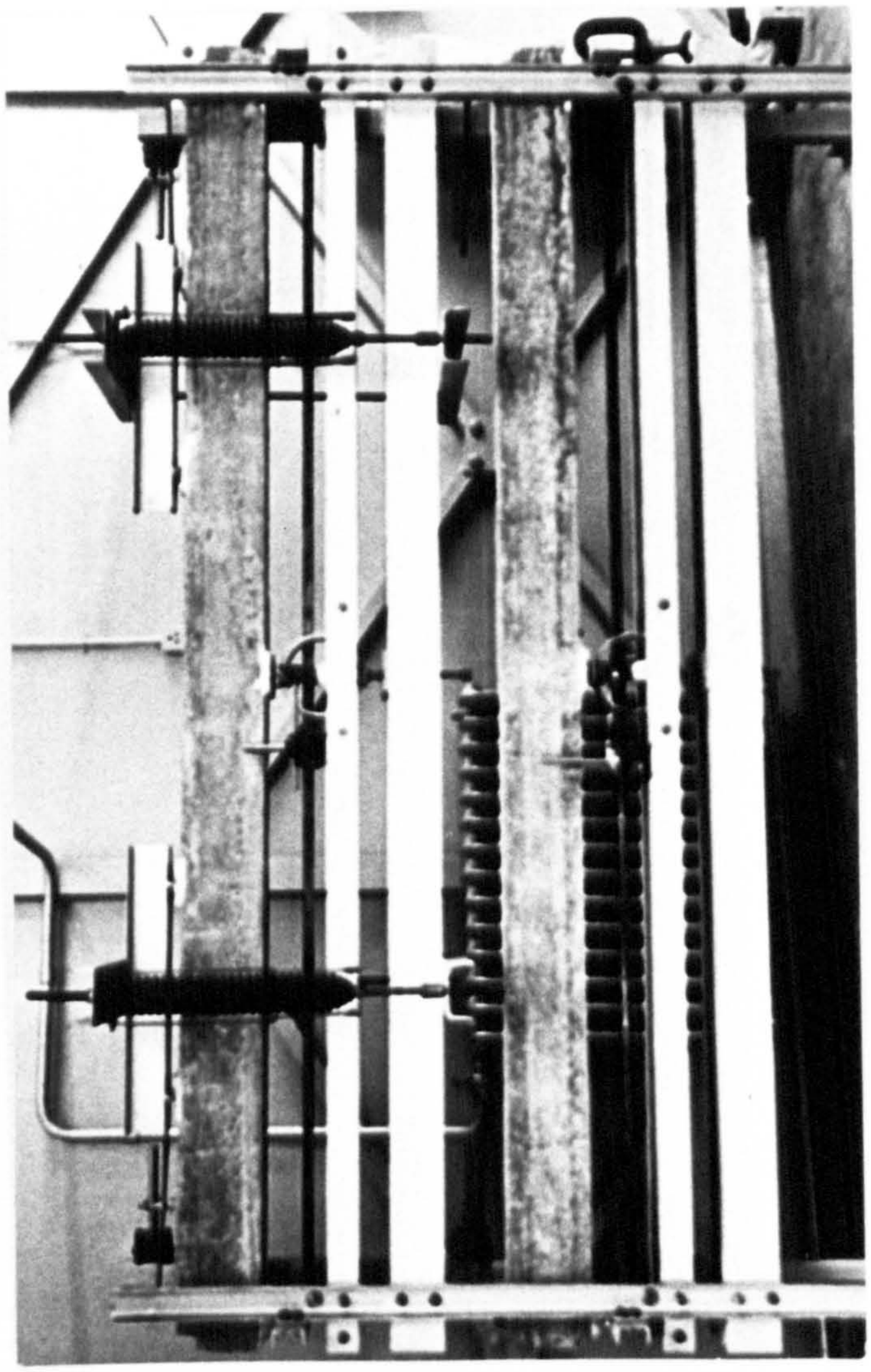

Photo 3.6 General view of the testing rig showing loaded and shrinkage control beams

CHAPTER 4

Experimental Work - Results, discussions and conclusions of the experiments reported in Chapter 3

4.1 SYNOPSIS

Experimental and theoretical results on long-term behaviour of experimental beams reported in Chapter 3 are presented. The assumptions of the analytical numerical approach reported in Chapter 6 permitted prediction of measured reactions and deflections with satisfactory accuracy.

4.2 INTRODUCTION

Results of long-term test programme carried out at laboratory temperature on the three types of two span continuous concrete beams resting on three level supports reported in Chapter 3 showed the beneficial effect of prestressed concrete plank of composite beam in reducing the elastic and long-term deflections in comparison with the reinforced concrete beam. The results also show the difference in behaviour between the three types of concrete beams during the 270 days of sustained loading while all the beams have virtually the same ultimate capacity.

4.3 RESULTS

4.3.1 Reinforced, Prestressed and Composite Prestressed Beams

(a) Dimensions

The cross sections of the continuous beams were 127 x 204 mm and the second moment of inertia of uncracked section was 89.85 x 10^{-6} m^4.

(b) Loads

(i) Dead Load

The elastic centre support reaction due to dead load with level supports was calculated to be 1.22 kN.

(ii) Transverse Load

The applied transverse load was 7.472 kN at the third points of each span, with level supports. The elastic reaction at centre support was calculated to be 19.927 kN. The bending moment diagram is shown below.

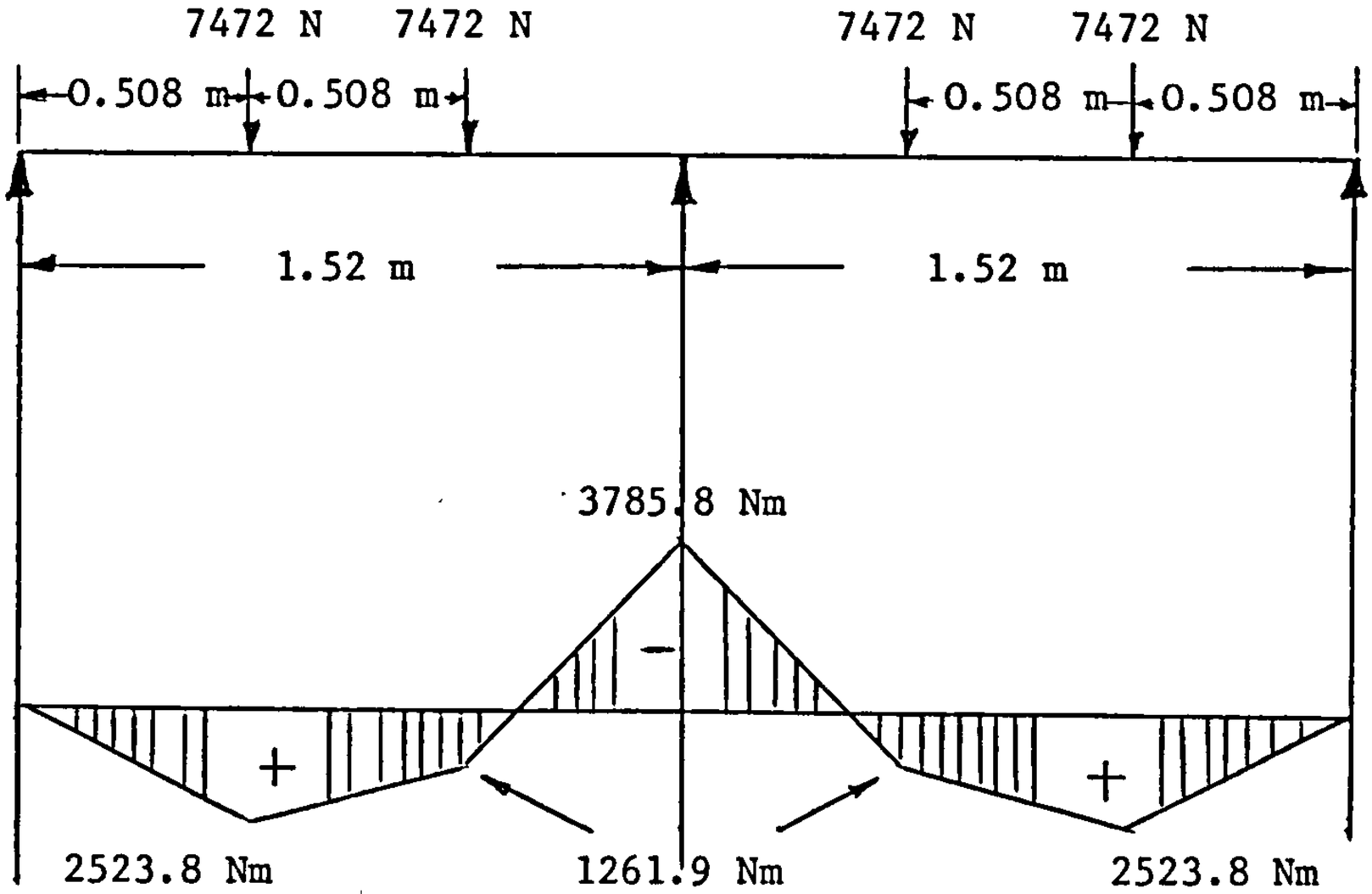

Strains were measured over 8" (203 mm) gauge length.

(iii) Prestressing Force

In the case of prestressed and composite prestressed beams each 5 mm diameter, prestressing wire was initially tensioned to 22.24 kN. The result is that the prestressed beam was initially subjected to a constant stress of 3447 MN/m^2 and each plank of the composite beam was initially subjected to a constant stress of 6.895 MN/m^2.

(c) Temperatures

All the beams were tested at laboratory temperature and any thermal strains in the beams caused by small temperature variation in the laboratory have been deducted from the measured strains assuming a value of $12.0 \times 10^{-6}/^{o}C$ for the coefficient of

expansion of steel and concrete and a datum temperature of results 15°C.

4.3.2 Reinforced Concrete Beam

(a) Centre Reaction

Graph 4.1 shows the variation of centre support reaction with time for 270 days of sustained transverse load and dead load. The elastic support reaction is also shown. The theoretical variation of centre reaction predicted from the numerical analysis of Chapter 6 is also plotted.

(b) Deflection

Graph 4.2 shows the time deflection behaviour at Section I-I for the period of sustained load. Graph 4.3 shows the deflection profile of half of the beam after various days of sustained loading. The theoretical elastic deflection values predicted from the numerical analysis of Chapter 6 are also plotted for comparison.

(c) Strains

Graph 4.4 and 4.5 show the measured strain curves after loading for the top and bottom gauge lengths at sections I-I and II-II. Graphs 4.6 and 4.7 show the measured strain distribution at sections I-I and II-II gauge lengths after various days of sustained loading.

4.3.3 Prestressed Concrete Beam

(a) Centre Reaction

The variation of centre support reaction for the entire period of sustained loading is shown in Graph 4.8. Also plotted the theoretical and long-term centre reaction variations predicted

from the numerical analysis of Chapter 6 for comparison.

(b) Deflection

Graph 4.9 shows the time deflection behaviour at Section I-I plotted as a function of time together with the theoretical long-term deflection. The deflection profile for half the beam at various times after loading is shown in Graph 4.10. The theoretical elastic deflection profile predicted from the numerical analysis is also plotted.

(c) Strains

The variation of measured top and bottom strain curves after loading at Sec. I-I and Sec. II-II are plotted in Graphs 4.11 and 4.12. Graphs 4.13 and 4.14 show the measured strain distribution at Sec. I-I and Sec. II-II gauge lengths after various days of sustained loading.

4.3.4 Composite Prestressed Concrete Beam

(a) Centre Reaction

Graph 4.15 shows variation of centre support reaction with time. The theoretical variation of centre reaction predicted from the numerical analysis of Chapter 6 is also plotted.

(b) Deflection

The measured time deflection behaviour at Sec. I-I together with the theoretical deflection profile are plotted in Graph 4.16. Graph 4.17 shows the deflection profile for half the beam at various times after loading. The theoretical elastic deflection profile predicted from the numerical analysis is also plotted for comparison.

(c) Strains

Graphs 4.18 and 4.19 show the variation of measured strain curves at the top and bottom gauge lengths at Sec. I-I and Sec. II-II for the whole period of sustained loading. Measured strain distributions at Sec. I-I and Sec. II-II gauge lengths after various days of sustained loading are plotted in graphs 4.20 and 4.21.

4.4 DISCUSSIONS

Central Support Reaction

Graphs 4.1, 4.8 and 4.15 show relatively little change with time of measured centre support reaction due to sustained transverse loading for the three types of concrete beams. The measured centre support reaction for the whole period of sustained loading w.r.t. the reinforced and prestressed beams is approximately the same and about 5% less in value for the composite beam after 270 days of sustained loading.

Deflections at span section I-I

Graphs 4.2, 4.9 and 4.16 show the measured and calculated elastic and creep deflection behaviour at Sec. I-I for the whole period of sustained loading w.r.t. the three beam types. The graphs show that the measured creep deflection at Sec. I-I after 270 days of sustained loading w.r.t. the reinforced, prestressed and composite beams is 1.8, 0.75 and 1.6 times the elastic deflection respectively. The graphs also show that there is a little difference between the experimental and theoretical deflection curves for prestressed and composite beams for the whole period of sustained loading. It is also obvious from Graph 4.2 that the measured deflection of reinforced concrete beam is greater

than the theoretical predicted values by 4% and 40% after 30 and 270 days of sustained loading respectively.

Deflection Profiles

Graphs 4.3, 4.10 and 4.17 show the variation of the deflection profiles of the three types of beams at various times after loading. The variation between the experimental and theoretical elastic deflection profiles is not significant w.r.t. the three beam types.

Strain at selected sections

Graphs 4.4, 4.11 and 4.18 show the complete strain variation with time at Sec. I-I due to elastic, creep and shrinking w.r.t. the three types of concrete beams. The Graphs show that the strain at gauge length 1 is increasing at a decreasing rate for the three types of beams due to creep and shrinkage, but the strain at gauge length 7 is decreasing at a decreasing rate w.r.t. the prestressed and composite beam due to creep and shrinkage but there was little change with time in the tensile strain at gauge length 7 which is close to steel level in the reinforced concrete beam.

Graphs 4.5, 4.12 and 4.19 show the measured complete strain variation with time at Sec. II-II due to elastic, creep and shrinkage w.r.t. the three beam types. It is obvious from the graphs that the strain near to the compression side of the beams at gauge length 7 is increasing at a decreasing rate due to creep and shrinkage w.r.t. the three types of beams. The graphs also show that the strain near the tensile side of the beams at gauge length 1 is decreasing at a decreasing rate w.r.t. the prestressed beam due to creep and shrinkage but the variation of the tensile strain at the same level showed relatively little change with time w.r.t. the reinforced and

composite concrete beams as that level is close to the tensile steel level.

Strain distribution at selected sections

Graphs 4.6, 4.13 and 4.20 show a slight deviation from a straight line strain distribution at Sec. I-I w.r.t. the three types of concrete beams. The same behaviour is also noticed in Graphs 4.7, 4.14 and 4.21 which represents the measured strain distributions at Sec. II-II for the three types of concrete beams.

4.5 CONCLUSIONS

(a) There is a good agreement between the measured and calculated long-term variation of centre support reaction from the numerical analysis of Chapter 6 for the three types of concrete beams.

(b) Ratio of measured creep deflection for reinforced, prestressed and composite concrete beams after 270 days of sustained loading was 1.8, 0.75 and 1.6 respectively.

(c) There was a little difference between the measured and calculated creep deflection from the numerical analysis w.r.t. prestressed and composite concrete beams, but there was about 40% difference between measured and computed creep deflection after 270 days of sustained loading for reinforced concrete beam.

(d) The measured elastic deflection profile was in good agreement with the computed elastic deflection profile for the three types of concrete beams.

(e) Measured variation of compressive creep and shrinkage strains in the positive moment region were approximately the same for prestressed and composite concrete beams despite the difference in compressive reinforcement in the positive moment region, but the measured compressive creep strain for reinforced concrete beam was relatively large in this region.

(f) Measured long-term variations of tensile and compressive creep and shrinkage strains in the negative moment region showed nearly the same behaviour for reinforced and composite beams.

(g) Measured tensile creep and shrinkage strains at positions of negative moment showed relatively little change with time in the case of reinforced and composite concrete beams.

(h) Measured long term variation of tensile and compressive creep and shrinkage strains in the positive moment region showed nearly the same behaviour for prestressed and composite beams despite the difference in material and the initial stresses between the two beams due to prestressing force.

(i) Comparison between measured and computed time deflection behaviour at section I-I for the whole period of sustained loading w.r.t. the three types of concrete beams are shown in graphs 4.2, 4.9 and 4.16. Comparison between measured and computed time deflection profile for half of the beam w.r.t. reinforced, prestressed and composite concrete beams can be made from graphs 4.3, 4.10 and 4.17 respectively for measured values and from Chapter 6 Graphs 6.3, 6.7 and 6.11 respectively for computed values.

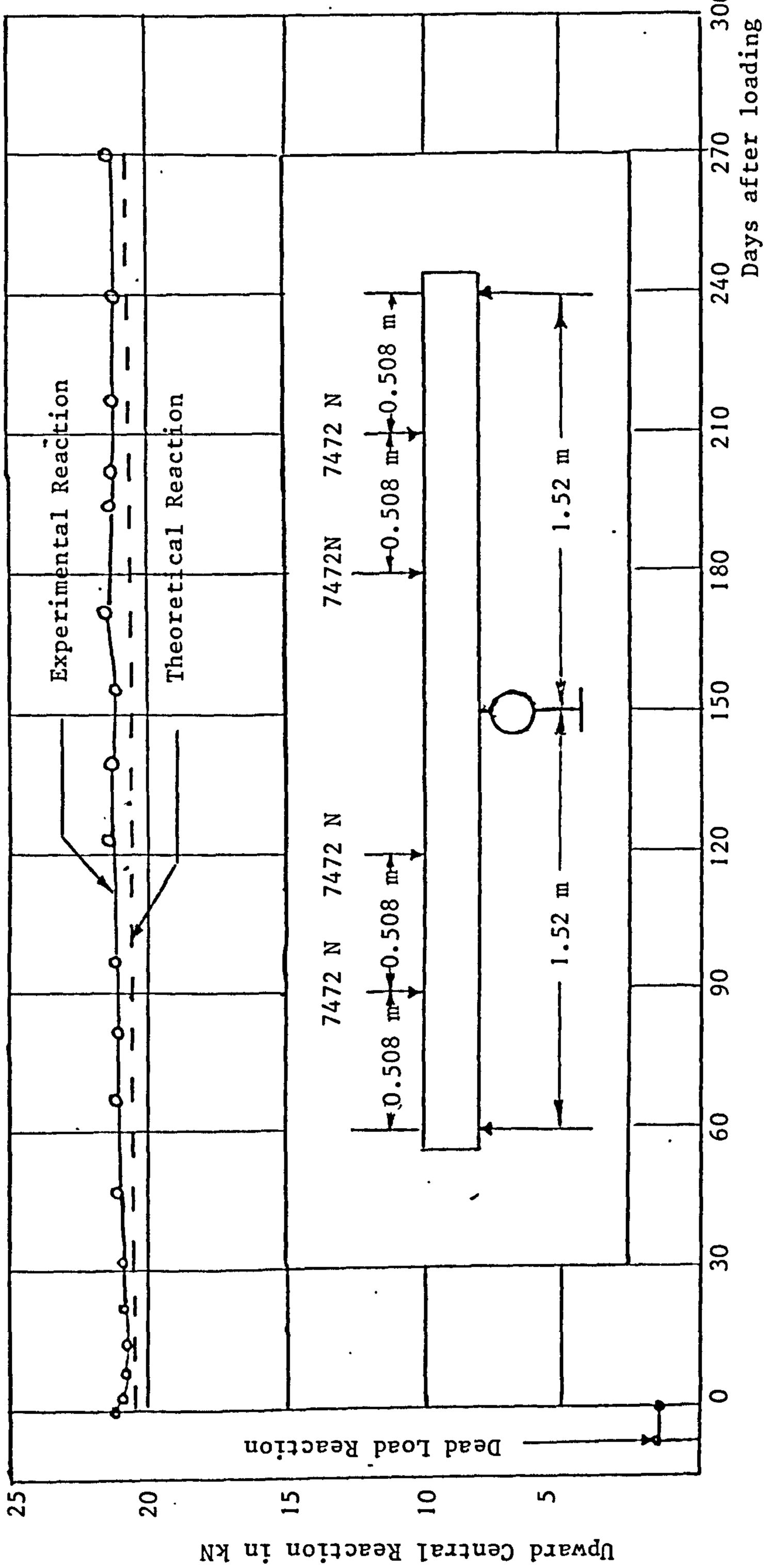

Graph 4.1 Variation with time of central reaction of reinforced concrete continuous beam

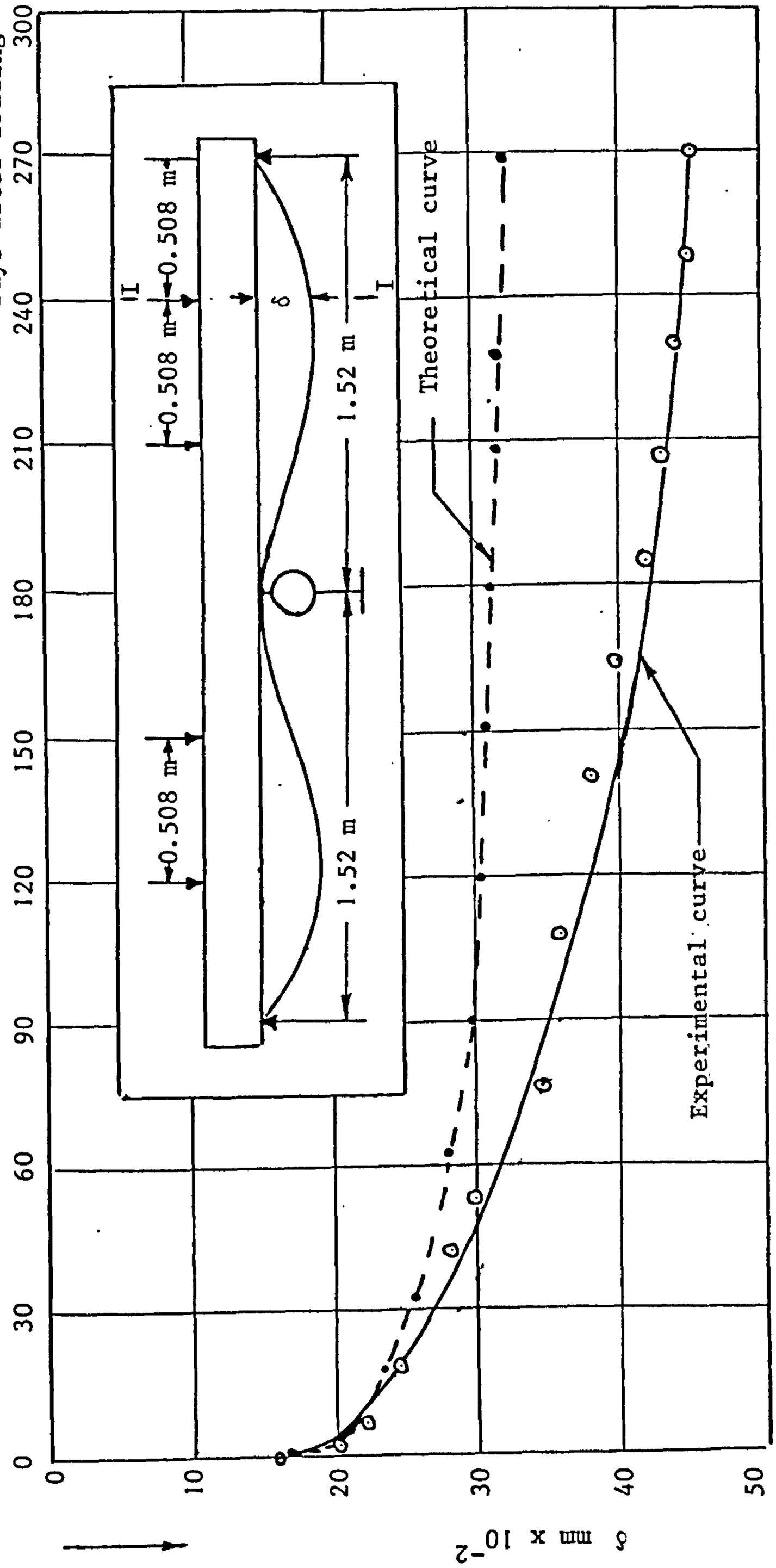

Graph 4.2 Time deflection behaviour at Sec. I-I of reinforced concrete continuous beam

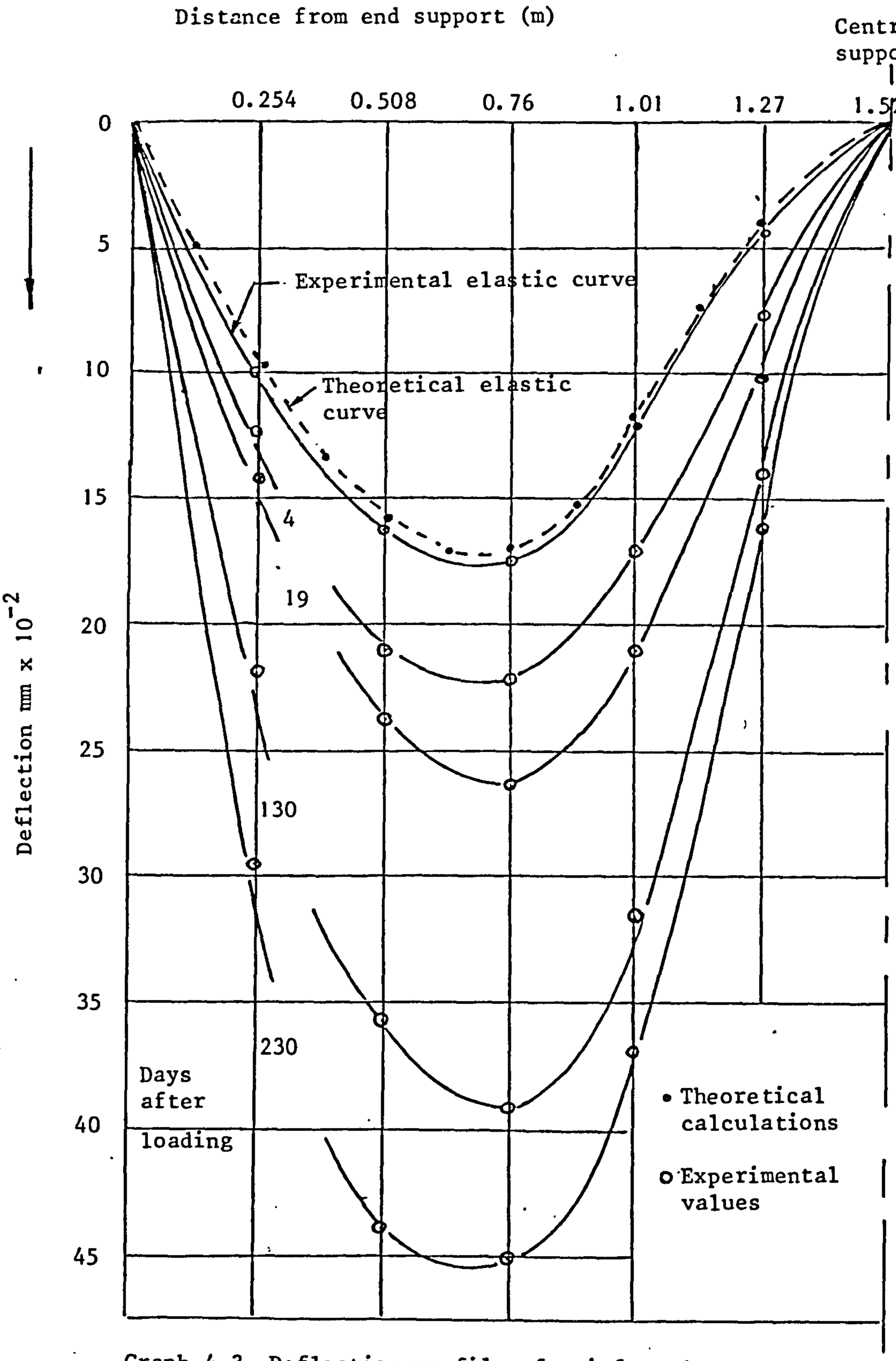

Graph 4.3 Deflection profile of reinforced concrete continuous beam after loading

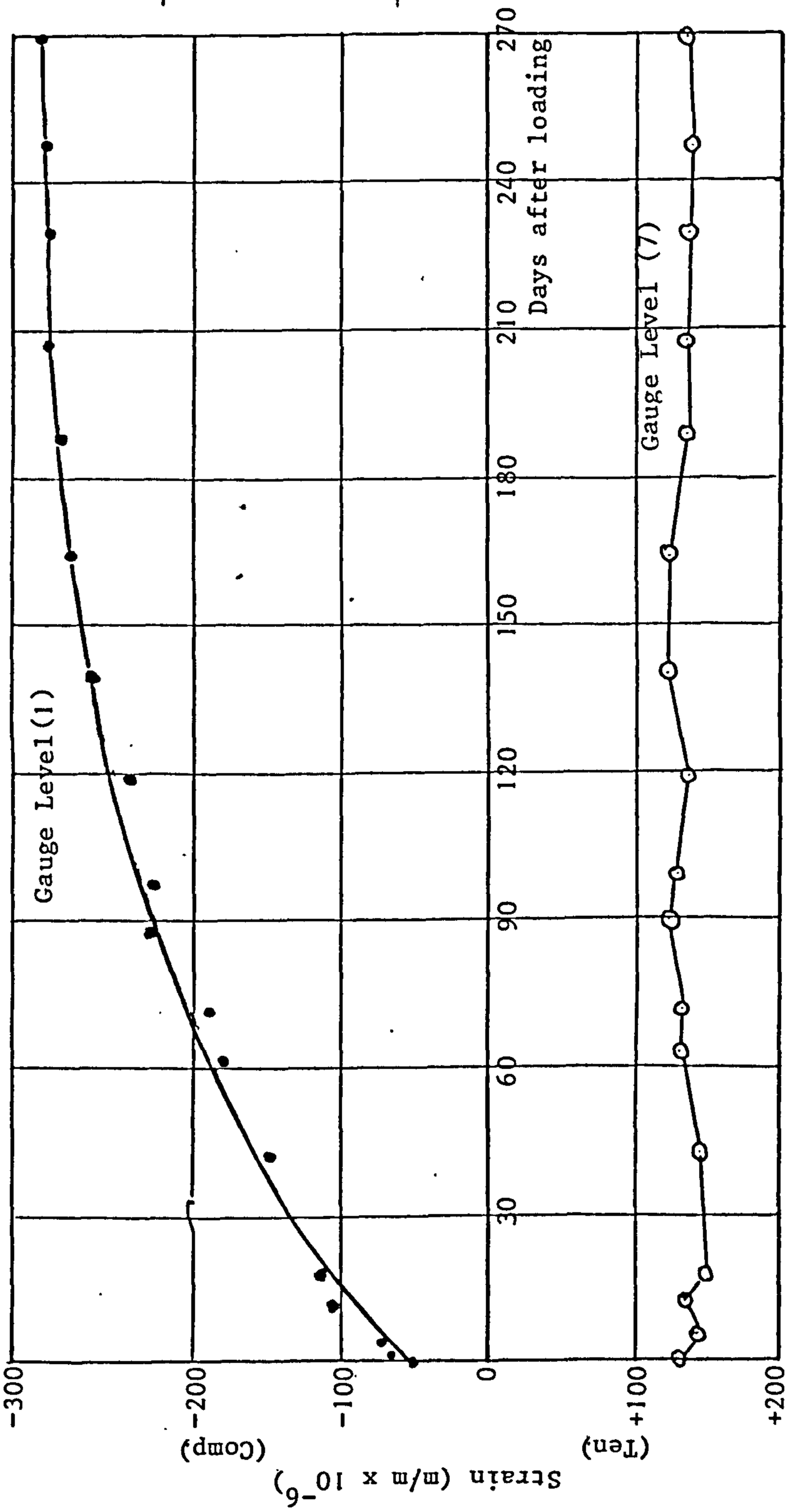

Graph 4.4 Measured concrete strains of reinforced concrete continuous beam at Sec. I-I i.e. sum of elastic, creep and shrinkage

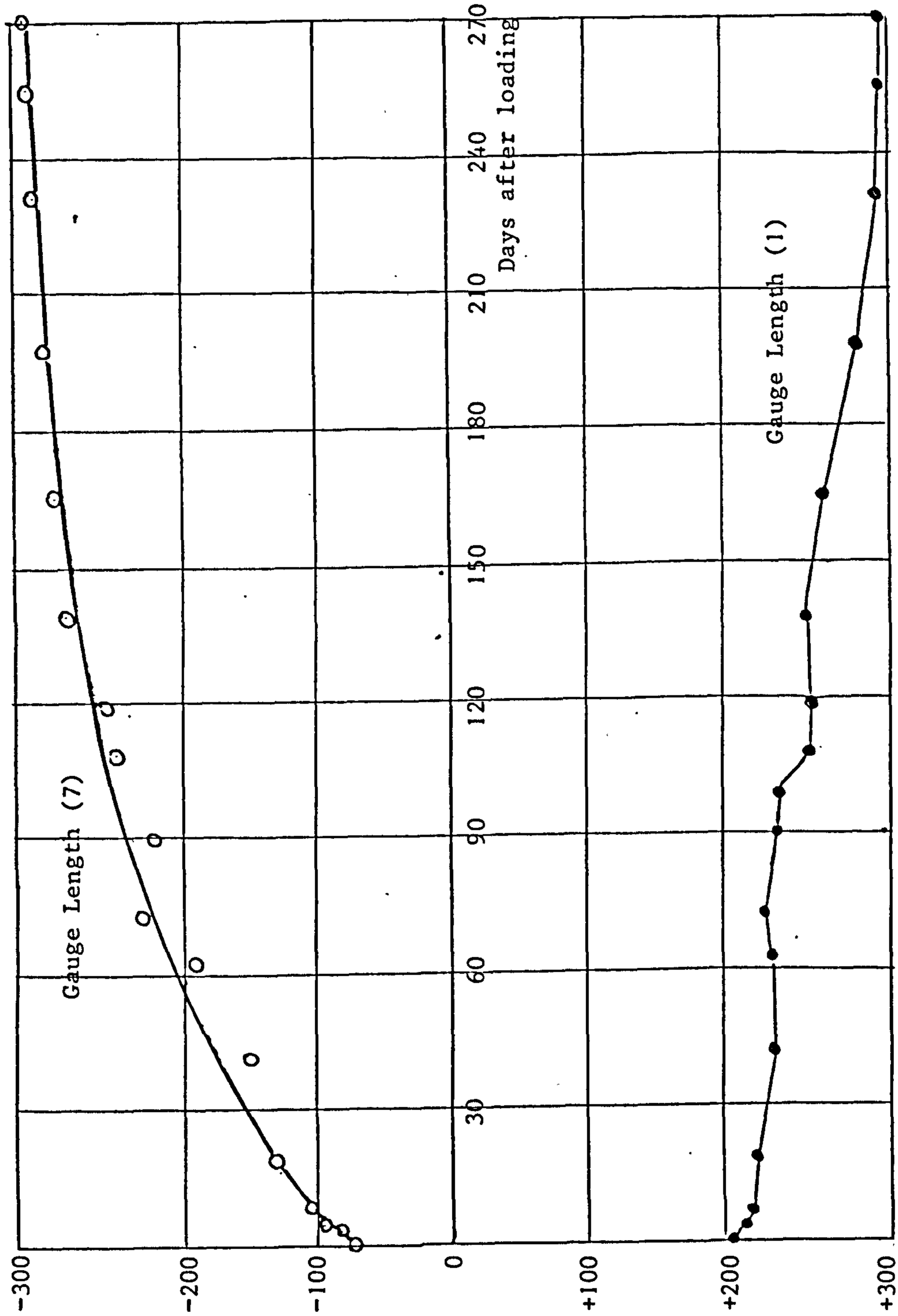

Graph 4.5 Measured concrete strains of reinforced concrete continuous beam at Section II-II i.e. sum of elastic, creep and shrinkage

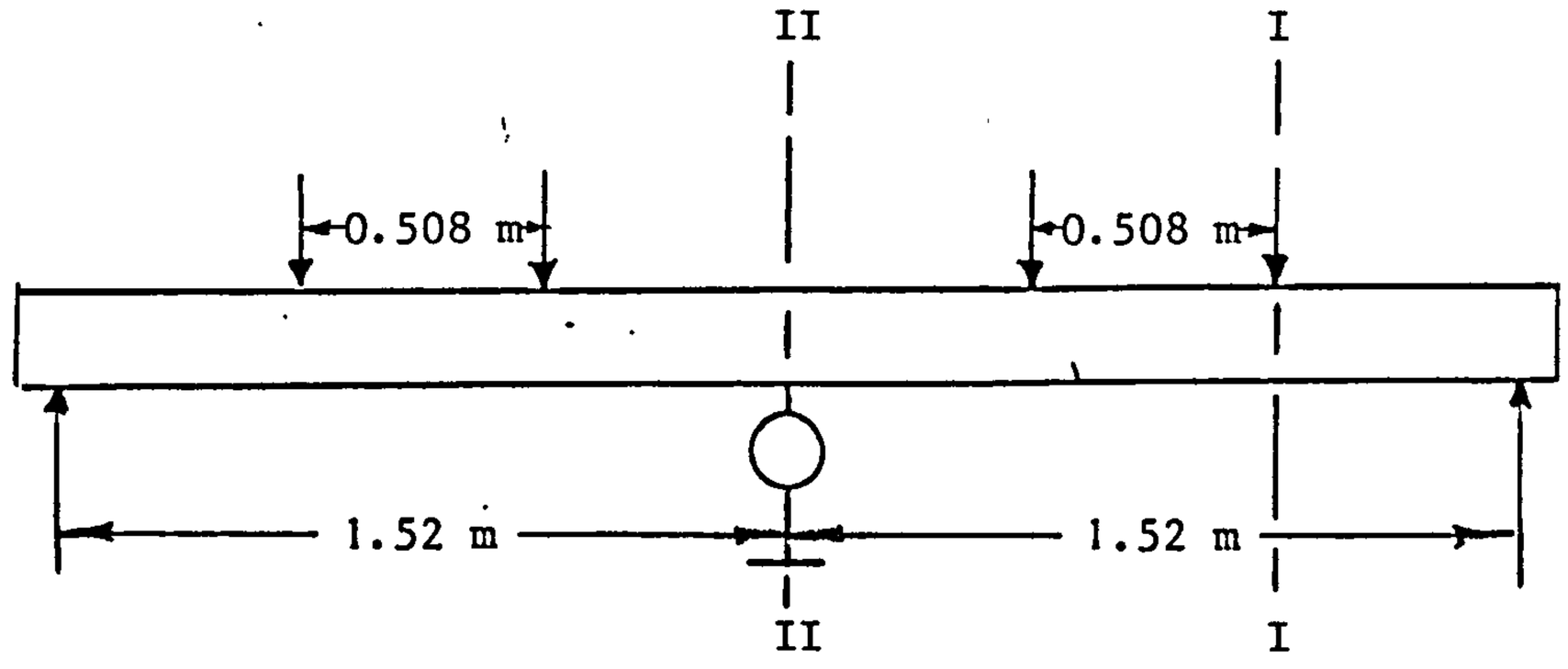

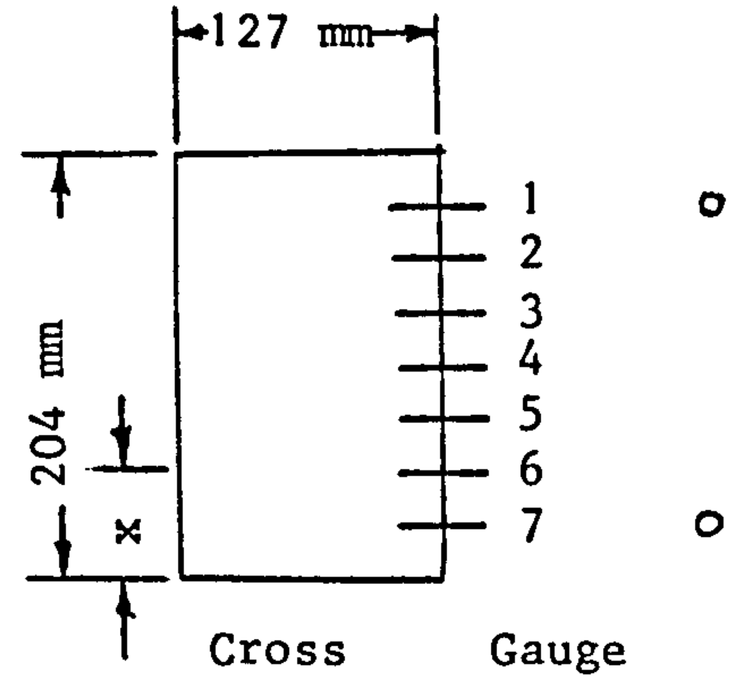

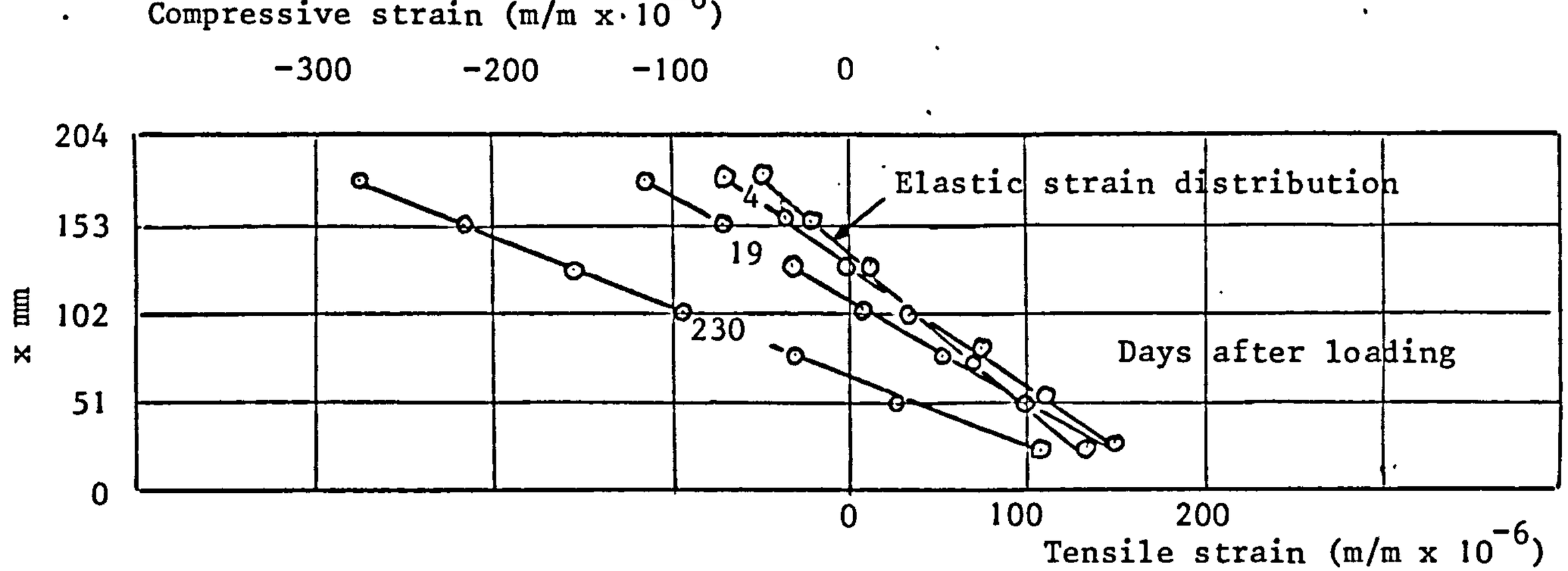

Graph 4.6 Measured strain distributions (elastic, creep and shrinkage) of reinforced concrete continuous beam at Sec. I-I gauge lengths with time

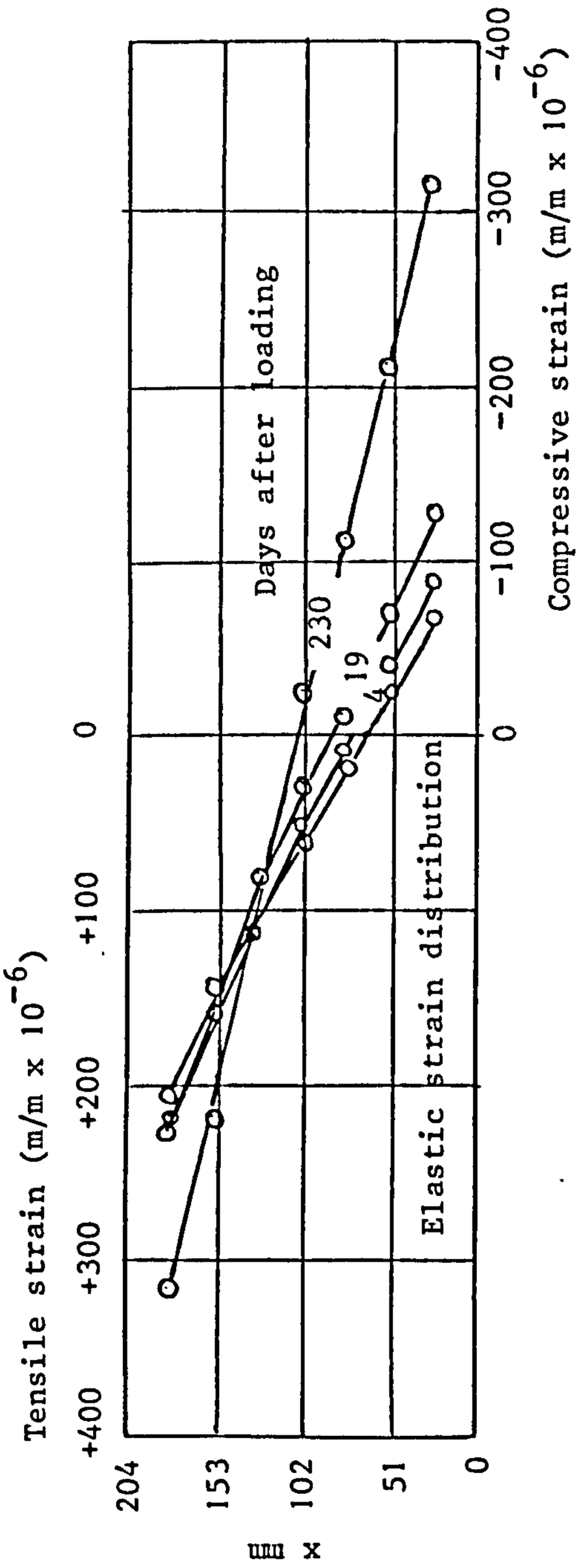

Graph 4.7 Measured strain distributions (elastic, creep and shrinkage) of reinforced concrete continuous beam at Sec. II-II gauge lengths with time

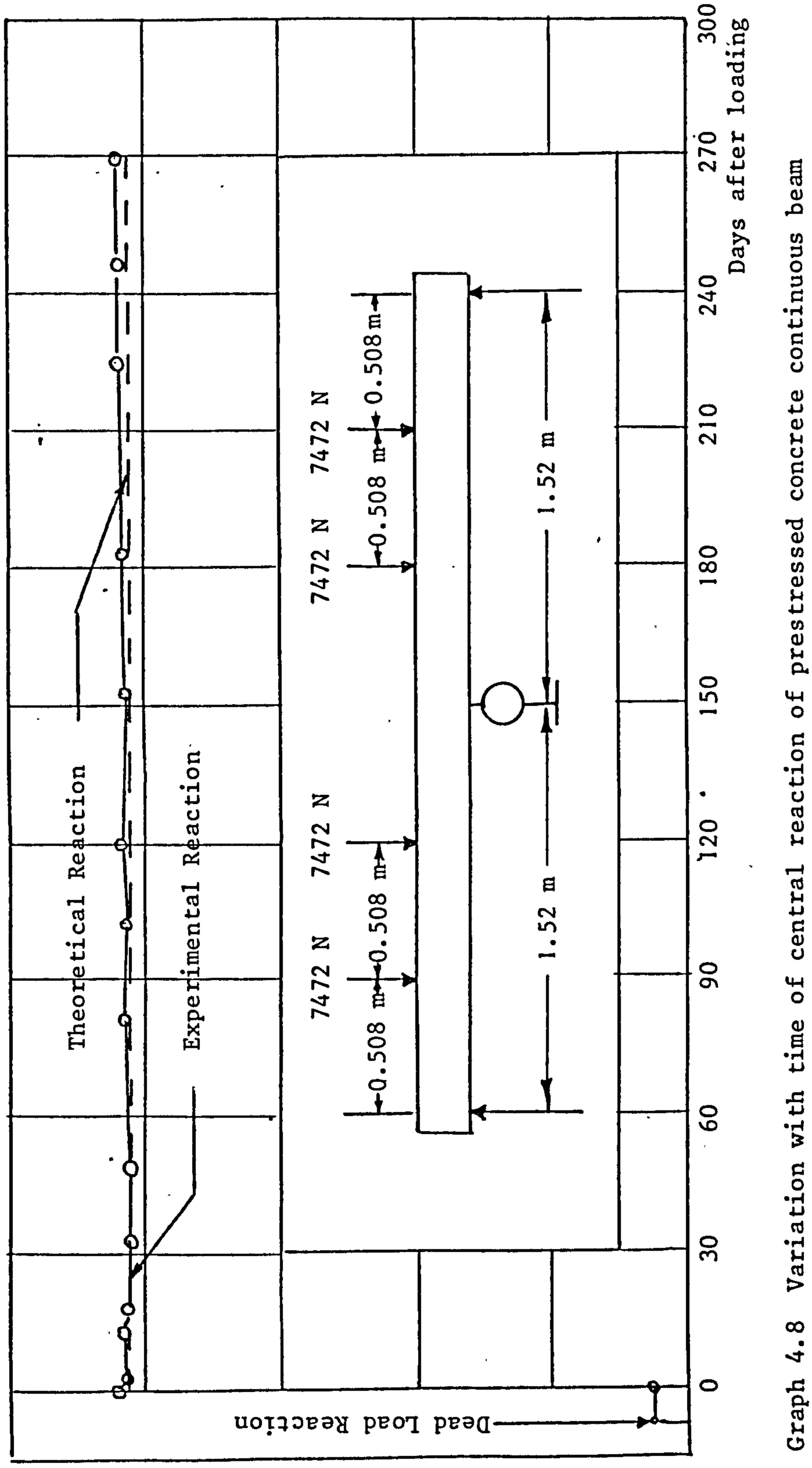

Graph 4.8 Variation with time of central reaction of prestressed concrete continuous beam

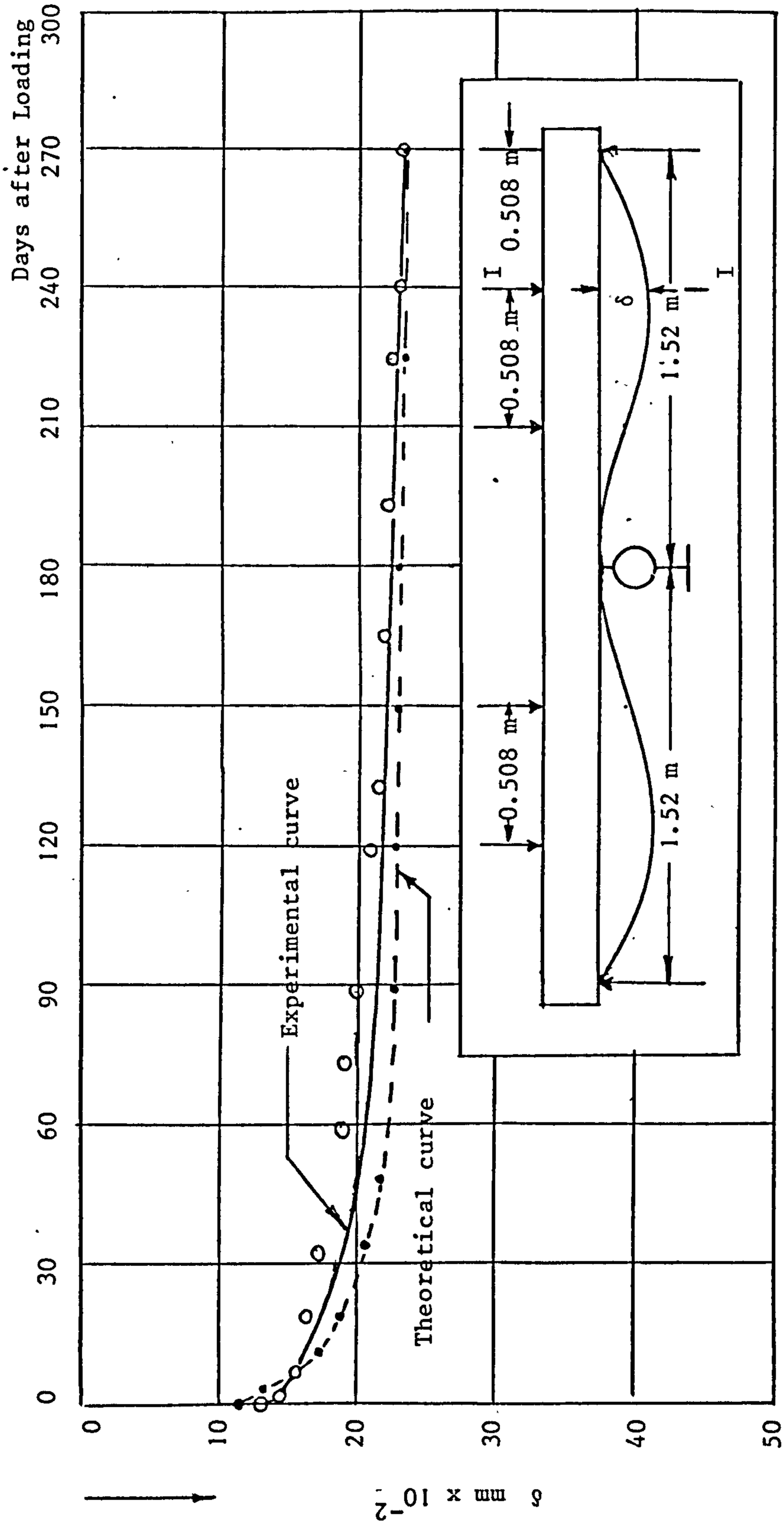

Graph 4.9 Time deflection behaviour at Sec. I-I of prestressed concrete continuous beam

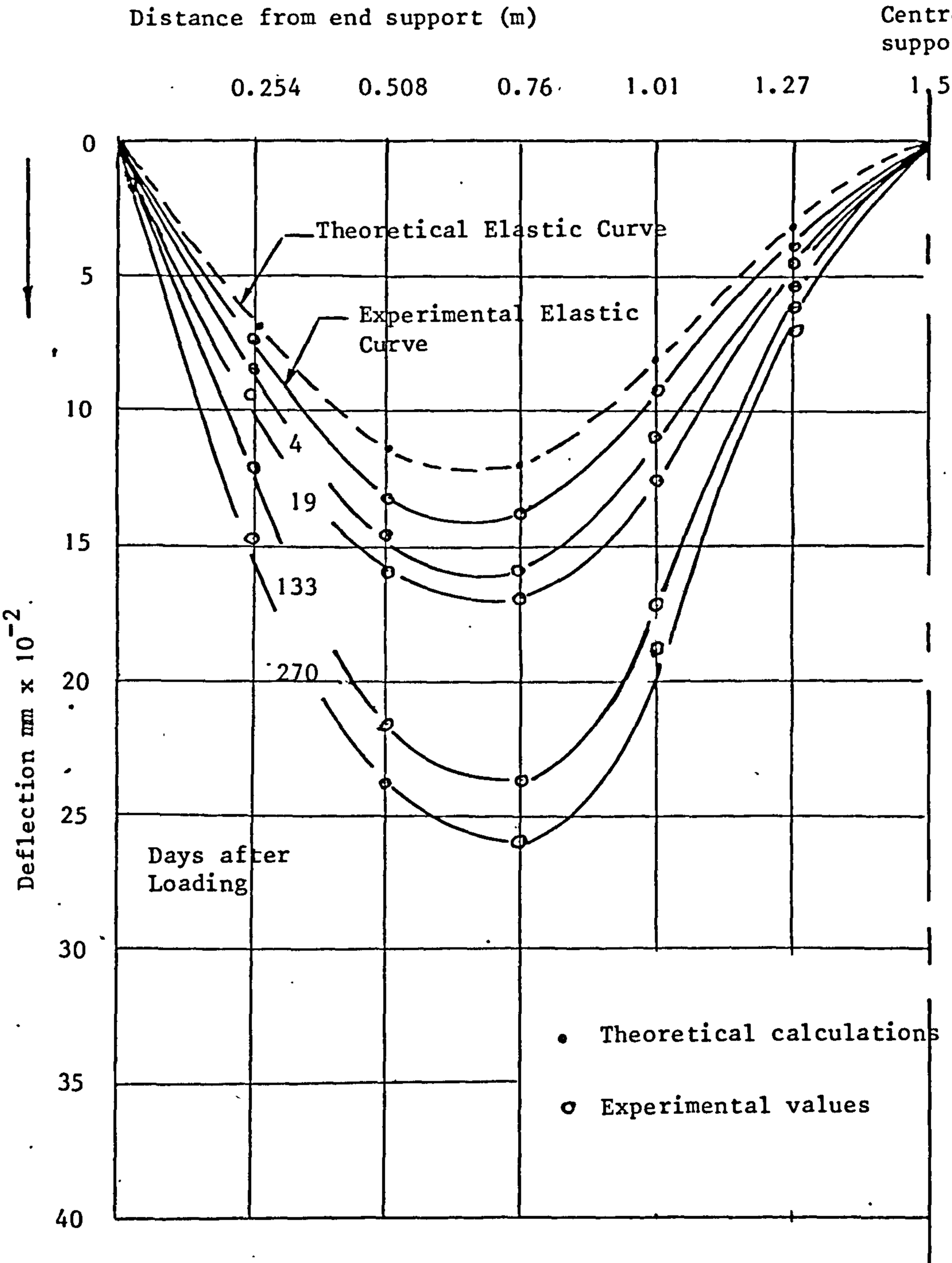

Graph 4.10 Deflection profile of prestressed concrete continuous beam after loading

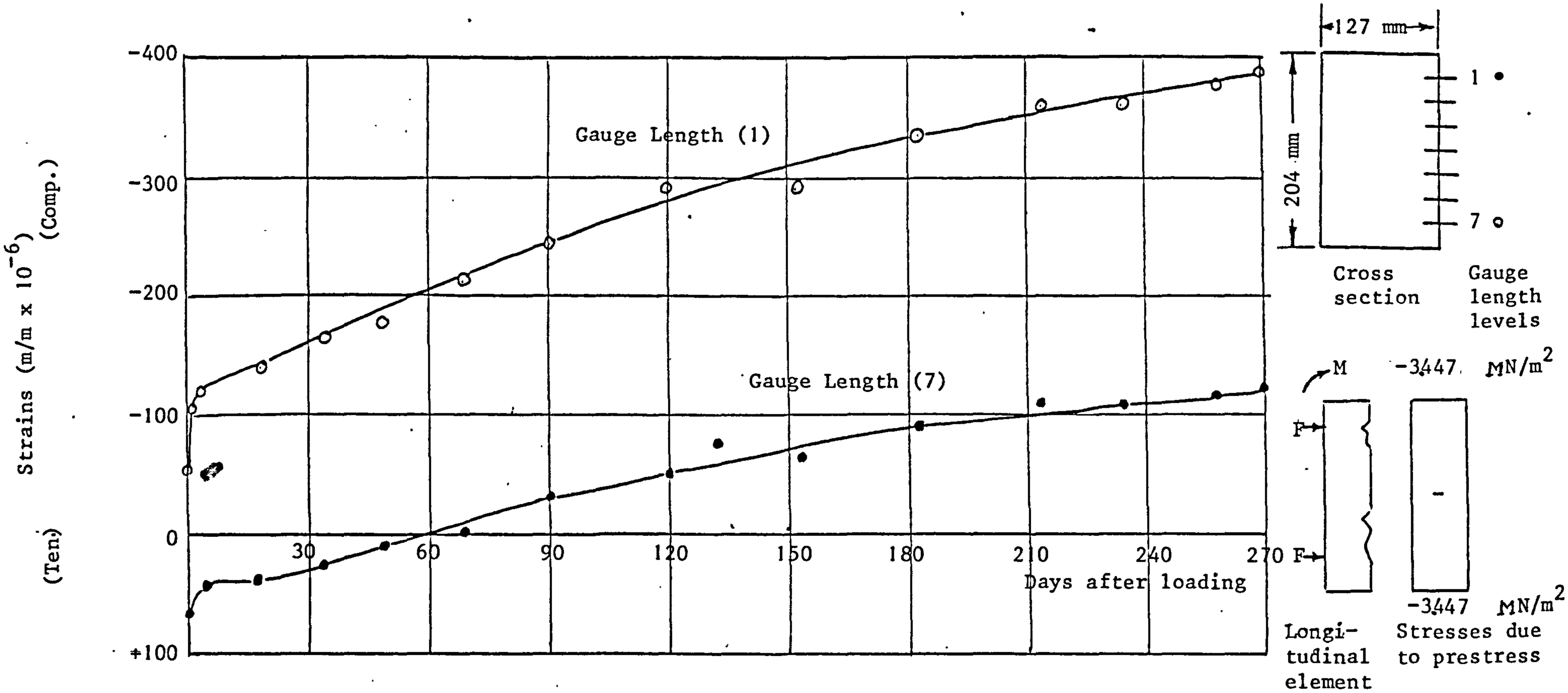

Graph 4.11 Measured concrete strains of prestressed concrete continuous beam at Section I-I i.e. sum of elastic, creep and shrinkage, after loading only

F = Prestressing Force
M = Applied bending moment = 2523.8 Nm

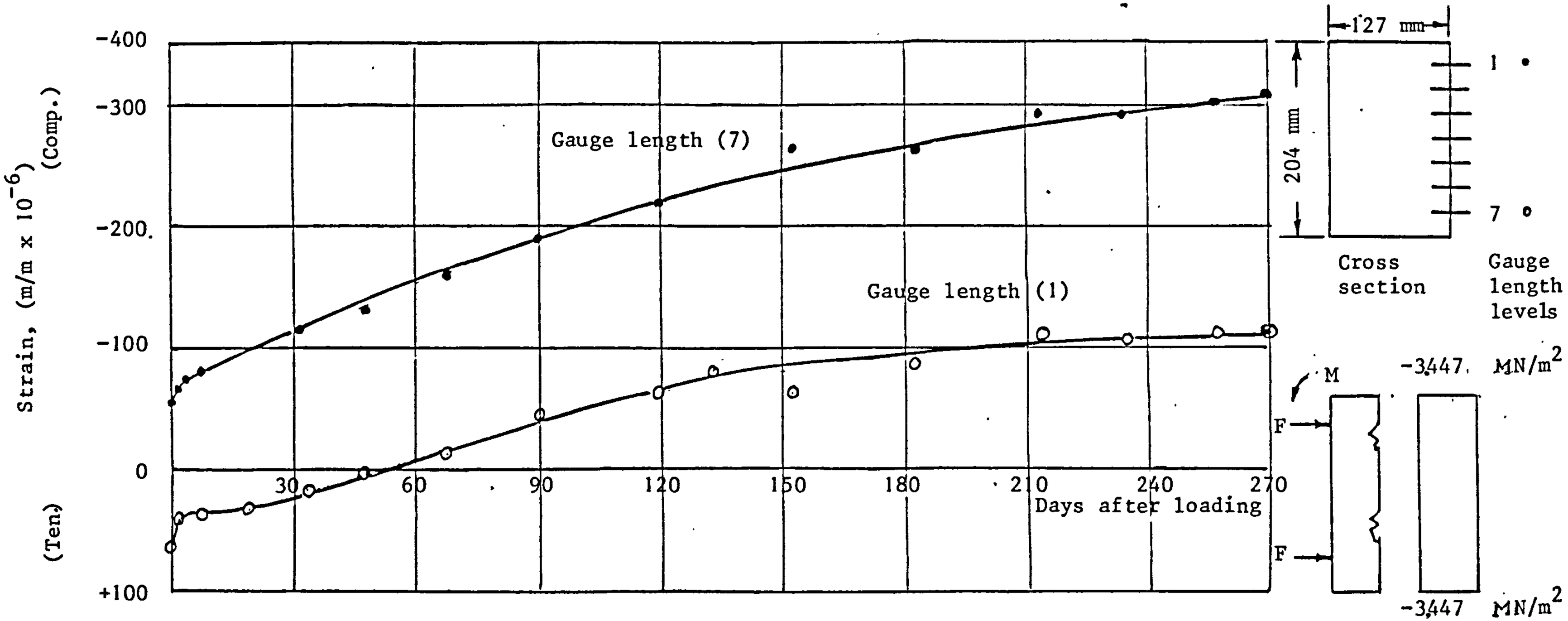

Graph 4.12 Measured concrete strains of prestressed concrete continuous beam at Sec. II-II i.e. sum of elastic, creep and shrinkage, after loading only

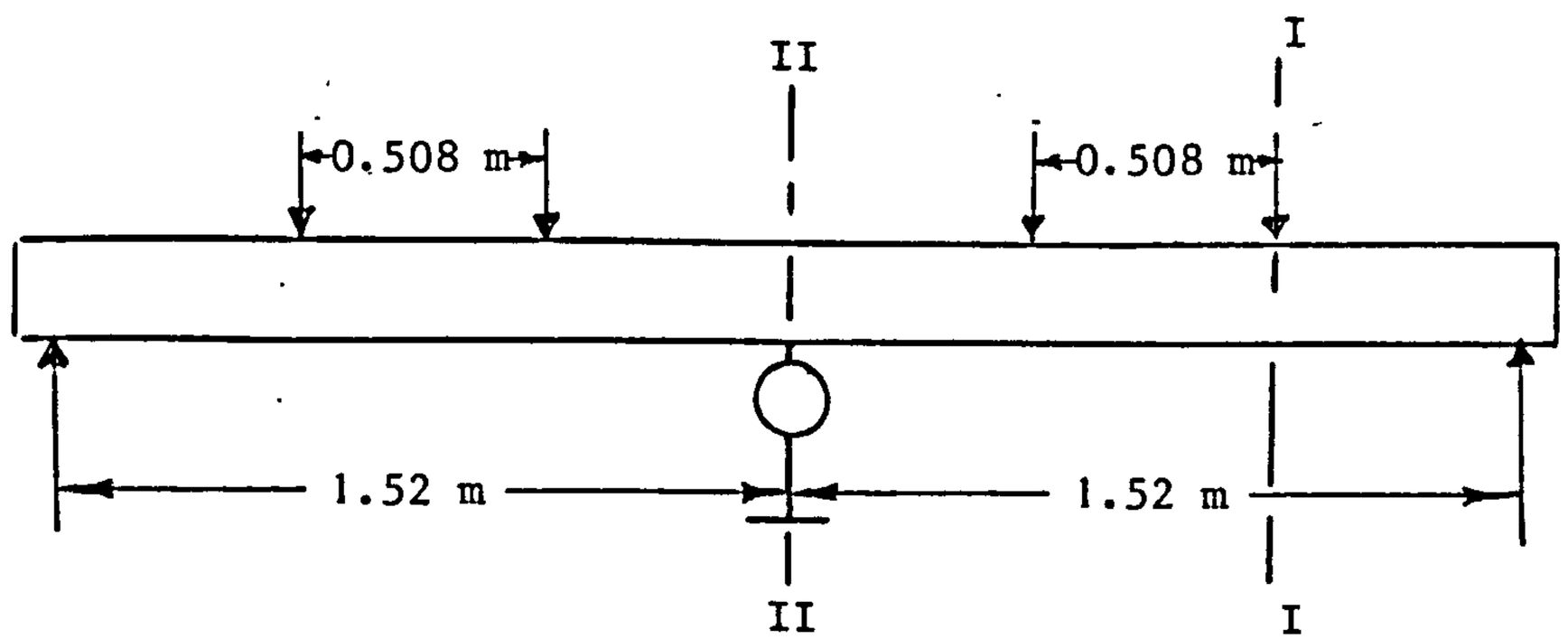

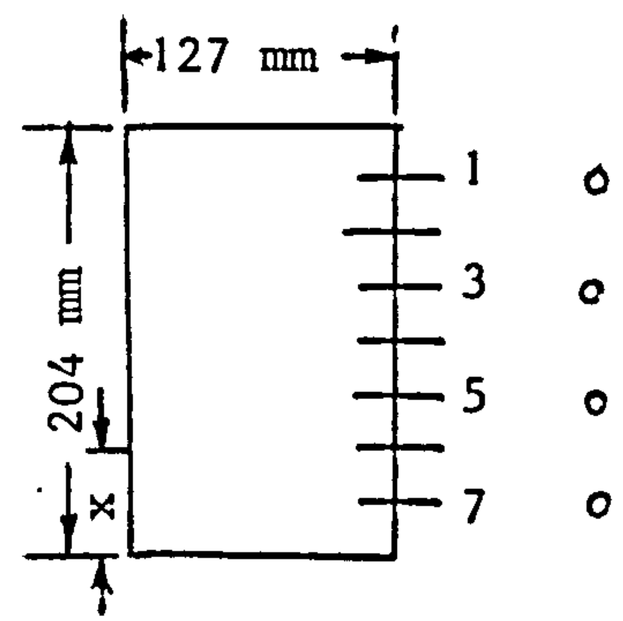

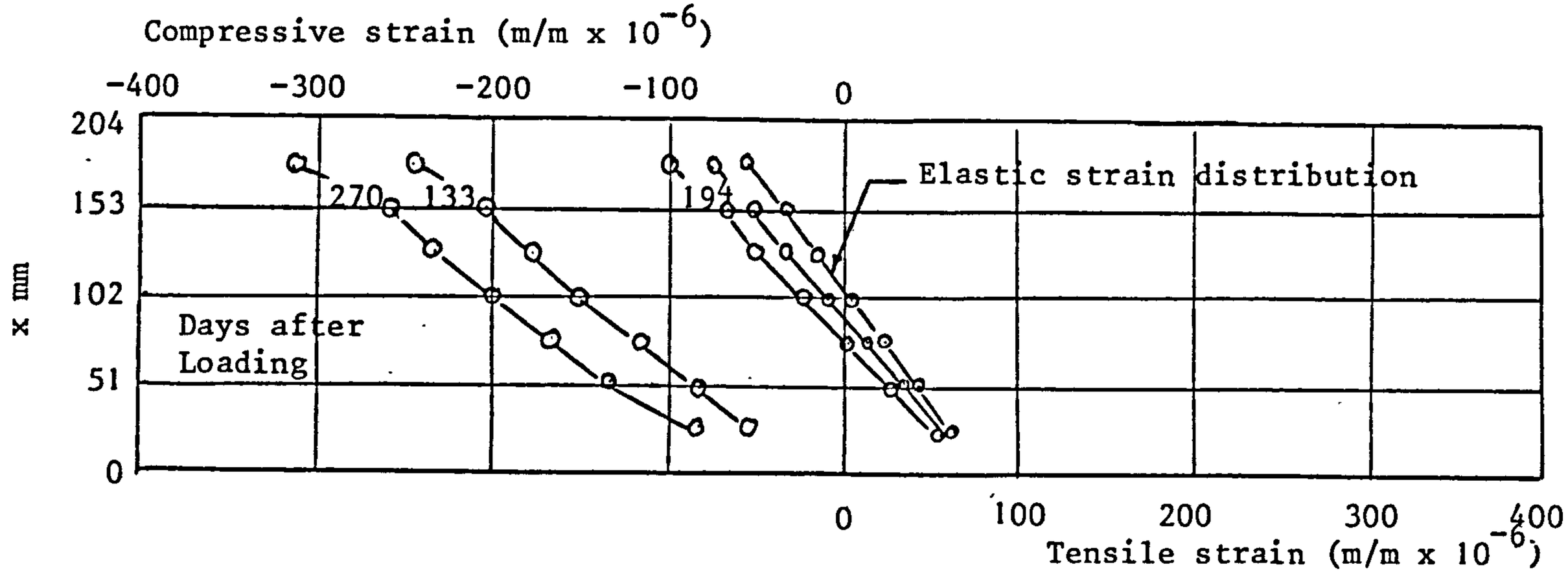

Graph 4.13 Measured strain distribution (elastic, creep and shrinkage) of prestressed concrete continuous beam at sec. I-I gauge lengths with time

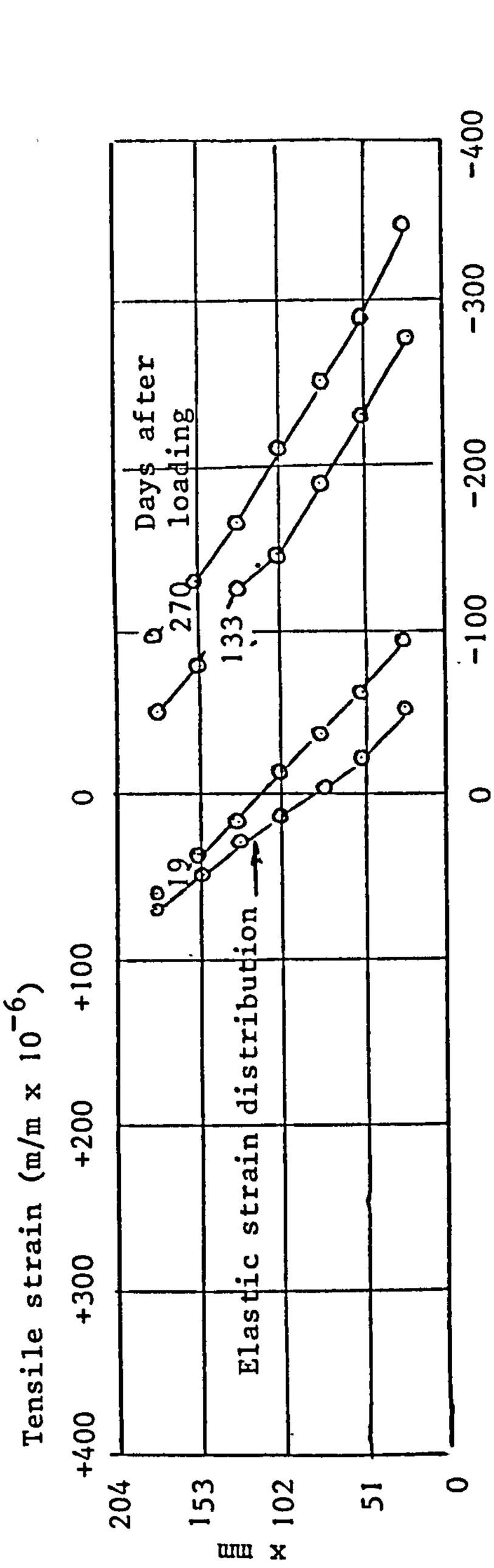

Graph 4.14 Measured strain distributions (elastic, creep and shrinkage) of prestressed concrete continuous beam at sec. II-II gauge lengths with time

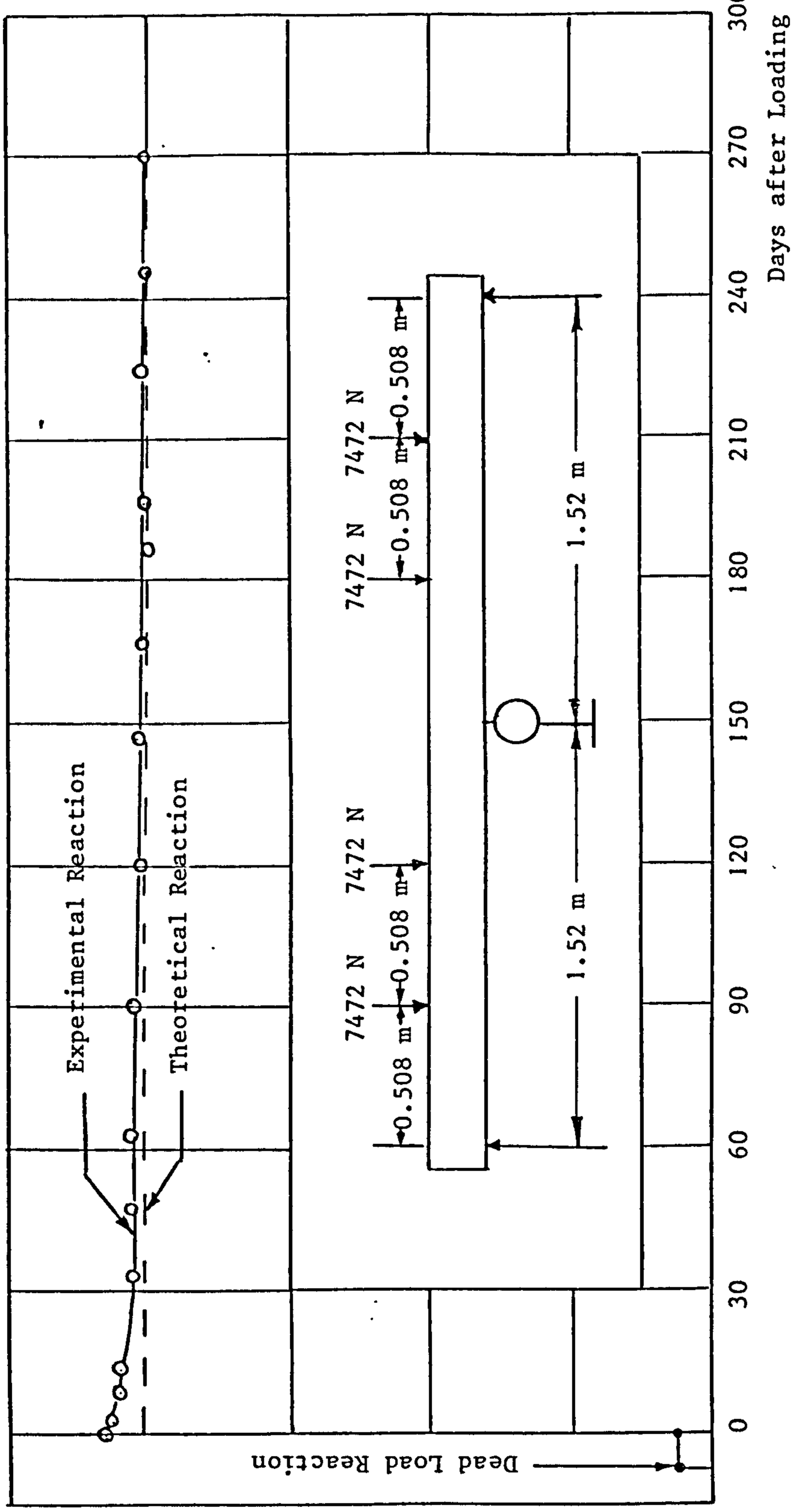

Graph 4.15 Variation with time of central reaction of composite prestressed concrete continuous beam

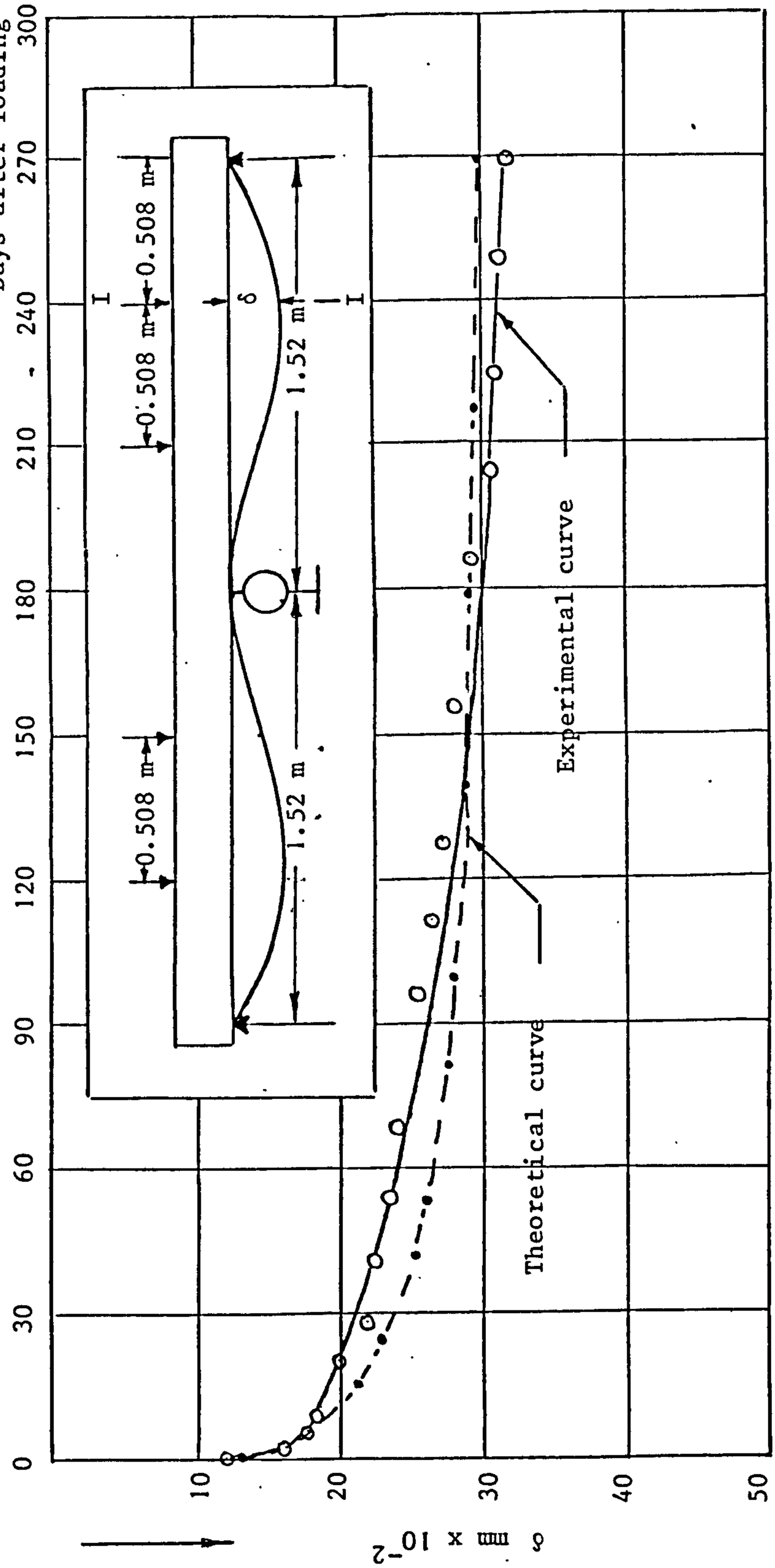

Graph. 4.16 Time deflection behaviour at Sec. I-I of composite prestressed concrete continuous beam

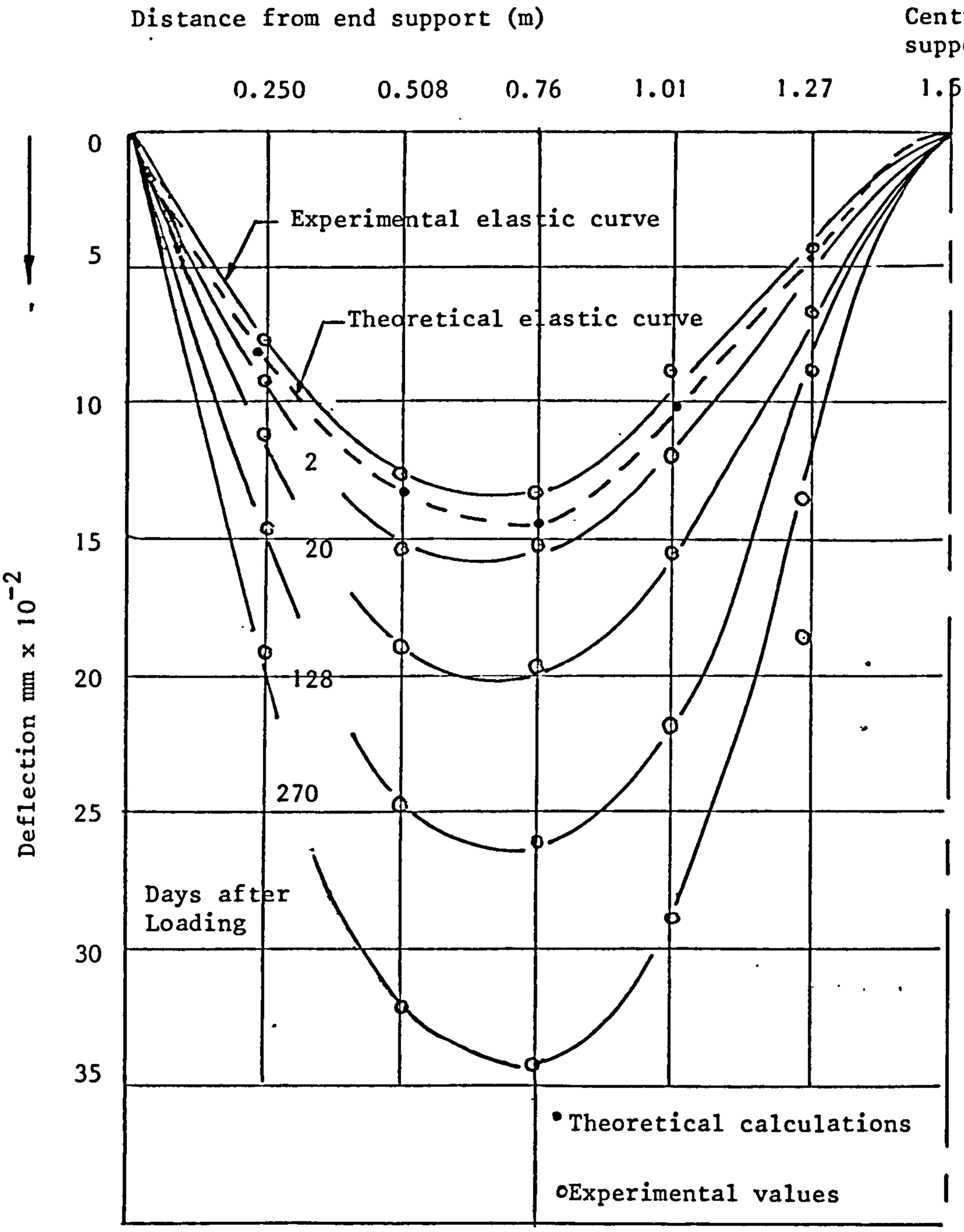

Graph 4.17 Deflection profile of composite prestressed concrete continuous beam after loading

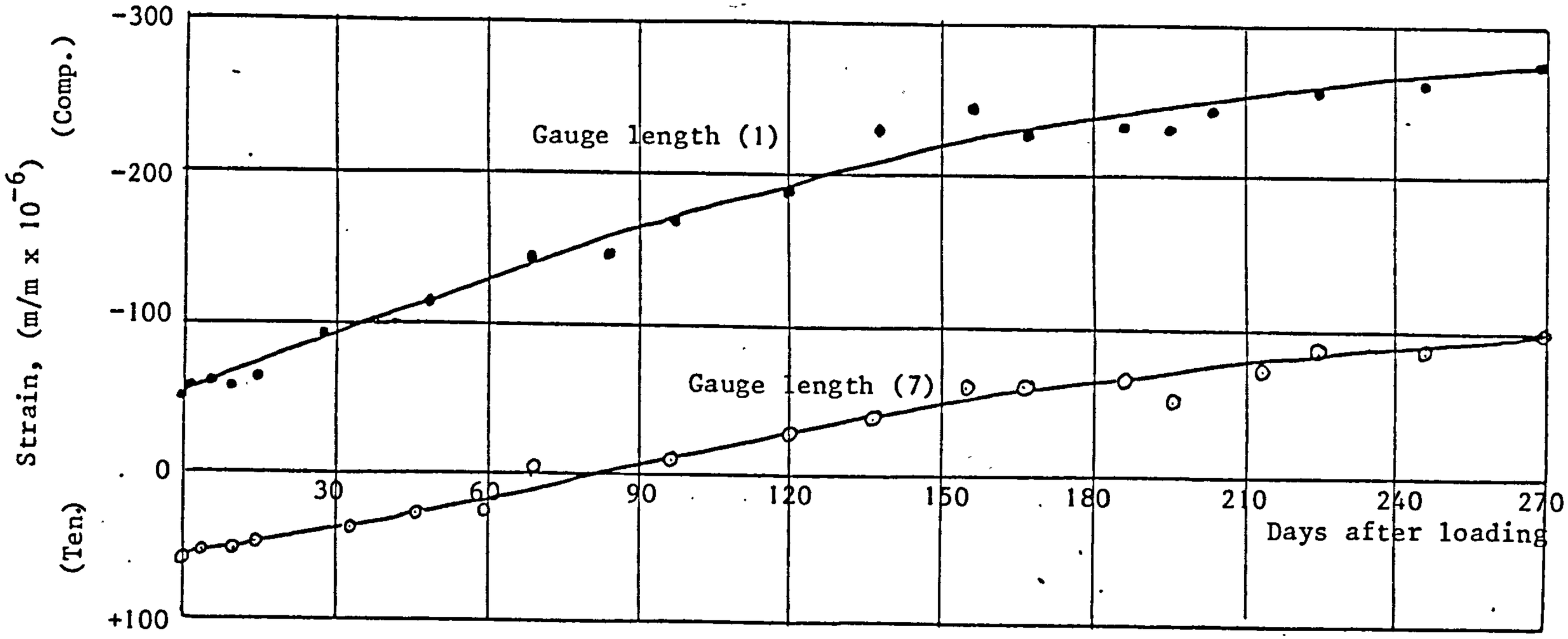

Graph 4.18 Measured concrete strains of composite prestressed concrete continuous beam at Sec. I-I i.e. sum of elastic, creep and shrinkage, after loading only

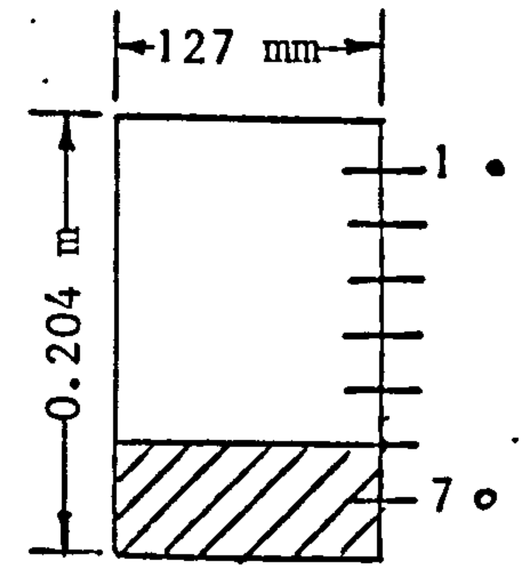

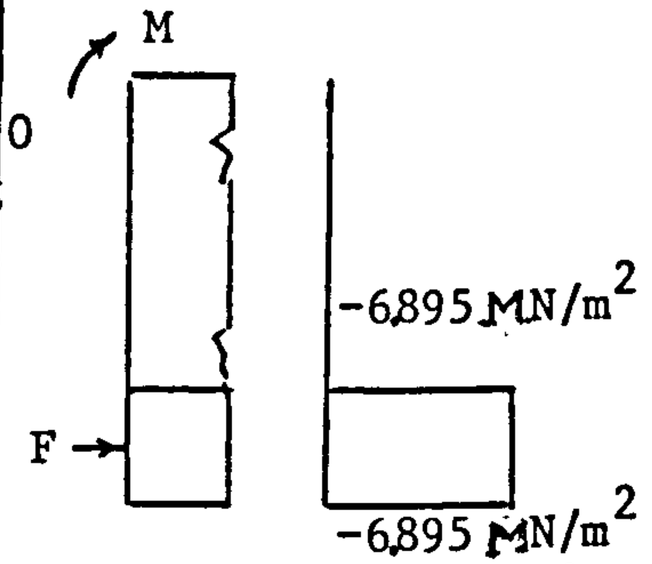

F = Prestressing force
M = Applied bending moment

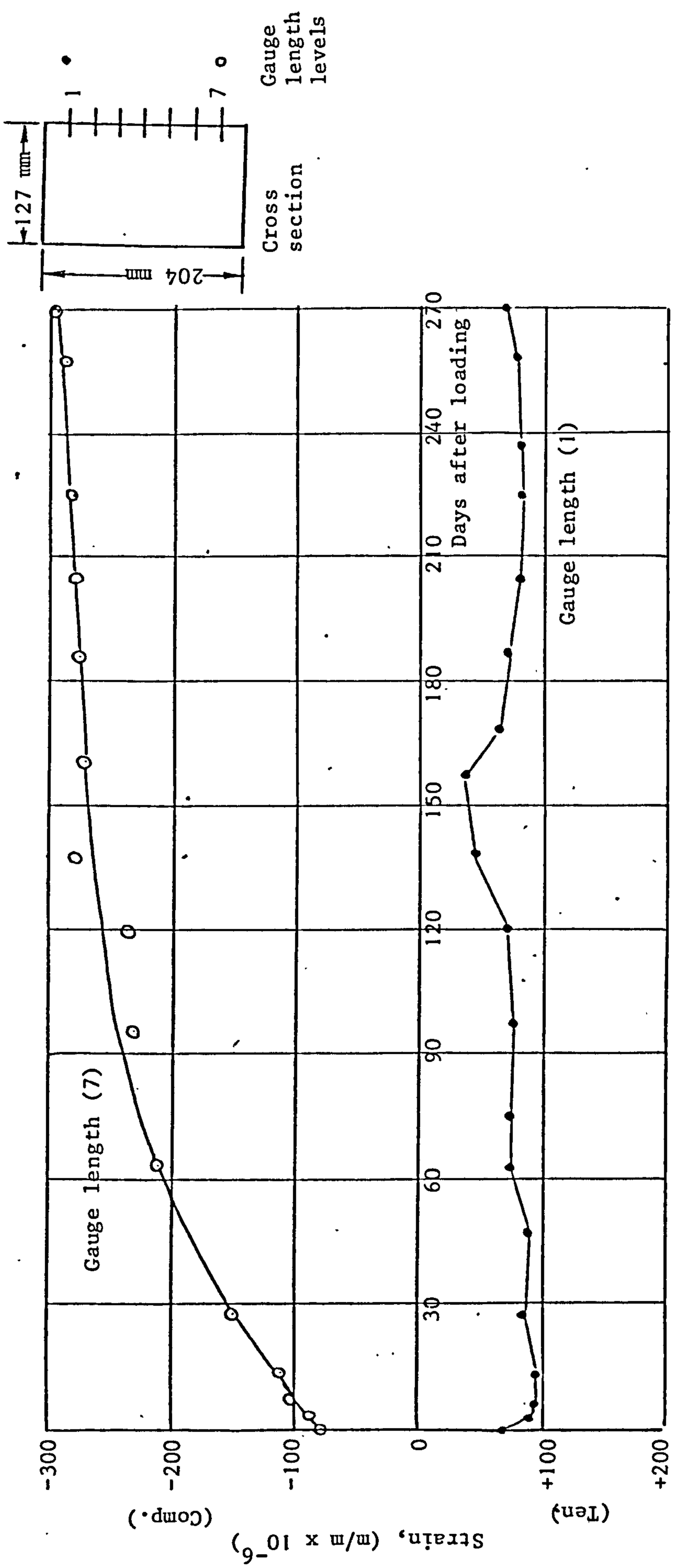

Graph 4.19 Measured concrete strains of composite prestressed concrete continuous beam at Sec. II-II i.e. sum of elastic, creep and shrinkage, after loading only

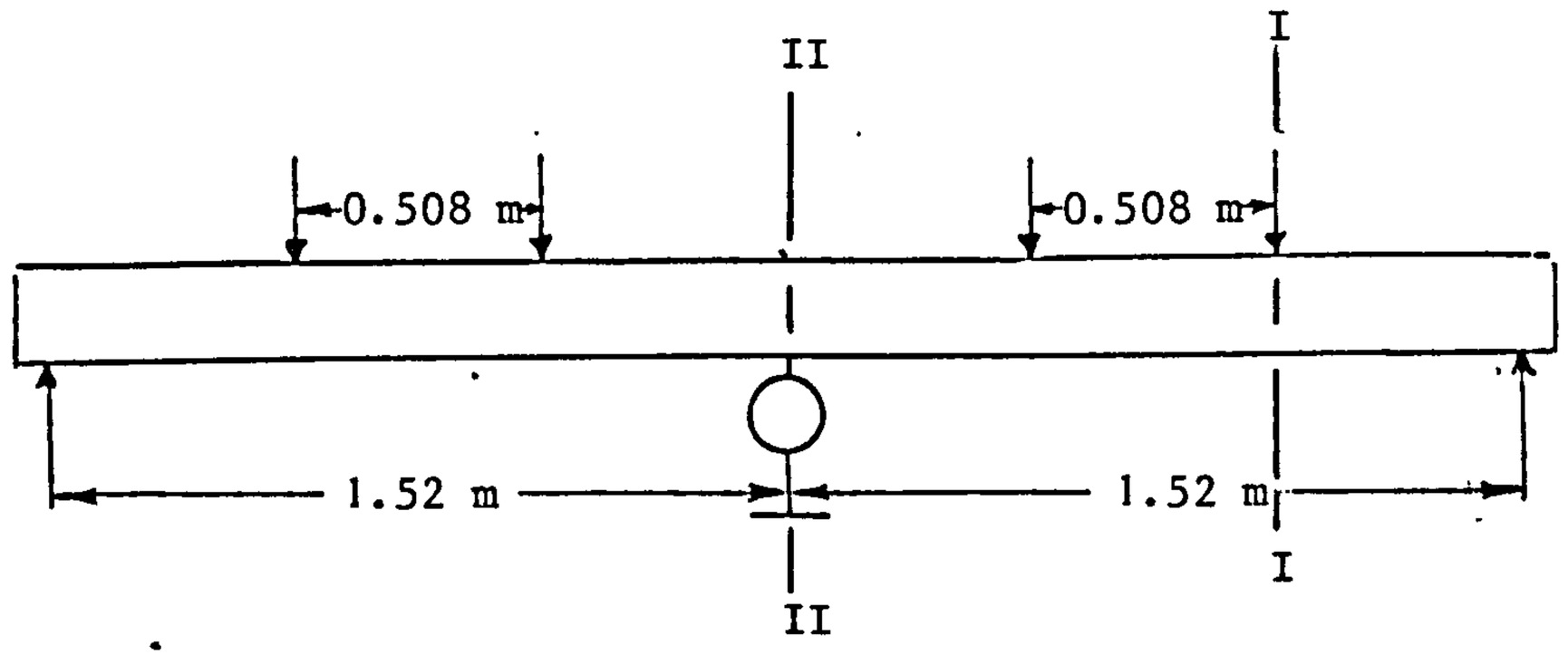

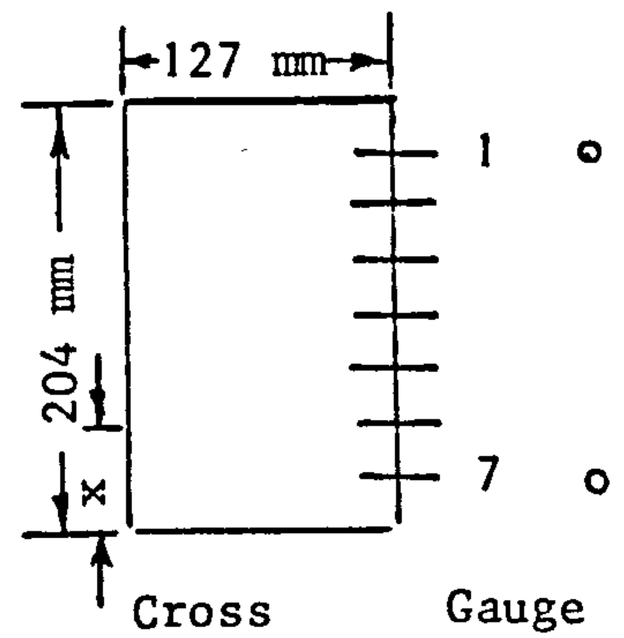

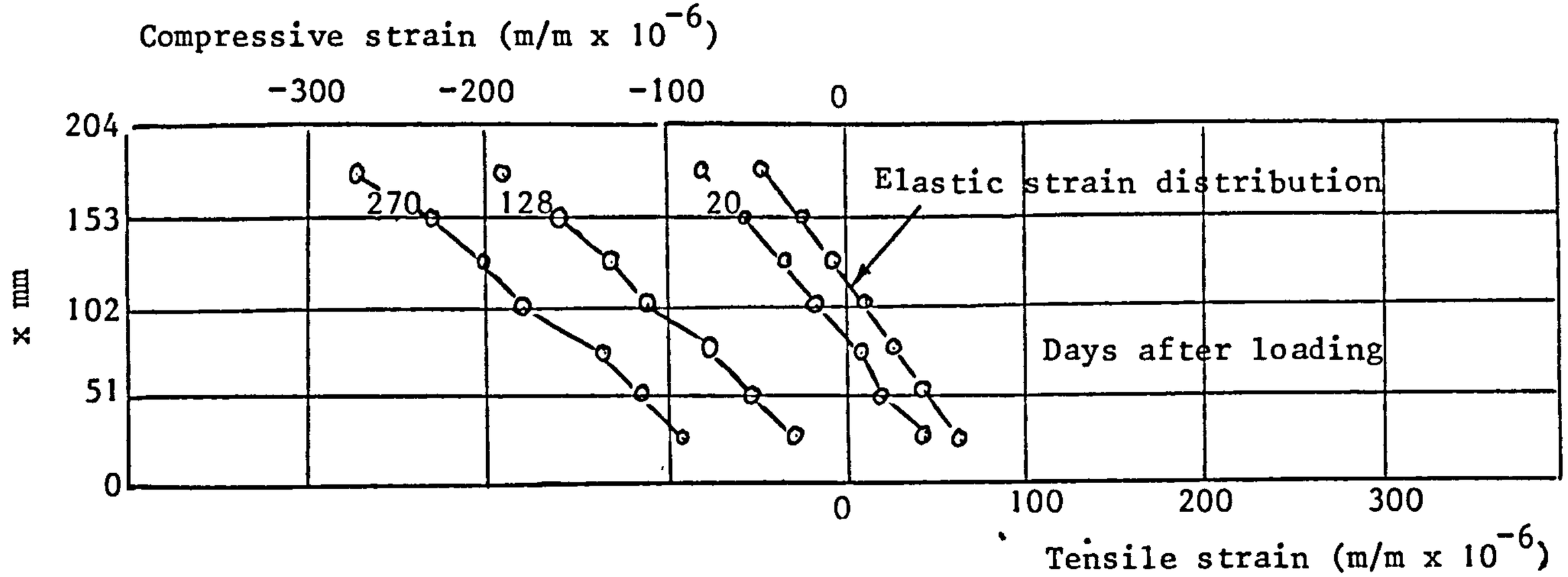

Graph 4.20 Measured strain distributions (elastic, creep and shrinkage) of composite prestressed concrete continuous beam at section I-I gauge length with time

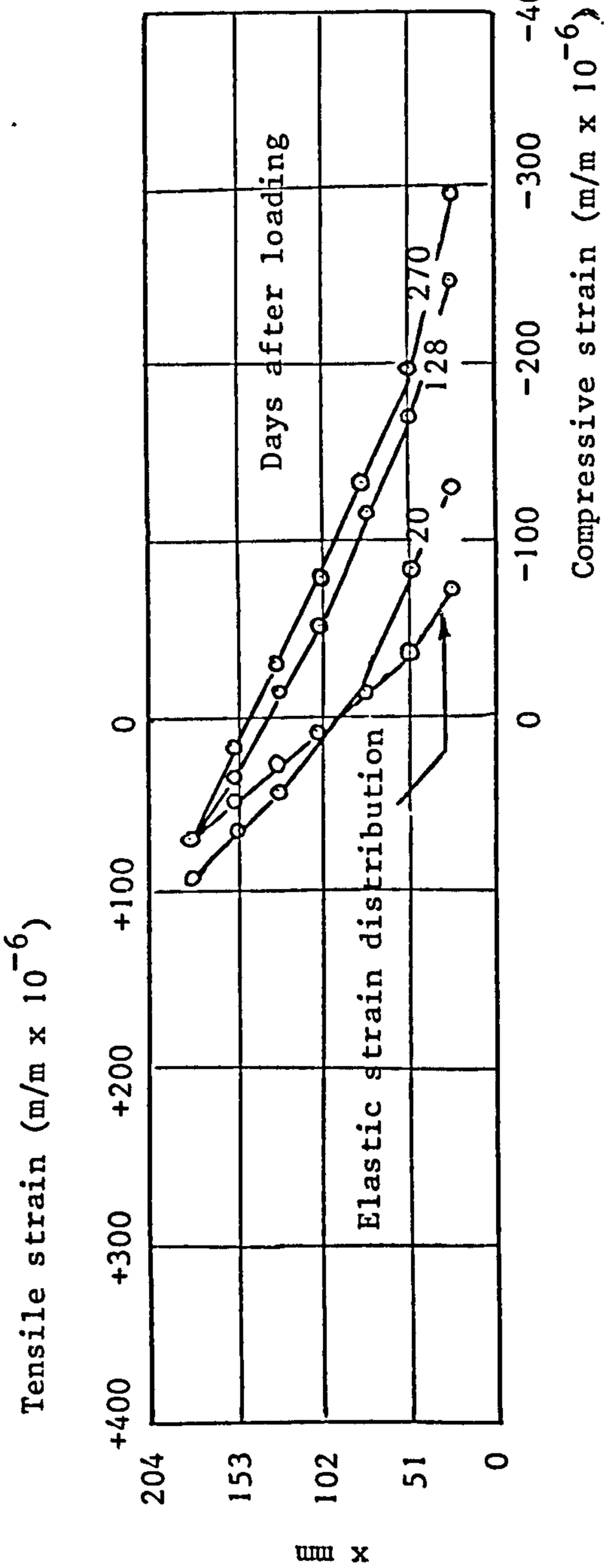

Graph 4.21 Measured strain distributions (elastic, creep and shrinking) of composite prestressed concrete continuous beam at Sec. II-II
Gauge lengths with time

CHAPTER 5

Experimental work - creep and shrinkage tests on control specimens of concrete cylinders, plain concrete and pre-stressed concrete planks - mixes A and B.

5.1 SYNOPSIS

Experimental studies on long-term behaviour at laboratory temperature of plain concrete cylinders and planks(the same dimensions as used in the experimental beams),Mix A, plain and prestressed concrete planks, Mix B, are reported.

Test results of two plain concrete planks and six cylinders Mix A prqportions are reported , one plain and one prestressed concrete plank Mix B proportions are presented.

In order to follow the stressing procedure of the tested concrete beams, long-term tests on concrete cylinders were carried out at an age of 35 days and at 7 days on prestressed concrete plank.

5.2 INTRODUCTION

The principal object of the investigation was to obtain creep and shrinkage strains for concrete subjected to known constant stress and using this creep data in the theoretical prediction of long-term behaviour of the three types of concrete beams. Six cylinders 113 mm in diameter and 304 mm long were tested for creep and shrinkage of concrete Mix A. Three of the above cylinders were subjected to constant stress of 6.895 MN/m^2 after 35 days from casting. Two concrete planks Mix A proportions 51 x 127 mm in cross section and 1.67 metres long were tested for shrinkage only. The top surface of one of the planks was sealed at an age of 24 hours in order to follow the casting procedure of the composite beam. Two concrete planks same dimensions as the previous planks were tested for creep and shrinkage of concrete Mix B proportions, one of the planks was pretensioned and subjected to constant stress of 6.895 MN/m^2 after 7 days from casting and the top surface was

sealed at an age of 14 days in order to follow the casting procedure of the cast in place portion of the composite beam.

5.3 SPECIMENS AND DETAILS OF CONCRETE MIXES

5.3.1 Mix

The Mix proportions were the same as the tested concrete beams of Chapter 2 (see art. 2.1.3.2).

5.3.2 Casting

The cylinders and planks were cast on a vibrating table. The concrete in the cylinder moulds was vibrated in 50 mm layers and was filled to 6 mm below the top of the moulds. This 6 mm gap was later filled with a neat cement paste which provided a flat surface after careful finishing with a trowel. The concrete in the plank's mould was vibrated in 25 mm layer and after filling the mould the surface was finished flat with a trowel.

5.3.3 Strain Measurement Points

Concrete cylinder strain was measured along 203 mm gauge lengths spaced at 120^{o} apart by the Demec strain gauge. Knurled brass knobs, internally threaded were cast into the concrete. 25 mm Long brass studs with Demec holes drilled at their ends were then inserted into the insets. Concrete plank strain was measured along twelve 203 mm gauge lengths from each side (see fig. in Graph 5.6) with surface studs stick to concrete.

5.4 TESTING APPARATUS

Photo 5.1 shows concrete cylinder specimens under test at laboratory temperature. The load was applied by three 12 mm diameter medium

tensile steel rods which compressed the concrete specimen and a mild steel tube. The steel tube was previously calibrated so that the applied stress of 6.895 MN/m^2 due to applied load could be obtained. A more detailed account of the testing apparatus has been reported elsewhere[34].

Photo 5.2 shows concrete plank specimens under test at laboratory temperature. The load on the prestressed plank was applied at an age of 7 days by means of two prestressing wires, the stress on the plank due to the prestressing force was 6.895 MN/m^2.

5.5 TESTING PROCEDURE

Tests were carried out at laboratory temperature. In order to follow the stressing procedure of the tested concrete beams, three cylinders were stressed to 6.895 MN/m^2 at 35 days after casting and the pre-stressed plank was stressed to 6.895 MN/m^2 at 7 days after casting. Loads were sustained up to an age of 300 days. Three cylinders were shrinkage control specimens for the loaded cylinders, one concrete plank was the shrinkage control specimen for the prestressed plank. The top surface of the prestressed plank was sealed after 14 days from casting in order to follow the casting procedure of the cast in place portion of the composite beam.

5.6 RESULTS

5.6.1 Strains of Loaded Specimens

Long term strain variation with time for concrete cylinders Mix A proportions under a stress of 6.895 MN/m^2 is plotted in Graph 5.1.

Graph 5.2 shows the long-term strain variation with time for prestressed concrete plank Mix B proportions under a stress of 6.895 MN/m^2.

5.6.2 Strains of Control Specimens

Graph 5.3 shows the average shrinkage strains of three concrete cylinders same mix as the loaded cylinders and kept unloaded at room temperature.

Graph 5.4 shows the shrinkage strains of concrete plank same mix as the prestressed plank, the concrete plank kept in room temperature at the same conditions as the prestressed plank.

Graph 5.5 shows the shrinkage strains of a concrete plank the same mix as loaded cylinders.

Graph 5.6 shows the shrinkage strains of a concrete plank the same mix as loaded cylinders, top surface of the plank was sealed after 24 hours after casting.

From Graphs 5.1 and 5.3 we get Graph 5.7 which represents the specific creep curve of cylinders concrete Mix.A.

Graph 5.8 which represents the specific creep curve of prestressed concrete plank Mix B could be obtained from curves(a) and (b) in Graphs 5.2 and 5.4.

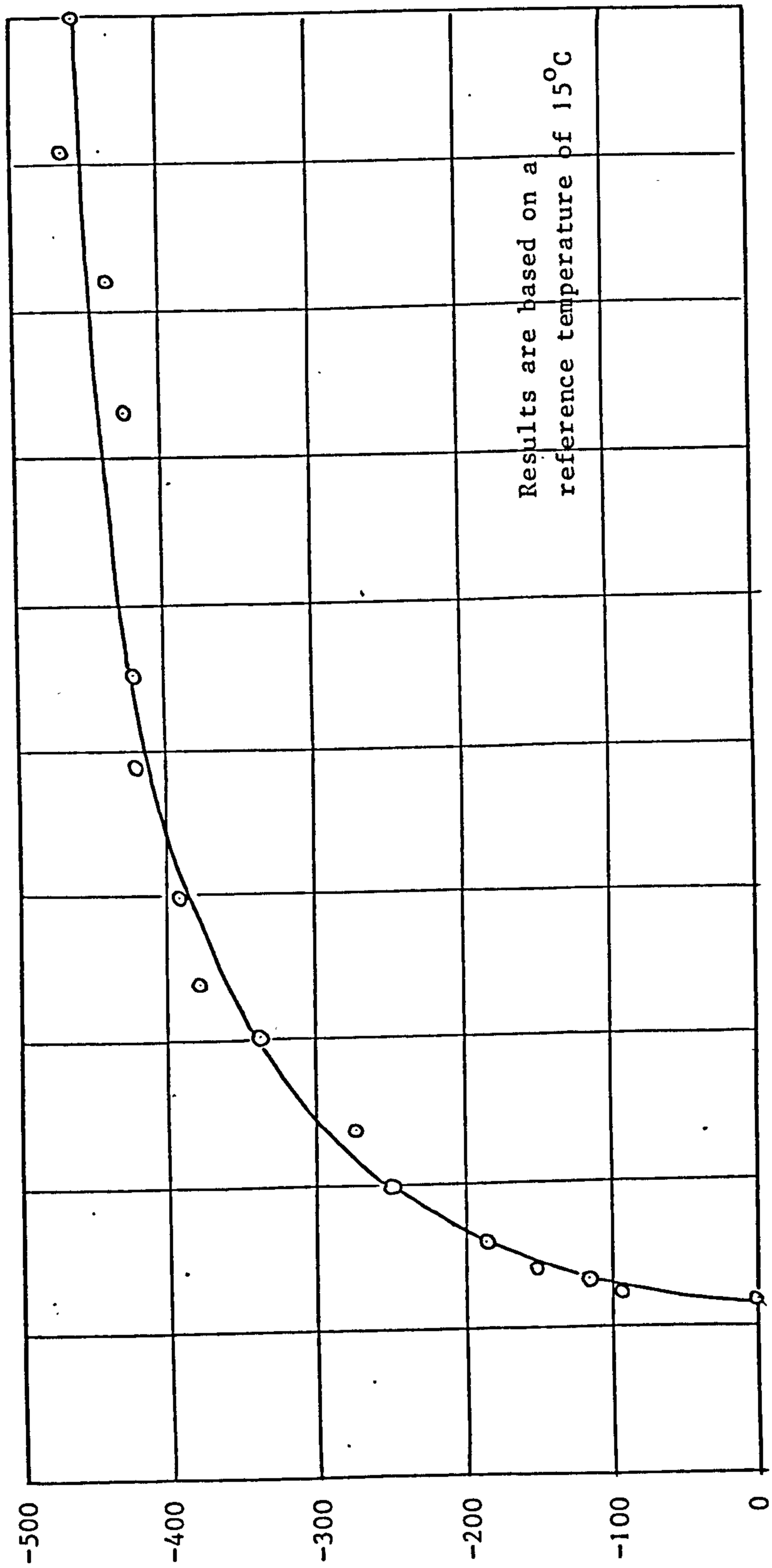

Graph 5.1 Measured concrete strains of concrete cylinders, loaded to 6895 MN/m^2 after 35 days from casting i.e. sum of creep and shrinkage - Concrete Mix A

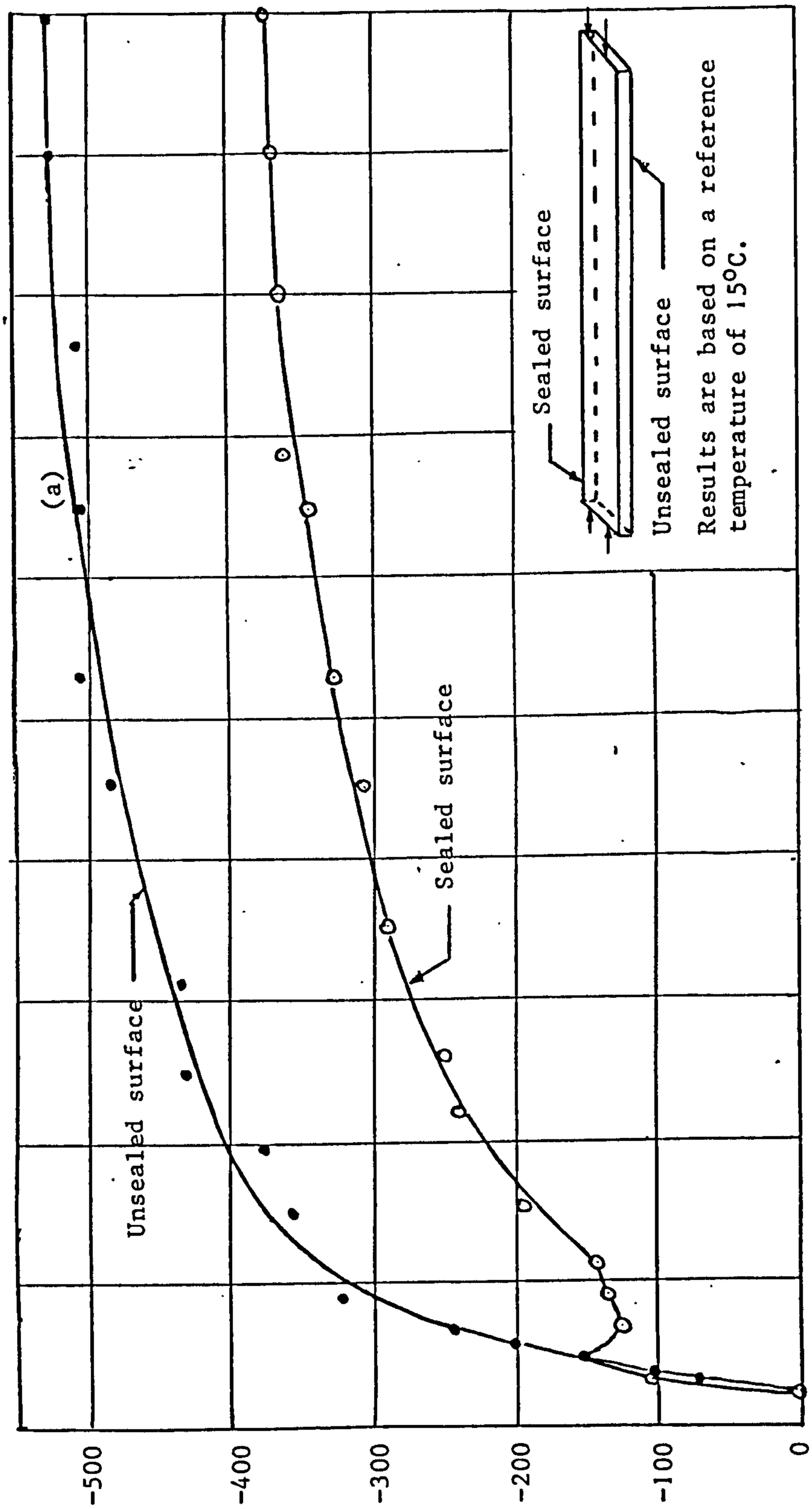

Graph 5.2 Measured concrete strains of prestressed concrete plank i.e. sum of creep and shrinkage - Concrete Mix B

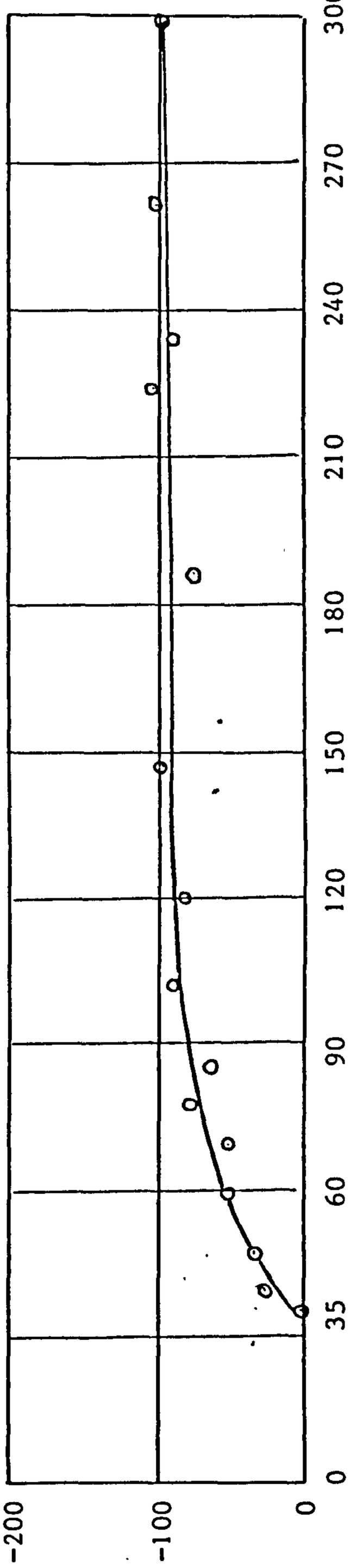

Graph 5.3 Measured concrete strains of concrete cylinders after 35 days from casting i.e. shrinkage - Concrete Mix A

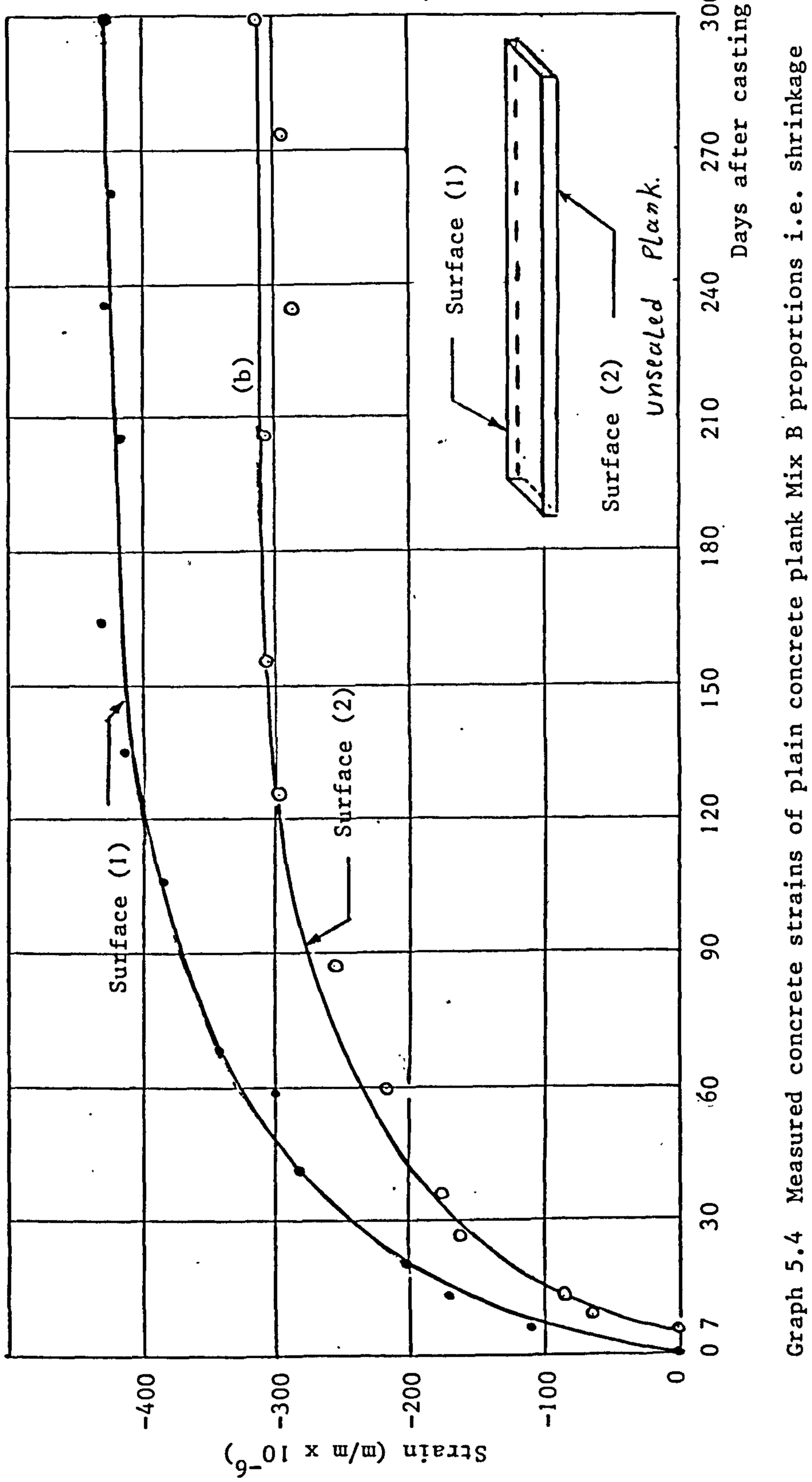

Graph 5.4 Measured concrete strains of plain concrete plank Mix B proportions i.e. shrinkage

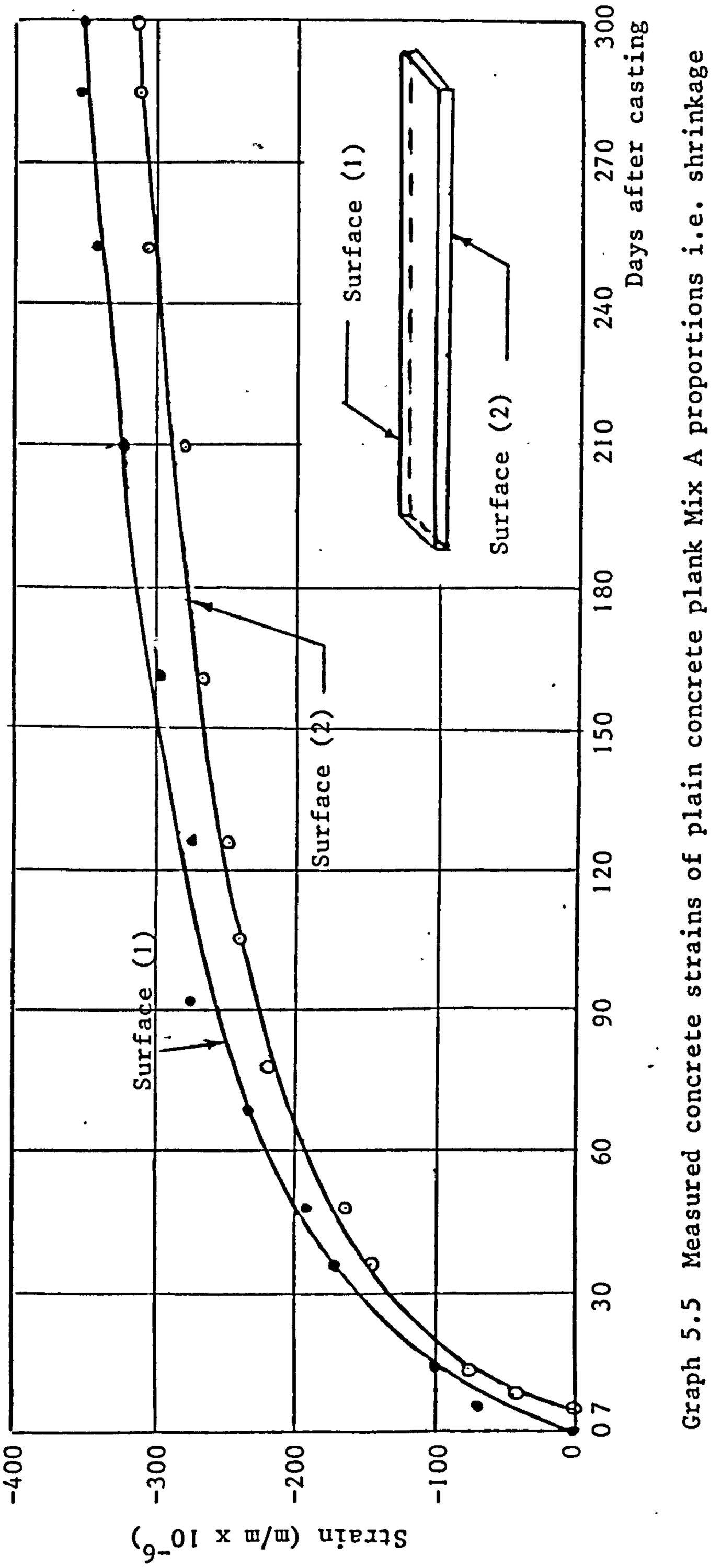

Graph 5.5 Measured concrete strains of plain concrete plank Mix A proportions i.e. shrinkage

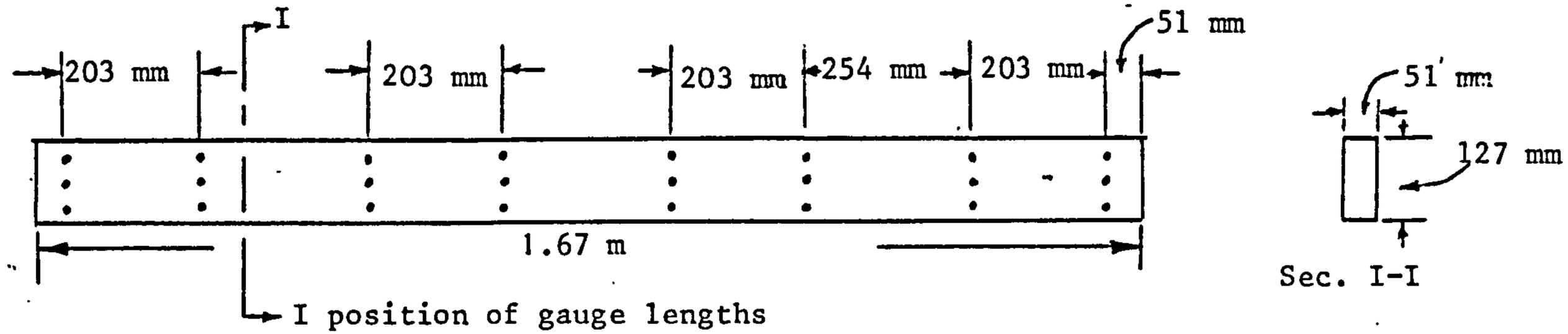

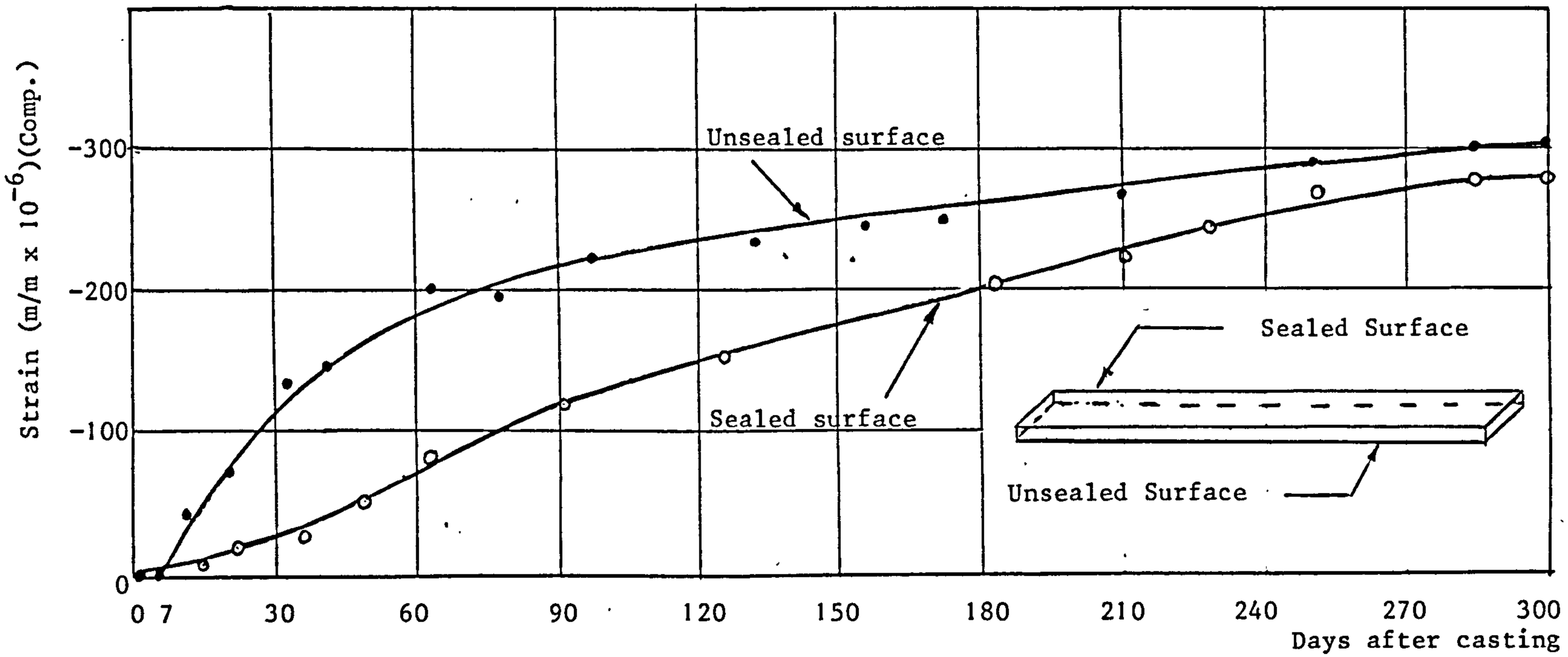

Graph 5.6 Measured concrete strains of plain concrete plank Mix A proportions i.e. shrinkage

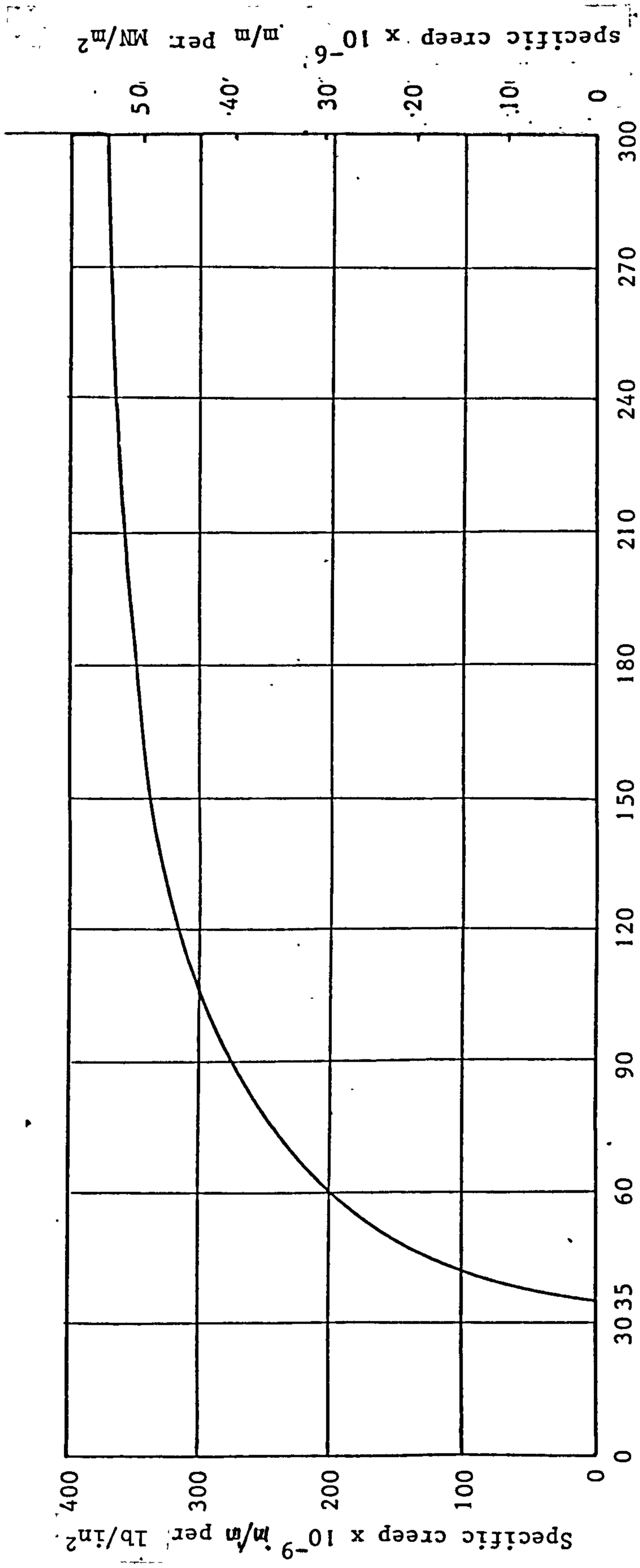

Graph 5.7 Specific creep of cylinders concrete Mix A plotted as a function of time

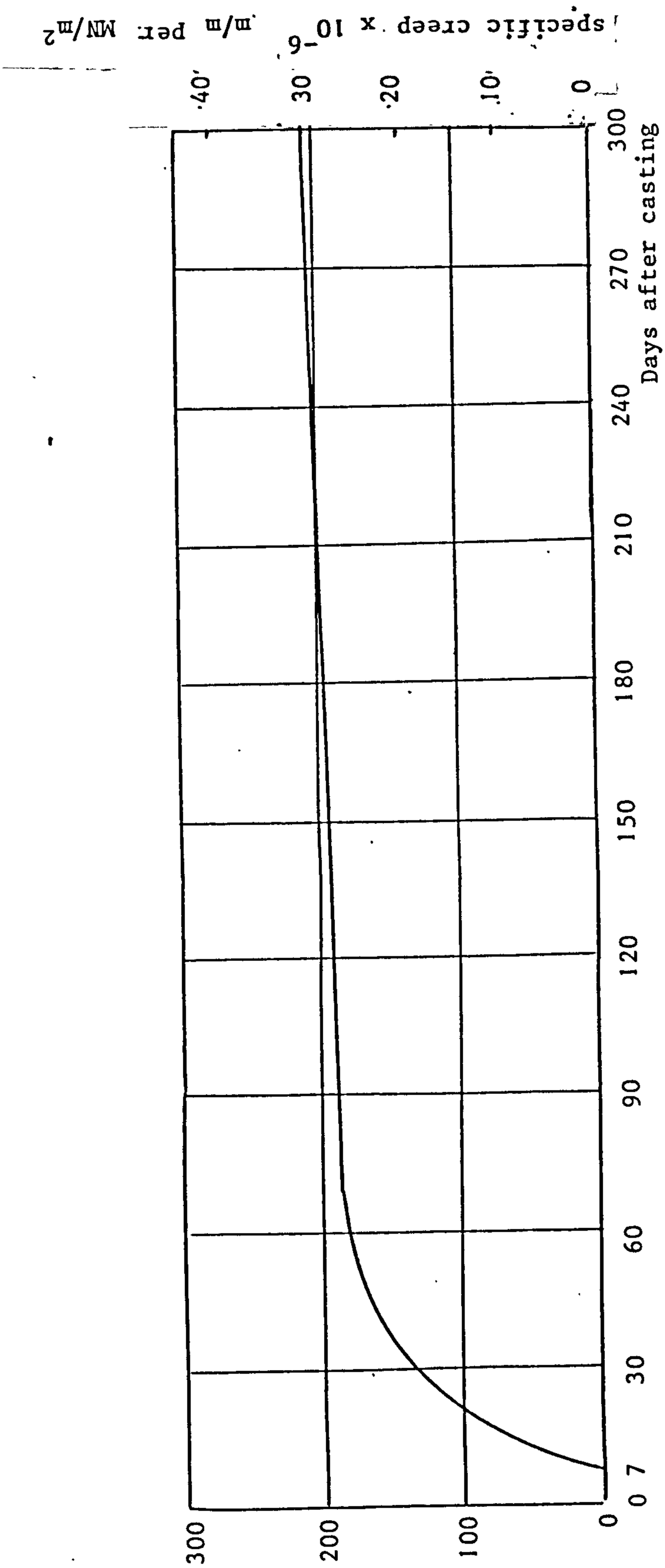

Graph 5.8 Specific creep of prestressed concrete plank Mix B plotted as a function of time

Photo 5.1 Cylinder creep rig units and control cylinders under test at laboratory temperature

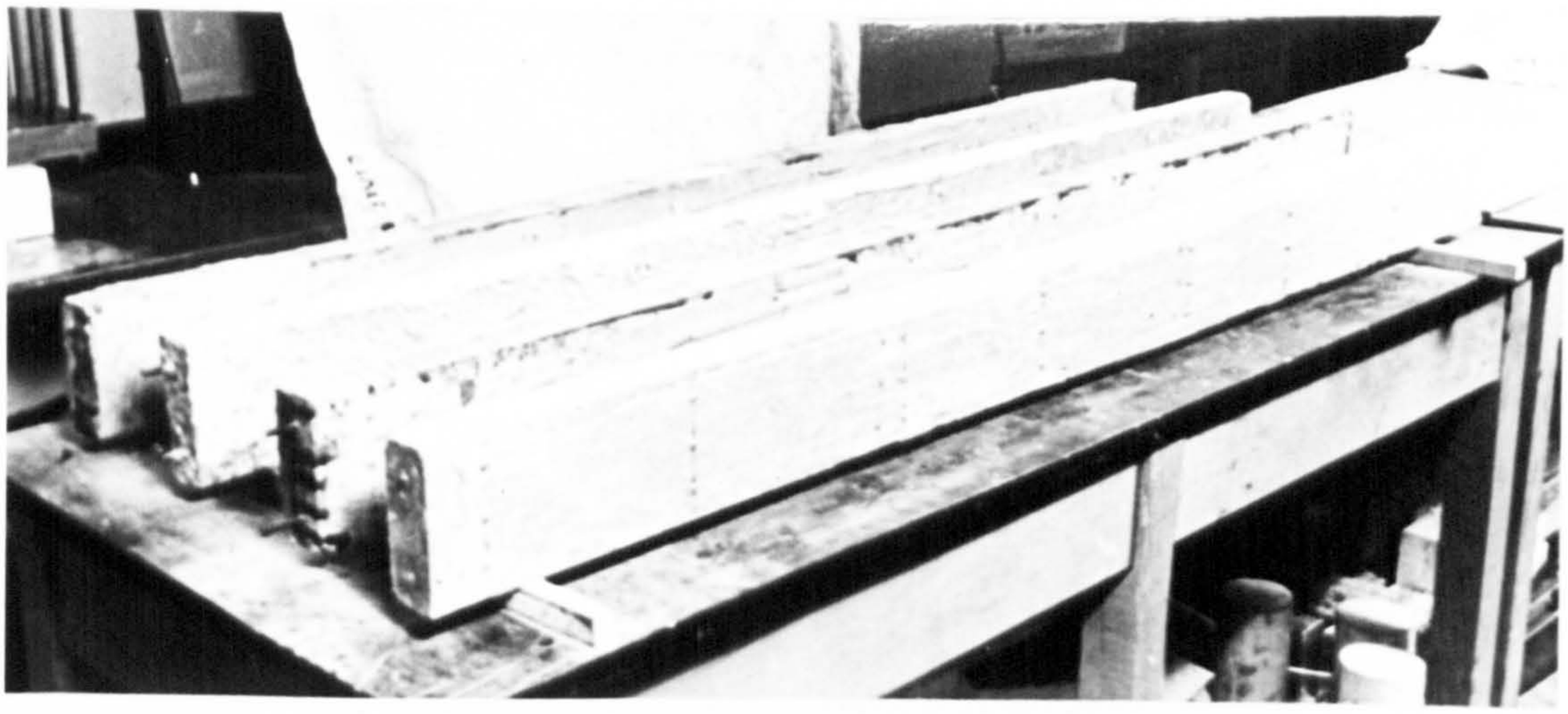

Photo 5.2 Concrete planks under test at laboratory temperature

CHAPTER 6

(Beams subjected to uniform temperature)

Theory for the prediction of elastic and long-term behaviour from numerical analysis corresponding to the experimental beams reported in Chapter 3 from control data in Chapter 5

6.1 SYNOPSIS

Theoretical studies on short and long-term behaviour at laboratory temperature of the three types of two span continuous concrete beams reported in Chapter 3 are reported in this Chapter.

Theory[18] reported in Appendix C for cracked prestressed concrete simple beam is adopted here to take into account in the continuous beams cracking which occurs in some parts of reinforced and composite prestressed concrete beams due to applied loads in the elastic analysis.

The Effective Modulus approach is used in connection with the above-mentioned theory to predict the long-term deformations by using creep data from control specimens in Chapter 5.

6.2 INTRODUCTION

This Chapter is concerned with the elastic and creep analysis at uniform temperature of three types of two span continuous concrete beams.

The objective of this Chapter is to provide an analytical numerical approach for the prediction of the elastic and long-term behaviour of the three types of concrete beams taking into consideration the effect of concrete tension between cracks developed in reinforced and composite prestressed concrete beams, and to compare the behaviour of the three types of beam construction, elastic and long-term stress distributions, vertical deflections and variation of support reactions with time, from the basis of the numerical predictions.

Comparison of the above mentioned numerical approach with some experimental data are reported in Table 6.5 in order to indicate the agreement of the theory.

6.3 ASSUMPTIONS

1. Concrete does not crack in the case of prestressed beams.
2. Concrete does crack in the case of reinforced and composite prestressed concrete beams.
3. Elastic strain is proportional to stress and up to cracking in tension.
4. Creep is proportional to stress.
5. Instantaneous Modulus of Elasticity is reduced with time under load. An effective modulus approach is adopted.
6. Plane sections of beam remain plane at all times.
7. Specific creep values of concrete are known from control data in Chapter 5.
8. The Effective Modulus at any instant neglects the stress history and predicts complete recovery of creep after removal of stress and is given by:

$$E_c' = \frac{1}{e + C}$$

$$e = \frac{1}{\text{instantaneous Modulus of concrete}}$$

C = specific creep at constant temperature

See (Chapter 1 art. 1.2) Effective Modulus Method for calculating creep at varying stress.

9. Coefficient of expansion is known and is constant.
10. Total strain = elastic strain + creep strain.
11. The effect of shearing stresses on deflections is negligible.
12. Compressive stresses defined by negative sign.
13. Shrinkage has been excluded from the analysis in order to compare the behaviour of the three beam types at uniform and elevated temperatures, due to influence of creep only.

6.4 NOTATIONS

r = horizontal strip of beam section of thickness $\frac{d}{n}$

b = breadth of beam

d = depth of beam

d_1 = distance of the bottom reinforcement from the upper face of the section

d_2 = distance of the top reinforcement from the upper face of the section

n = number of horizontal elements

m = number of horizontal elements in prestressed portion of composite beam

E_s = Modulus of Elasticity of steel

E_c = instantaneous Modulus of Elasticity of concrete Mix A (units for reinforced and composite concrete beams)

E = instantaneous Modulus of Elasticity of concrete Mix B (prestressed units)

E_c' = Effective Modulus

N = modular ratio $\frac{E_s}{E_c}$

M = Bending Moment

M_{cr} = Cracking Moment

A_s = Area of the bottom reinforcement of the section

A_s' = Area of the top reinforcement of the section

ε_o = Longitudinal strain of the extreme compression fibre of the section

ε_{cr} = Longitudinal strain of the extreme compression fibre of the section at a crack when $M \geq M_{cr}$

ε_{β} = Longitudinal strain of the extreme compression fibre of the section just before cracking when $M \leq M_{cr}$

ε_A = Longitudinal strain of the extreme compression fibre of the section at a crack when $M = M_{cr}$

ε_r = Longitudinal strain of the rth element.

f_{ct} = Maximum allowable tensile stress of concrete Mix A 2620 $\mu N/m^2$

θ = curvature

θ_{cr} = curvature at a crack when $M \geqslant M_{cr}$

θ_{β} = curvature just before cracking when $M \leqslant M_{cr}$

θ_A = curvature at a crack when $M = M_{cr}$

$\Delta F_{,r}$ = Longitudinal force on the rth element

F = Prestressing force

e_s = tensile steel strain

e_s' = compressive steel strain

f_{scr} = steel stress at a crack when $M \geqslant M_{cr}$

$f_{s\beta}$ = steel stress just before cracking when $M \leqslant M_{cr}$

f_{sA} = steel stress at a crack when $M = M_{cr}$

f_s = tensile steel stress

f_s' = compressive steel stress

ℓ = distance from a crack

ℓ_{β} = minimum distance from a crack over which sufficient tension can be transferred from the steel to concrete by bond to crack the concrete

u = bond stress

ΣO = Total surface area of tensile steel reinforcement per unit length

u_m = Maximum bond stress

u_{av} = Average bond stress

T_c = Tensile force in concrete

T_s = Tensile force in steel

K_1 = Parameter for distance from neutral axis to centroid of concrete tension

C_1 = Compressive force in concrete

f_{cc} = Concrete compressive stress at extreme compression fibre

K = Parameter for distance from neutral axis to extreme compression fibre

x = distance from neutral axis to a fibre

C = specific creep (creep/unit stress at that instant)

R = central support reaction

Δ = deflection

6.5 THEORY

6.5.1 Behaviour of Reinforced Concrete Two-Span Continuous Beam

Effective Modulus Method

The Modulus is governed by a Law of the Form

$$E_c' = \frac{E_c}{1 + E_c.C}$$

in which the instantaneous modulus E_c is reduced to take into account creep strains.

The parameter C is the specific creep at that instant i.e. the creep strain due to unit stress.
The strain at any instant is the stress at that instant divided by the Effective Modulus at that instant. The method neglects the stress history and predicts complete recovery of creep after removal of stress.

The method is applied here to predict the elastic and long-term behaviour of the continuous reinforced concrete beam in bending. The beam is divided into small longitudinal elements and each element will have associated with it particular value of M as shown in Fig. 6.1(b) and this is assumed to change with respect to time. Further subdivision of the longitudinal element into n elements

each of equal thickness as shown in Fig. 6.1(a) is necessary in order that the stress distribution over the cross section may be determined.

The analysis proceeds by applying a particular value of M to each longitudinal element thus producing strain diagram as shown by line AA in Fig. 6.1(c). The two unknown quantities to be determined for each longitudinal element are therefore the longitudinal strain ε_o and the curvature θ.

With reference to the r th element in Fig. 6.1(a) the strain is denoted by ε_r:

$$\varepsilon_r = \left[\varepsilon_o - \frac{(2r - 1)}{2n} \theta d\right] \tag{6.1}$$

The resulting longitudinal force on the element is

$$\Delta F_r = \frac{bd}{n} E_c \varepsilon_r \tag{6.2}$$

The total longitudinal force is the summation of the force increments from equation (6.2). However, the external longitudinal force is equal to zero.

Therefore:

$$0 = \sum_{r=1}^{r=n} \frac{bd}{n} E_c \left[\varepsilon_o - \frac{(2r - 1)}{2n} \theta d\right] + A_s' E_s(\varepsilon_o - \theta d_2) + A_s E_s(\varepsilon_o - \theta d_1) \tag{6.3}$$

where E_c is uniform over the cross ection.

From equation (6.3) we obtain:

$$\theta = \varepsilon_o \frac{bdE_c + E_s(A_s + A_s')}{\frac{bd^2}{2n^2} E_c \sum_{r=1}^{r=n} (2r - 1) + E_s(d_1 A_s + d_2 As')} \tag{6.4}$$

A second equation of equilibrium of the longitudinal element is obtained by consideration of flexure. Taking moments with respect to the upper face of the section gives:

$$M = d_1 A_s E_s(\theta d_1 - \varepsilon_o) - d_2 A_s' E_s(\varepsilon_o - \theta d_2) - \sum_{r=1}^{r=n} \frac{bd}{n} E_c \left[\varepsilon_o - \frac{(2r-1)}{2n}\theta d\right] \frac{(2r-1)}{2n} d \qquad (6.5)$$

from equation 6.5 we obtain:

$$\theta = \frac{M + \varepsilon_o \left[\frac{bd^2}{2n^2} E_c \sum_{r=1}^{r=n}(2r-1) + E_s(d_1 A_s + d_2 A_s')\right]}{\frac{bd^3}{4n^3} E_c \sum_{r=1}^{r=n}(2r-1)^2 + E_s(d_1^2 A_s + d_2^2 A_s')} \qquad (6.6)$$

The solution of equation 6.4 and (6.6) yields the following expression for the longitudinal strain ε_o:

$$\varepsilon_o = M \Big/ \left\{ \left[\left[bdE_c + E_s(A_s + A_s') \right] \left[\frac{bd^3}{4n^3} E_c \sum_{r=1}^{r=n}(2r-1)^2 + E_s(d_1^2 A_s + d_2^2 A_s') \right] \Big/ \right. \right.$$
$$\left. \left. \frac{bd^2}{2n^2} E_c \sum_{r=1}^{r=n}(2r-1) + E_s(d_1 A_s + d_2 A_s') \right] - \frac{bd^2}{2n^2} E_c \sum_{r=1}^{r=n}(2r-1) + E_s(d_1 A_s + d_2 A_s') \right\} \qquad (6.7)$$

The curvature θ may be obtained from equation 6.4 by substitution for ε_o from equation (6.7). The stress distribution over the cross section is then found from equation (6.1) on multiplication by E_c.

Initial calculations of ε_o and θ will refer to elastic effects only without taking into consideration the effects of cracks occurring in some parts of the beam. So the theory[18] will be adopted here

to take into account in the analysis cracking which occurs in the beam. The theory takes into consideration the variation of curvature between cracks caused by concrete tension and makes possible the prediction of both the curvature at a crack and the average curvature along the length of the beam between two cracks. Moment curvature relationships for reinforced concrete members are usually derived for the sections at which cracks form, the behaviour of the member between the cracks being ignored. However, the bond between the steel and concrete will mean that tension is transferred from the steel to the concrete between the cracks. This build-up of concrete tension depends upon the distribution of bond stress and will only lead to new cracks between existing cracks when the tensile strength of concrete is exceeded. Because of the tension carried by the concrete the curvature between the cracks will be less than at a crack.

Development of the Theory

1. Calculation of ε_{cr} and θ_{cr} after the formation of cracks

(a) Conditions at a crack when $M \geq M_{cr}$

At each step of the previous analysis for calculation of ε_o and θ the concrete stress in tension in the tensile region of the section is compared with maximum allowable concrete stresses in tension f_{ct} and if in excess of this quantity the calculation follows an iterative procedure excluding the elements carrying high tensile stresses which are thus assumed to crack. This cycling procedure continues until the equilibrium of the section is secured with stresses in the tensile zone everywhere below the critical value f_{ct} which causes cracking. Thus we obtain ε_{cr} and θ_{cr} after cracking

from which we calculate the stress in the tensile reinforcement f_{scr}

$$f_{scr} = (d_1\theta - \varepsilon_o)F_s$$

(b) Condition at a crack when $M = M_{cr}$

Same procedure as in (a) may be followed here in order to calculate ε_A, θ_A and f_{sA}.

(c) Condition at a crack when $M \leq M_{cr}$

Same procedure as in (a) may be followed here in order to calculate ε_β, θ_β and $f_{s\beta}$.

(d) Condition at distance ℓ from a crack ($\ell \leq \ell_\beta$)

The assumption is made that at section some distance from a crack, the steel strain is still linearly related to the concrete compressive strain. At a distance ℓ from a crack, the steel stress will be reduced by bond and the concrete tension will build up. At this stage of the analysis no assumption is made regarding the shape and distribution of tensile stresses and strains in the concrete across the section. The conditions at a distance from a crack are shown in Fig. 6.2. The reduction of steel tension force over length ℓ from the crack is given by $\int_0^\ell u\Sigma O d\ell$ where u is the bond stress and may vary with ℓ. Therefore, the tensile stress in the steel at distance ℓ from the crack is:

$$f_s = f_{scr} - \int_0^\ell \frac{u\Sigma O}{A_s}\, d\ell \qquad (6.8)$$

and the steel strain is:

$$e_s = (f_{scr} - \int_0^\ell \frac{u\Sigma O d\ell}{A_s})/E_s \qquad (6.9)$$

The actual stress-strain curves for the steel and concrete can be obtained from test results. It is generally agreed that the bond stress is a maximum very close to the crack and decreases in some fashion further away from the crack, see Evans and Robinson[50] and Leonhard[51] for examples. For this analysis it will be assumed that, at first cracking, the bond stress decreases linearly from a maximum u_m at a crack to a zero at a distance ℓ_β, equal to the bond length, away from the crack. It will be further assumed that the gradient of the bond stress is independent of the distance between cracks but is purely a function of the distance from the nearest crack. Thus for the average condition of two cracks spaced a distance 1.5 ℓ_B apart, the bond stress distribution will be as shown in Fig. 6.3. The bond stress distribution at $\ell \leq 0.75\ \ell_\beta$ from a crack is then given by:

$$u = u_m\left(1 - \frac{\ell}{\ell_\beta}\right) \tag{6.10}$$

at a distance $\ell \leq 0.75\ \ell_\beta$ from a crack the tensile steel stress is given by equation (6.8) and (6.10):

$$f_s = f_{scr} - \int_0^\ell u_m\left(1 - \frac{\ell}{\ell_\beta}\right) \frac{\Sigma O}{A_s}\, d\ell$$

$$= f_{scr} - \frac{u_m \Sigma O}{A_s}\left(1 - \frac{\ell^2}{2\ell_\beta}\right) \tag{6.11}$$

Average bond stress at a distance $\ell \leq 0.75\ \ell_\beta$ from a crack is given by:

$$u_{av} = \frac{A_s(f_{sA} - f_{s\beta})}{\ell_\beta \Sigma O} \tag{6.12}$$

and since a linear bond distribution is assumed:

$$u_m = 2u_{av} = \frac{2A_s(f_{sA} - f_{s\beta})}{\ell_\beta \Sigma O} \qquad (6.13)$$

Substituting u_m from equation (6.13) into (6.11) gives the steel stress at distance $\ell \leq 0.75\ \ell_\beta$ from a crack as:

$$f_s = f_{scr} - 2(f_{sA} - f_{s\beta})\left(\frac{\ell}{\ell_\beta} - \frac{\ell^2}{2\ell_\beta^2}\right) \qquad (6.14)$$

in equation (6.14) f_{scr} is the tensile steel stress at the crack for the particular moment acting and f_{sA} and $f_{s\beta}$ are the steel stresses when $M = M_{cr}$ and $M \leq M_{cr}$.

The value of f_s given by equation (6.14) is the value which will be used to find the average ε_o and θ at a distance $\ell \leq 0.75\ \ell_\beta$ from a crack and consequently the full stress and strain conditions at a distance $\ell \leq 0.75\ \ell_\beta$ from a crack. Note that f_s from equation (6.14) is independent of the maximum bond stress u_m and thus the magnitude of the maximum bond stress does not affect the moment curvature relationship. This is to be expected because given a certain bond stress distribution (for example triangular, as used here) the magnitude of u_m will only alter the crack spacing.

The distribution of concrete tension at a section between two cracks is required in order that parameter K_1 which gives the distance from the centroid of the concrete tensile stresses to the neutral axis may be determined. As very little information is available as to the magnitude of K_1 the analysis is eventually insensitive to this variable and a value of $\frac{1}{2}$ was chosen.

From the strain distribution in Fig. 6.2:

$$K = \frac{\varepsilon_o}{\varepsilon_o + e_s} \tag{6.15}$$

$$\varepsilon_o = \frac{K . e_s}{1 - K} \tag{6.16}$$

For equilibrium:

$$C_1 = T_c + T_s \tag{6.17}$$

$$\varepsilon_o \frac{Kd_1}{2} E_c b + A_s' f_s' = T_c + A_s f_s$$

$$T_c = \varepsilon_o \frac{Kd_1}{2} E_c b + A_s' f_s' - A_s f_s \tag{6.18}$$

and if moments are taken about the neutral axis,

$$M = \varepsilon_o \frac{Kd_1}{2} E_c b\, x + T_c K_1 \left(d - \frac{\varepsilon_o d_1}{\varepsilon_o + e_s}\right) + A_s f_s \frac{e_s d_1}{\varepsilon_o + e_s}$$

$$+ A_s' f_s' (Kd_1 - d_2) \tag{6.19}$$

from the strain diagram:

$$\frac{e_s'}{\varepsilon_o} = \frac{(Kd_1 - d_2)}{Kd_1}$$

$$e_s' = \varepsilon_o (Kd_1 - d_2)/Kd_1 = \frac{Ke_s}{1-K} \frac{(Kd_1 - d_2)}{Kd_1} = e_s \frac{(Kd_1 - d_2)}{(1 - K)d_1} \tag{6.20}$$

$$f_s = e_s E_s \tag{6.21}$$

$$N = \frac{E_s}{E_c} \tag{6.22}$$

$$f_s' = e_s'.E_c(N - 1) \qquad (6.23)$$

or

$$f_s' = (N - 1)E_c.\frac{e_s\,(Kd_1 - d_2)}{(1 - K)d_1} \qquad (6.24)$$

The solution of the simultaneous equations (6.18) and (6.19) gives the unknowns ε_o and T_c and consequently we can obtain K and the curvature θ at this section at a particular moment M as:

$$\theta = \frac{\varepsilon_o + e_s}{d_1} \qquad (6.25)$$

with values of ε_o and θ for each longitudinal element known their integrated effects along the beam permit slopes and deflections to be evaluated as discussed in Appendix (B). Initial calculations will not include the effects of creep and hence the values of ε_o and θ refer to elastic effects only. The effects of creep may be included in the analysis by calculating the reduced modulus E_c' at any particular time after loading by using the specific creep data of Concrete Mix A reported in Table 6.1 which could be obtained from the specific creep curve of Concrete Mix A reported in Chapter 5 Graph 5.7. Using E_c' instead of E_c in the above analysis we may obtain ε_o, θ, stresses and reactions at any particular time after loading. In this analysis compatability of the whole beam is maintained throughout as discussed in Appendix (B).

6.5.2 Behaviour of Prestressed Concrete two span continuous beam

The effective modulus method is applied here to predict the elastic and long-term behaviour of the continuous prestressed beam in bending.

Days after Loading	1	2	4	7	11
C x 10^{-9}	57	69	89	119	139
Days after Loading	15	19	25	32	43
C x 10^{-9}	159	179	199	229	249
Days after Loading	53	63	71	81	90
C x 10^{-9}	269	279	294	309	319
Days after Loading	99	109	119	130	140
C x 10^{-9}	329	334	339	344	349
Days after Loading	152	165	179	186	198
C x 10^{-9}	354	359	361	362	363
Days after Loading	208	218	230	250	270
C x 10^{-9}	364	365	367	368	369

Table 6.1 Specific creep data of Concrete Mix A
(See Chapter 5 Graph 5.7)

The analysis proceeds by applying two forces each equal to F and a particular value of M to each longitudinal element as shown in Fig. 6.4(b)*. Thus producing a strain diagram as shown by line AA in fig. 6.4(c). The two unknown quantities to be determined for each longitudinal element are therefore the longitudinal strain ε_o and the curvature θ.

With reference to the rth element in fig. 6.4(a) the strain is denoted by ε_r

$$\varepsilon_r = \left[\varepsilon_o - \frac{(2r - 1)}{2n} \theta d\right] \tag{6.26}$$

The resulting longitudinal force on the element is

$$\Delta F_r = \frac{bd}{n} E \varepsilon_r \tag{6.27}$$

in which E is Young's Modulus for concrete.

The total longitudinal force is the summation of the force increments from equation (6.27), thus

$$2F = \sum_{r=1}^{r=n} \frac{bd}{n} E\left[\varepsilon_o - \frac{(2r - 1)}{2n} \theta d\right] \tag{6.28}$$

where E is uniform over the cross section.

From equation (6.28) we obtain:

$$\theta = \frac{bdE\ \varepsilon_o - 2F}{\frac{bd^2}{2n^2} E \sum_{r=1}^{r=n} (2r - 1)} \tag{6.29}$$

A second equation of equilibrium of the longitudinal element is obtained by consideration of flexure, taking moments with respect

* Page 195

to the upper face of the section gives:

$$(d_1 + d_2)F - M = \sum_{r=1}^{r=n} \frac{bd}{n}\left[\varepsilon_o - \frac{(2r-1)}{2n}\theta d\right]\frac{(2r-1)}{2n}\,dE \qquad (6.30)$$

from equation (6.30) we obtain:

$$\theta = \frac{\frac{bd^2}{2n^2}E\,\varepsilon_o \sum_{r=1}^{r=n}(2r-1) - \left[(d_1 + d_2)F - M\right]}{\frac{bd^3}{4n^3}E \sum_{r=1}^{r=n}(2r-1)^2} \qquad (6.31)$$

The solution of equations (6.29) and (6.31) yields the following expression for the longitudinal strain ε_o.

$$\varepsilon_o = \frac{\frac{Fd}{n}\sum_{r=1}^{r=n}(2r-1)^2 - \left[(d_1 + d_2)F - M\right]\sum_{r=1}^{r=n}(2r-1)}{\frac{bd^2}{2n^2}E\left[\sum_{r=1}^{r=n}(2r-1)^2 - \frac{1}{n}\left(\sum_{r=1}^{r=n}2r-1\right)^2\right]} \qquad (6.32)$$

The curvature θ may be obtained from equation (6.29) by substitution for ε_o from equation (6.32). The stress distribution over the cross section is then found from equation (6.26) on multiplication by E. With the values of ε_o and θ for each longitudinal element known their integrated effects along the beam permit slopes and deflections to be evaluated. Initial calculations will not include the effects of creep and hence the values of ε_o, θ refer to elastic effects only.

The effects of creep may be included in the analysis by calculating the reduced modulus, E_c' at any particular time after loading using the specific creep data of concrete Mix B reported in Table 6.2 (see Graph 5.8.) Using E_c' instead of E in the above-mentioned equations we may obtain ε_o, θ, stresses and reactions at any particular time after loading. In this analysis compatibility of the whole beam is maintained throughout as reported in Appendix B.

Days after Loading	2	5	7	10	12
C x 10^{-9}	25	55	70	80	100
Days after Loading	15	20	25	30	35
C x 10^{-9}	115	135	150	160	165
Days after Loading	40	45	50	55	60
C x 10^{-9}	170	175	180	185	187
Days after Loading	90	120	150	180	270
C x 10^{-9}	190	192	195	198	200

Table 6.2 Specific creep data of Concrete Mix B
(See Chapter 5 Graph 5.8)

6.5.3 Behaviour of composite prestressed concrete two span continuous beam

The effective modulus method is applied here to predict the elastic and long-term behaviour of the continuous composite beam in bending.

The prestressed portion is divided into m elements.

The analysis proceeds by applying the force F and a particular value of M to each longitudinal element as shown in Fig. 6.5(b) Page 195 thus producing a strain diagram as shown by line AA Fig. 6.5(d). The two unknown quantities to be determined for each longitudinal element are, therefore, the longitudinal strain ε_o and the curvature θ . With reference to the rth element in Fig. 6.5(a), the strain is denoted by ε_r.

$$\varepsilon_r = \left[\varepsilon_o - \frac{(2r - 1)}{2n} \theta d \right] \tag{6.33}$$

The resulting longitudinal force on the element is:

$$\Delta F_r = \frac{bd}{n} E_c \varepsilon_r \tag{6.34}$$

in which E_c is Young's Modulus for cast-in-place portion of concrete.

The total longitudinal force is the summation of the force increments from equation (6.34)

Thus:

$$0 = \sum_{r=1}^{r=n-m} \frac{bd}{n} E_c \left[\varepsilon_o - \frac{(2r - 1)}{2n} \theta d \right] + A_s' E_s (\varepsilon_o - d_2 \theta) + \sum_{r=n-(m-1)}^{r=n} \frac{bd}{n} E \left[\varepsilon_o - \frac{(2r - 1)}{2n} \theta d \right] \tag{6.35}$$

from equation (6.35) we obtain:

$$\theta = \frac{\varepsilon_o \left[\frac{(n - m)}{n} bdE_c + A_s'E_s + \frac{m}{n} bdE \right]}{d_2 A_s'E_s + \frac{bd^2}{2n^2} \left[E_c \sum_{r=1}^{r=n-m} (2r - 1) + E \sum_{r=n-(m-1)}^{r=n} (2r - 1) \right]} \qquad (6.36)$$

It is obvious that omission of the longitudinal force F from the lefthand side of equation (6.35) will lead to a constant elastic and long-term solution at all times because of using the effective modulus approach.

A second equation of equilibrium of the longitudinal element is obtained by consideration of flexure moments with respect to the upper face of the section.

$$-M = \sum_{r=1}^{r=n-m} \frac{bd}{n} E_c \left[\varepsilon_o - \frac{(2r - 1)}{2n} \theta d \right] \frac{(2r - 1)}{2n} d + d_2 A_s' E_s (\varepsilon_o - d_2 \theta)$$

$$+ \sum_{r=n-(m-1)}^{r=n} \frac{bd}{n} E \left[\varepsilon_o - \frac{(2r - 1)}{2n} \theta d \right] \frac{(2r - 1)}{2n} d \qquad (6.37)$$

from equation (6.37) we obtain:

$$\theta = \frac{\varepsilon_o \left[d_2 A_s' E_s + \frac{bd^2}{2n^2} \left(E_c \sum_{r=1}^{r=n-m} (2r - 1) + E \sum_{r=n-(m-1)}^{r=n} (2r-1) \right) \right] + M}{d_2^2 A_s' E_s + \frac{bd^3}{4n^3} \left[E_c \sum_{r=1}^{r=n-m} (2r - 1)^2 + E \sum_{r=n-(m-1)}^{r=n} (2r - 1)^2 \right]} \qquad (6.38)$$

The solution of equation (6.36) and (6.38) yields the following expression for the longitudinal strain ε_o.

$$\varepsilon_o \doteq -M \left[d_2 A_s' E_s + \frac{bd^2}{2n^2} \left(E_c \sum_{r=1}^{r=n-m} (2r-1) + E \sum_{r=n-(m-1)}^{r=n} (2r-1) \right) \right] \Bigg/$$

$$\left[d_2 A_s' E_s + \frac{bd^2}{2n^2} \left(E_c \sum_{r=1}^{r=n-m} (2r-1) + E \sum_{r=n-(m-1)}^{r=n} (2r-1) \right) \right]^2 -$$

$$\left[\frac{(n-m)}{n} bdE_c + A_s' E_s + \frac{m}{n} bdE \right] \left[d_2^2 A_s' E_s + \right.$$

$$\left. \frac{bd^3}{4n^3} \left(E_c \sum_{r=1}^{r=n-m} (2r-1)^2 + E \sum_{r=n-(m-1)}^{r=n} (2r-1)^2 \right) \right] \qquad (6.39)$$

The curvature θ may be obtained from equation (6.36) by substitution for ε_o from equation (6.39). To take into consideration the effects of cracks in some parts in the beam, the same procedure used in reinforced concrete continuous beam to deal with this problem could be followed here to evaluate ε_o and θ at a distance ℓ from a crack ($\ell \leq \ell_\beta'$) for each longitudinal element. Integration of ε_o and θ along the beam permit slopes and deflections to be evaluated. Initial calculations will not include the effects of creep and hence ε_o and θ refer to elastic effects only. The effects of creep may be included in the analysis by calculating the reduced modulus E_c' at any particular time with regard to prestressed and cast-in-place portion using the specific creep data of concrete Mixes A and B reported in Table 6.3 which could be obtained from the specific creep curves of concrete mixes A and B reported in Chapter 5 Graphs 5.7 and 5.8.

Using the reduced Modulus of E_c and E in the above analysis we may obtain ε_o, θ, stresses and reactions at any particular time after loading.

Concrete Mix type	Days after loading	1	2	4	7	11
A	C x 10^{-9}	57	69	89	119	139
B	C x 10^{-9}	15	25	45	70	95
	Days after loading	15	19	25	32	43
A	C x 10^{-9}	159	179	199	229	249
B	C x 10^{-9}	115	130	148	162	175
	Days after loading	53	63	71	81	90
A	C x 10^{-9}	269	279	294	309	319
B	C x 10^{-9}	183	185	187	189	190
	Days after loading	99	109	119	130	140
A	C x 10^{-9}	329	334	339	344	349
B	C x 10^{-9}	191	192	193	194	195
	Days after loading	152	165	179	186	198
A	C x 10^{-9}	354	359	361	362	363
B	C x 10^{-9}	196	197	198	199	200
	Days after loading	208	218	230	250	270
A	C x 10^{-9}	364	365	367	368	369
B	C x 10^{-9}	200	200	200	200	200

Table 6.3 Specific creep data of concrete Mixes A and B

6.6 PREDICTED VALUES FOR EXPERIMENTAL CONDITIONS

6.6.1 Reinforced Concrete Beam (see fig. in Graph 6.1)

(a) Centre Reaction

Graph 6.1 shows the calculated elastic and long-term variation of centre reaction with time for 270 days of sustained loading.

(b) Deflection

Graph 6.2 shows the computed time deflection profile at Sec. I-I (see fig. in Graph 6.2) for the period of sustained load. Graph 6.3 shows the calculated elastic and long-term variation with time of the deflection profile for half of the beam.

(c) Stresses

Graph 6.4 shows the computed elastic and long-term variation with time of the stress distribution for two cross sections of the beam at Sec. I-I and over the centre support.

6.6.2 Prestressed Concrete Beam (see fig. in Graph 6.5)

(a) Centre Reaction

Graph 6.5 shows the calculated elastic and long-term variation of centre reaction with time for 270 days of sustained loading.

(b) Deflection

Graph 6.6 shows the computed time deflection profile at Sec. I-I (see fig. in Graph 6.6) for the period of sustained loading. Graph 6.7 shows the calculated elastic and long-term variation with time of the deflection profile for half of the beam.

(c) Stresses

Graph 6.8 shows the computed elastic and long-term variation with time of the stress distribution for two cross sections of the beam.

6.6.3 Composite Concrete Beam (see fig. in Graph 6.9)

(a) Centre Reaction

Graph 6.9 shows the calculated elastic and long-term variation of centre support reaction with time for 270 days of sustained loading.

(b) Deflection

Graph 6.10 shows the computed time deflection profile at Sec. I-I (see fig. in Graph 6.10) for the whole period of sustained loading.

Graph 6.11 shows the calculated elastic and long-term variation with time of the deflection profile for half of the beam.

(c) Stresses

Graph 6.12 shows the computed elastic and long-term variation with time of the stress distribution for two cross sections of the beam.

6.7 DISCUSSIONS

Central Support Reaction

Graphs 6.1, 6.5 and 6.9 show that there is no significant variation in centre support reaction in the long-term behaviour of the three types of continuous concrete beams.

Deflections at span section I-I

Graphs 6.2, 6.6 and 6.10 show the calculated values of elastic and long-term deflection behaviour at Sec. I-I for the three types of concrete beams. It is obvious from the graphs that the rate of increase in deflection is increasing at a decreasing rate for the three types of concrete beams. Table 6.4 shows the calculated deflections at various times for the three types of concrete beams.

Beam Type / days after Loading	Deflection mm x 10^{-2}		
	R.C.	P.C.	C.P.C.
0	16.2	11	13.2
15	23.2	17.5	21.2
30	25.5	20	24
60	28	22	26.5
90	30	22.5	27.5
150	31	23	29
270	32.5	23.5	30

Table 6.4 Calculated deflections at Sec. I-I at various times Comparison for the three beam types subjected to same applied loading

Deflection Profiles

Graphs 6.3, 6.7 and 6.11 show the calculated variation of deflection profile of the three types of beams after loading. The deflections do increase with time because of creep but the rate of increase in

deflections decreases with time as the rate of creep decreases. This can be explained by the fact that creep and stress are proportional so that the structure functions as an elastic one in which Young's Modulus merely reduces with time.

Stress distribution at selected sections

Graphs 6.4, 6.8 and 6.12 show the calculated variation of the stress distribution after loading for the three types of continuous concrete beams for two sections of each beam.

We notice a similarity in behaviour of reinforced and composite prestressed beams over the centre support due to loading as the stresses decline and the travel of the neutral axis towards the tensile zone due to creep. This behaviour is expected as the tensile reinforcement and the properties of concrete at that particular section for the two beams are the same. The calculated variation of the stress distribution at Sec. I-I of the composite beam has a different pattern because of the prestressed concrete plank. The variation with time of stress distributions at both sections of the prestressed concrete beam is not significant.

6.8 CONCLUSIONS

The theory presented in this Chapter for the analysis of reinforced, prestressed and composite prestressed concrete continuous beams to predict the elastic and long-term behaviour including the effect of concrete tension between cracks is developed by analytical numerical approach. The only empirical data included is used to define the bond stress distribution between cracks. It is noticeable in Graphs in Chapters 2 and 4 the agreement is good between theoretical curves calculated from the above-mentioned theory and the experimental results in the case of prestressed and composite beams only.

Comparison between measured and computed time deflection behaviour at section I-I for the whole period of sustained loading w.r.t the three types of concrete beams are shown in graphs 4.2, 4.9 and 4.16 in Chapter 4.

Comparison between measured and computed time deflection profile for half of the beam w.r.t reinforced, prestressed and composite concrete beams can be made from graphs 4.3, 4.10 and 4.17 respectively for measured values and from graphs 6.3, 6.7 and 6.11 respectively for computed values.

Table 6.5 indicates that the proposed method gave reasonably good agreement with estimated elastic deflection in reinforced concrete beams, but tending to underestimate the long-term deflection. The method is too complex for hand calculations, but the appropriate equations were programmed for solution by digital computer.

Ref. No.	Beam No.	Meas. Elast. def. mm	Cal. Elast. def. mm	Loading Period	A Meas. def. mm	B Cal. def. mm	A/B
Suan[20]	B4	3.03	2.87	120 days	5.74	4.25	1.35
Glanville & Thomas[37]	88D	1.57	1.34	225 days	3.63	2.42	1.50
Washa & Fluck[36]	B3, B6	26.42	25.10	2½ years	86.36	62.23	1.38
Stevens[88]	B	1.02	1.09	2 years	2.16	1.49	1.45
Stevens[88]	D	0.79	0.86	2 years	2.16	1.46	1.47

Table 6.5 Calculated deflections at various times by the proposed numerical approach - comparison with measured values carried out by some investigators - simple reinforced concrete beams.

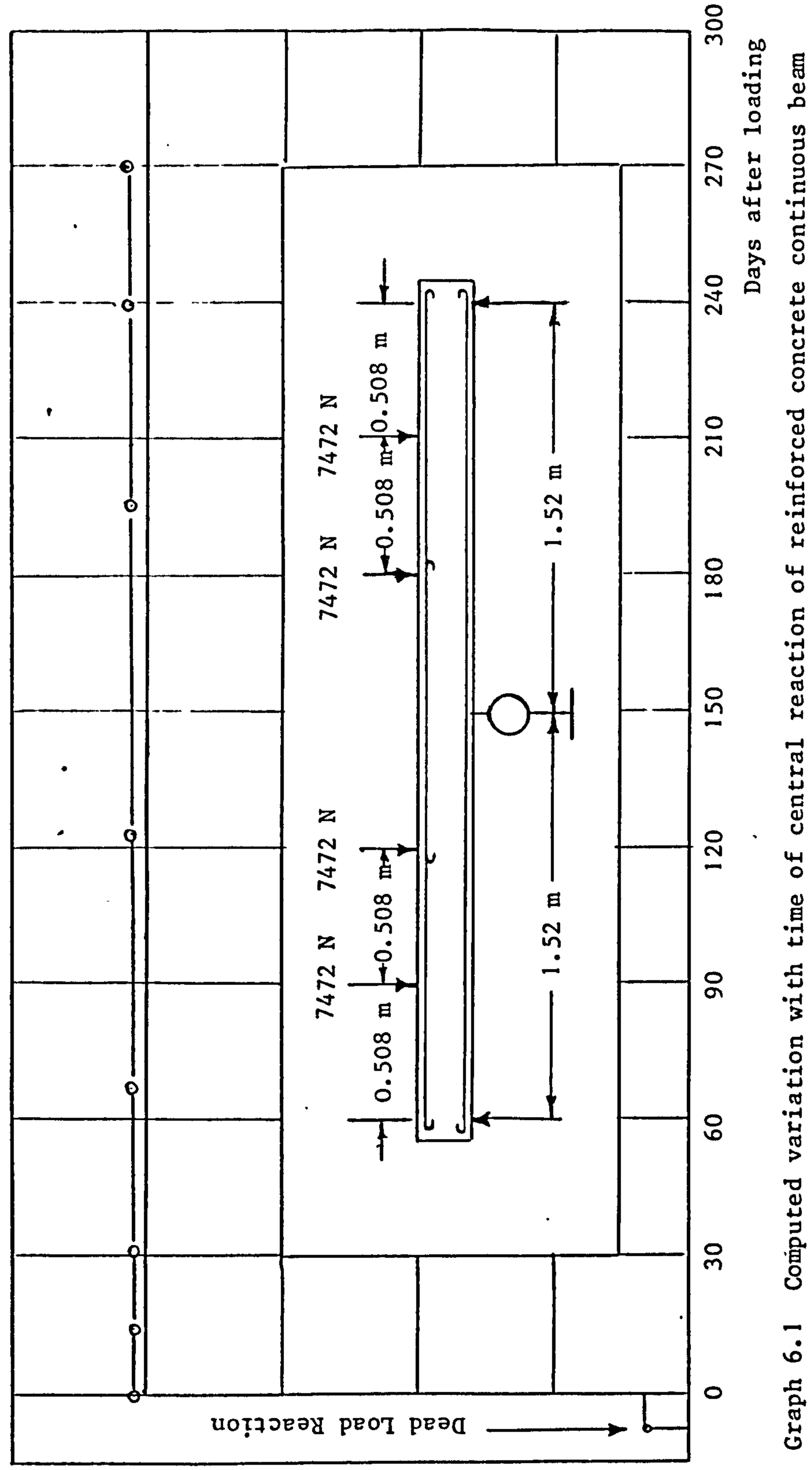

Graph 6.1 Computed variation with time of central reaction of reinforced concrete continuous beam after loading

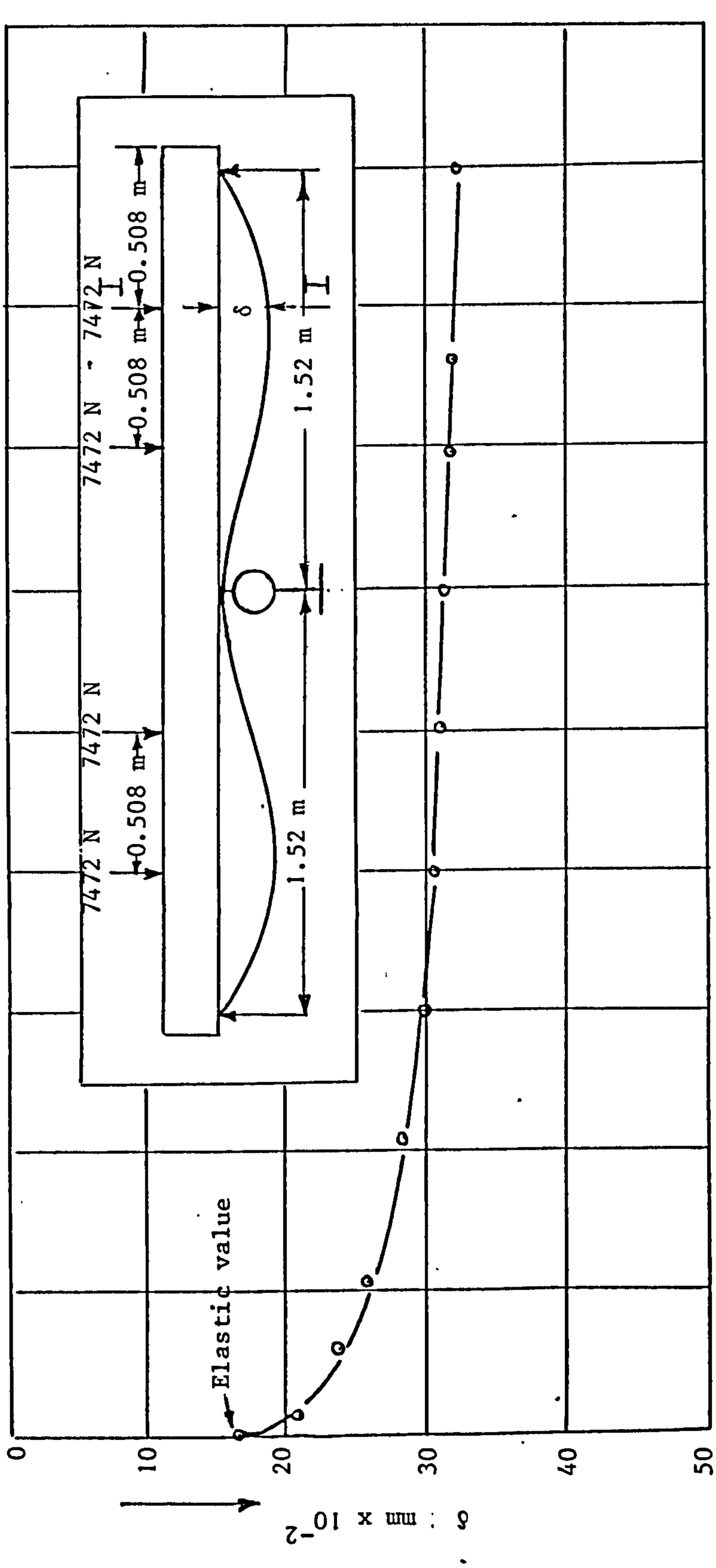

Graph 6.2 Computed time deflection behaviour at Sec. I-I of reinforced concrete continuous beam after loading

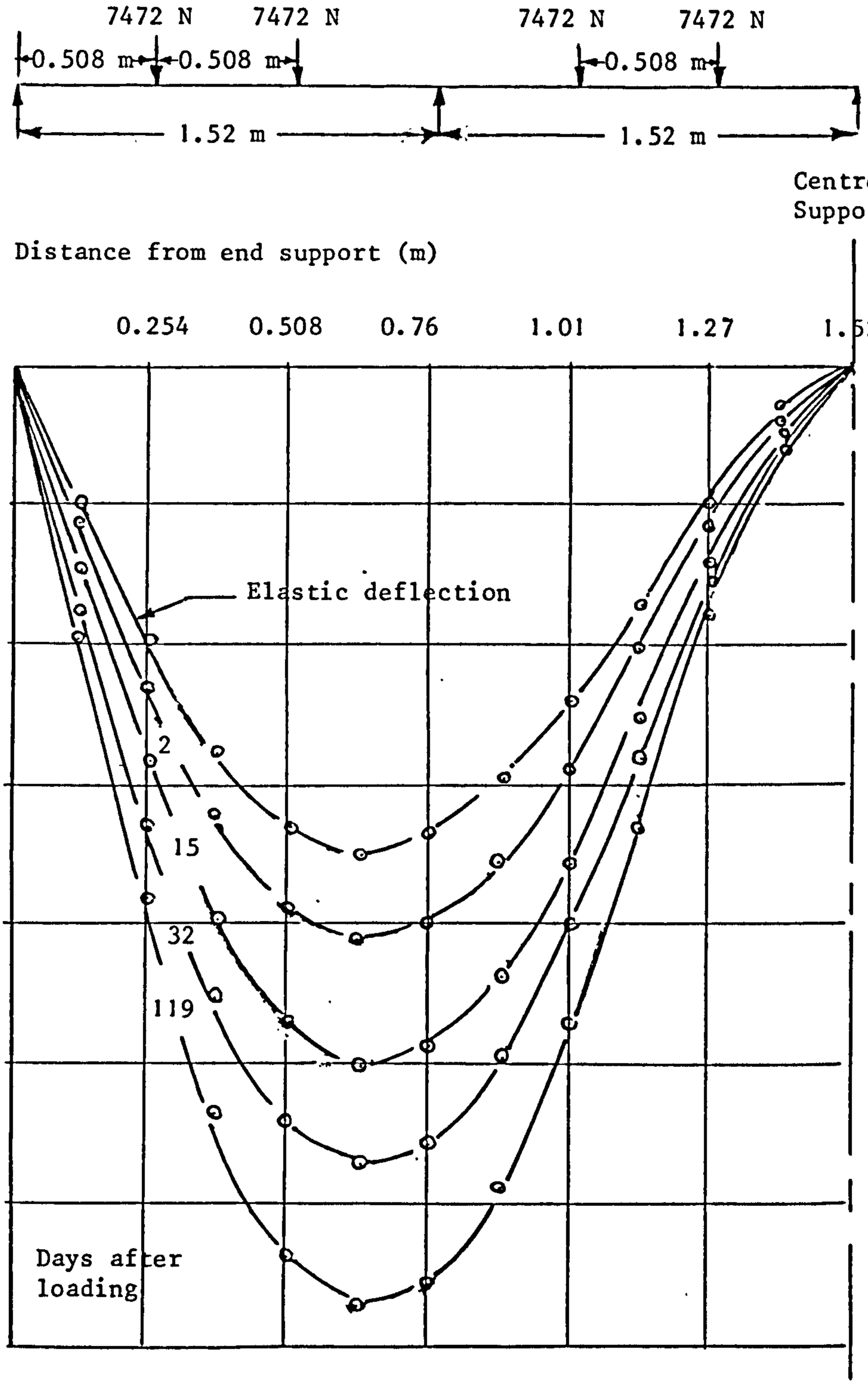

Graph 6.3 Computed deflection profile of reinforced concrete continuous beam after loading

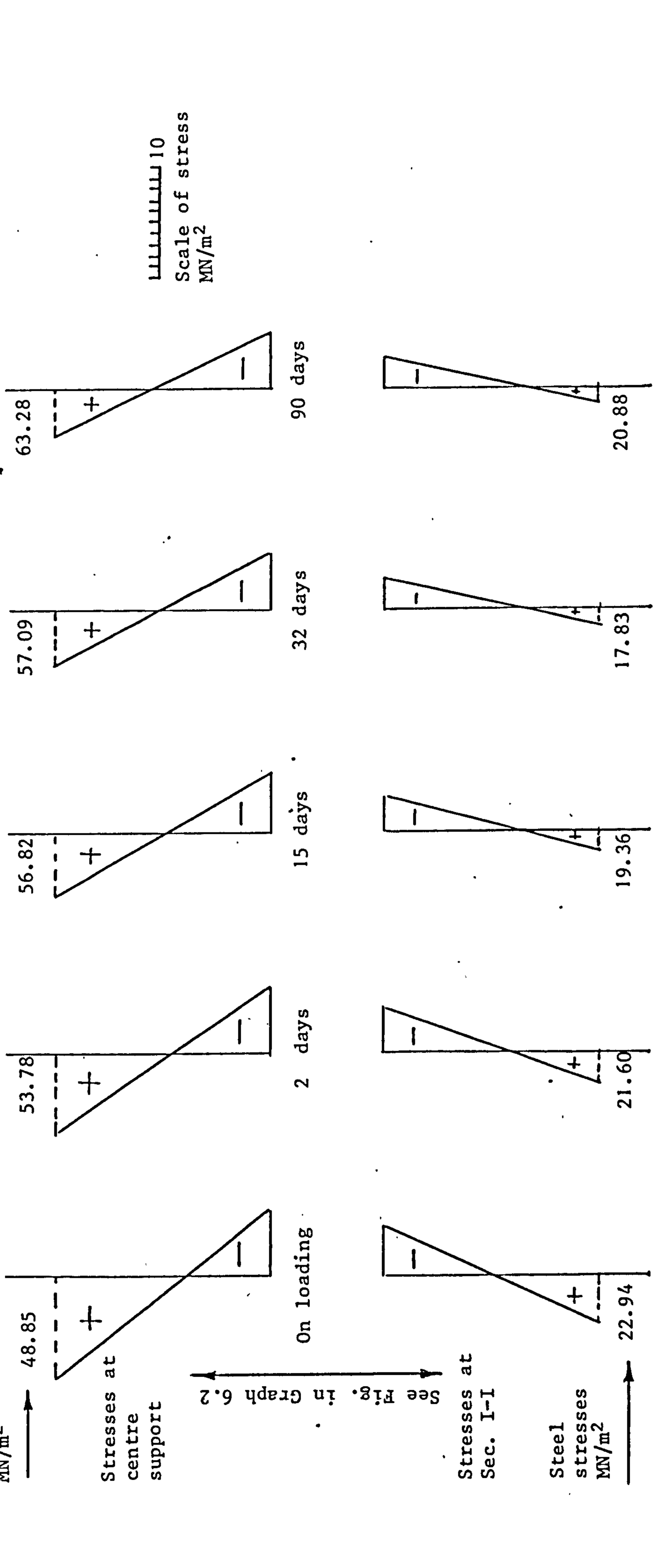

Graph 6.4 Computed concrete stress distribution (elastic, creep) of reinforced concrete continuous beam for two cross sections of the beam

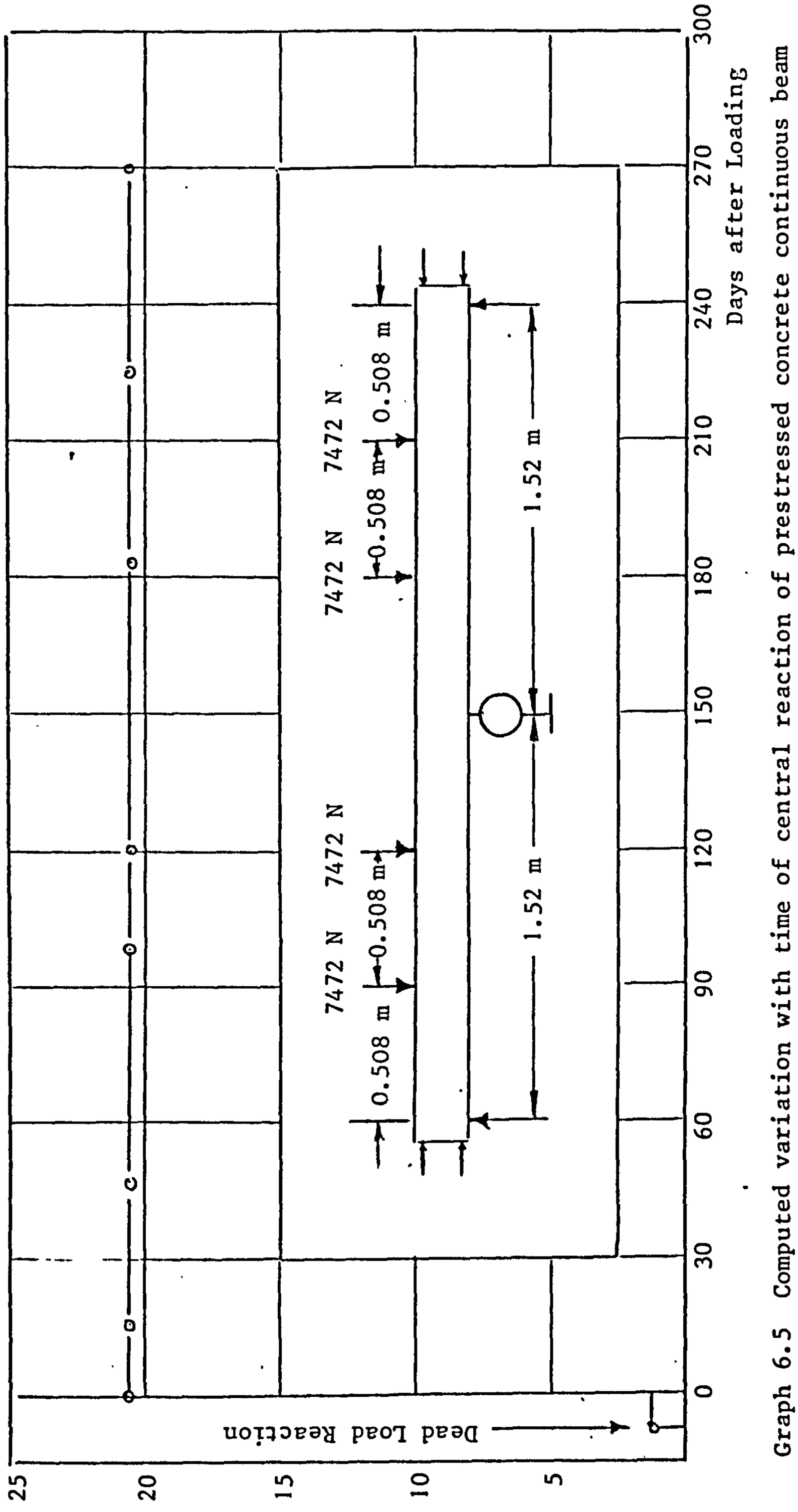

Graph 6.5 Computed variation with time of central reaction of prestressed concrete continuous beam after loading

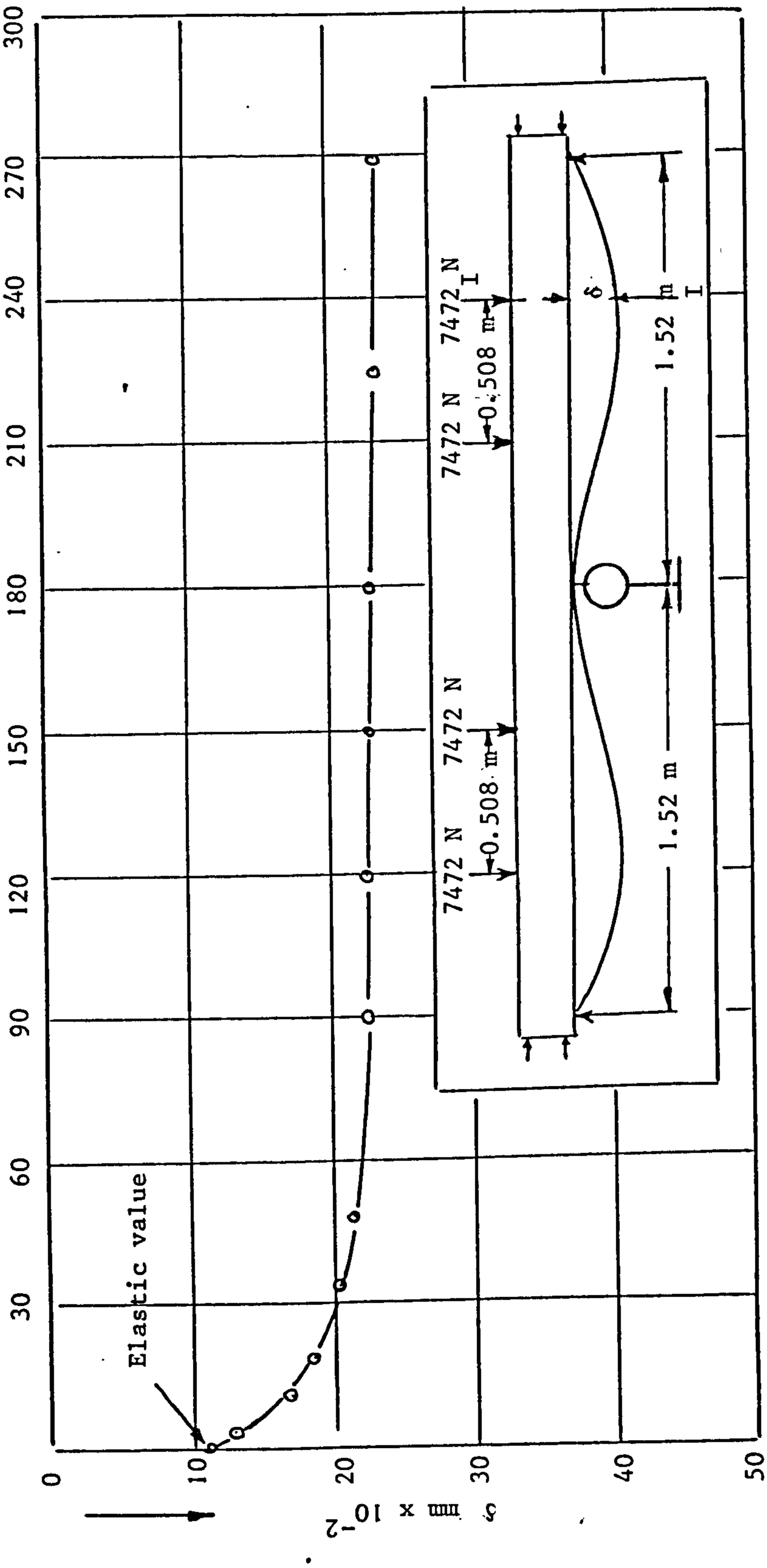

Graph 6.6 Computed time deflection behaviour at Sec. I-I of prestressed concrete continuous beam after loading

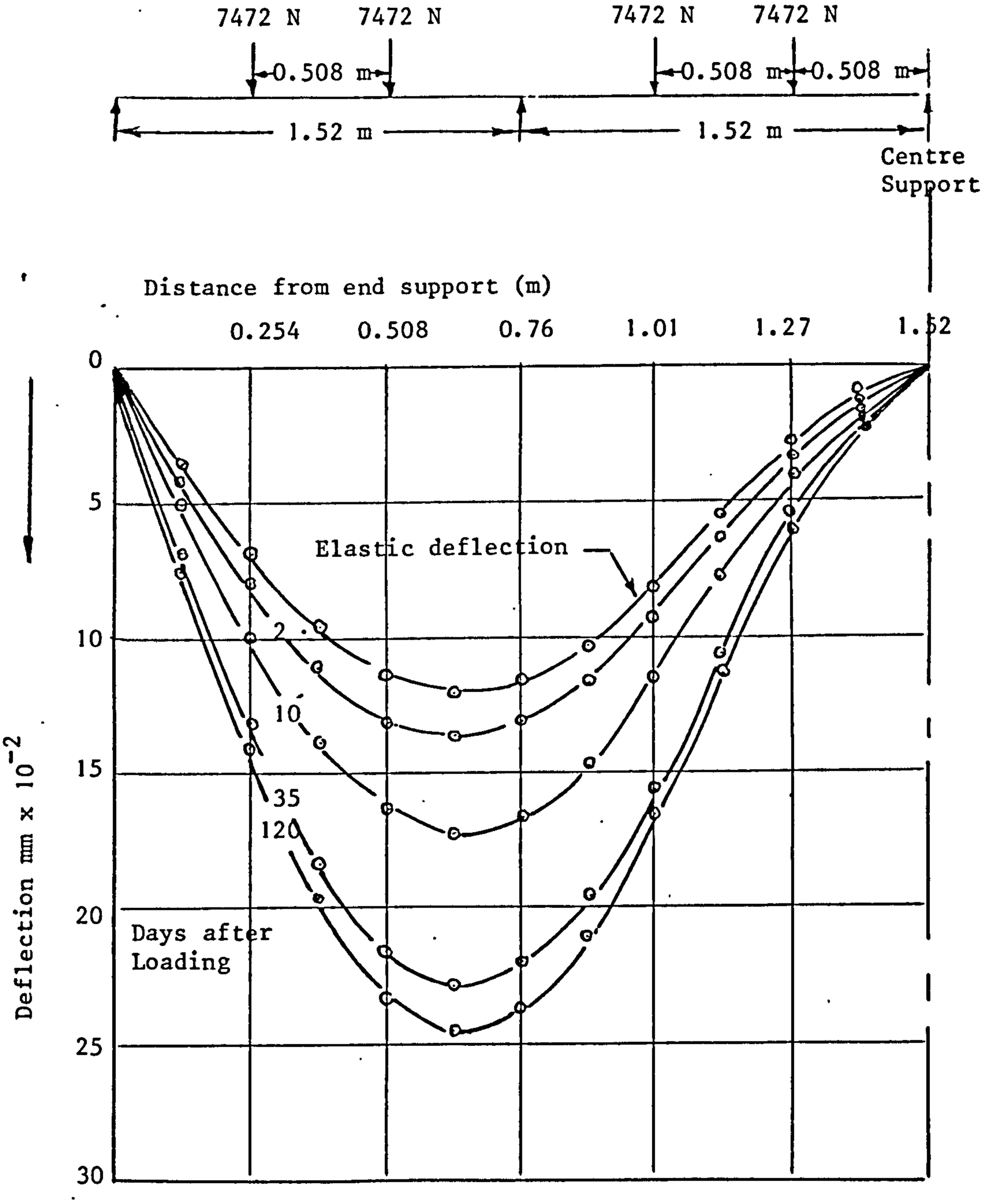

Graph 6.7 Computed deflection profile of prestressed concrete continuous beam after loading

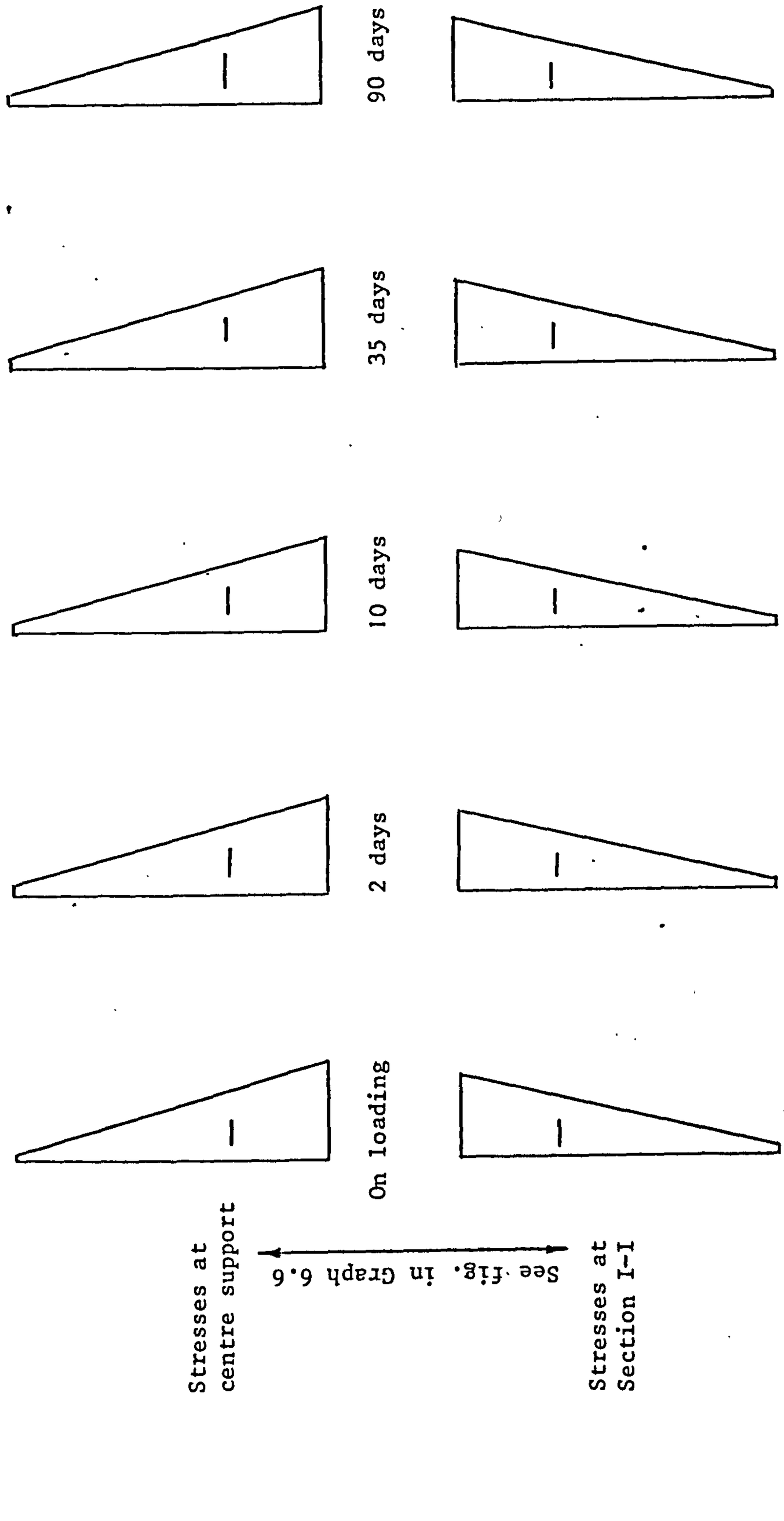

Graph 6.8 Computed concrete stress distribution (elastic, creep) of prestressed concrete continuous beam for two cross-sections of the beam

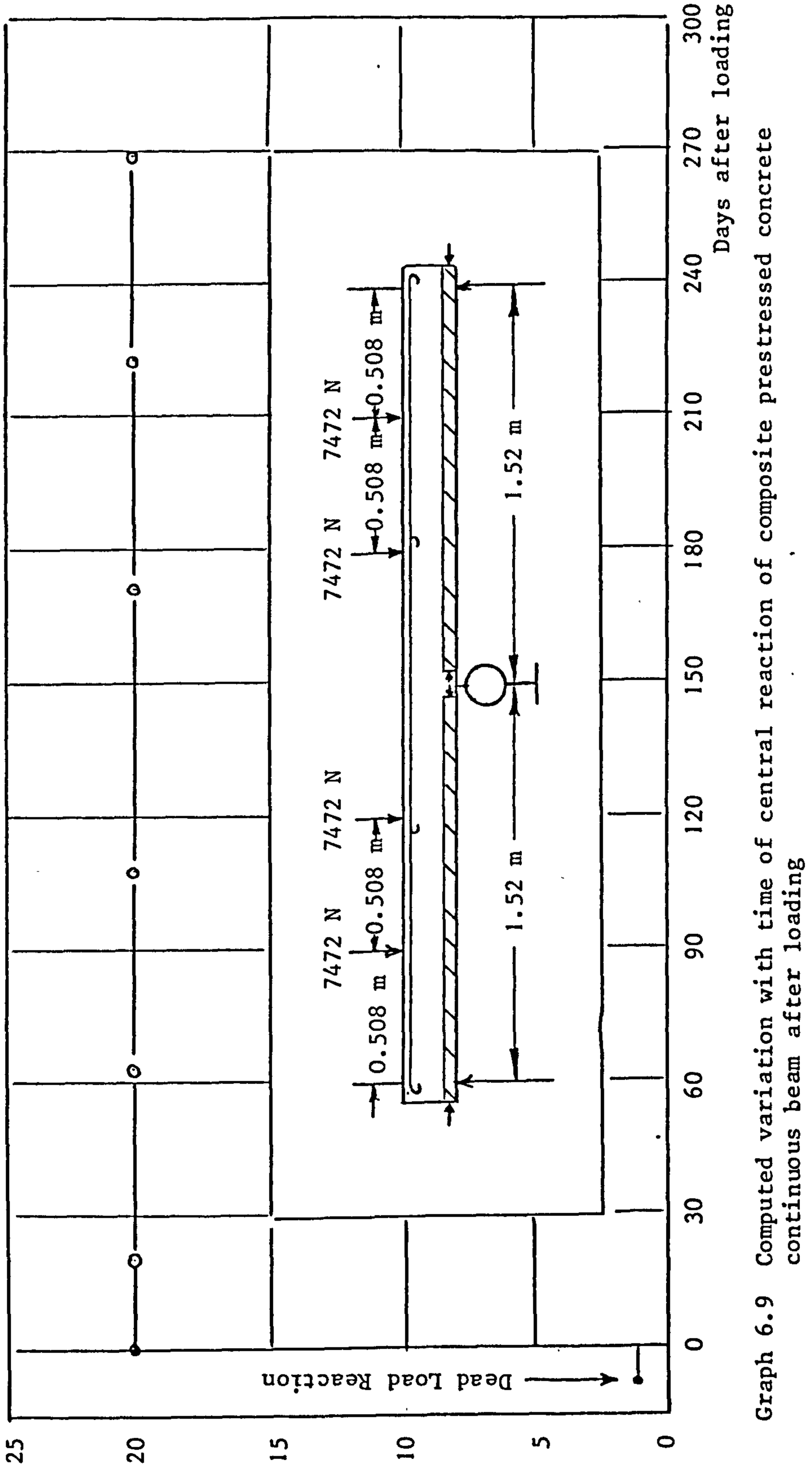

Graph 6.9 Computed variation with time of central reaction of composite prestressed continuous beam after loading

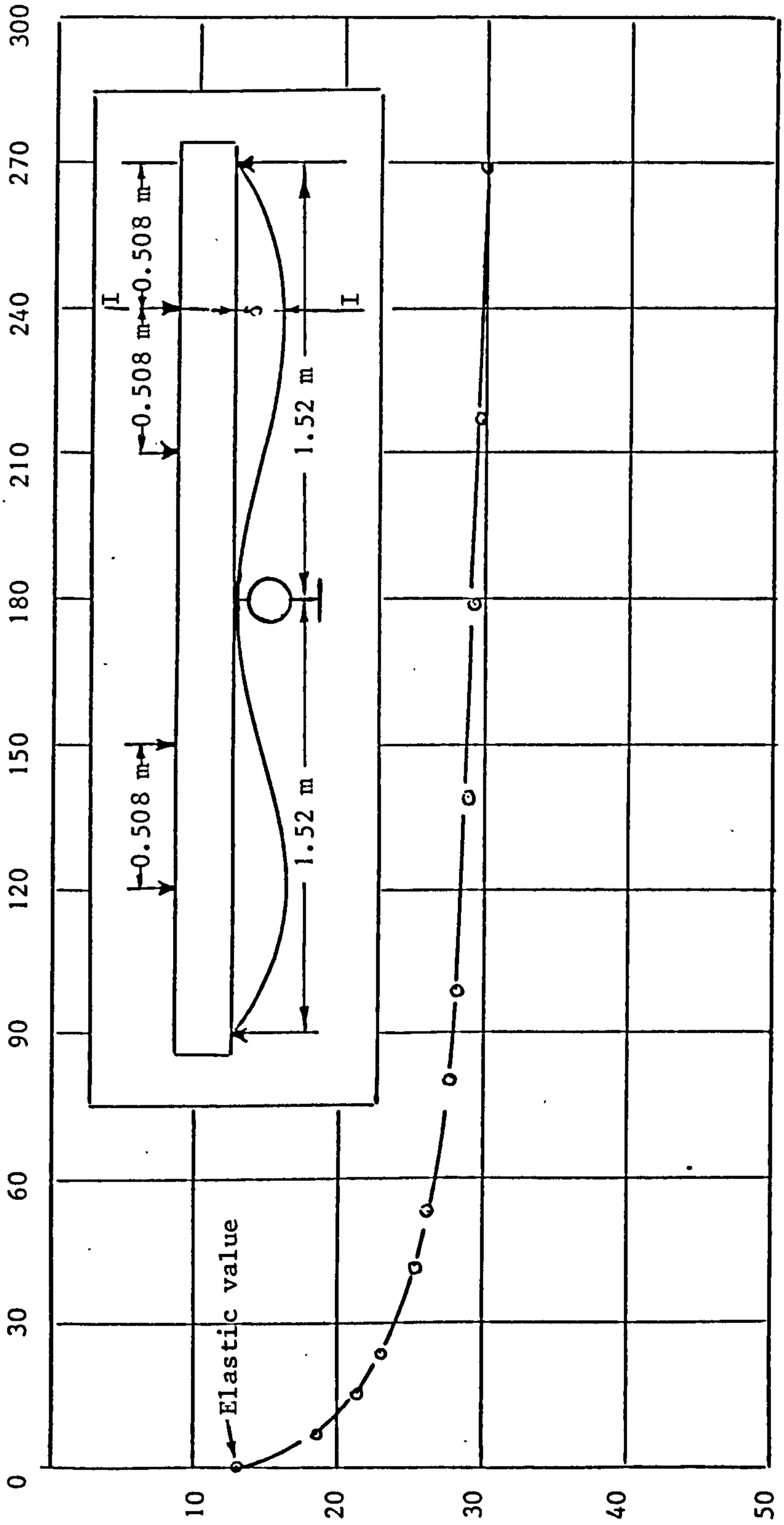

Graph 6.10 Computed time deflection behaviour at Sec. I-I of composite prestressed concrete continuous beam after loading

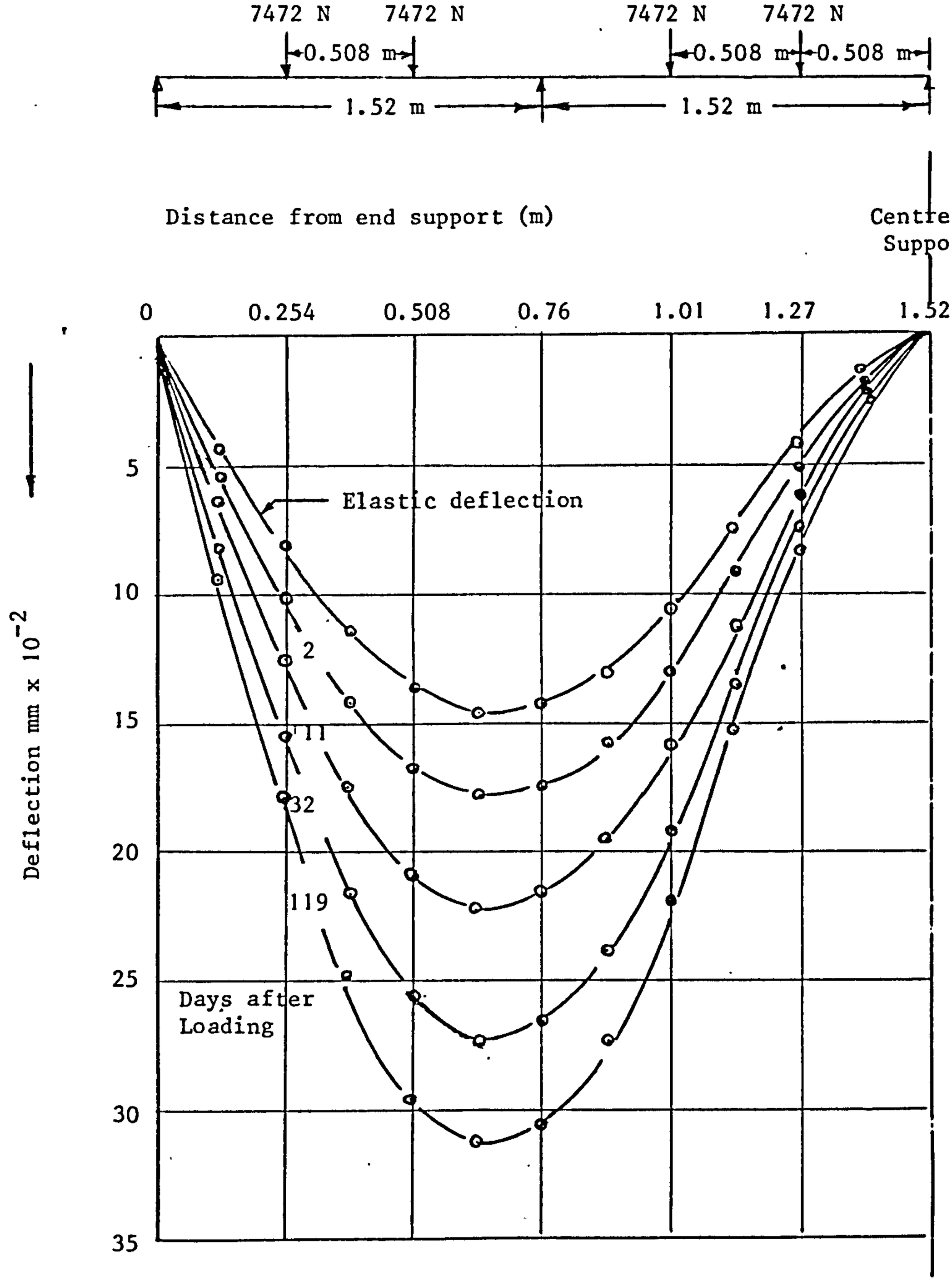

Graph 6.11 Computed deflection profile of composite prestressed concrete continuous beam after loading

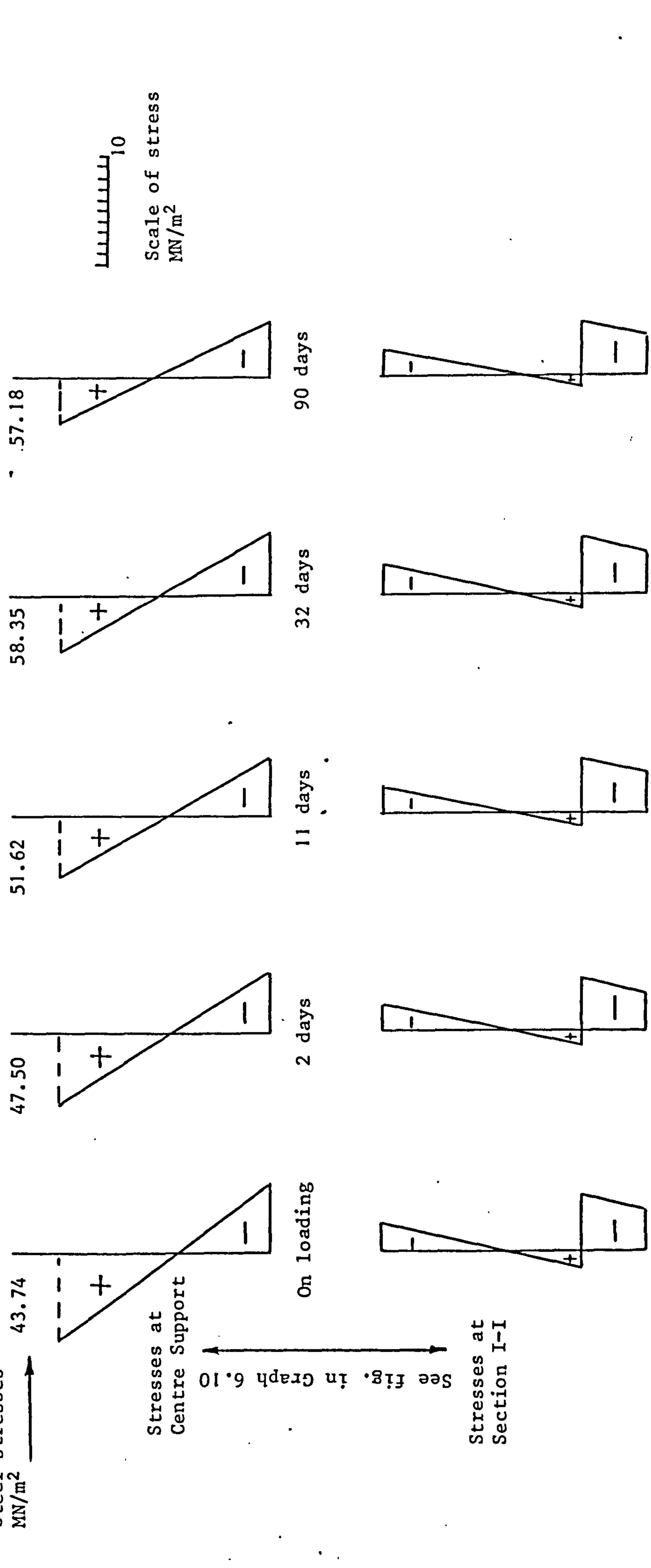

Graph 6.12 Computed concrete stress distribution (elastic, creep) of composite prestressed concrete continuous beam for two cross sections of the beam

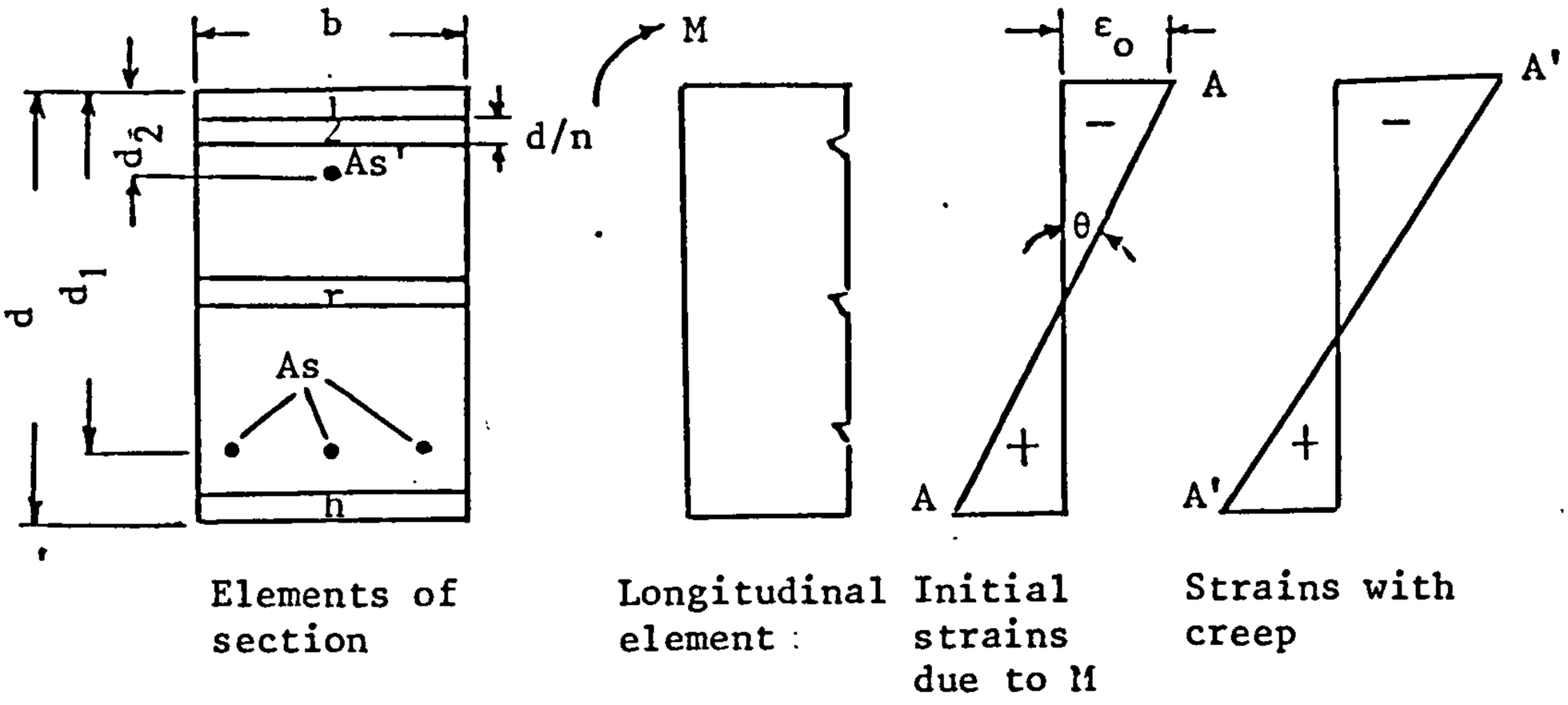

Fig. 6.1 Strains in reinforced concrete beam by the Effective Modulus Method

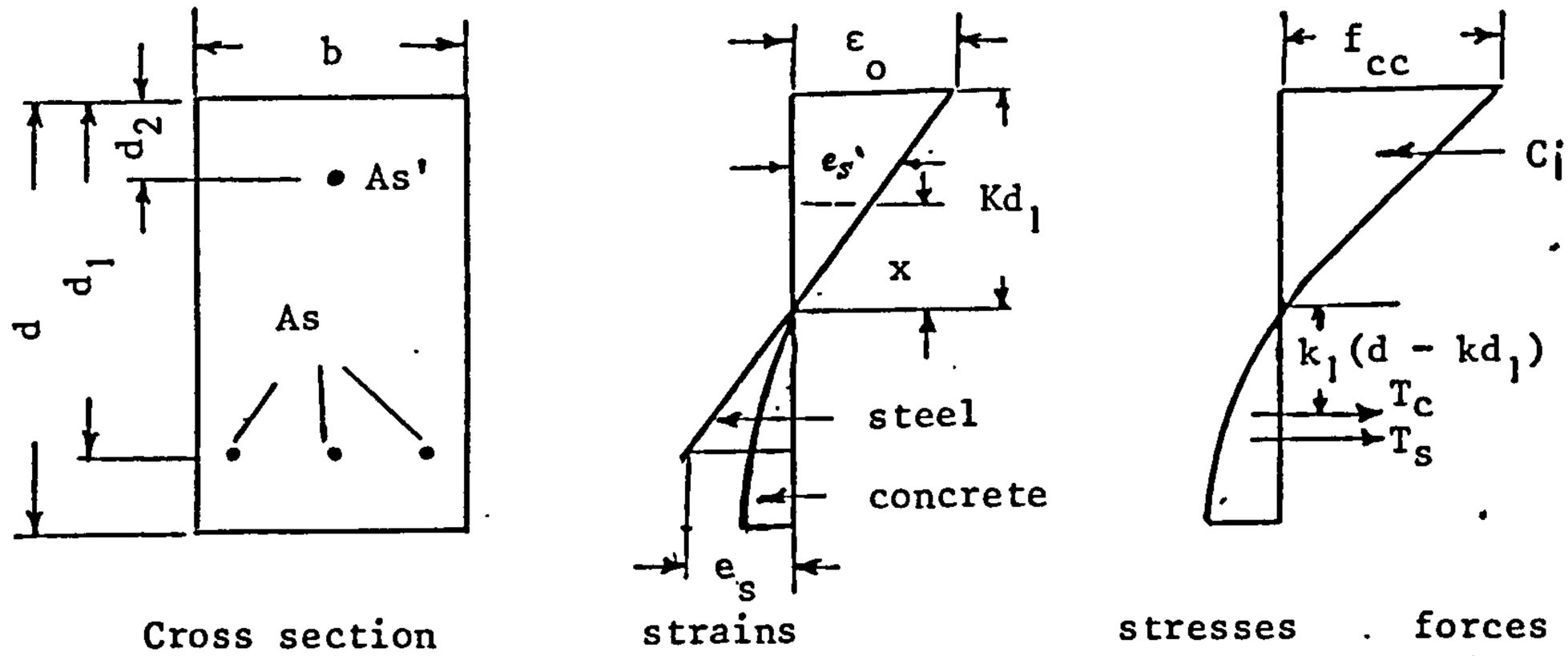

Fig. 6.2 Conditions at a distance $\ell < \ell_\beta$ from a crack

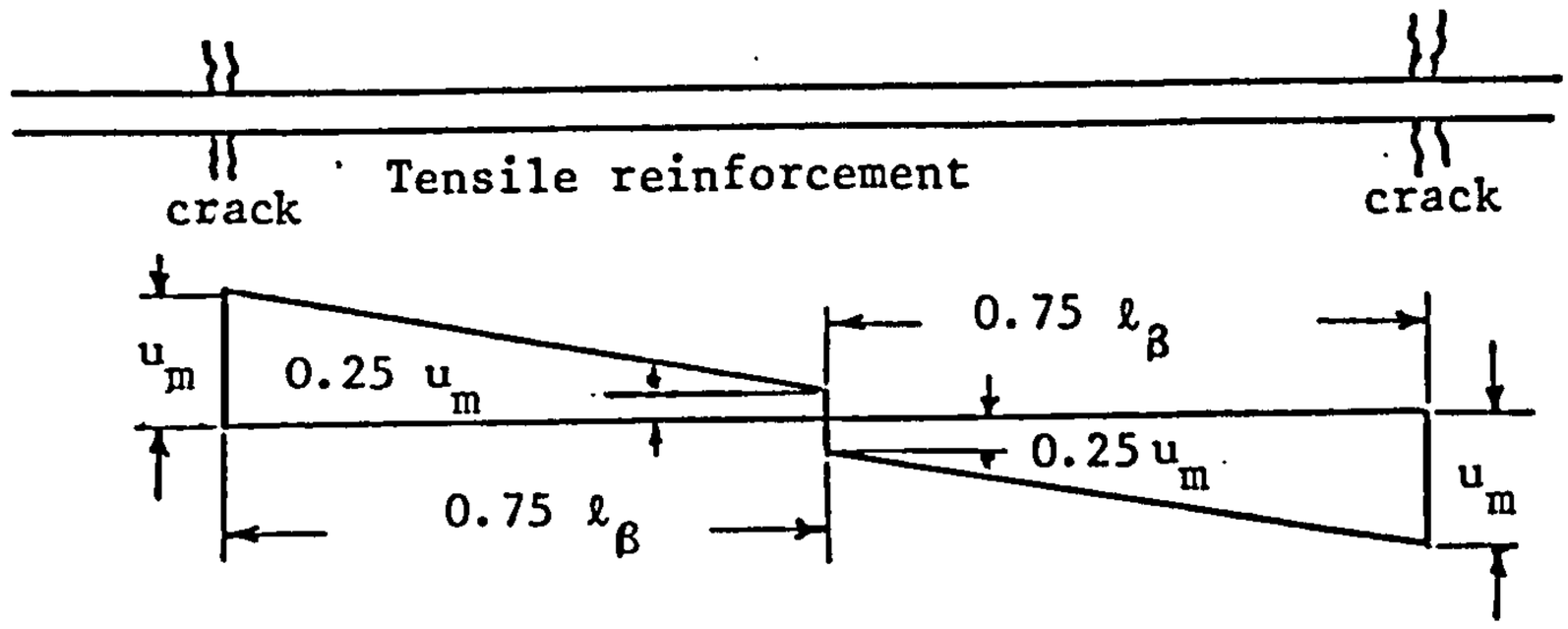

Fig. 6.3 Bond stress distribution between adjacent cracks

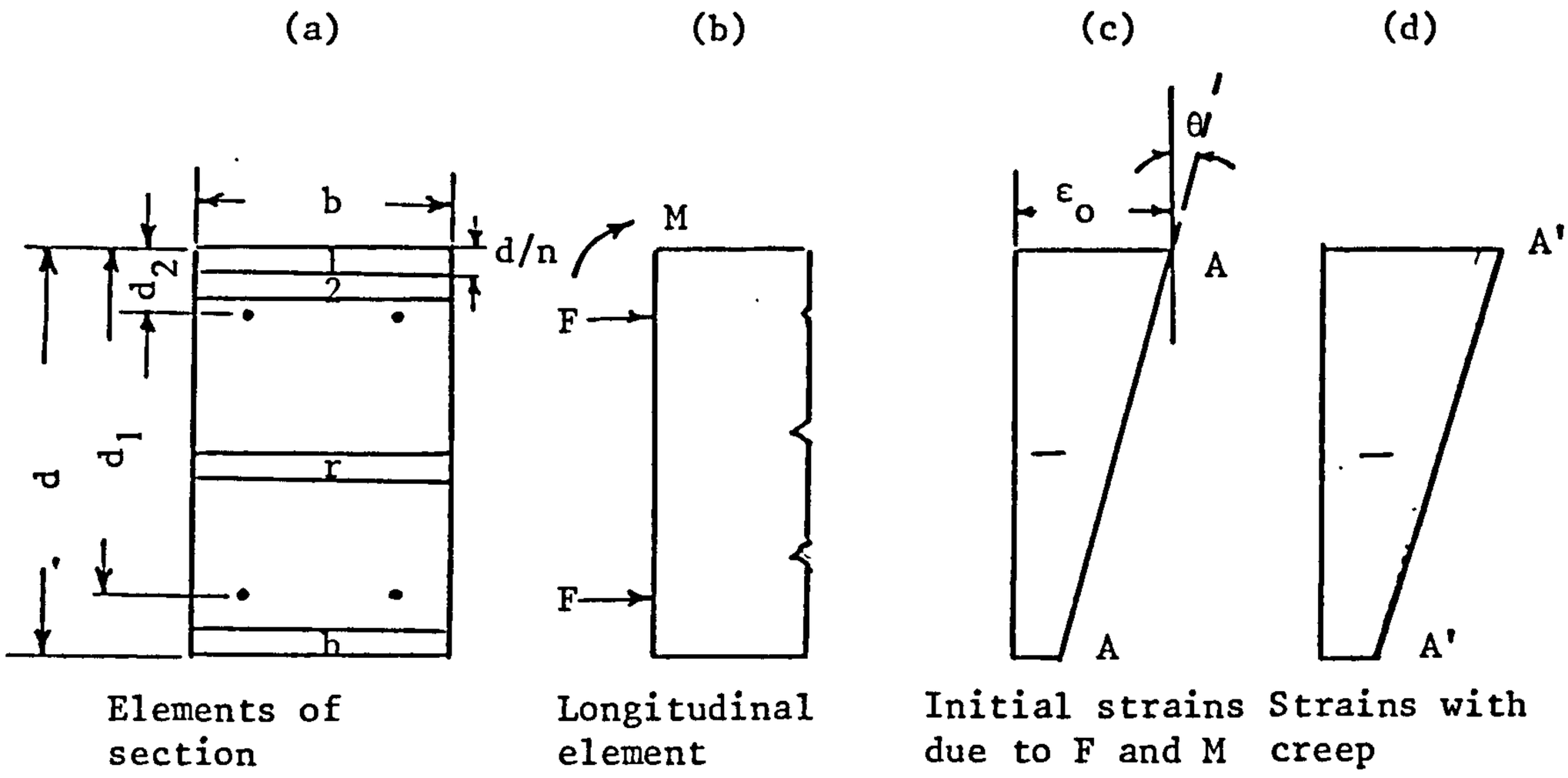

Elements of section | Longitudinal element | Initial strains due to F and M | Strains with creep

Fig. 6.4 Strains in prestressed concrete beam by the Effective Modulus Method

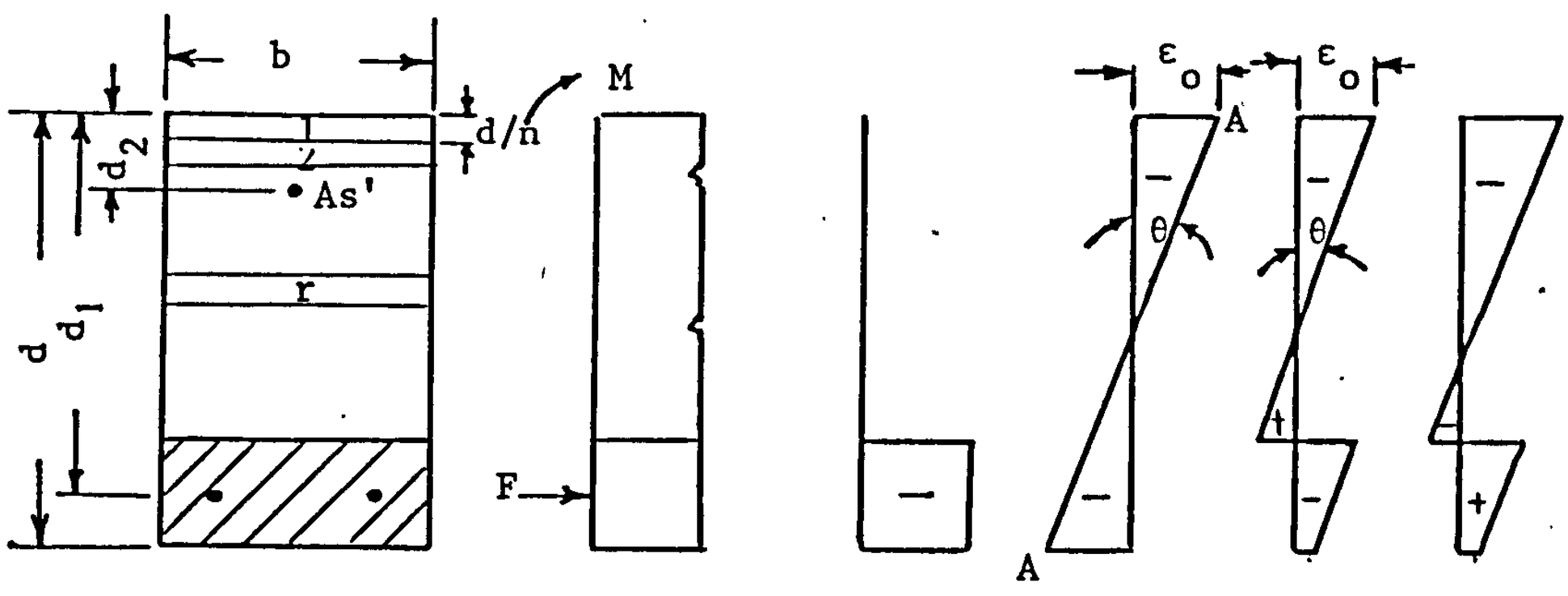

Elements of section | Longitudinal element | Initial strains due to F | Initial strains due to M | Initial strains due to F and M | Strains with creep

Fig. 6.5 Strains in composite prestressed concrete beam by the Effective Modulus Method

CHAPTER 7

(Beams subjected to temperature gradient)

The influence of temperature gradient on the theoretical behaviour of continuous concrete beams (similar to those of Chapter 3) i.e. reinforced, prestressed and composite pre-stressed concrete beams.

7.1 SYNOPSIS

Theoretical studies taking into account the influence of temperature gradient on the short and long-term behaviour of the three types of two span continuous concrete beams reported in Chapter 3 are presented in this Chapter. The numerical procedure used in Chapter 6 is extended here to calculate the elastic and long-term stresses and displacements of the three types of concrete beams subject to temperature crossfalls in terms of the stress strain temperature - time properties of concrete. First a temperature gradient is chosen for each type of beam in order not to create cracks due to heating and loading at the bottom side of any beam over the centre support and the analysis was carried out to predict the behaviour of the three types of beams under that condition. Secondly, the analysis was carried out by applying the same constant temperature gradient to each beam in order to compare the theoretical behaviour of the three types of beam under the previous condition.

Thirdly, the analysis was carried out with respect to the composite beam only using constant concrete properties for prestressed portion and variable reduced properties for cast-in-place portion. There was a slight increase in centre support reaction due to creep accompanied by significant increase in approximately the mid-span deflection due to reduction in cast-in-place concrete properties.

Finally, the analysis was carried out with respect to reinforced concrete beam only by assuming increase of maximum allowable concrete stress in tension f_{ct} to prevent the formation of any

cracks at any time during the whole period of sustained loading and heating. Two temperature gradients have been considered in the analysis for comparison.

Significant increase in the computed thermo-elastic deflection with respect to the computed elastic deflection of a cracked reinforced concrete beam is recorded due to increase in temperature gradient.

7.2 INTRODUCTION

This Chapter is concerned with the short and long-term creep analysis under thermal gradients while carrying a constant sustained working load for the three types of concrete beams, similar to those reported in Chapter 3. (Laboratory temperature assumed 15^{o}C)

The analysis has been carried out on the basis of certain assumptions and provisions reported in Table 7.1.

Beam Type	Temperature Gradient ^{o}C		Cases of Study
	Top Surface	Bottom Surface	
R.C.	60	30	1 - Cracks are allowed
	40	30	2 - Cracks are not allowed
P.C.	50	30	Cracks are not allowed
	40	30	
C.P.C.	40	30	1 - Cracks are allowed 2 - Cracks are allowed with the provision of constant precast concrete properties and variable reduced cast-in-place concrete properties

Table 7.1 Assumptions and provisions used in the analysis of the three types of concrete beams

The analysis shows the effect of variation of cast-in-place concrete properties with respect to constant prestressed concrete portion properties on the long-term behaviour of composite beam and also shows the significant effect of cracking due to increase in temperature gradient on the thermoelastic deflection behaviour of the reinforced concrete beam. The object of this Chapter is to provide a numerical analytical solution for the prediction of elastic and long-term stress distributions, vertical deflections and variation of reactions and to show the main difference in behaviour between the same beams reported in Chapter 6 when subjected to uniform temperature.

7.3 ASSUMPTIONS

1. Concrete does not crack in the case of prestressed beam.

2. Concrete does crack in the case of reinforced concrete beam when the maximum allowable tensile stress of concrete is exceeded.

3. The prestressed portion and the cast-in-place portion at the bottom surface of the beam over the centre support when subjected to tensile stresses due to temperature does not crack in the case of composite prestressed beam.

4. Elastic strain is proportional to stress and up to cracking in tension. Compressive stresses defined by negative sign.

5. Sections that are plane before heating remain plane after heating.

6. Creep in tension is the same as creep in compression and is proportional to stress.

7. Creep strain is proportional to temperature in the range 20-80°C.

8. The effective modulus at any instant neglects the stress history and predicts complete recovery of creep after removal of stress and is given by

$$E_c' = \frac{1}{e + ct}$$

where $e = \frac{1}{\text{instantaneous modulus of concrete}}$

t = temperature

c = specific thermal creep (i.e. creep/unit stress/ unit temperature) See Chapter 1 art. 1.2 Effective Modulus method for calculating creep at varying stress.

9. Coefficient of expansion is known and is constant and is taken 12×10^{-6} as an average value for steel and concrete.

10. Total strain = Elastic strain + thermal strain + creep strain.

11. Strength of concrete Mix A in tension 2620 MN/m^2.

12. The effect of shearing stress on deflections is negligible.

7.4 NOTATIONS

r = horizontal strip of beam section of thickness $\frac{d}{n}$

b = breadth of beam

d = depth of beam

d_1 = distance of the bottom reinforcement from the upper face of the section

d_2 = distance of the top reinforcement from the upper face of the section

n = number of horizontal elements

m = number of horizontal elements in prestressed portion of composite beam

E_s = Modulus of elasticity of steel

E_c = instantaneous modulus of elasticity of concrete Mix A (units for reinforced and composite concrete beams)

E = instantaneous modulus of elasticity of concrete Mix B (prestressed units)

E_{cr} = Effective modulus of Concrete Mix A at the rth element (units for reinforced and composite concrete beams)

E_r = effective modulus of concrete Mix B at the rth element (prestressed units)

N = modular ratio

M = bending moment

A_s = Area of the bottom reinforcement of the section

A_s' = Area of the top reinforcement of the section

ε_o = longitudinal strain of the upper face of the section

$\varepsilon_{r,\sigma}$ = longitudinal strain associated with stress of the rth element

$\varepsilon_{r,f}$ = longitudinal free strain of the rth element due to temperature

$\varepsilon_{,fs}$ = longitudinal free strain of the section due to temperature at the level of tensile reinforcement

$\varepsilon_{,fs'}$ = longitudinal free strain of the section due to temperature at the level of compressive reinforcement.

f_{ct} = maximum allowable tensile stress of concrete Mix A 2620 MN/m^2

$'_{\theta}$ = curvature

ΔF_r = longitudinal force on the rth element

F = Prestressing force

f_s = tensile steel stress

f_s' = compressive steel stress

c = specific thermal creep (i.e. creep/unit stress/unit temperature)

7.5 THEORY

7.5.1 Behaviour of reinforced concrete two span continuous beam

The analysis proceeds by applying transverse temperature distribution and a particular value of M to each longitudinal element as shown in Fig. 7.1(b) and (c) thus producing a free strain diagram as shown by line BB Fig. 7.1(d). Compatability and equilibrium are then achieved by introducing the straight line AA which represents the actual strains in the elements. Thus the strains represented between line AA and BB are associated with stresses which themselves satisfy the equilibrium conditions of the longitudinal element.

The two unknown quantities to be determined for each longitudinal element are therefore the longitudinal strain ε_o and the curvature θ.

With reference to the rth element in Fig. 7.1(a), the strain associated with stress is denoted by:

$$\varepsilon_{r,\sigma} = \varepsilon_{r,f} - \left[\varepsilon_o - \frac{(2r-1)}{2n}\theta d\right] \qquad (7.1)$$

The resulting longitudinal force on the element is

$$\Delta F_r = \frac{bd}{n} E_{cr} \varepsilon_{r,\sigma} \qquad (7.2)$$

The total longitudinal force is the summation of the force increments from equation (7.2) thus:

$$0 = \sum_{r=1}^{r=n} \frac{bd}{n} E_{cr}\left[\varepsilon_{r,f} - \left(\varepsilon_o - \frac{(2r-1)}{2n}\theta d\right)\right] + \left[\varepsilon_{,fs'} - (\varepsilon_o - \theta d_2)\right] A_s' E_s + \left[\varepsilon_{,fs} - (\varepsilon_o - \theta d_1)\right] A_s E_s \qquad (7.3)$$

from equation (7.3) we obtain:

$$\theta = \frac{\varepsilon_o\left[\frac{bd}{n}\sum_{r=1}^{r=n} E_{cr} + E_s(A_s + A_s')\right] - \frac{bd}{n}\sum_{r=1}^{r=n} E_{cr}\varepsilon_{r,f} - E_s(\varepsilon_{,fs}A_s + \varepsilon_{,fs'}A_s')}{\frac{bd^2}{2n^2}\sum_{r=1}^{r=n} E_{cr}(2r-1) + E_s(d_1A_s + d_2A_s')} \qquad (7.4)$$

A second equation of equilibrium of the longitudinal element is obtained by consideration of flexure. Taking moments with respect to the upper face of the section gives:

$$-M = d_1 A_s E_s \left[\varepsilon_{,fs} - (\varepsilon_o - \theta d_1)\right] + d_2 A_s' E_s \left[\varepsilon_{,fs}' - (\varepsilon_o - \theta d_2)\right] +$$

$$\sum_{r=1}^{r=n} \frac{bd}{n} E_{cr} \left[\varepsilon_{r,f} - \left(\varepsilon_o - \frac{(2r-1)}{2n}\theta d\right)\right] \frac{(2r-1)}{2n} d \qquad (7.5)$$

from equation (7.5) we obtain:

$$\theta = \left\{ \varepsilon_o \left[\frac{bd^2}{2n^2} \sum_{r=1}^{r=n} E_{cr}(2r-1) + E_s(d_1 A_s + d_2 A_s')\right] - \frac{bd^2}{2n^2} \sum_{r=1}^{r=n} E_{cr}\varepsilon_{r,f}(2r-1) - E_s\left[d_1 A_s \varepsilon_{,fs} + d_2 A_s' \varepsilon_{,fs}'\right] - M \right\} \Big/$$

$$\left[\frac{bd^3}{4n^3} \sum_{r=1}^{r=n} E_{cr}(2r-1)^2 + E_s(d_1^2 A_s + d_2^2 A_s')\right] \qquad (7.6)$$

The solution of equations (7.4) and (7.6) yield the following expression for the longitudinal strain ε_o:

$$\varepsilon_o = \frac{PA + RY - QQ - ZZ - M/C_1}{\left[\frac{A_1 C_1 - B_1^2}{B_1 C_1}\right]} \qquad (7.7)$$

where

$$PA = \frac{\frac{bd}{n} \sum_{r=1}^{r=n} E_{cr}\varepsilon_{r,f}}{\frac{bd^2}{2n^2} \sum_{r=1}^{r=n} E_{cr}(2r-1) + E_s(d_1 A_s + d_2 A_s')}$$

$$RY = \frac{E_s(\varepsilon_{,fs}A_s + \varepsilon_{,fs}'A_s')}{\frac{bd^2}{2n^2}\sum_{r=1}^{r=n}E_{cr}(2r-1) + E_s(d_1A_s + d_2A_s')}$$

$$QQ = \frac{\frac{bd^2}{2n^2}\sum_{r=1}^{r=n}E_{cr}\varepsilon_{r,f}(2r-1)}{\frac{bd^3}{4n^3}\sum_{r=1}^{r=n}E_{cr}(2r-1)^2 + E_s(d_1^2A_s + d_2^2A_s')}$$

$$ZZ = \frac{E_s(d_1A_s\varepsilon_{,fs} + d_2A_s'\varepsilon_{,fs}')}{\frac{bd^3}{4n^3}\sum_{r=1}^{r=n}E_{cr}(2r-1)^2 + E_s(d_1^2A_s + d_2^2A_s')}$$

$$A_1 = \frac{bd}{n}\sum_{r=1}^{r=n}E_{cr} + E_s(A_s + A_s')$$

$$B_1 = \frac{bd^2}{2n^2}\sum_{r=1}^{r=n}E_{cr}(2r-1) + E_s(d_1A_s + d_2A_s')$$

$$C_1 = \frac{bd^3}{4n^3}\sum_{r=1}^{r=n}E_{cr}(2r-1)^2 + E_s(d_1^2A_s + d_2^2A_s')$$

The curvature θ may be obtained from equation 7.4 by substitution for ε_o from equation (7.7).

The effects of cracks in some parts of the beam could be taken into consideration using the same procedure used in reinforced concrete beam reported in Chapter 6 (art.6.5.1) with values of ε_o and θ for each longitudinal element known, their integrated effect along the beam permit slopes and deflections to be evaluated.

7.5.2 Behaviour of prestressed concrete two span continuous beam

The same method of analysis used in Chapter 6 (art. 6.5.2) is used here to predict the behaviour of prestressed beam subjected to a sustained transverse temperature distribution and bending moment.

The analysis proceeds by applying two forces each equal to F, transverse temperature distribution and a particular value of M to each longitudinal element as shown in Fig. 7.2(b) and (c), thus producing a free strain diagram as shown by line BB Fig. 7.2(d). Compatability and equilibrium are then achieved by introducing the straight line AA which represents the actual strains in the elements. Thus the strains represented between line AA and BB are associated with stresses which themselves satisfy the equilibrium conditions of the longitudinal element. The two unknown quantities to be determined for each longitudinal element are therefore the longitudinal strain ε_o and the curvature θ.

With reference to the rth element in Fig. 7.2(a), the strain associated with stress is:

$$\varepsilon_{r,\sigma} = \varepsilon_{r,f} - \left[\varepsilon_o - \frac{(2r-1)}{2n}\theta\, d\right] \qquad (7.8)$$

The resulting longitudinal force on the element is:

$$\Delta F_r = \frac{bd}{n} E_r \varepsilon_{r,\sigma} \qquad (7.9)$$

In which E_r is the effective modulus for concrete in the rth element.

The total longitudinal force is the summation of the force increments from equation (7.9) thus:

$$2F = \sum_{r=1}^{r=n} \frac{bd}{n} E_r \left[\varepsilon_{r,f} - \left(\varepsilon_o - \frac{(2r - 1)}{2n} \theta d\right)\right] \qquad (7.10)$$

from equation (7.10) we obtain:

$$\theta = \frac{\frac{bd}{n} \varepsilon_o \sum_{r=1}^{r=n} E_r + 2F - \frac{bd}{n} \sum_{r=1}^{r=n} \varepsilon_{r,f} E_r}{\frac{bd^2}{2n^2} \sum_{r=1}^{r=n} (2r - 1) E_r} \qquad (7.11)$$

A second equation of equilibrium of the longitudinal element is obtained by consideration of flexure. Taking moments with respect to the upper face of the section gives:

$$(d_1 + d_2)F - M = \sum_{r=1}^{r=n} \frac{bd}{n} E_r \left[\varepsilon_{r,f} - \left(\varepsilon_o - \frac{(2r - 1)}{2n} \theta d\right)\right] \frac{(2r - 1)}{2n} d \qquad (7.12)$$

from equation (7.12) we obtain:

$$\theta = \frac{\frac{bd^2}{2n^2} \varepsilon_o \sum_{r=1}^{r=n} E_r (2r - 1) + \left((d_1 + d_2)F - M\right) - \frac{bd^2}{2n^2} \sum_{r=1}^{r=n} \varepsilon_{r,f} E_r (2r - 1)}{\frac{bd^3}{4n^3} \sum_{r=1}^{r=n} E_r (2r - 1)^2} \qquad (7.13)$$

The solution of equations (7.11) and (7.13) yields the following expression for the longitudinal strain ε_o:

$$\varepsilon_o = \left\{ -\frac{Fd}{n} \sum_{r=1}^{r=n} E_r(2r-1)^2 + \left((d_1 + d_2)F - M \right) \sum_{r=1}^{r=n} E_r(2r-1) + \right.$$

$$\left. \frac{bd^2}{2n^2} \left[\sum_{r=1}^{r=n} E_r(2r-1)^2 \sum_{r=1}^{r=n} \varepsilon_{r,f} E_r - \sum_{r=1}^{r=n} E_r(2r-1) \sum_{r=1}^{r=n} \varepsilon_{r,f} E_r(2r-1) \right] \right\} \Big/$$

$$\frac{bd^2}{2n^2} \left[\sum_{r=1}^{r=n} E_r \sum_{r=1}^{r=n} E_r(2r-1)^2 - \left(\sum_{r=1}^{r=n} E_r(2r-1) \right)^2 \right] \qquad (7.14)$$

The curvature θ may be obtained from euqation (7.11) by substitution for ε_o from equation (7.14).

The stress distribution over the cross section is then found from equation (7.8) on multiplication by E_r.

With values of ε_o and θ for each longitudinal element known, their integrated effect along the member permits slopes and deflections to be evaluated.

7.5.3 Behaviour of composite prestressed concrete two span continuous beam

Assuming that the prestressed portion is divided into m elements, the analysis proceeds by applying the force F, transverse temperature distribution and a particular value of M to each longitudinal element as shown in Fig. 7.3(b) and (c), thus producing a free strain diagram as shown by line BB Fig. 7.3(d). Compatability and equilibrium are then achieved by introducing the lines AA and CC which represent the actual strains in the elements. Thus the strains represented between lines AA, CC

and BB are associated with stresses which themselves satisfy the equilibrium conditions of the longitudinal element.

The two unknown quantities to be determined for each longitudinal element are therefore the longitudinal strain ε_o and the curvature θ.

With reference to the rth element in Fig. 7.3(a), the strain associated with stress is:

$$\varepsilon_{r,\sigma} = \varepsilon_{r,f} - \left[\varepsilon_o - \frac{(2r-1)}{2n}\theta d\right] \tag{7.15}$$

The resulting longitudinal force on the element is

$$\Delta F_r = \frac{bd}{n} E_{cr} \varepsilon_{r,\sigma} \tag{7.16}$$

The total longitudinal force is the summation of the force increments from equation (7.16):

$$0 = \sum_{r=1}^{r=n-m} \frac{bd}{n} E_{cr}\left[\varepsilon_{r,f} - \left(\varepsilon_o - \frac{(2r-1)}{2n}\theta d\right)\right] + \left[\varepsilon_{,fs}' - (\varepsilon_o - \theta d_2)\right] A_s' E_s$$

$$+ \sum_{r=n-(m-1)}^{r=n} \frac{bd}{n} E_r\left[\varepsilon_{r,f} - \left(\varepsilon_o - \frac{(2r-1)}{2n}\theta d\right)\right] \tag{7.17}$$

from equation (7.17) we obtain:

$$\theta = \left\{ \varepsilon_o \left[\frac{bd}{n} \left(\sum_{r=1}^{r=n-m} E_{cr} + \sum_{r=n-(m-1)}^{r=n} E_r \right) + A_s' E_s \right] - \right.$$

$$\left. \frac{bd}{n} \left(\sum_{r=1}^{r=n-m} E_{cr} \varepsilon_{r,f} + \sum_{r=n-(m-1)}^{r=n} E_r \varepsilon_{r,f} \right) - \varepsilon_{,fs}' A_s' E_s \right\} \Big/$$

$$\left[\frac{bd^2}{2n^2} \left(\sum_{r=1}^{r=n-m} E_{cr}(2r-1) + \sum_{r=n-(m-1)}^{r=n} E_r(2r-1) \right) + d_2 A_s' E_s \right]$$

(7.18)

A second equation of equilibrium of the longitudinal element is obtained by consideration of flexure. Taking moments with respect to the upper face of the section gives:

$$-M = \sum_{r=1}^{r=n-m} \frac{bd}{n} E_{cr} \left[\varepsilon_{r,f} - \left(\varepsilon_o - \frac{(2r-1)}{2n} \theta d \right) \right] \frac{(2r-1)}{2n} d +$$

$$d_2 A_s' E_s \left[\varepsilon_{,fs}' - (\varepsilon_o - \theta d_2) \right] + \sum_{r=n-(m-1)}^{r=n} \frac{bd}{n} E_r \left[\varepsilon_{r,f} - \right.$$

$$\left. \left(\varepsilon_o - \frac{(2r-1)}{2n} \theta d \right) \right] \frac{(2r-1)}{2n} d \qquad (7.19)$$

from equation (7.19) we obtain:

$$\theta = \left\{ \varepsilon_o \left[\frac{bd^2}{2n^2} \left(\sum_{r=1}^{r=n-m} E_{cr}(2r-1) + \sum_{r=n-(m-1)}^{r=n} E_r(2r-1) \right) + d_2 A_s' E_s \right] - \right.$$

$$\frac{bd^2}{2n^2} \left[\sum_{r=1}^{r=n-m} E_{cr}\varepsilon_{r,f}(2r-1) + \sum_{r=n-(m-1)}^{r=n} E_r \varepsilon_{r,f}(2r-1) \right] -$$

$$\left. d_2 A_s' E_s \varepsilon_{,fs}' - M \right\} \Bigg/$$

$$\left[\frac{bd^3}{4n^3} \left(\sum_{r=1}^{r=n-m} E_{cr}(2r-1)^2 + \sum_{r=n-(m-1)}^{r=n} E_r(2r-1)^2 \right) + d_2^2 A_s' E_s \right] \quad . \quad (7.20)$$

The solution of equations (7.18) and (7.20) yields the following expression for the longitudinal strain ε_o:

$$\varepsilon_o = \frac{(PA + RY - QQ - ZZ - (\frac{M}{D}))}{(\frac{AD - B^2}{BD})} \qquad (7.21)$$

Where

$$A = \frac{bd}{n} \left(\sum_{r=1}^{r=n-m} E_{cr} + \sum_{r=n-(m-1)}^{r=n} E_r \right) + A_s' E_s$$

$$B = \frac{bd^2}{2n^2} \left[\sum_{r=1}^{r=n-m} E_{cr}(2r-1) + \sum_{r=n-(m-1)}^{r=n} E_r(2r-1) \right] + d_2 A_s' E_s$$

$$D = \frac{bd^3}{4n^3} \left[\sum_{r=1}^{r=n-m} E_{cr}(2r-1)^2 + \sum_{r=n-(m-1)}^{r=n} E_r(2r-1)^2 \right] + d_2^2 A_s' E_s$$

$$PA = \frac{bd}{n}\left(\sum_{r=1}^{r=n-m} E_{cr}\,\varepsilon_{r,f} + \sum_{r=n-(m-1)}^{r=n} E_r\,\varepsilon_{r,f} \right) \Big/ B$$

$$RY = \varepsilon_{,fs}' A_s' E_s / B$$

$$QQ = \frac{bd^2}{2n^2}\left[\sum_{r=1}^{r=n-m} E_{cr}\varepsilon_{r,f}(2r-1) + \sum_{r=n-(m-1)}^{r=n} E_r\varepsilon_{r,f}(2r-1) \right] \Big/ D$$

$$ZZ = d_2 A_s' E_s \varepsilon_{,fs}' / D$$

The curvature θ may be obtained from equation (7.18) by substitution for ε_o from equation (7.21). The effect of cracks in some parts of the beam could be taken into consideration by following the same procedure used in reinforced concrete beam reported in Chapter 6 (art. 6.5.1). With values of ε_o and θ for each longitudinal element known, their integrated effect along the beams permit slopes and deflections to be evaluated.

7.6 NUMERICAL EXAMPLES

7.6.1 Reinforced, prestressed and composite prestressed concrete continuous beams each subjected to different constant temperature gradient (see figs. in Graphs 7.1, 7.5 & 7.9)

(a) Centre Reaction

Graphs 7.1, 7.5 and 7.9 show the calculated variation of centre support reaction with time for 270 days of sustained heating and loading.

(b) Deflection

Graphs 7.2, 7.6 and 7.10 show the computed time deflection behaviour at Sec. I-I. Graphs 7.3, 7.7 and 7.11 show the calculated elastic and long-term variation with time of the deflection profile for half of the beam due to loading and heating.

(c) Stresses

Graphs 7.4, 7.8 and 7.12 show the computed elastic and long-term variation with time of the stress distribution for two cross sections of the beam at Sec. I-I and over the centre support.

7.6.2 Reinforced, prestressed and composite prestressed concrete continuous beams subjected to the same constant temperature gradient (see figs. in Graphs 7.13, 7.17 and 7.9)

(a) Centre Reaction

Graphs 7.13, 7.17 and 7.9 show the calculated variation of centre support reaction with time after heating and loading for 270 days.

(b) Deflection

Graphs 7.14, 7.18 and 7.10 show the computed time deflection behaviour at Sec. I-I. Graphs 7.15, 7.19 and 7.11 show the calculated elastic and long-term variation with time of the deflection profile for half of the beam due to loading and heating.

(c) Stresses

Graphs 7.16, 7.20 and 7.12 show the computed elastic and long-term variation with time of the stress distribution for two cross sections of each beam.

7.6.3 Composite prestressed concrete beam assuming constant concrete properties for prestressed portion and variable reduced properties for cast-in-place portion (see fig. in Graph 7.21.)

(a) Deflections

Graph 7.21 shows the calculated time deflection behaviour at Sec. I-I for the whole period of sustained loading and heating. Graph 7.22 shows the computed deflection profiles for half of the beam at 11 days after loading and heating.

(b) Stresses

Graph 7.23 shows the computed stress distribution at 11 days after loading and heating for two cross sections of the beam at Sec. I-I and over the centre support.

(c) Bending Moment

Graph 7.24 shows the computed variation with time of the bending

moment over the centre support for 270 days of sustained loading and heating.

7.7 DISCUSSIONS

(a) Beams subjected to different temperature gradient

Central Support Reaction

Graphs 7.1, 7.5 and 7.9 show the calculated variation of centre support reaction due to heating and loading of the three types of continuous concrete beams. A very large variation in the central reaction which is due to uniform temperature gradient is noticed. It is interesting to see that this reaction changes sign just after heating and loading of the beams. Creep would play a main part after that to bring the centre reaction back gradually to its original direction upwards to maintain co-linear supports. The behaviour of the three types of continuous beams concerning the variation of centre reaction is the same despite the difference inthe temperature crossfall between the three types of beams.

Deflections at spans Section I-I

Graph 7.2 shows the calculated variation of deflection behaviour of the reinforced concrete beam at Sec. I-I, the deflection is greatly increased by heating and loading.

Graphs 7.6 and 7.10 show the calculated variation with time of deflection behaviour of the prestressed and composite beams at Sec. I-I. A sudden reduction in the value of calculated deflection because of heating is noticed but gradually the creep effect would greatly increase the deflection at this section in the downward direction.

Deflection Profiles

Graph 7.3 shows the calculated variation with time of the deflection profile of half of the reinforced concrete beam. The deflection profile is greatly increasing due to heating and loading, but the rate of increase is decreasing by time as the rate of creep is decreasing.

Graph 7.7 shows the calculated variation with time of the deflection profile of the prestressed concrete beam. This diagram indicates the massive effect of temperature and creep on the elastic and long-term behaviour of the beam. Instant reduction in the deflection profile just after loading and heating is noticed but gradual increase in deflection profile is noticed in the downward direction because of the creep effect.

Graph 7.11 shows the calculated variation with time of deflection profile of half of the composite beam. The form of the changes occurring in the deflection profile by time is similar to that of the prestressed beam.

Stress distribution at selected sections

Graphs 7.4 and 7.12 show the calculated variation with time of the stress distribution after loading and heating for the reinforced and composite concrete beams. The form of the changes occurring in the stress distribution over the centre support by time for both beams is the same. The calculated variation of the stress distribution at Sec. I-I of the composite beam has a pattern different from that of the reinforced concrete beam because of the prestressed concrete plank.

Graph 7.8 shows the calculated variation with time of the stress distribution after loading and heating for the prestressed concrete beam at the section over the centre support. Initially, the stress distribution has the same form as the temperature distribution, but changes rapidly with time as concrete creeps. Redistribution is greater over the central support than at Sec. I-I because there is a greater and more rapid change of bending moment there.

(b) Beams subjected to the same temperature gradient

Central Support Reaction

Graphs 7.13, 7.17 and 7.9 show the calculated variation of centre support reaction due to loading and heating by applying the same constant temperature gradient to the three types of continuous concrete beams. A sudden reduction in central reaction is noticed in all types of beams just after heating and loading, but the reduction in reaction varies considerably from one beam to another with ratio 1:2:3.5 approximately with respect to reinforced, composite and prestressed beam respectively, depending upon the magnitude and direction of the bending moment at that section and the prestressing force, if any.

Deflections at span section I-I

Graphs 7.14, 7.18 and 7.10 show the calculated variation of deflection behaviour of reinforced, prestressed and composite beams at Sec. I-I. A sudden reduction in the value of calculated deflection because of heating is noticed in all types of beams, but the reduction varies considerably from one beam to another with a ratio 1:5:7 approximately with respect to reinforced, prestressed and composite beams. By time the creep would greatly

increase the deflection at this section in the downward direction and after 90 days of loading and heating the deflection at this particular section with respect to the three types of beams varies from 10-12%.

Deflection Profiles

Graphs 7.15, 7.19 and 7.11 show the calculated variation of deflection profile with time of half of reinforced, prestressed and composite beams. The diagrams indicate the massive effect of loading and heating the beams on the elastic and long-term behaviour of the beams. For all types of beams we notice instant reduction in deflection profile just after loading and heating, but gradual increase in deflection profile is noticed in the downward direction due to creep effect, but the rate of increase is decreasing by time as the rate of creep is decreasing.

Stress distribution at selected sections

Graph 7.16, 7.20 and 7.12 show the calculated variation with time of the stress distribution after loading and heating the three types of concrete beams to the same constant temperature gradient. We notice rapid changes in the stress distribution of pre-stressed concrete beam at the section over the support as con-crete creeps. It is also clear that the redistribution is greater over the central support than at Sec. I-I because of the rapid change of bending moment over the centre support. The form of variation in the stress distribution over the centre support by time for both reinforced and composite beams is the same. At Sec. I-I the composite beam has a pattern different from that of reinforced concrete beam because of the prestressed plank.

(c) Composite Prestressed Beam subjected to variable reduced cast-in-place concrete properties

Deflections at span section I-I

Graph 7.21 shows the calculated variation of deflection behaviour at Section I-I of the composite beam loaded and heated using different cast-in-place concrete properties with respect to constant concrete properties of the prestressed portion. We notice from the graph that creep greatly increases the deflection at that section in the downward direction due to heating and loading, but the rate of increase is decreasing by time as the rate of creep is decreasing. We can notice also that the increase in deflection at that section is decreasing as the properties of the cast-in-place concrete portion are increasing.

Deflection Profile

Graph 7.22 shows the computed variation of deflection profile of composite prestressed beam at 11 days after loading and heating using constant concrete properties for the prestressed portion (Mix B) and variable concrete properties for the cast-in-place portion (Mix A). It is clear from the graph that the deflection increases by reducing concrete properties of the cast-in-place portion. We notice that the deflection at nearly the middle of the span is 1.7 times the deflection at the same point when the creep of Mix A increases from 2 to 6 times the creep of Mix B.

Stress distributions at selected sections

Graph 7.23 shows the calculated variation of the stress distribution after 11 days of loading and heating the composite beam assuming different concrete properties for cast-in-place portion

it is clear from the graph that the rate of variation in stresses at the centre support is greater than the rate of variation at Section I-I, this is because of the rapid variation of the bending moment over the centre support due to creep.

Bending Moment at Centre Support

Graph 7.24 shows the variation with time of the bending moment at the centre support of the composite beam due to loading and heating. It also shows the effect of variation of cast-in-place concrete properties on the bending moment. It is obvious from the graph the sudden great drop in bending moment just after heating and loading the beam followed by a gradual great increase in bending moment in the early days after heating due to the effect of creep, but the rate of increase in bending moment is decreasing by time as the rate of creep is decreasing. The pattern of variation of bending moment with respect to the different cast-in-place concrete properties is the same. It is also noticed that the rate of increase in bending moment increases as creep of cast-in-place concrete increases.

(d) Effect of Cracking on Reinforced Concrete Beam

Deflection Profiles

Graphs 7.25 and 7.26 show the computed variation with time of the deflection profile of reinforced concrete beam due to loading and heating using two different temperature gradients and providing an increase in the allowable tensile strength of concrete to prevent the formation of cracks due to loading and heating at any time. It is clear from the above-mentioned graphs that the thermo-elastic deflection of the beam decreases due to

increase in temperature gradient providing cracks are not allowed, but there will be a substantial increase in thermo-elastic deflection by increasing the temperature gradient and allowing for cracking which will create a situation in which the thermo-elastic curve cuts the elastic curve due to increase in cracking.

7.8 CONCLUSIONS

1. Under sustained load and sustained temperature crossfall there are substantial changes in computed reactions in the three types of continuous concrete beams.

2. The computed deflections of the three types of concrete beams exhibit severe variations with time when subjected to sustained temperature crossfall.

3. The stresses of prestressed conctinuous beam when subjected to sustained temperature crossfall exhibit severe variations with time.

4. In composite beam the variation of cast-in-place concrete properties with respect to a constant concrete properties of precast portion causes substantial increase in computed deflections as creep of cast-in-place concrete increases.

5. Sagging moments may develop at the centre support sections in the composite prestressed beam by increasing the applied temperature crossfall from $40^{o}C$ to, say, $60^{o}C$ on the top side of the beam. As long as there is no positive moment continuity connection is provided cracking may occur at the bottom of the beam at these sections. This will create a situation in which nominally tensile steel at the centre

support sections is actually in compression. These cracks will develop only just after loading and heating. However, there will be a very rapid reduction of the positive moments set up at the centre support at the early stage of loading and heating accompanies by redistribution of bending moment over the whole beam gradually by time due to creep. The result is closing up the cracks at these sections after a very short time of loading and heating. Certainly these cracks are not desirable at this particular section which is not provided with any reinforcement to carry that tension, but as long as these cracks will close up due to creep this will not affect the subsequent life or the ultimate load carrying capacity of the structure. Estension of the whole plank over the whole length of the beam will prevent the creation of these cracks at centre support sections, but this is not the most economical solution to the problem as long as these cracks will close up after a few days of loading and heating.

6. Cracking has a significant influence on increasing the deflections of reinforced concrete beam when subjected to large temperature crossfalls.

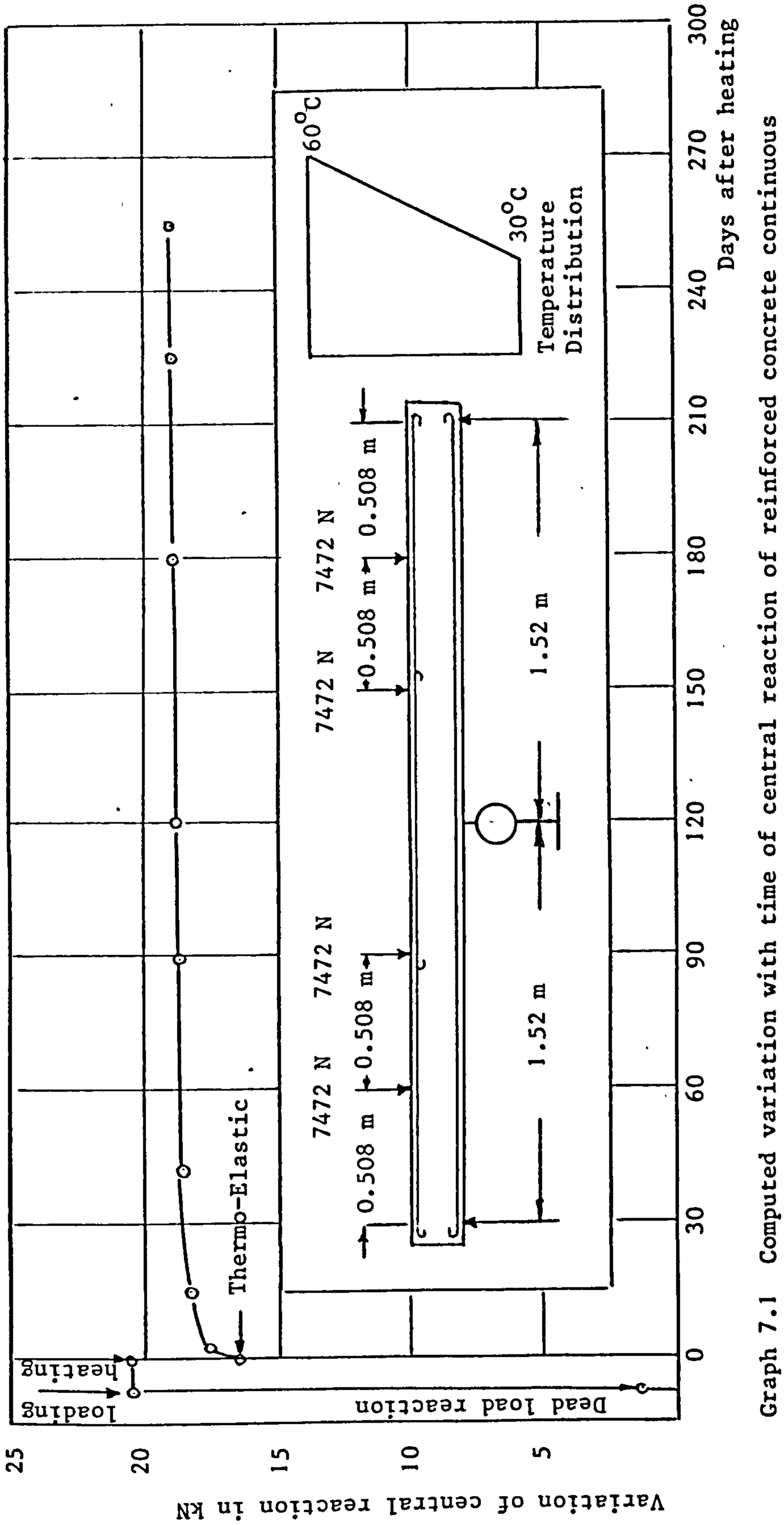

Graph 7.1 Computed variation with time of central reaction of reinforced concrete continuous beam loaded and heated

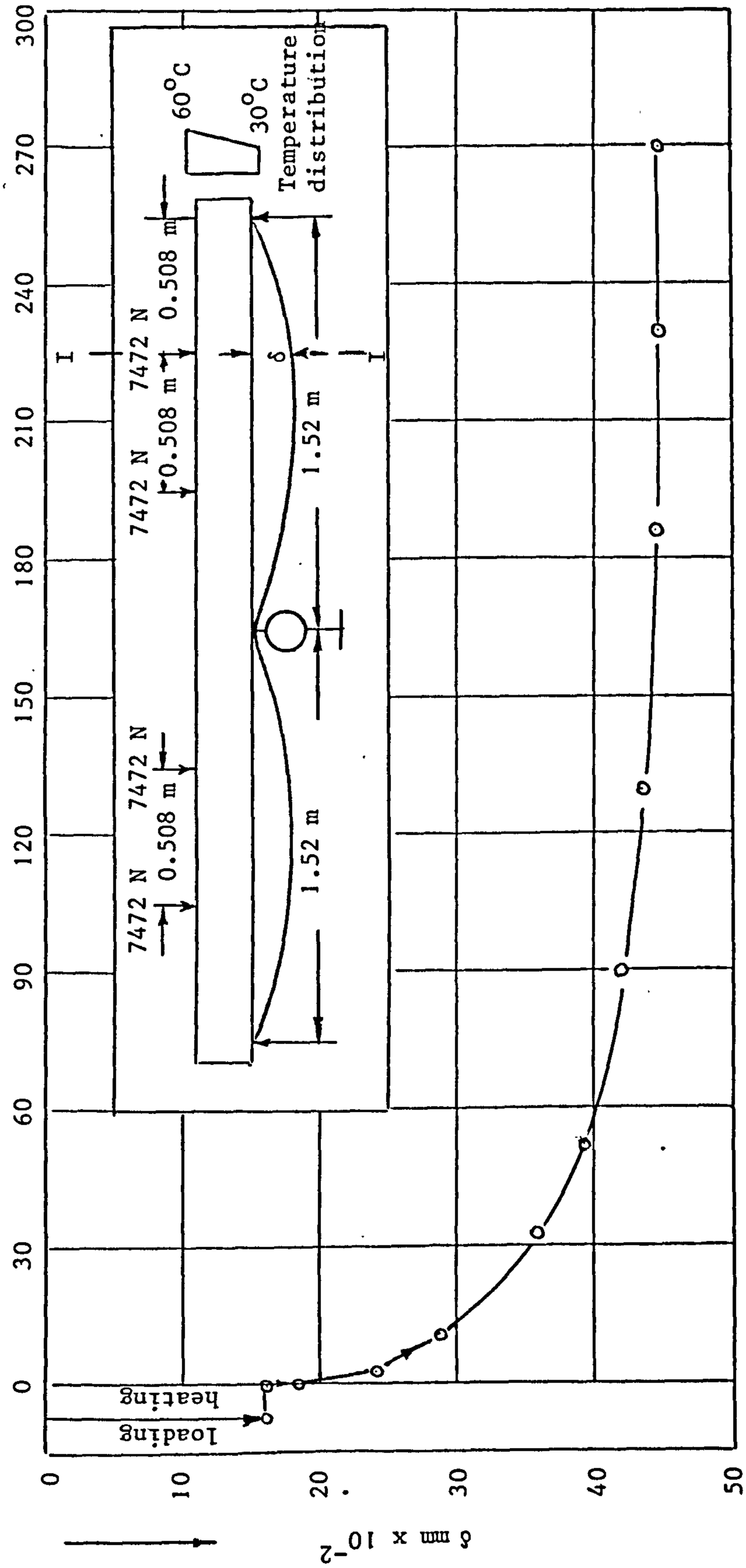

Graph 7.2 Computed time deflection behaviour at section I-I of reinforced concrete continuous beam loaded and heated

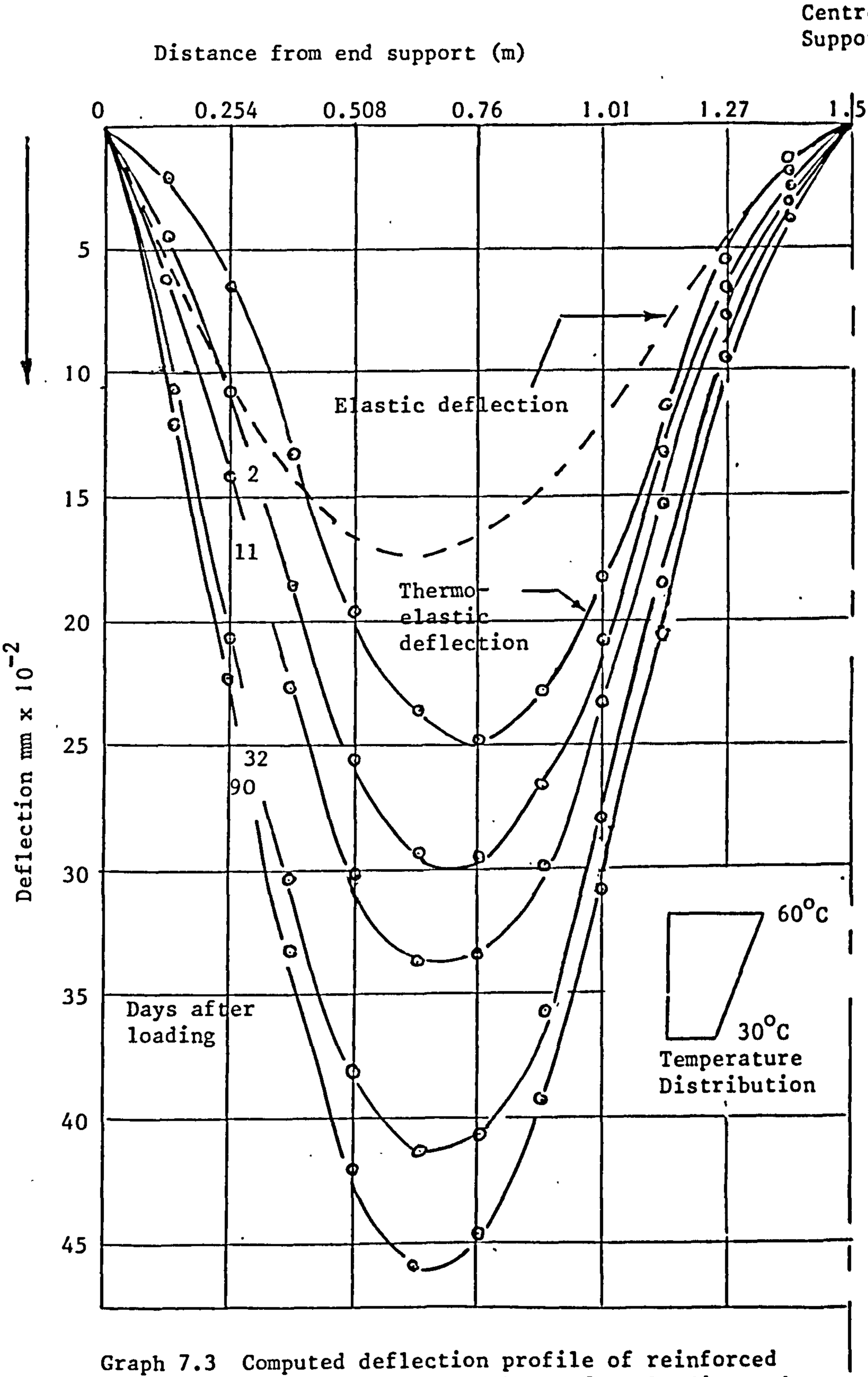

Graph 7.3 Computed deflection profile of reinforced concrete continuous beam after loading and heating

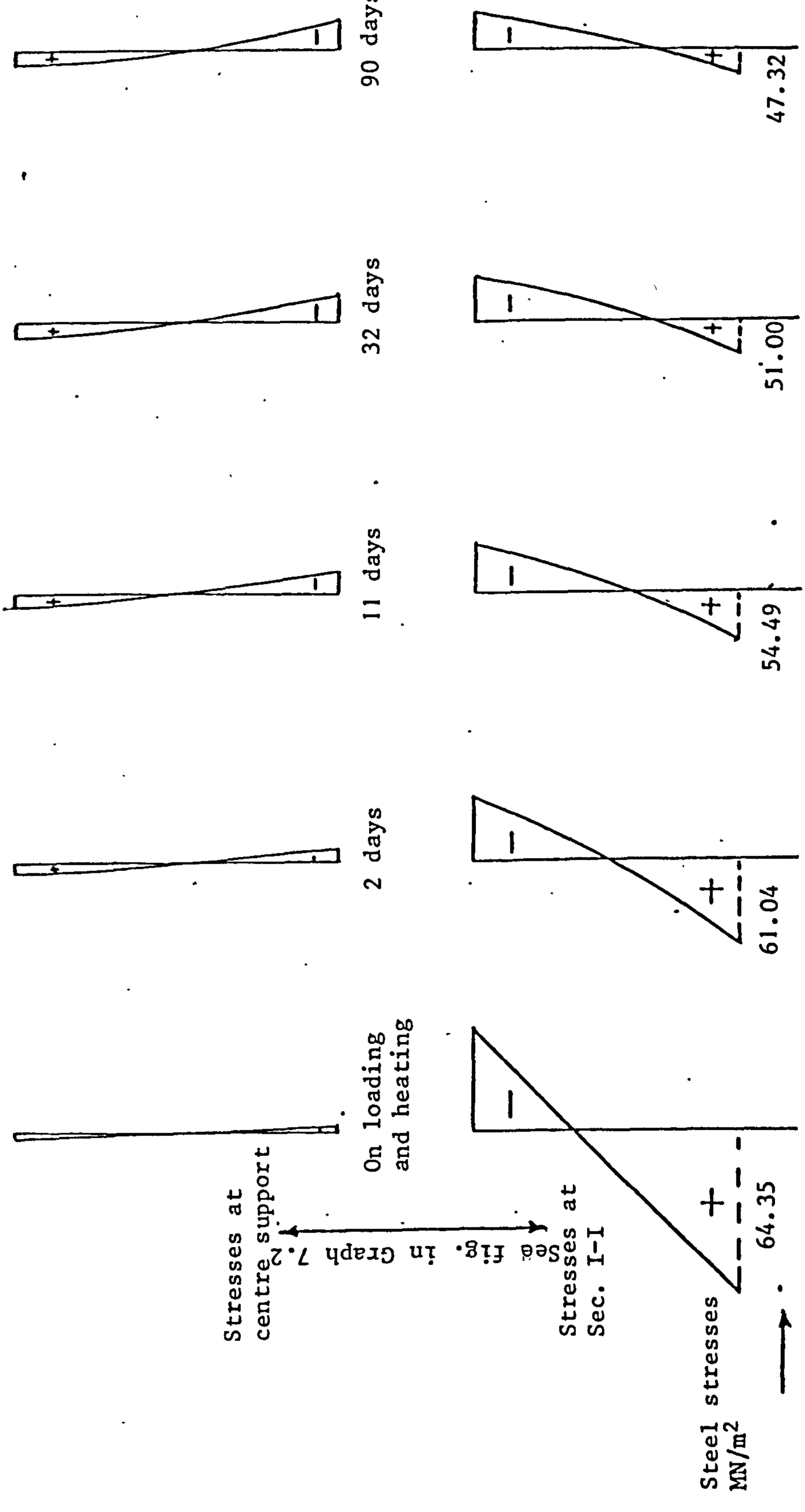

Graph 7.4 Computed concrete stress distribution (elastic, creep) of reinforced concrete continuous beam for two cross sections of the beam

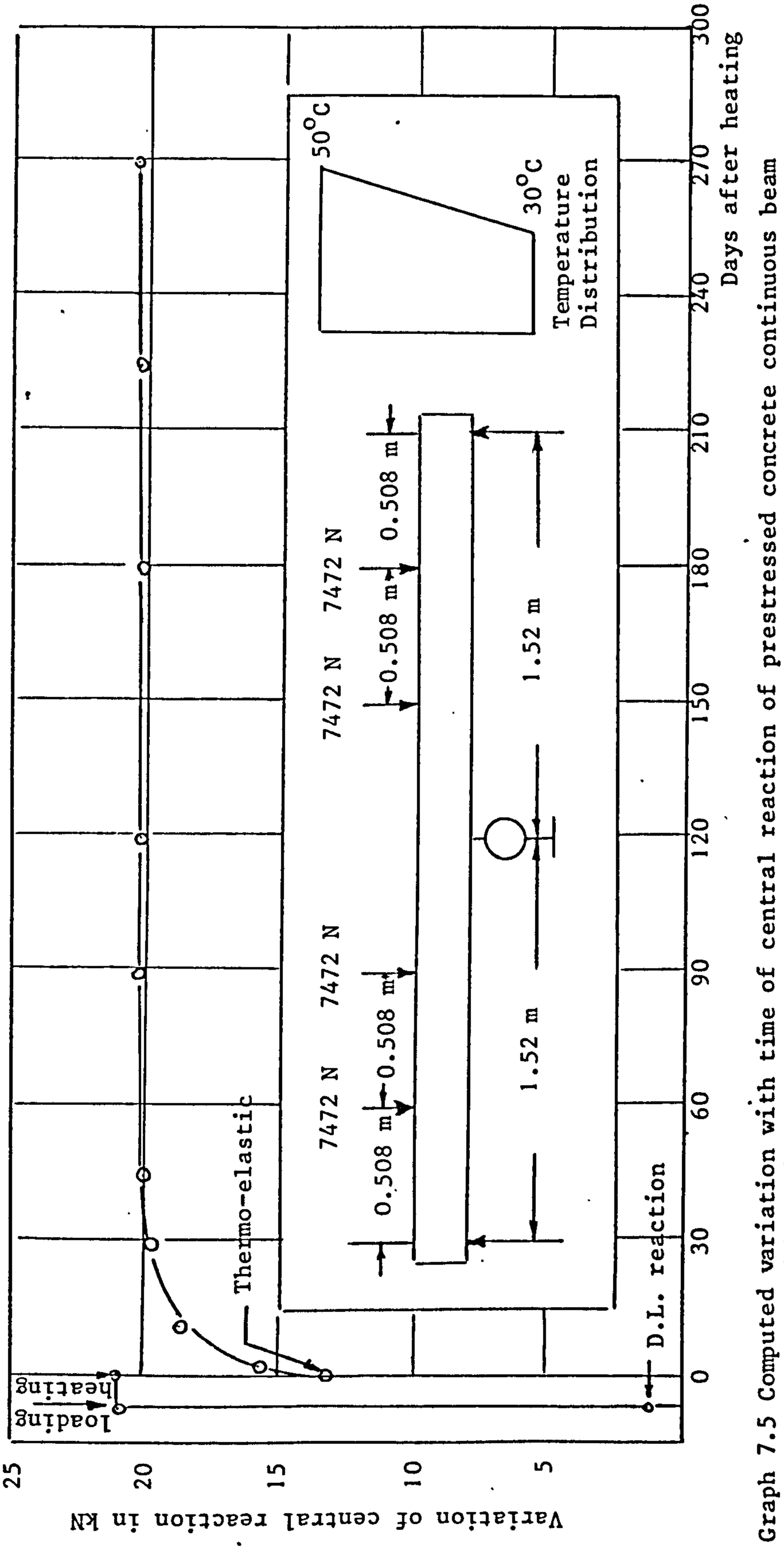

Graph 7.5 Computed variation with time of central reaction of prestressed concrete continuous beam loaded and heated

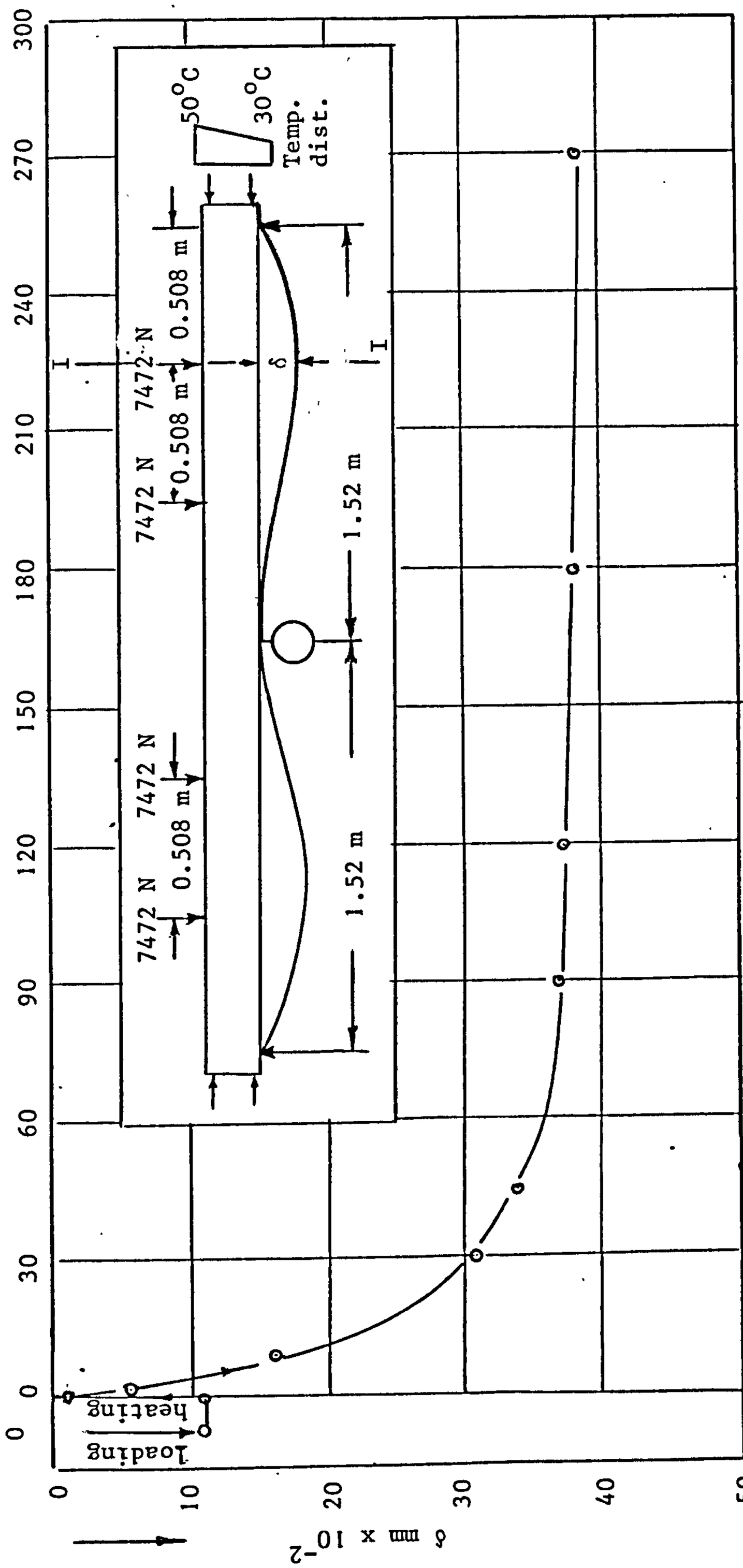

Graph 7.6 Computed time deflection behaviour at Section I-I of prestressed concrete continuous beam loaded and heated

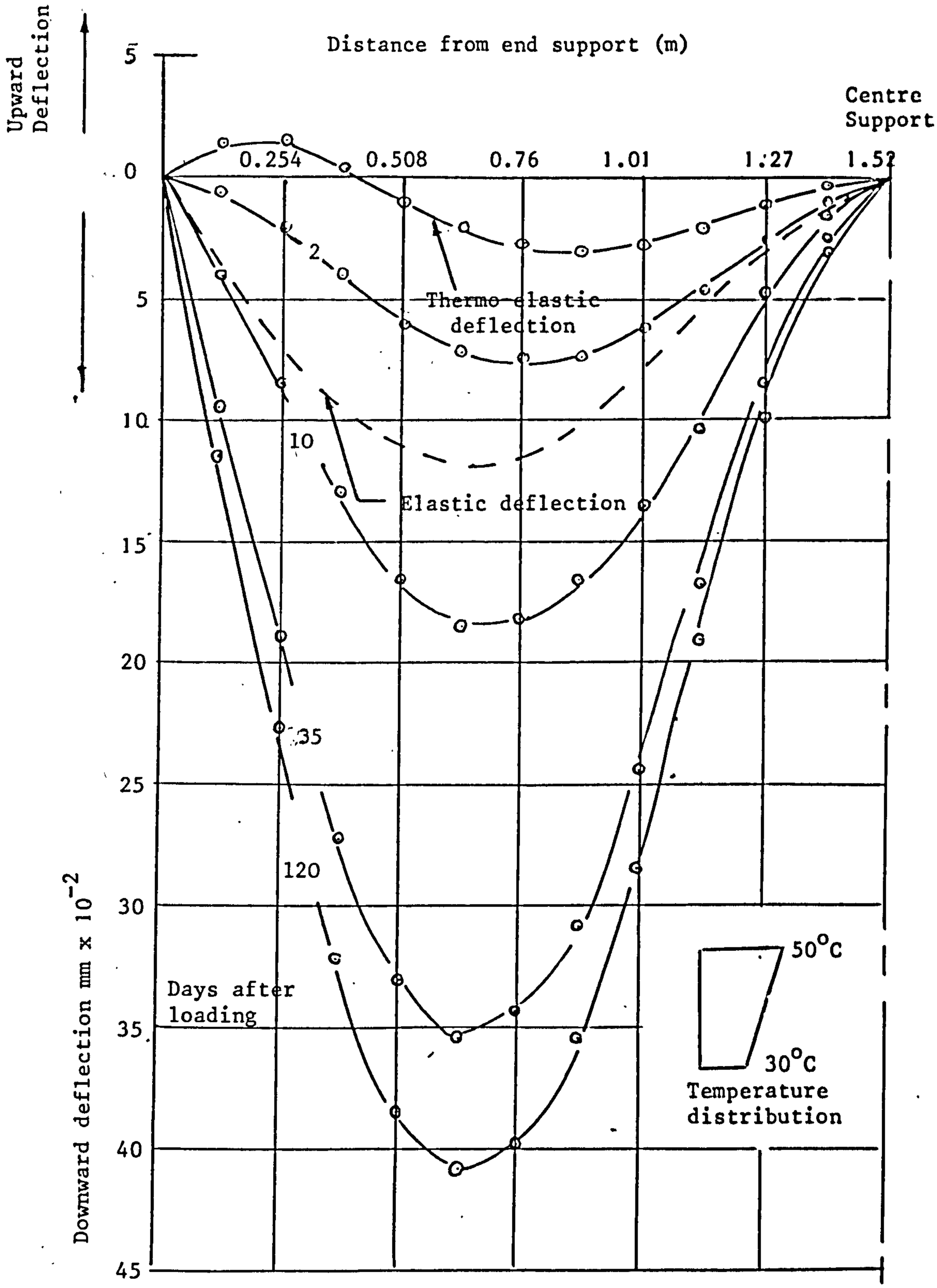

Graph 7.7 Computed deflection profile of prestressed concrete continuous beam after loading and heating

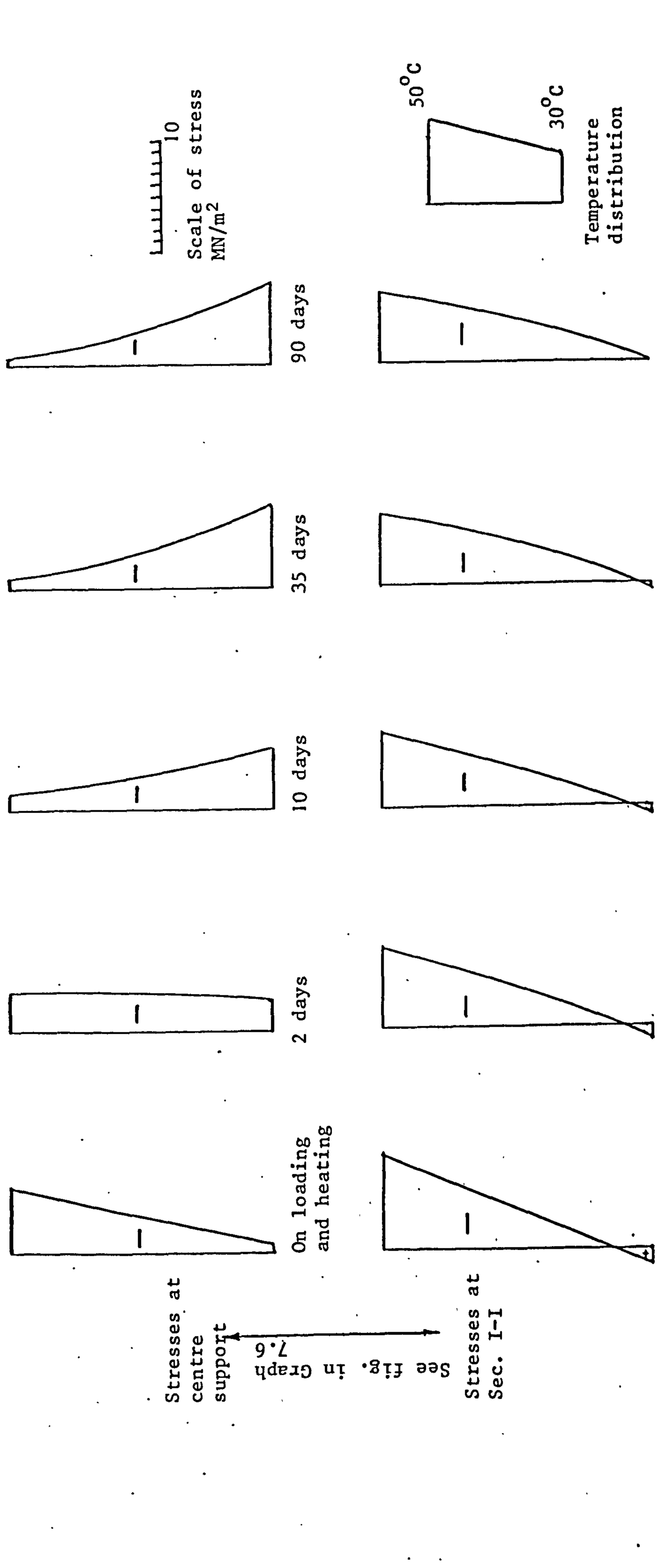

Graph 7.8 Computed concrete stress distribution (elastic, creep) of prestressed concrete continuous beam for two cross-sections of the beam

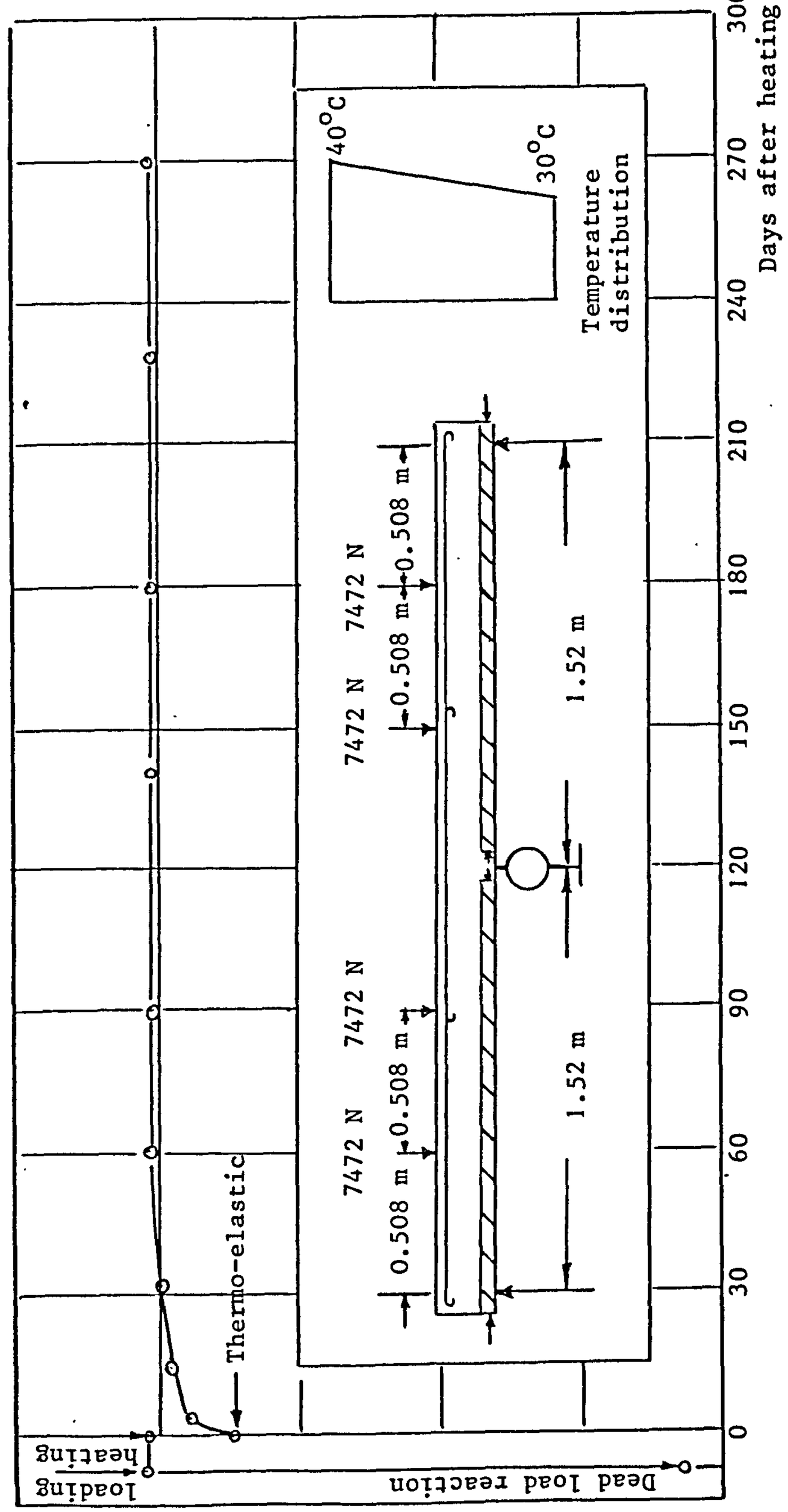

Graph 7.9 Computed variation with time of central reaction of composite prestressed concrete continuous beam loaded and heated

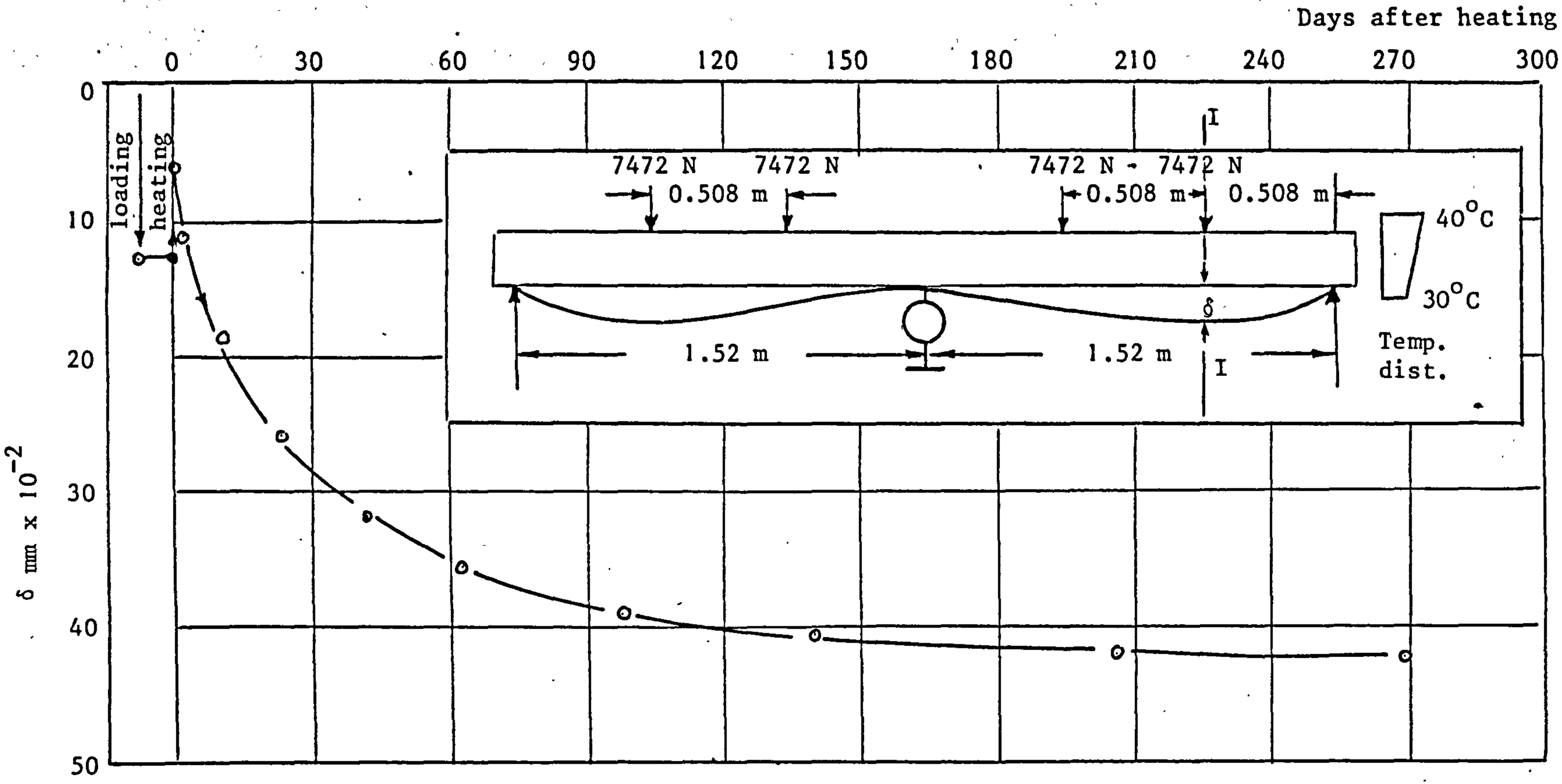

Graph 7.10 Computed time deflection behaviour at Section I–I of composite prestressed concrete continuous beam loaded and heated.

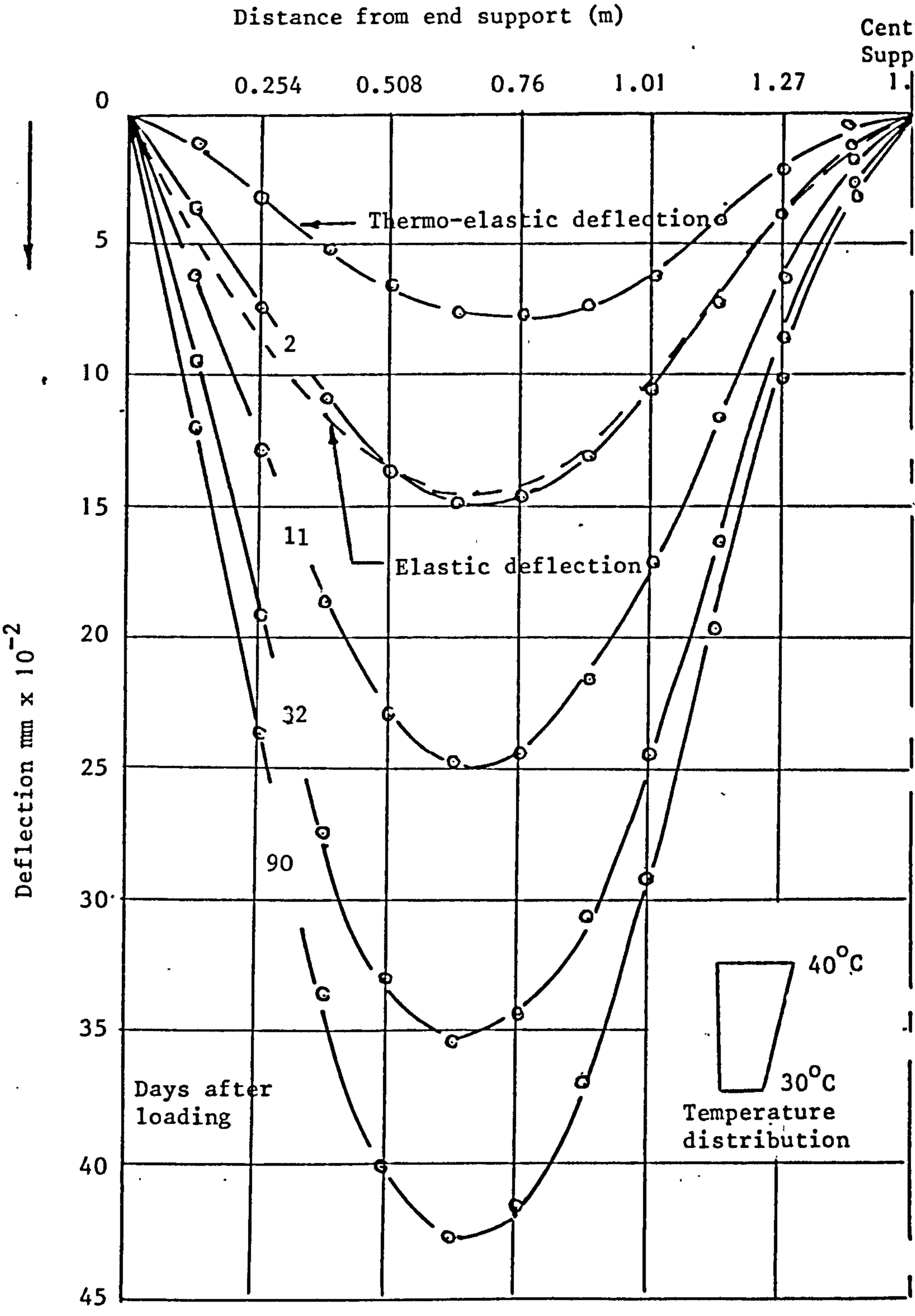

Graph 7.11 Computed deflection profile of composite prestressed concrete continuous beam after loading and heating

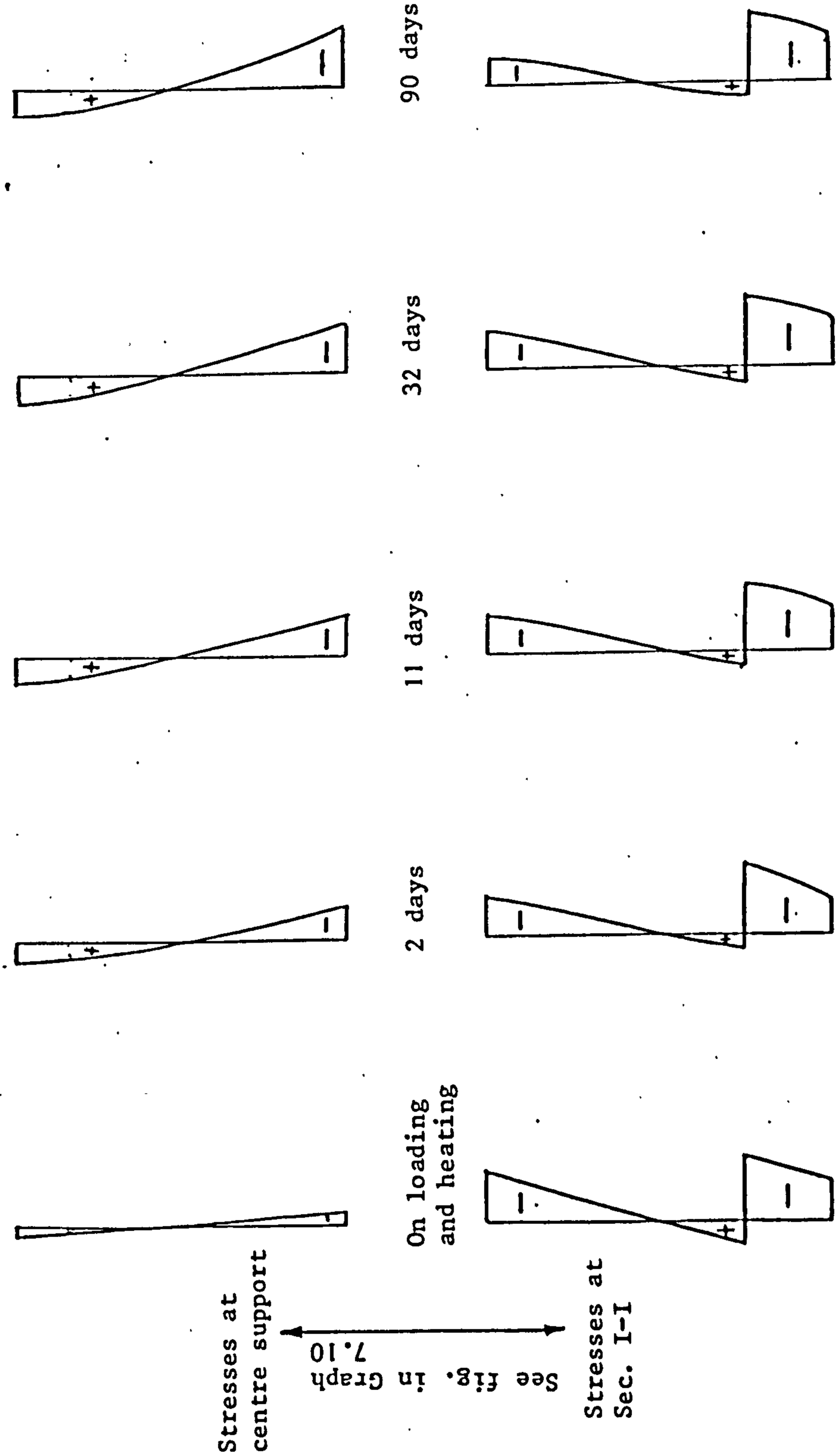

Graph 7.12 Computed concrete stress distribution (elastic, creep) of composite prestressed concrete continuous beam for two cross sections of the beam

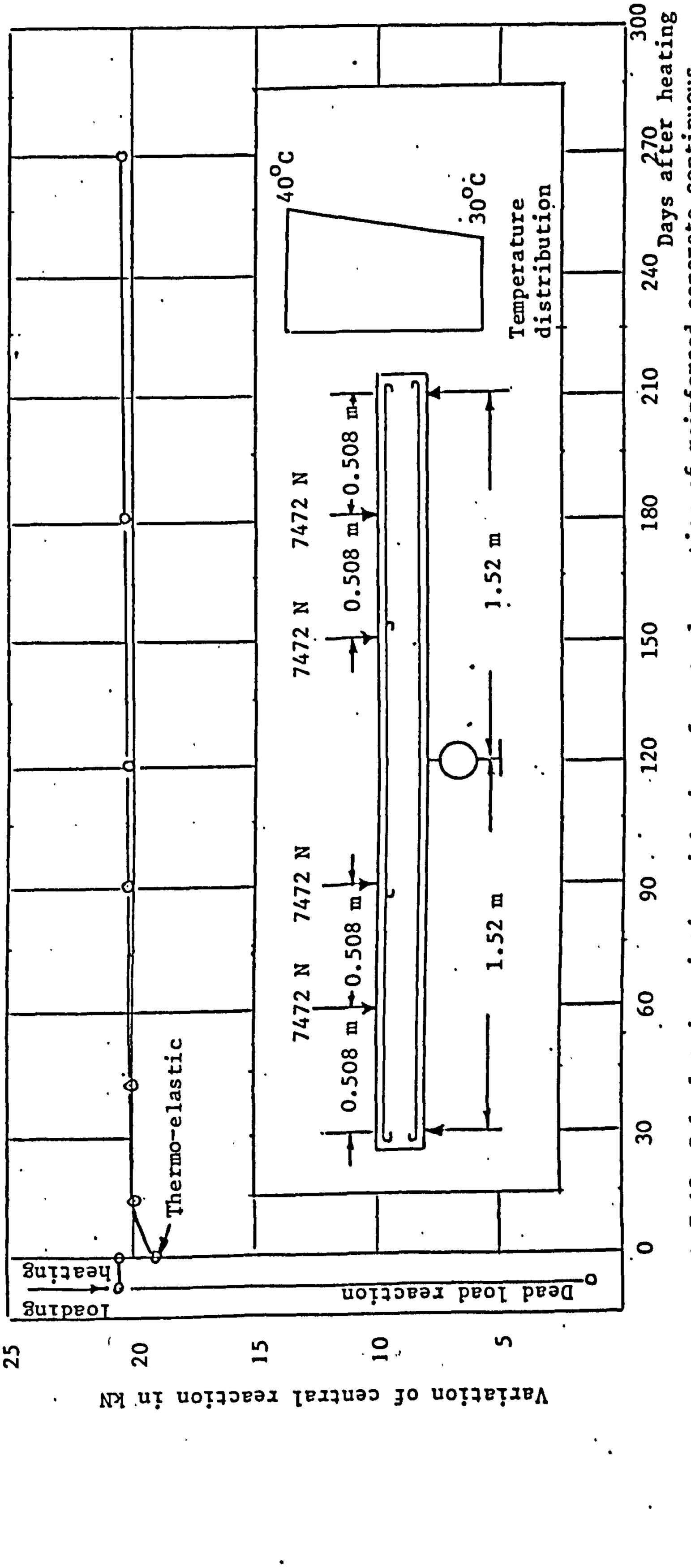

Graph 7.13 Calculated variation with time of central reaction of reinforced concrete continuous beam loaded and heated

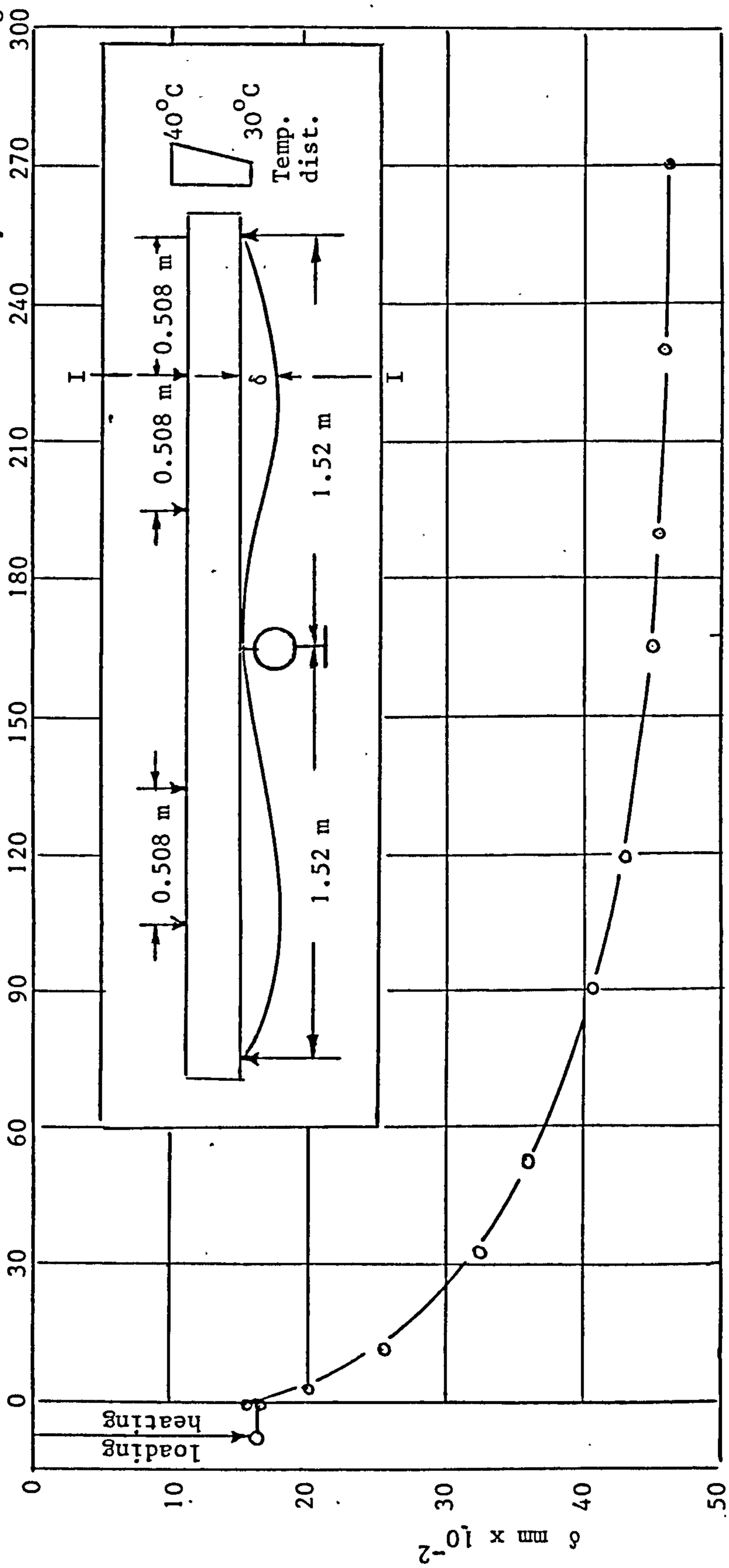

Graph 7.14 Computed time deflection behaviour at Section I-I of reinforced concrete continuous beam loaded and heated

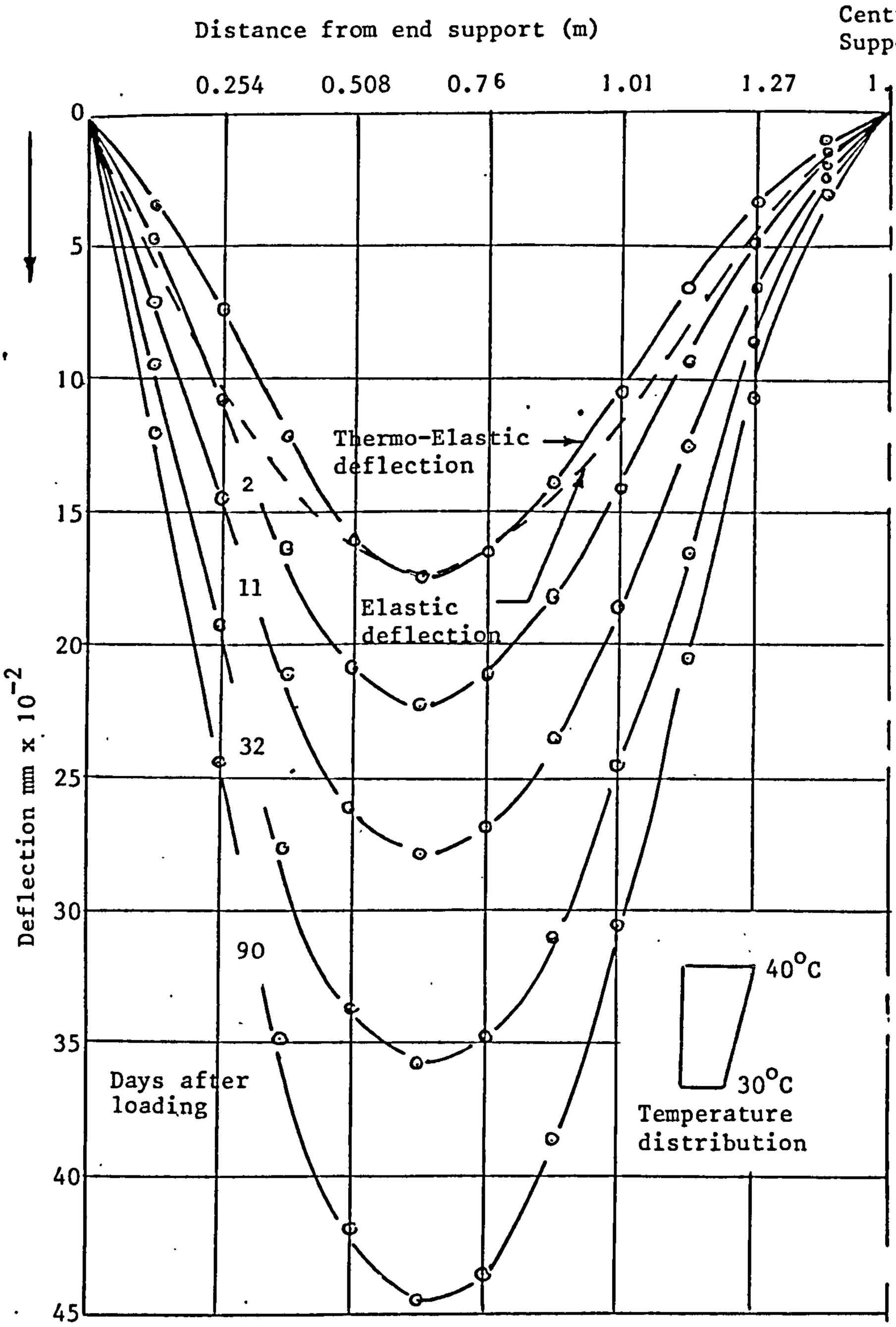

Graph 7.15 Computed deflection profile of reinfoced concrete continuous beam after loading and heating

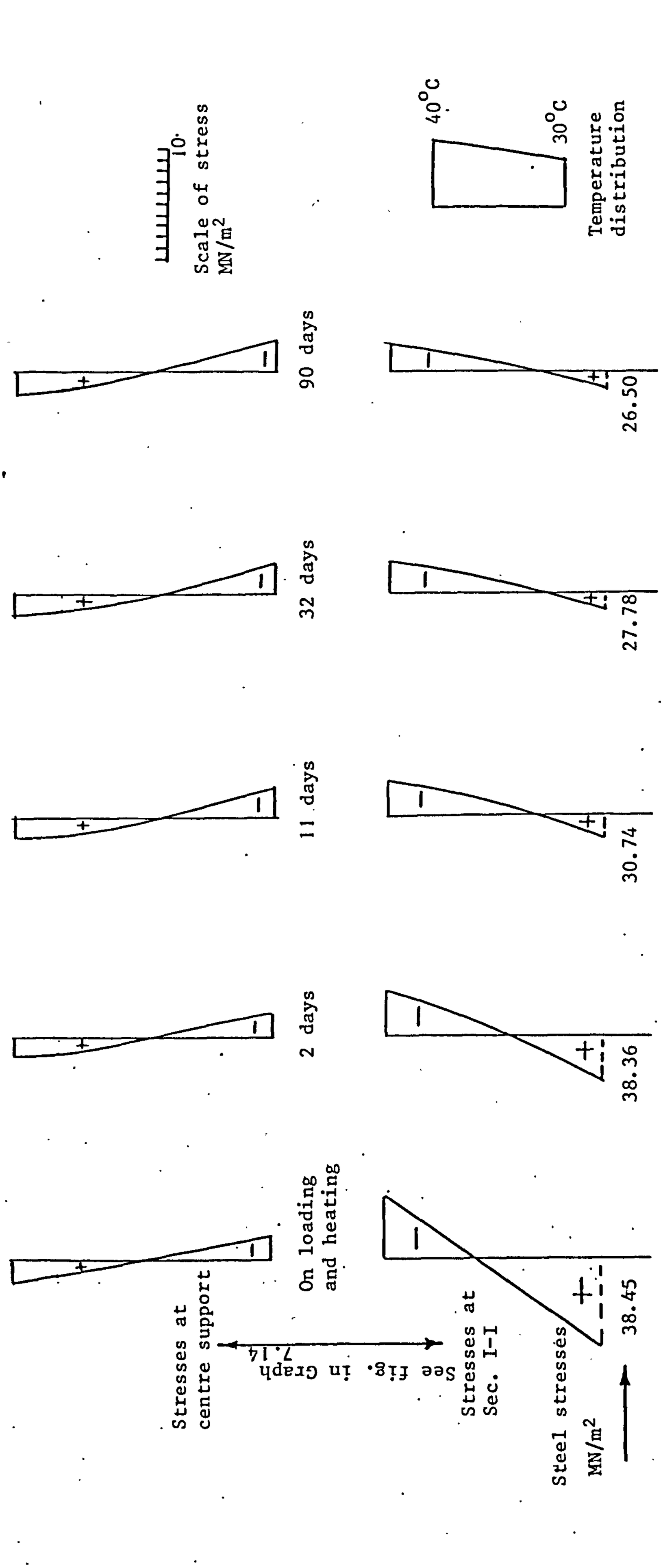

Graph 7.16 Computed concrete stress distribution (elastic, creep) of reinforced concrete continuous beam for two cross sections of the beam

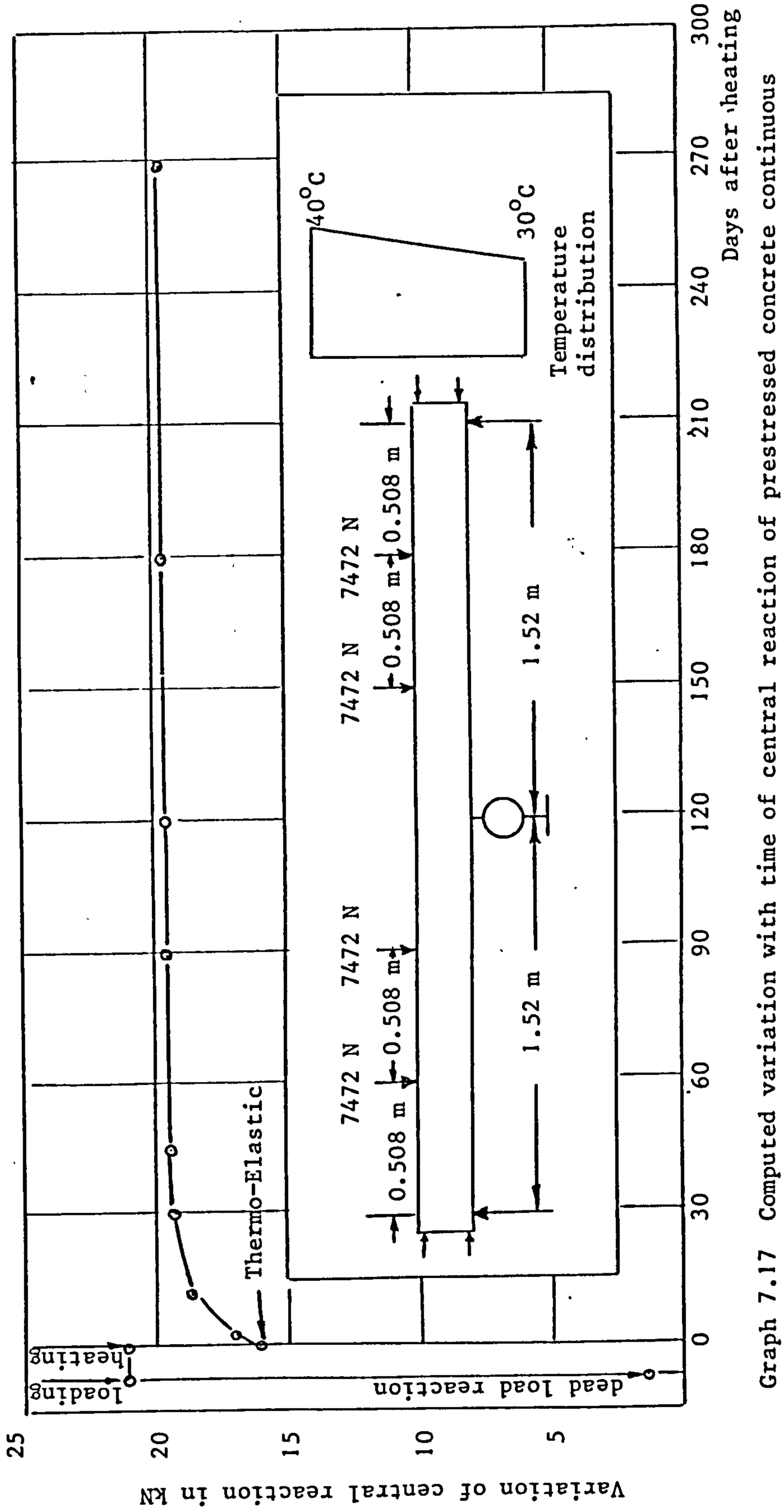

Graph 7.17 Computed variation with time of central reaction of prestressed concrete continuous beam loaded and heated

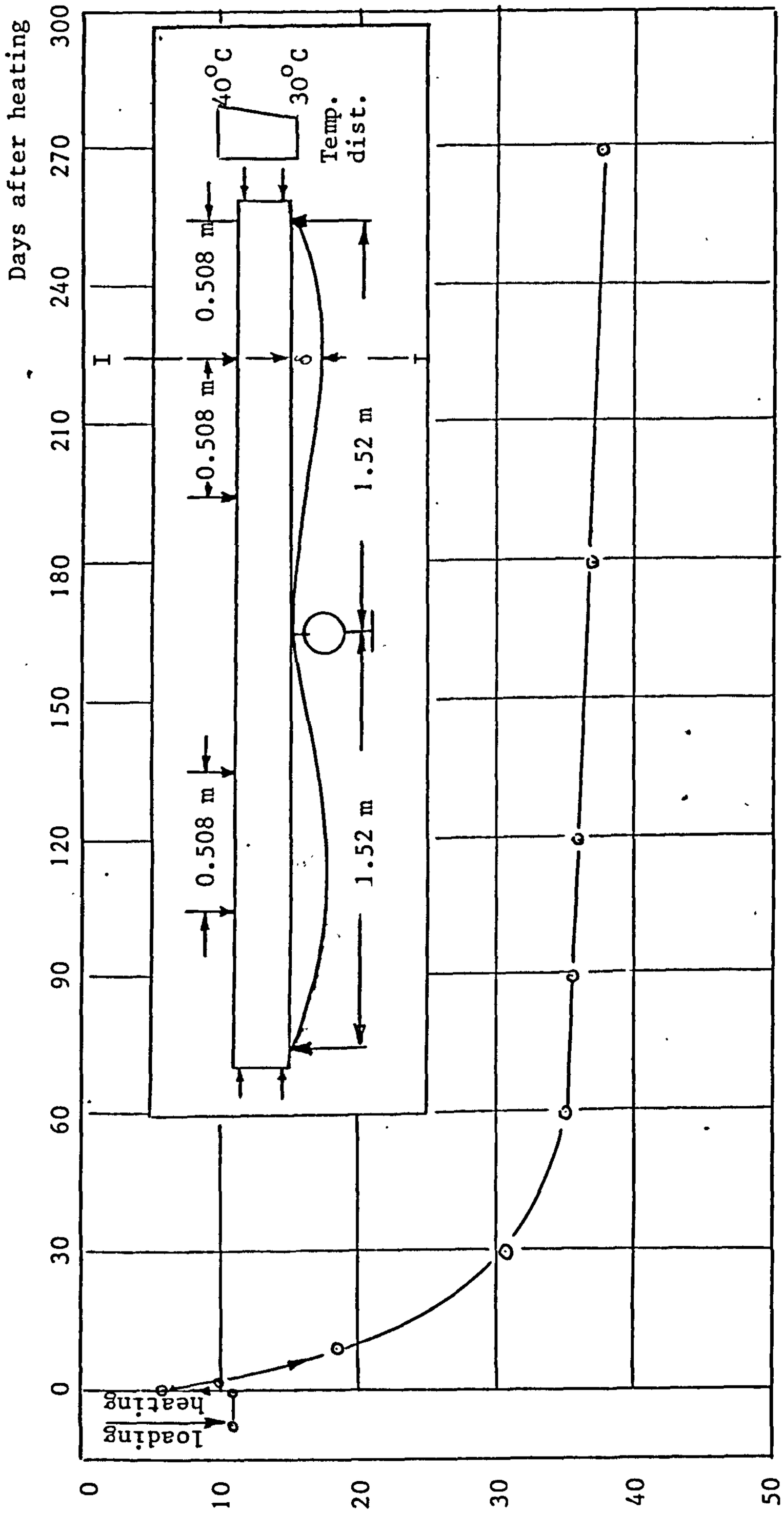

Graph 7.18 Computed time deflection behaviour at Sec. I-I of prestressed concrete continuous beam loaded and heated

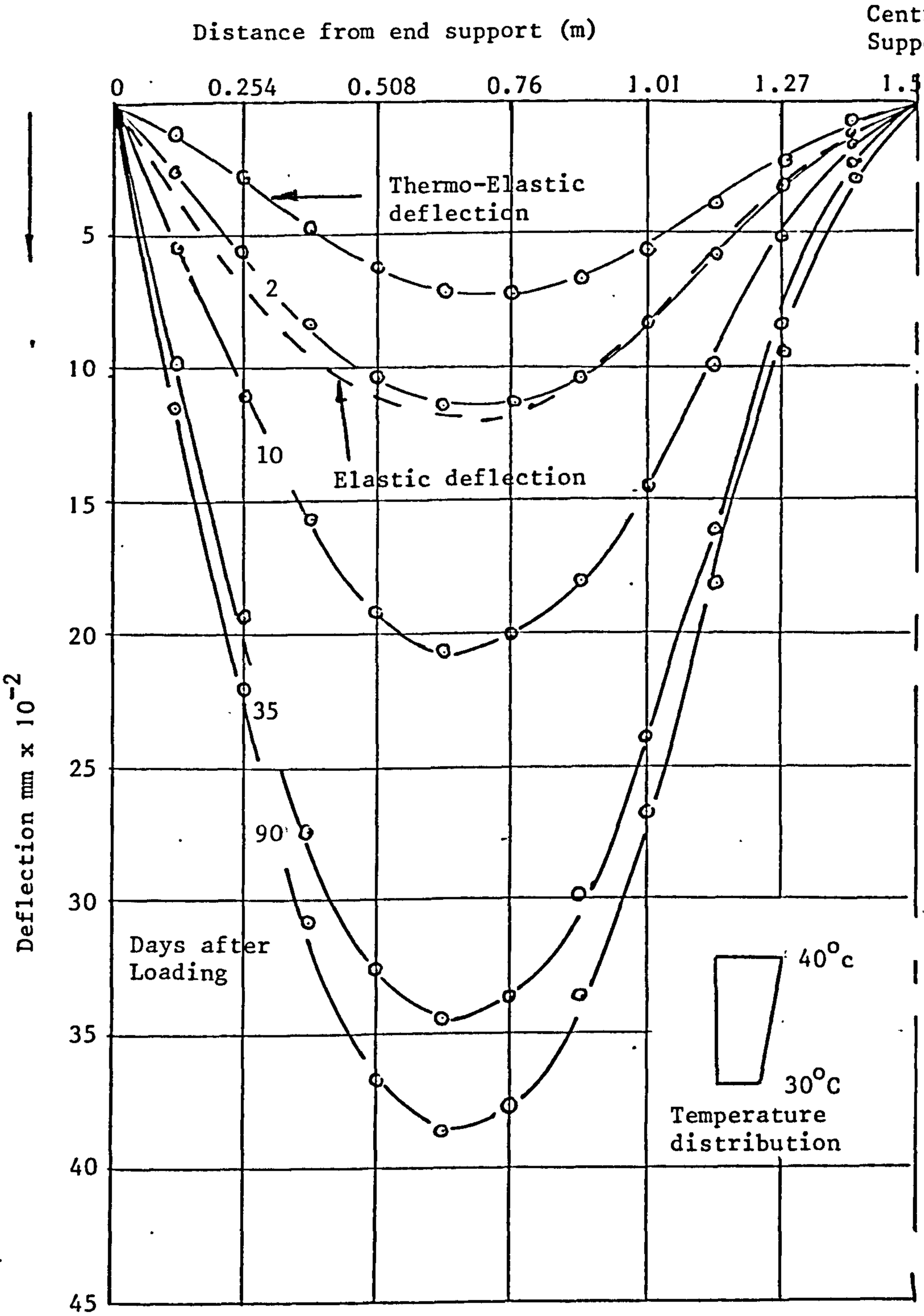

Graph 7.19 Computed deflection profile of prestressed concrete continuous beam after loading and heating

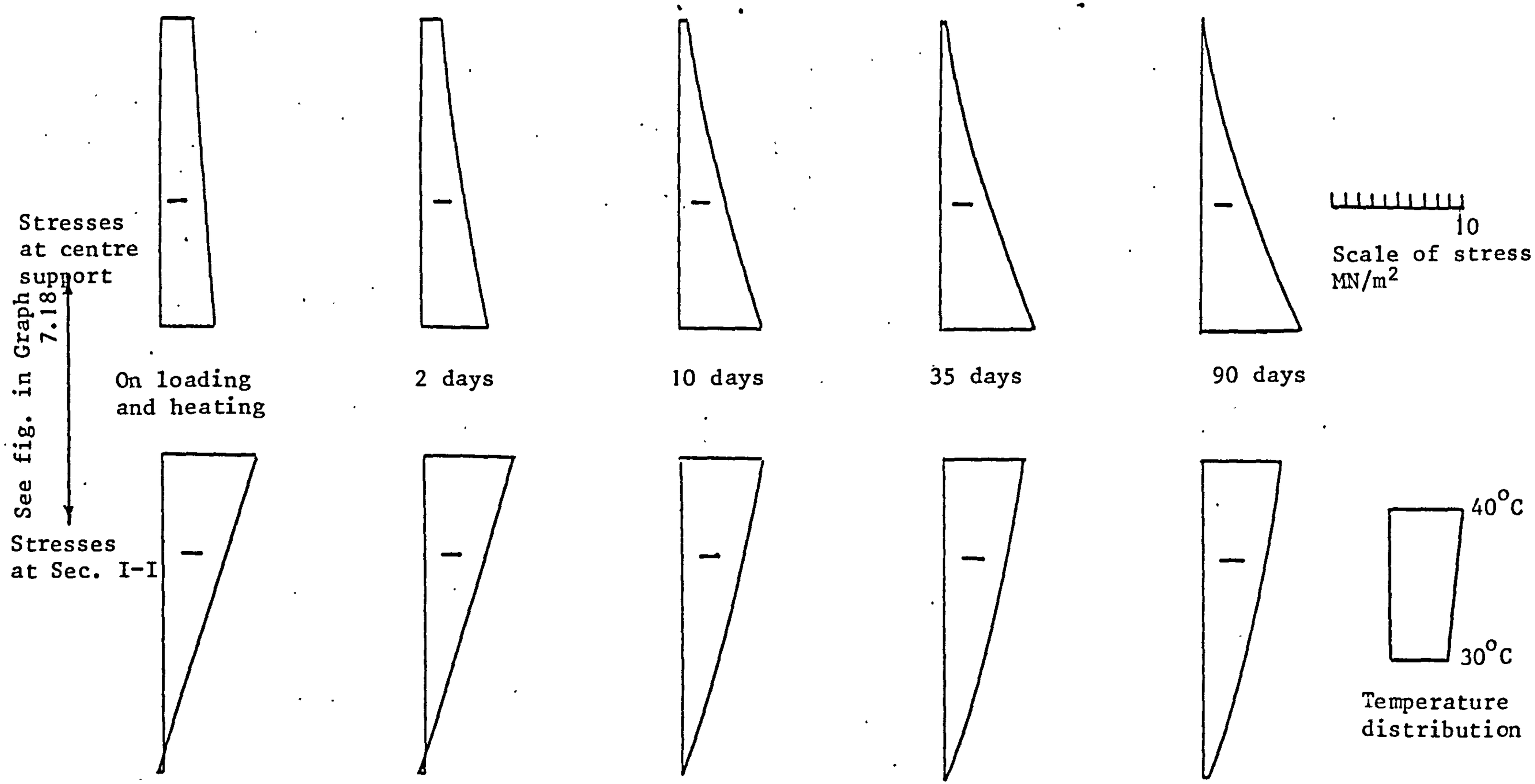

Graph 7.20 Computed concrete stress distribution (elastic and creep) of prestressed concrete continuous beam for two cross-sections of the beam

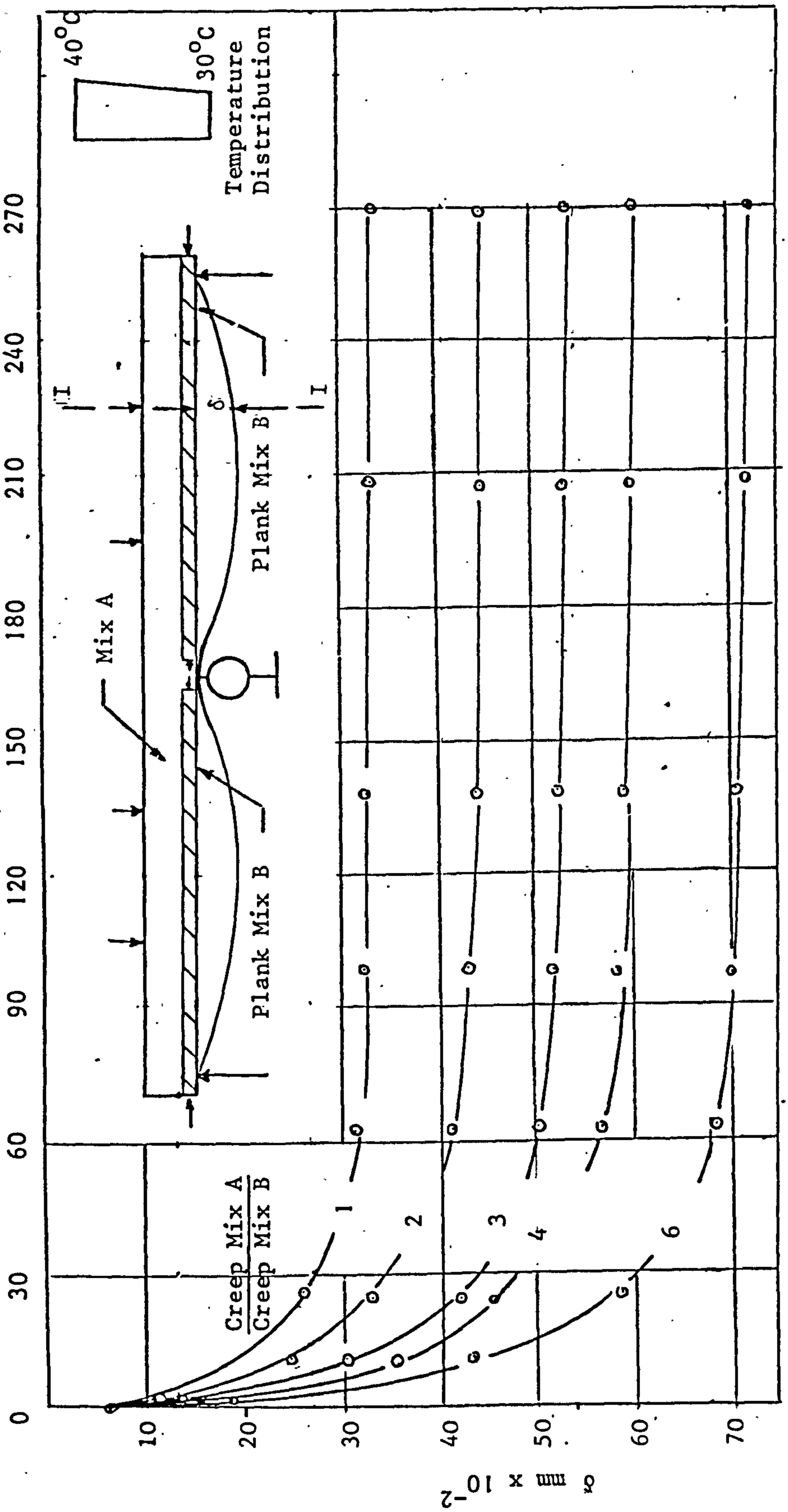

Graph 7.21 Computed time deflection behaviour at Section I-I of composite prestressed concrete beam loaded and heated using variable cast in place concrete properties.

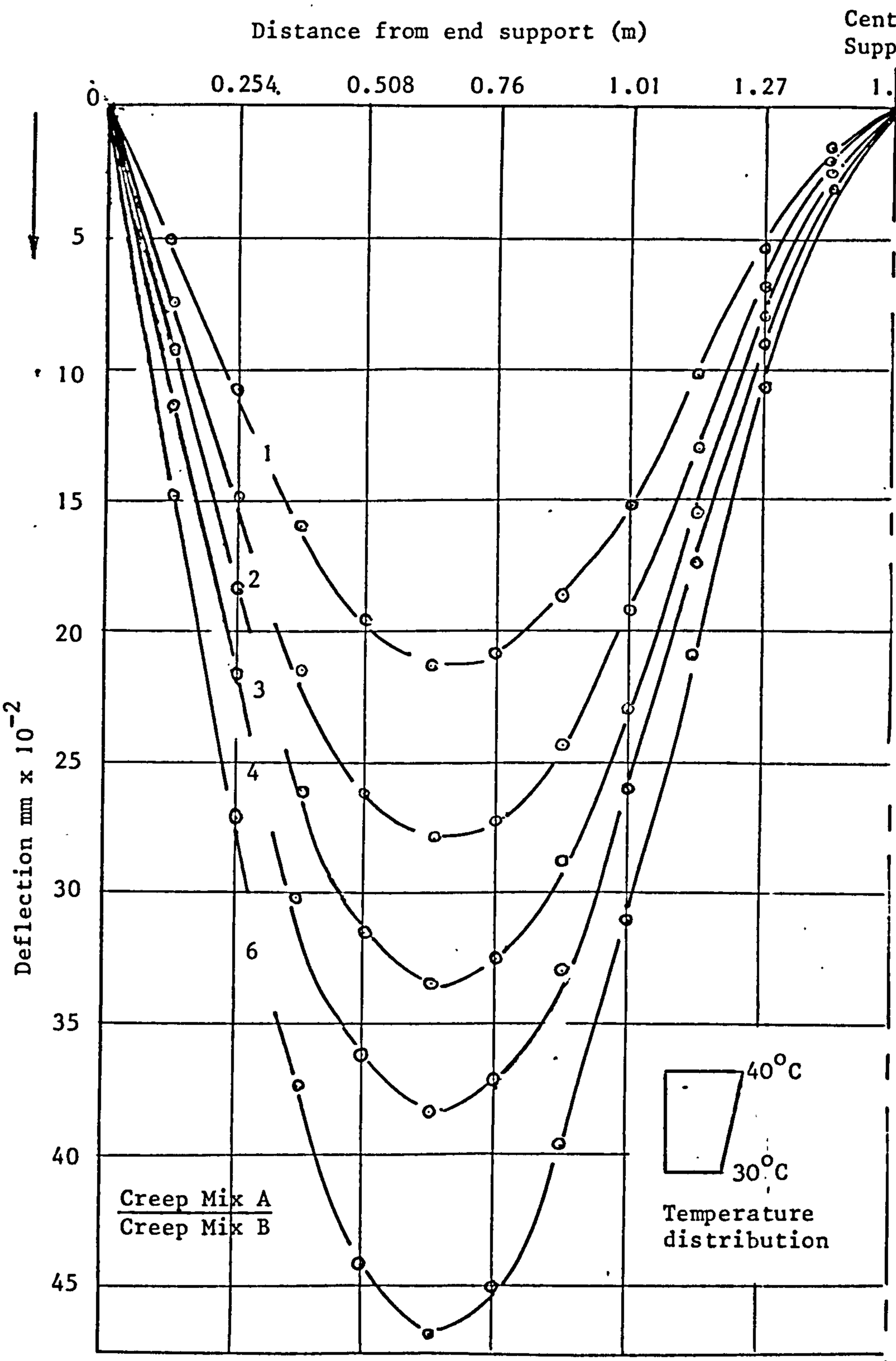

Graph 7.22 Computed deflection profile of composite prestressed concrete continuous beam at 11 days after loading and heating using variable cast-in place concrete properties

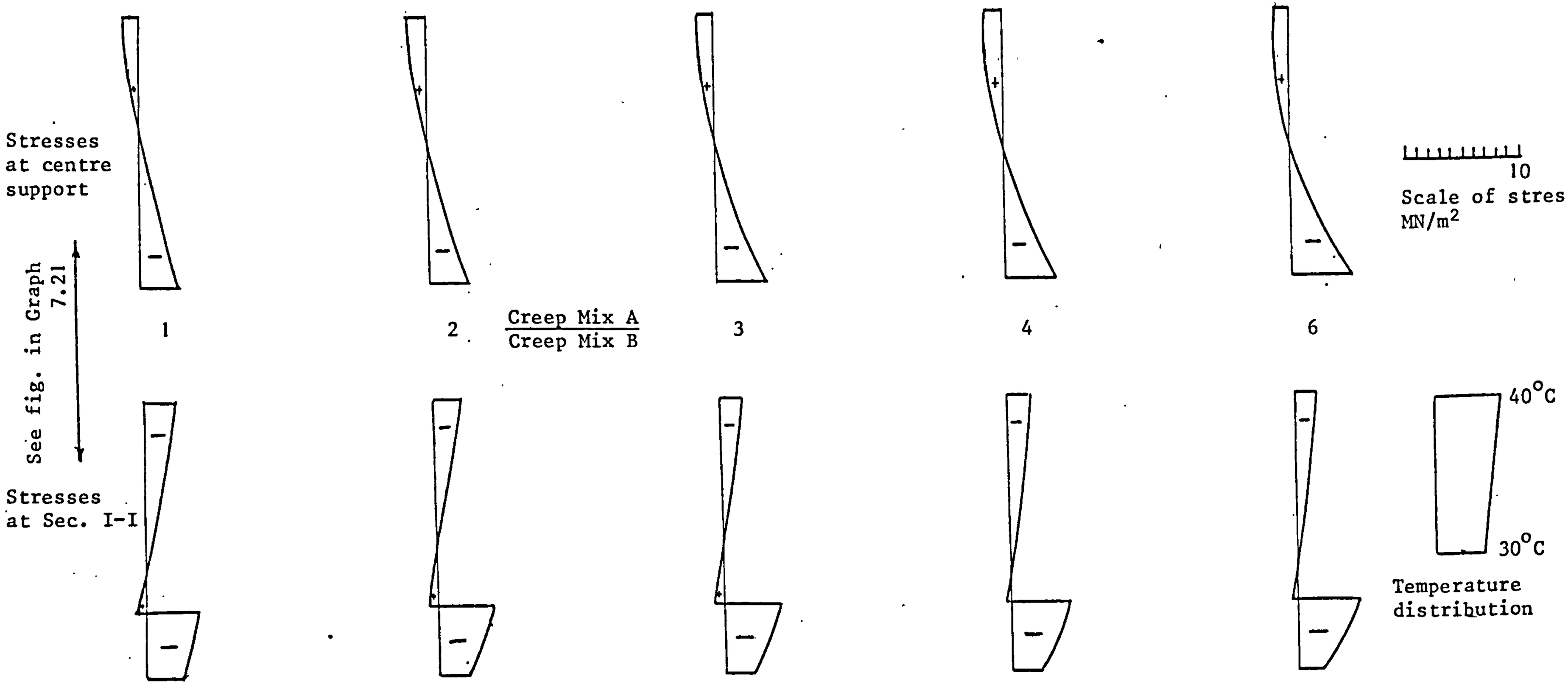

Graph 7.23 Computed concrete stress distribution (creep, shrinkage) of composite prestressed concrete continuous beam for two cross-sections of the beam at 11 days after loading and heating using variable cast in place concrete properties

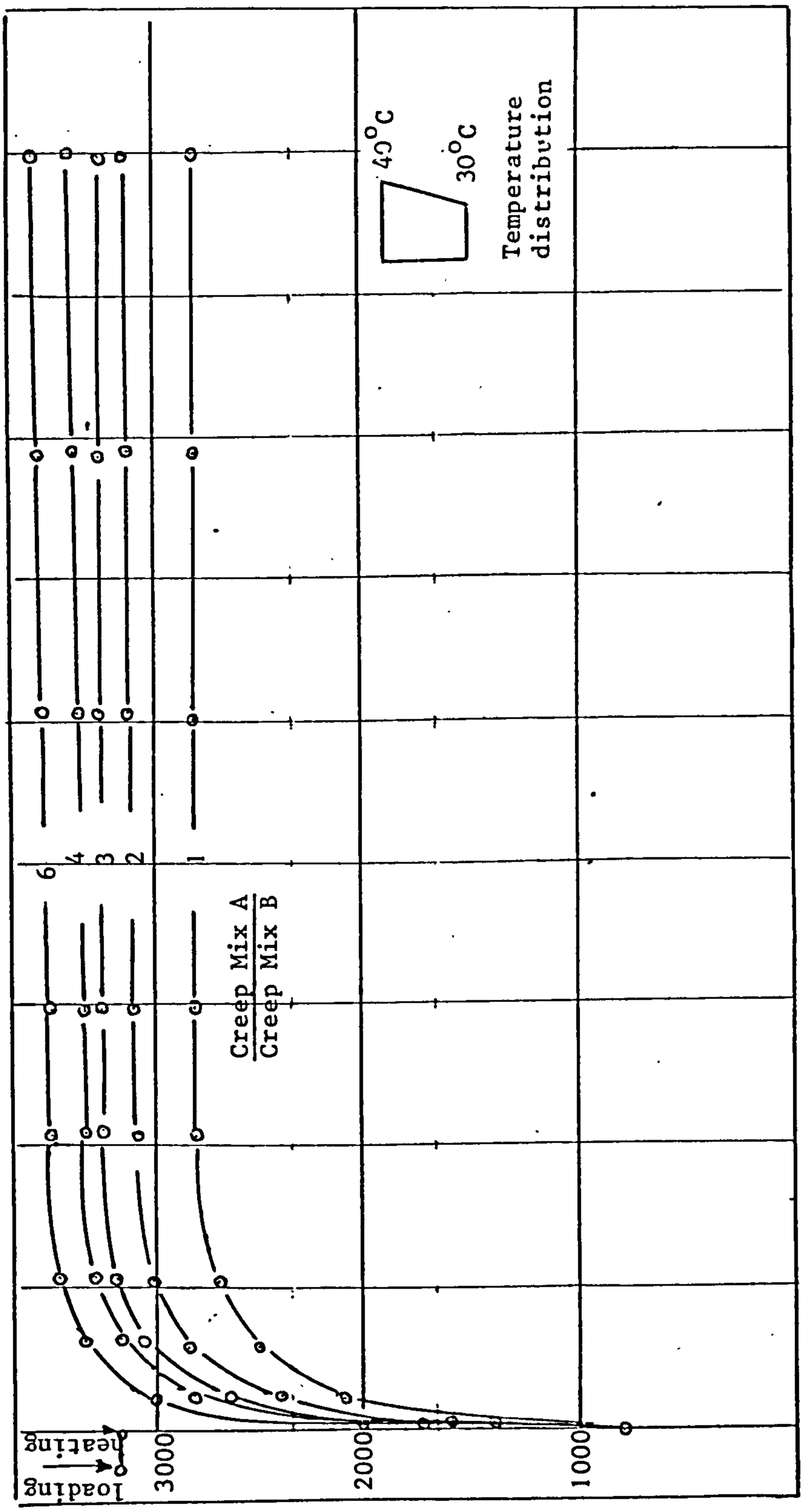

Graph 7.24 Computed variation with time of bending moment at centre support of composite prestressed concrete continuous beam loaded and heated using variable cast in place concrete properties

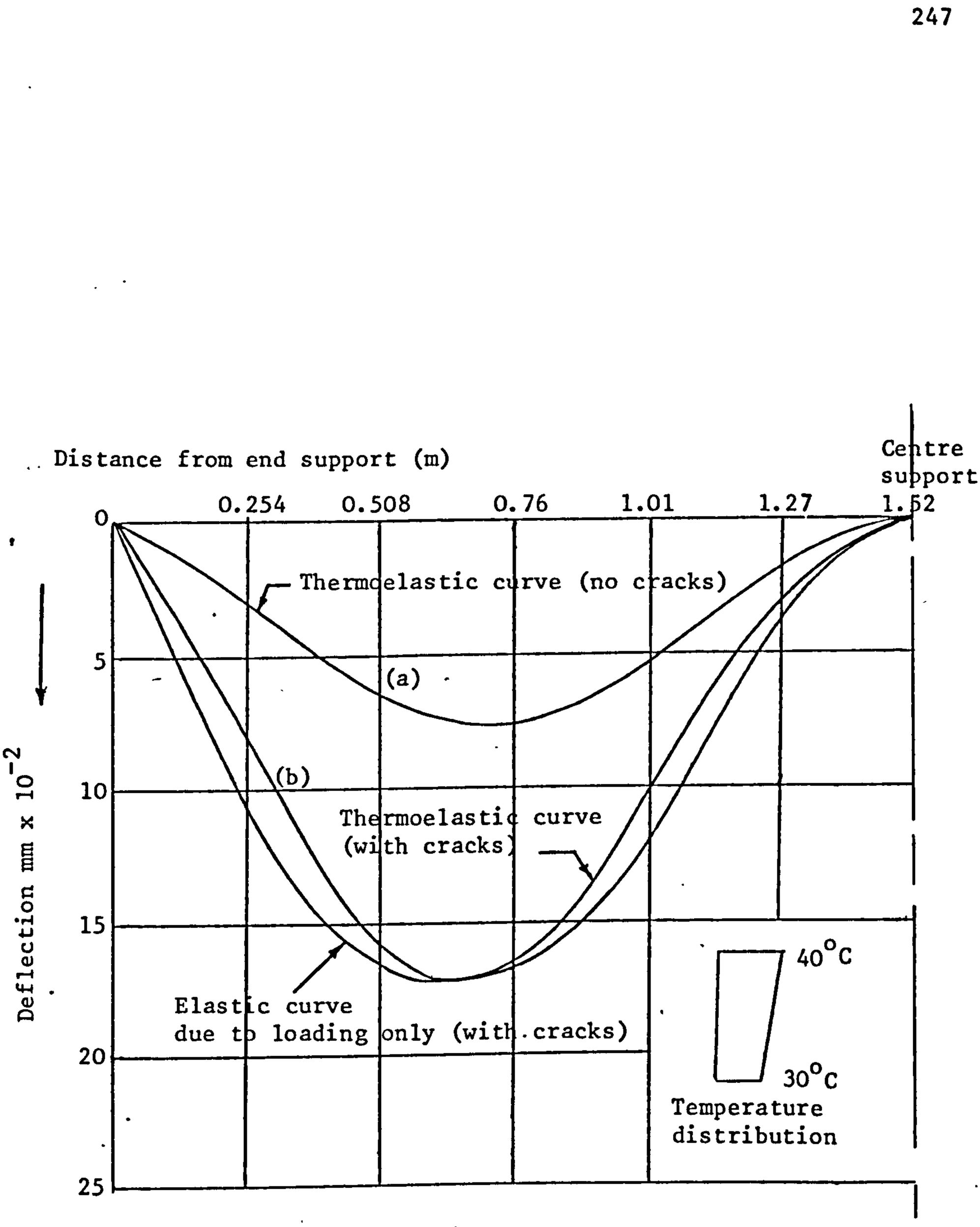

Graph 7.25 Computed deflection profile of reinforced concrete continuous beam after loading and heating.

Curves (a) and (b) indicate the influence that cracking has on deflections

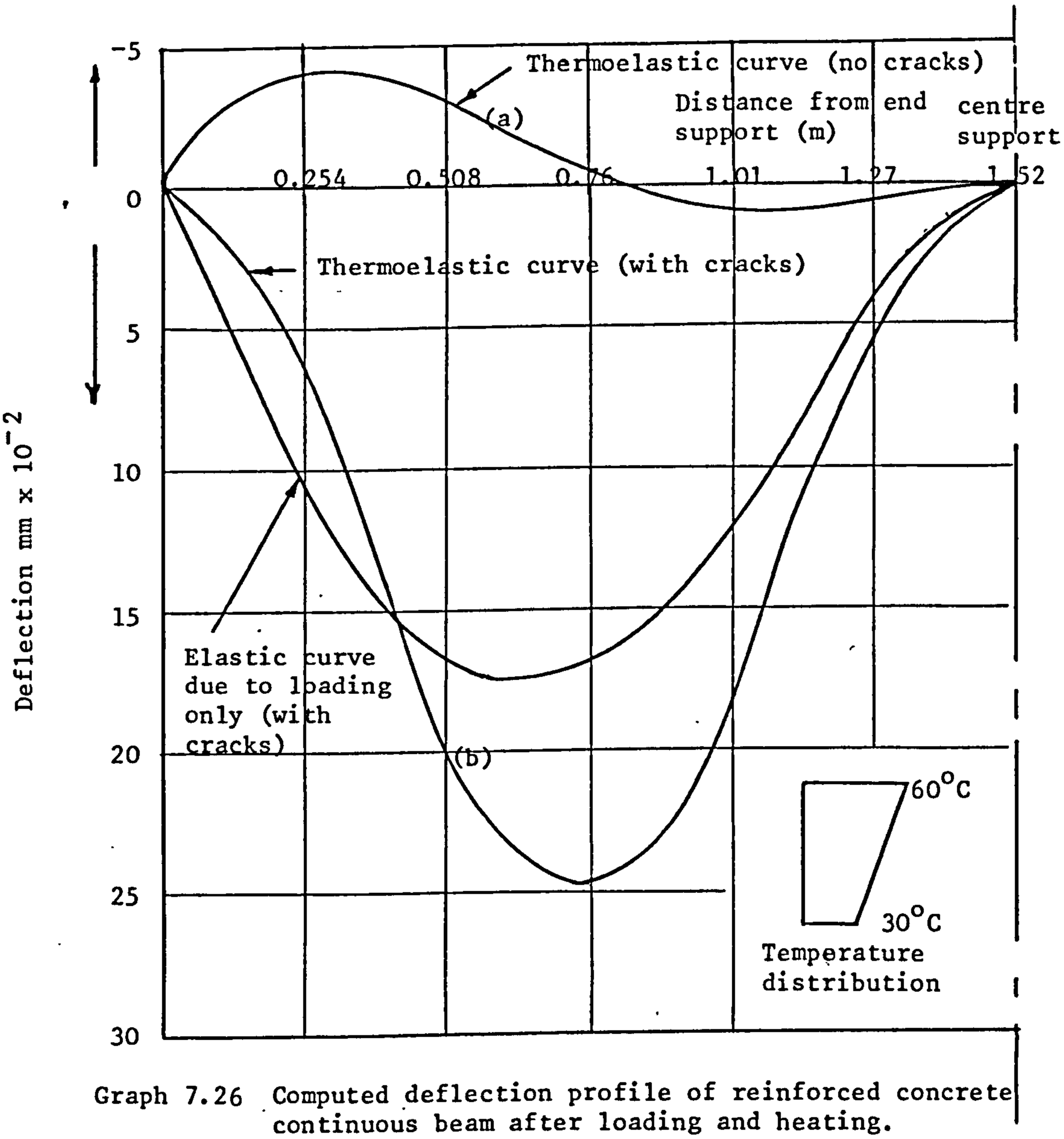

Graph 7.26 Computed deflection profile of reinforced concrete continuous beam after loading and heating.

Curves (a) and (b) indicate the significant influence that cracking has on deflection at large temperature crossfalls

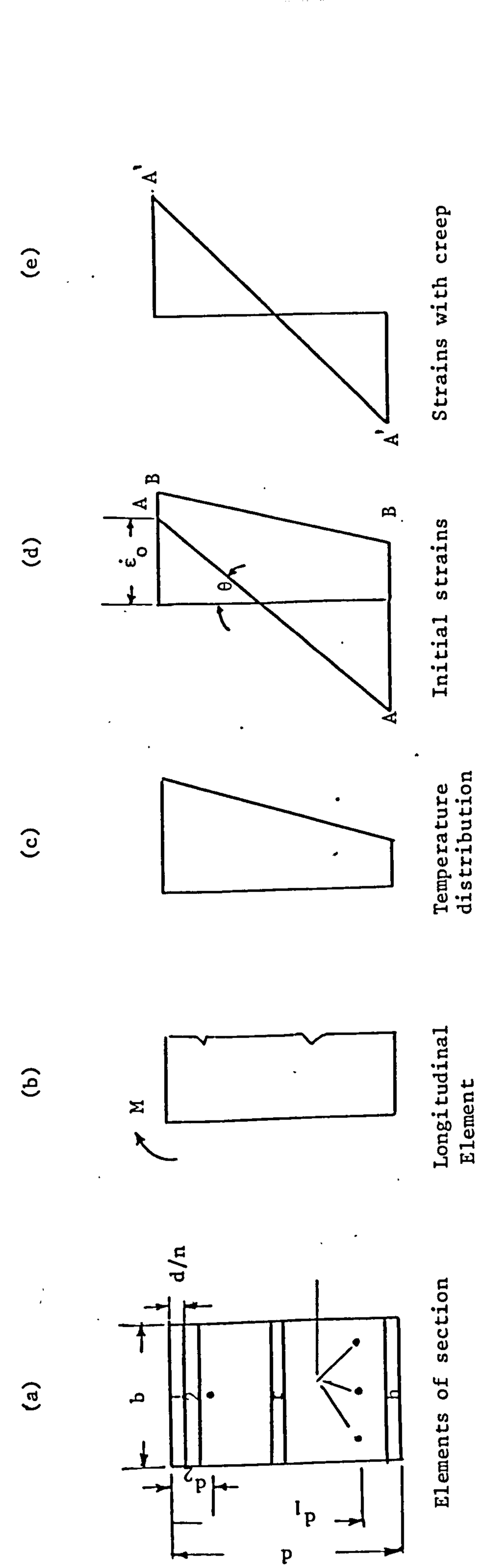

Fig. 7.1 Strains in reinforced concrete beam subject to temperature cro ssfall

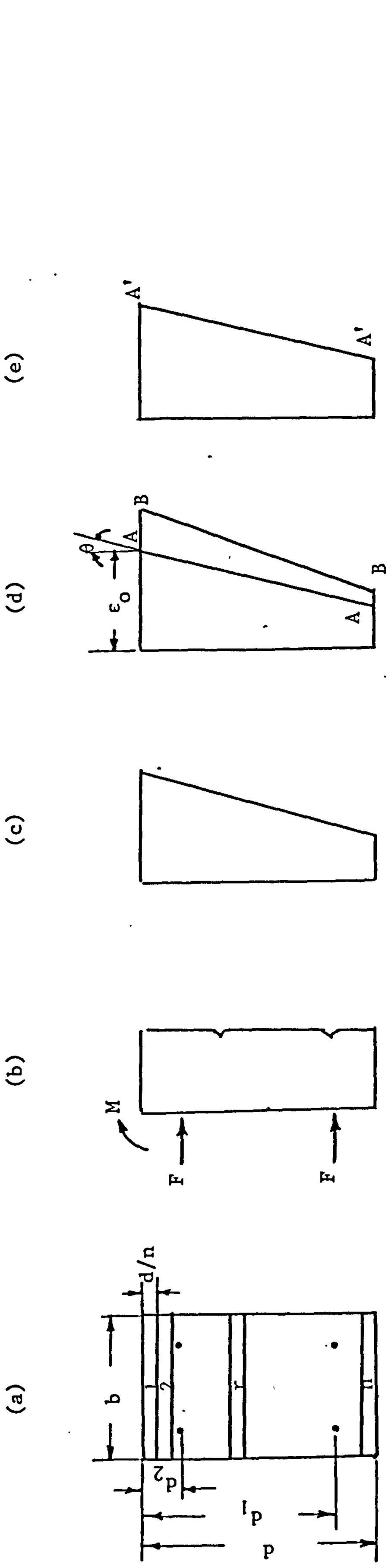

Fig. 7.2 Strains in prestressed concrete beam subject to temperature crossfall

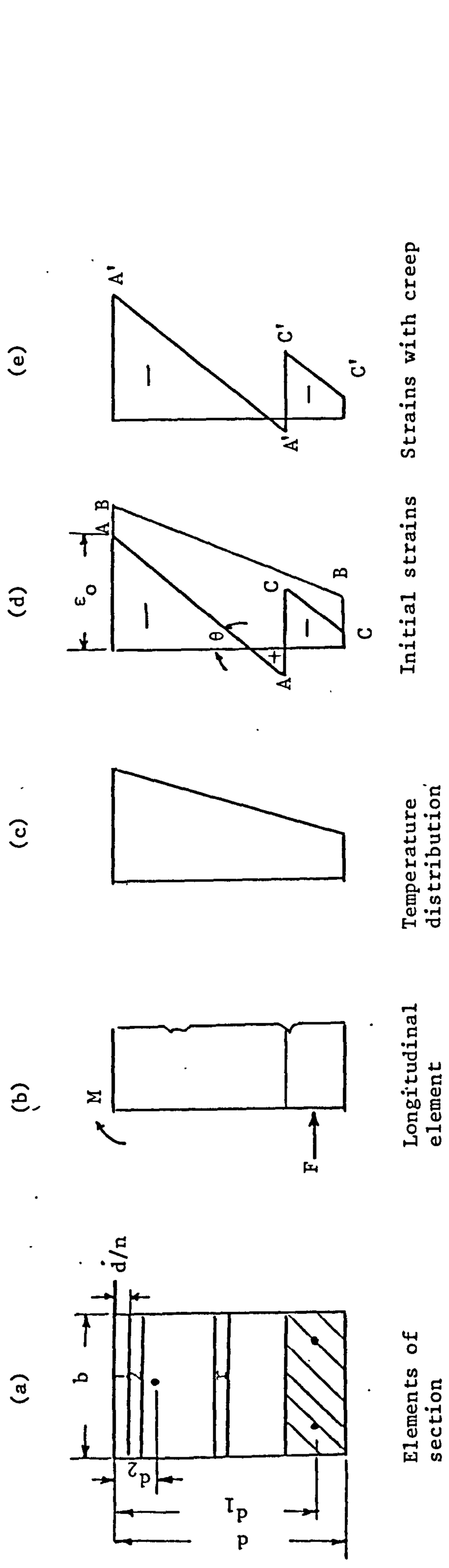

Fig. 7.3 Strains in composite prestressed concrete beam subject to temperature crossfall

Chapter 8

Conclusions and suggestions for further research

8.1 CONCLUSIONS

In this Chapter the essential points arising from the entire investigation in the preceding chapters are summarised in the following points:

1. The deflection behaviour of simply supported and continuous concrete beams tested to failure followed the elastic theory predictions until cracking. The experimental and theoretical loads at ultimate showed good agreement.

2. Long-term tests at laboratory temperature indicate decrease in the magnitude of the centre support reaction during the sustained loading period with regard to the reinforced and composite prestressed beams. The decrease was about 2% for reinforced concrete beam, and 5% for composite beam. No time dependent variation of the centre support reaction was observed in the prestressed concrete beam.

3. The ratio of the creep deflection at 9 months after loading to the elastic deflection for reinforced, prestressed and composite beams was approximately 1.57, 0.87 and 1.55 respectively.

4. Tensile concrete strains at the steel level at positions of maximum positive bending moment showed little change with time in reinforced concrete beam.

5. The proposed numerical method of analysis which takes into consideration the effect of concrete tension between cracks has been verified by comparison with experimental results. There is fair agreement between theoretical predictions and the experimental results in the case of prestressed and composite concrete beams only. The method underestimates the long-term deflection of reinforced concrete beam.

6. Calculated long-term variation of centre reaction and deflections of the three types of continuous concrete beams when subjected to a crossfall of 10°C between the hot and cold faces showed severe variation with time.

7. Calculated elastic thermal deflections decreased by increasing the temperature crossfall in the case of prestressed and composite prestressed beams and often increases in the case of reinforced concrete beam. The increase in the latter case results from the increased cracking which is created by large temperature crossfalls.

8.2 SUGGESTIONS FOR FURTHER RESEARCH

1. In some prestressed concrete structures, cracks are permissible in design. The present investigation should be extended experimentally to study the long-term behaviour of a cracked prestressed concrete continuous beam and the present analysis should be extended to account for the effect of cracks and their propagation with time in prestressed beams.

2. The present investigation should be extended experimentally to study the elastic and long-term behaviour of the three types of continuous concrete beams when subjected to temperature gradient and compare the results with the predictions from the numerical method used in this investigation.

APPENDIX A

Design details of the experimental test beams

A simple empirical method for determining the ultimate flexural strength of reinforced, prestressed and composite prestressed concrete beams is presented herewith, based on the tests carried out by some investigators. The method is limited to the following conditions:

1. The failure is primarily a flexural failure with no shear, bond or anchorage failure which might decrease the strength of the section.

2. Prestressed beams are bonded.

3. The beams are statically determinate, although discussions apply equally well to individual sections of continuous beams, the ultimate strength of continuous beams as a whole could be calculated by using the plastic hinge theory.

4. The load considered is the ultimate load obtained as a result of a short static test.

5. For the purpose of practical design it is assumed that the steel is stressed to the ultimate strength at rupture of under-reinforced prestressed beams.

6. Tension failure by yielding of the steel in under-reinforced, reinforced concrete beams.

The computation of the ultimate resisting moment can be calculated from the laws of equilibrium and from the assumption that plane cross sections remain plane. Referring to Fig. A-1, the ultimate compressive force in concrete C' equals the ultimate tensile force in the steel T', thus,

$$C' = T' = A_s f_s' \qquad (A\text{-}1)$$

Let a' be the lever arm between the forces C' and T', then the ultimate resisting moment is given by

$$M' = T'a' = A_s f_s' a' \qquad (A-2)$$

to determine the lever arm a', it is only necessary to locate the centre of pressure C'. There are many plastic theories for the distribution of compressive stress in concrete at failure[84].

Choosing the rectangular stress block for the ultimate compression in concrete, the depth to the ultimate neutral axis k'd is computed by

$$C' = k_1 f_c' k' bd$$

where $k_1 f_c'$ is the average compressive stress in concrete at rupture, b is the width of the beam and d is the depth of the beam. Hence

$$k'd = \frac{C'}{k_1 f_c' b} = \frac{A_s f_s'}{k_1 f_c' b}$$

$$k' = \frac{A_s f_s'}{k_1 f_c' bd} \qquad (A-3)$$

Where A_s is the cross-sectional area of steel and f_s' is the ultimate unit stress in steel.

Locating C' at the centre of the rectangular stress block, we have the lever arm

$$a' = d - k'd/2$$

$$= d(1 - \frac{k'}{2}) \qquad (A-4)$$

Hence the ultimate resisting moment is

$$M' = A_s f_s' d(1 - \frac{k'}{2}) \qquad (A-5)$$

According to Whitney's plastic theory of reinforced concrete beams, k_1 should be 0.85 based on cylinder strength.

Using 0.85 for k_1 formula (A-3) can be written as

$$k' = \frac{A_s f_s'}{0.85 f_c' bd}$$

By substituting this expression for k' into equation (A-5), we have

$$M' = A_s f_s' d(1 - \frac{A_s f_s'}{2 \times 0.85 f_c' bd}) \qquad (A-6)$$

for a rectangular section we put $P = \frac{A_s}{bd}$. Then using f_{su} for f_s', we have the following formula:

$$M' = A_s f_{su} d(1 - \frac{0.59\ P f_{su}}{f_c'}) \qquad (A-7)$$

which is almost identical to that given in the building code requirements of the Prestressed Concrete Institute, 1961 and as first proposed by the ACI-ASCE recommendations (85).

A.1 Design of Composite Prestressed Concrete Simple Beam

Assumptions (See Fig. A.2)

$b = 0.127$ m

$d = 0.204$ m

$d_1 = 0.178$ m

$t = 51$ mm (depth of prestressed portion)

$\ell = 1.52$ m

$A_s = 3.926 \times 10^{-5}$ m^2 (area of 2-5 mm Ø H.T.S. bars)

$f_c' = 30710$ MN/m^2

f_{ct} = 2800 MN/m^2 (maximum allowable tensile stress of Concrete Mix B)

f_{su} = 1652590 MN/m^2

f_i = 22240 N (initial Prestressing force in steel before transfer)

Cracking Load

Assuming total loss at loading = 15%

Therefore concrete stress in precast unit just before loading

$$= \frac{85}{100} \times \frac{2 \times 22240}{0.127 \times 0.051} = 5837.27\ MN/m^2$$

$$I = \frac{bd^3}{12} = \frac{0.127 \times 0.204^3}{12} = 8.98 \times 10^{-5}\ m^4$$

where I is the moment of inertia of the section

$$M_{cr} = \frac{(\text{initial stress in precast unit} + f_{ct})}{\left(\frac{d}{2}\right)} \times I$$

$$= \frac{(5837270 + 2800000)}{\left(\frac{0.204}{2}\right)} \times 8.98 \times 10^{-5}$$

$$= 7604.1847\ Nm$$

where M_{cr} is the cracking moment.

$$W_{cr} = \frac{M_{cr}}{\left(\frac{\ell}{3}\right)} = \frac{7604.1847}{\left(\frac{1.52}{3}\right)} = 15008.25\ N$$

where W_{cr} is the point load on the beam at cracking.

Total cracking load = $2W_{cr}$ = 30.0165 kN

Ultimate Load

Using equation (A-7) for calculation of ultimate bending moment

$$P = \frac{A_s}{bd_1} = \frac{3.926 \times 10^{-5}}{0.127 \times 0.178} = 0.001737$$

$$M' = 3.926 \times 10^{-5} \times 1652590 \times 10^3 \times 0.178 \times$$

$$\left(1 - \frac{0.59 \times 0.001737 \times 1652590 \times 10^3}{30710 \times 10^3}\right)$$

$$= 10911.847 \text{ Nm}$$

$$W_{ult} = \frac{3M'}{\ell}$$

$$= \frac{3 \times 10911.847}{1.52} = 21536.54 \text{ N}$$

where W_{ult} is the maximum point load at failure

Ultimate Failure Load = $2W_{ult}$

$$= 43073.08 \text{ N}$$

A.2 Design of Reinforced Concrete Simple Beam

Assumptions (See Fig. A.2)

$b = 0.127$ m

$d = 0.204$ m

$d_1 = 0.165$ m

$\ell = 1.52$ m

$A_s = 1{,}508 \times 10^{-4}$ m^2 (area of 3 No. 8 mm Ø deformed bars)

$f_c' = 30710$ MN/m^2

$f_{ct} = 2620$ MN/m^2 (maximum allowable tensile stress of concrete Mix A)

$f_y = 427490$ MN/m^2 (Steel stress at yield point)

Cracking Load

$$I = \frac{bd^3}{12} = 8.98 \times 10^{-5}\ m^4$$

where I is the moment of inertia of the section

$$M_{cr} = \frac{f_{ct}}{\left(\frac{d}{2}\right)} \times I$$

$$= \frac{2620000}{\left(\frac{0.204}{2}\right)} \times 8.98 \times 10^{-5} = 2306.62\ Nm$$

where M_{cr} is the cracking moment.

$$W_{cr} = \frac{M_{cr}}{\left(\frac{\ell}{3}\right)} = \frac{2306.62}{\left(\frac{1.52}{3}\right)} = 4552.53\ N$$

where W_{cr} is the point load on the beam at cracking.

Total Cracking Load = $2W_{cr}$ = 9.1 kN

Ultimate Load

Using f_y instead of f_{su} in equation (A-7) to calculate the ultimate bending moment

$$P = \frac{A_s}{bd_1} = \frac{1.508 \times 10^{-4}}{0.127 \times 0.165} = 0.00719$$

$$M' = 1.508 \times 10^{-4} \times 427490 \times 10^3 \times 0.165 \times \left(1 - \frac{0.59 \times 0.00719 \times 427490 \times 10^3}{30710 \times 10^3}\right)$$

$$= 10008.692\ Nm$$

$$W_{ult} = \frac{3M'}{\ell}$$

$$= \frac{3 \times 10008.692}{1.52} = 19753.99\ N$$

Where W_{ult} is the maximum point load at failure.

Ultimate failure load = $2W_{ult}$

= 39507.98 N

A.3 Design of Prestressed Concrete Simple Beam

Assumptions (See Fig. A.2)

b = 0.127 m

d = 0.204 m

d_1 = 0.171 m

ℓ = 1.52 m

A_s = 3.926×10^{-5} m^2 (area of 2-5 mm Ø H.T.S. bars)

f_c' = 35095 MN/m^2

f_{ct} = 2800 MN/m^2 (maximum allowable tensile stress of concrete Mix B)

f_{su} = 1652590 MN/m^2

f_i = 22240 N (initial Prestressing force in steel before transfer)

Cracking Load

Assuming total loss at loading = 15%

Therefore the initial concrete stress just before loading

$$= \frac{85}{100} \times \frac{2 \times 22240}{0.127 \times 0.204} = 1459.31\ MN/m^2$$

$$I = \frac{bd^3}{12} = 8.98 \times 10^{-5}\ m^4$$

where I is the moment of inertia of the section

$$M_{cr} = \frac{(\text{initial stress in the beam} + f_{ct})}{\left(\frac{d}{2}\right)} \times I$$

$$= \frac{(1459310 + 2800000)}{\left(\frac{0.204}{2}\right)} \times 8.98 \times 10^{-5} = 3749.86 \text{ Nm}$$

where M_{cr} is the cracking moment.

$$W_{cr} = \frac{M_{cr}}{\left(\frac{\ell}{3}\right)} = \frac{3749.86}{\left(\frac{1.52}{3}\right)} = 7401 \quad N$$

where W_{cr} is the point load on the beam at cracking.

Total Cracking Load $= 2W_{cr} = 14.8$ kN

Ultimate Load

From equation (A-7) we calculate the ultimate bending moment:

$$P = \frac{A_s}{bd_1} = \frac{3.926 \times 10^{-5}}{0.127 \times 0.171} = 1.807 \times 10^{-3}$$

$$M' = 3.926 \times 10^{-5} \times 1652590 \times 10^{3} \times 0.171 \times \left(1 - \frac{0.59 \times 1.807 \times 10^{-3} \times 1652590 \times 10^{3}}{35095 \times 10^{3}}\right)$$

$$= 10537.614 \text{ Nm}$$

$$W_{ult} = \frac{3M'}{\ell}$$

$$= \frac{3 \times 10537.614}{1.52} = 20797.923 \text{ N}$$

where W_{ult} is the maximum point load at failure

Ultimate Failure Load $= 2W_{ult}$

$= 41595.844$ N

We notice that the three types of beams have approximately the same ultimate capacity.

The design approach has been chosen because of preference in my own country. A similar result would be obtained by using the British code.

A.4 Design of reinforced concrete two span continuous beam

Assumptions used in reinforced concrete simple beam regarding beam cross sections and properties of steel and concrete are used here to calculate the ultimate moment at Sec. II-II (see Fig. A.3)(the section of maximum negative bending moment) by following the same procedure and using equation (A-7). The ultimate strength of the whole beam could be calculated by using the plastic hinge theory, as at ultimate load, the maximum positive bending moment at Sec. I-I will reach the value of the moment at Section II-II.

Cracking Load:

$M_{cr} = M_{cr}$ for reinforced concrete simple beam (see art. A.2)

Where M_{cr} is the cracking moment

$$W_{cr} = \frac{M_{cr}}{(\ell/3)} = \frac{2306.62}{1.52} \times 3 = 4552.53 \text{ N}$$

Total cracking load $= 4\ W_{cr} = 18.2$ kN

Ultimate Load

The ultimate moment M' at sections I-I and II-II are taken equal to the ultimate moment of simple beam (see art. A.2).

Therefore, when the bending moment at Section II-II reaches its ultimate value 10008.692 Nm

$$W_1 = \frac{3M'}{\ell}$$

$$= \frac{3 \times 10008.692}{1.52} = 19753.997 \text{ N}$$

Bending moment at Section I-I will reach its ultimate value M' when W_1 is given by:

$$(W_1 - \frac{M'}{\ell}) \times \frac{\ell}{3} = M' \quad \text{(See fig. A.4)}$$

$$(W_1 - \frac{10008.692}{1.52}) \times \frac{1.52}{3} = 10008.692$$

$$(W_1 - 6584.66) \times \frac{1.52}{3} = 10008.692$$

Therefore,

$W_1 = 26338.65$ N.

Ultimate failure load = $4W_1$ = 105.354 kN.

Design of stirrups

The shear stresses, q, at any cross-section in a reinforced concrete beam are calculated from the following equation:

$$q = \frac{Q}{b\ell a} \qquad \text{(A-8)}$$

where Q is the total shearing force across the section,

b is the breadth of the rectangular beam

ℓa is the arm of the resistance moment appropriate to the method of design being used.

Q max at ultimate = 32923.31 N

ℓa assumed $0.8\ d_1 = 0.8 \times 0.165$

b = 0.127 m

Therefore,

$$q = \frac{32923.31}{0.127 \times 0.8 \times 0.165} = 1.963929.\ MN/m^2$$

choose Ø 8 mm 2 branches.

Area of stirrups = $1.005 \times 10^{-4}\ m^2$

Calculation of stirrup spacing by using the following equation:

$$Q = \frac{P_{st}\ A_w\ \ell a}{S} \qquad \text{(A-9)}$$

Where P_{st} is the permissible tensile stress in shear reinforcement.

A_w is the cross sectional area of the stirrup

ℓa is the arm of the resistance moment

S is the spacing of stirrups

from equation (A-9)

$$S = \frac{P_{st}\ A_w\ \ell a}{Q} = \frac{P_{st}\ A_w\ \ell a}{qb\ell a}$$

$$= \frac{P_{st}\ A_w}{qb}$$

$$= \frac{427490 \times 10^3 \times 1.005 \times 10^{-4}}{1963929.2 \times 0.127}$$

$$= 0.172 \text{ m}$$

As the spacing of stirrups when required to resist shear should not exceed a distance equal to the arm of the resistance moment.(86) Therefore, the space S is taken as 0.127 m.

A.5 Design of Prestressed Concrete two span continuous beam

Cracking Load

Assuming total loss at loading = 15%

Therefore the initial concrete stress just before loading

$$= \frac{85}{100} \times \frac{4 \times 22240}{0.127 \times 0.204} = 2918\ 63\ MN/m^2$$

$$I = \frac{bd^3}{12} = 8.98 \times 10^{-5}\ m^4$$

where I is the moment of inertia of the section

$$M_{cr} = \frac{(\text{initial stress in the beam} + f_{cr})}{(d/2)} \times I$$

$$= \frac{(2918630 + 2800000)}{(\frac{0.204}{2})} \times 8.98 \times 10^{-5} = 5034.637\ Nm$$

where M_{cr} is the cracking moment

$$W_{cr} = \frac{M_{cr}}{(\ell/3)} = \frac{5034.637}{(\frac{1.52}{3})} = 9936.78\ N$$

where W_{cr} is the point load on the beam at cracking.

Total cracking load = $4W_{cr}$ = 39.764 kN

Ultimate Load

The ultimate moment M' at sections I-I and II-II are taken equal to the ultimate moment of prestressed concrete simple beam (see art. A.3).

Therefore,

when the bending moment at section II-II reaches its ultimate value

$$W_1 = \frac{3M'}{\ell}$$

$$= \frac{3 \times 10537.614}{1.52} = 20797.923 \text{ N}$$

Bending moment at section I-I will reach its ultimate value M' when W_1 is given by

$$(W_1 - \frac{M'}{\ell}) \times \ell/3 = M'$$

$$(W_1 - \frac{10537.614}{1.52}) \times \frac{1.52}{3} = 10537.614$$

Therefore

$$W_1 = 27730.56 \text{ N}$$

Ultimate failure load = $4W_1$ = 110.922 kN

A.6 Design of Composite Prestressed Concrete two span continuous beam

Cracking Load

M_{cr} at section II-II = M_{cr} for reinforced concrete continuous beam.

Therefore

Total, Cracking Load = 18.2 kN (see art. A.4)

Ultimate Load

The ultimate moment M' at section II-II is taken equal to the ultimate moment M' of reinforced continuous beam at section II-II.

Therefore

The ultimate failure load = ultimate failure load of reinforced concrete continuous beam = 105.354 kN (see art. A.4)

We notice that the three types of continuous beams have approximately the same ultimate capacity.

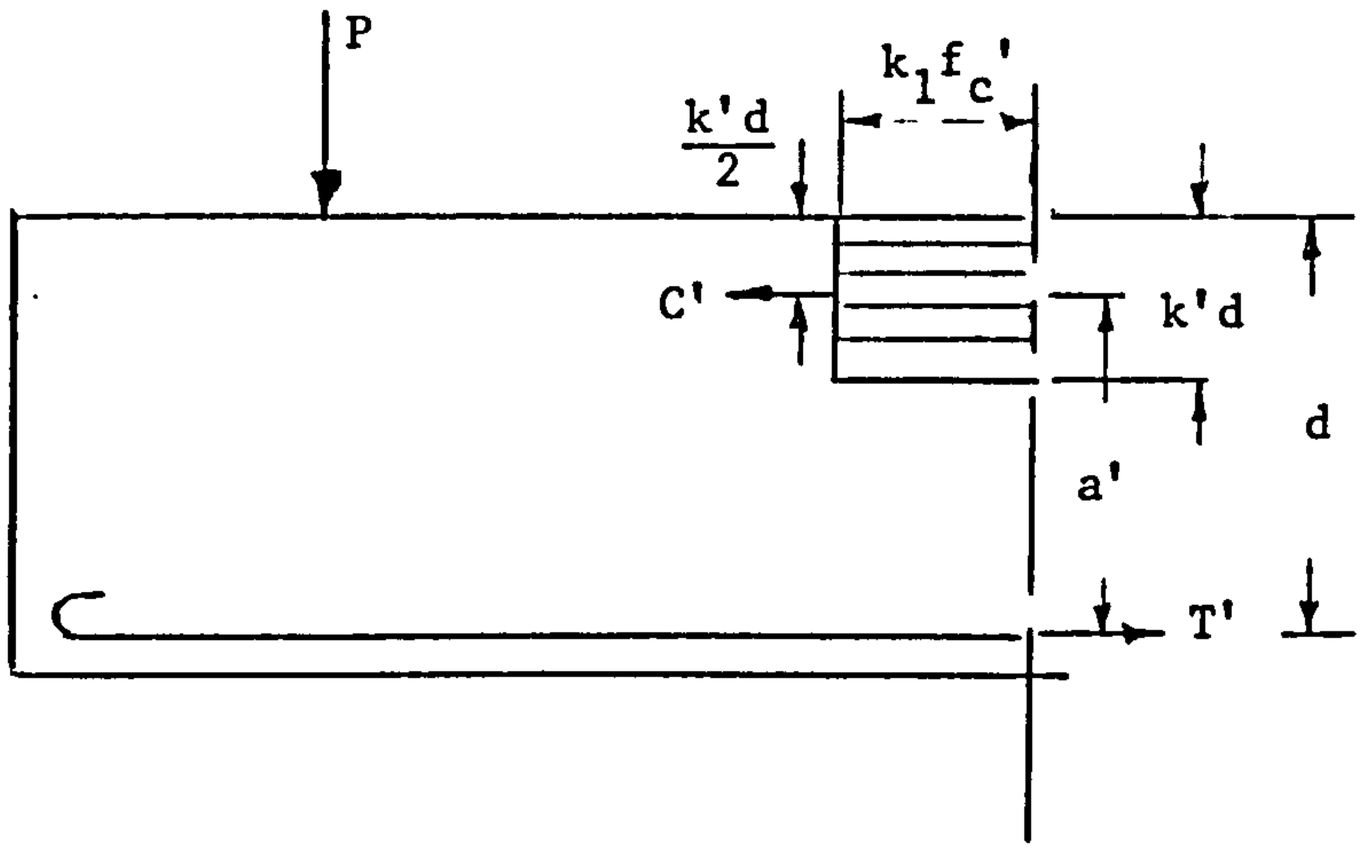

Fig. A.1 Concrete compressive stress distribution at I failure

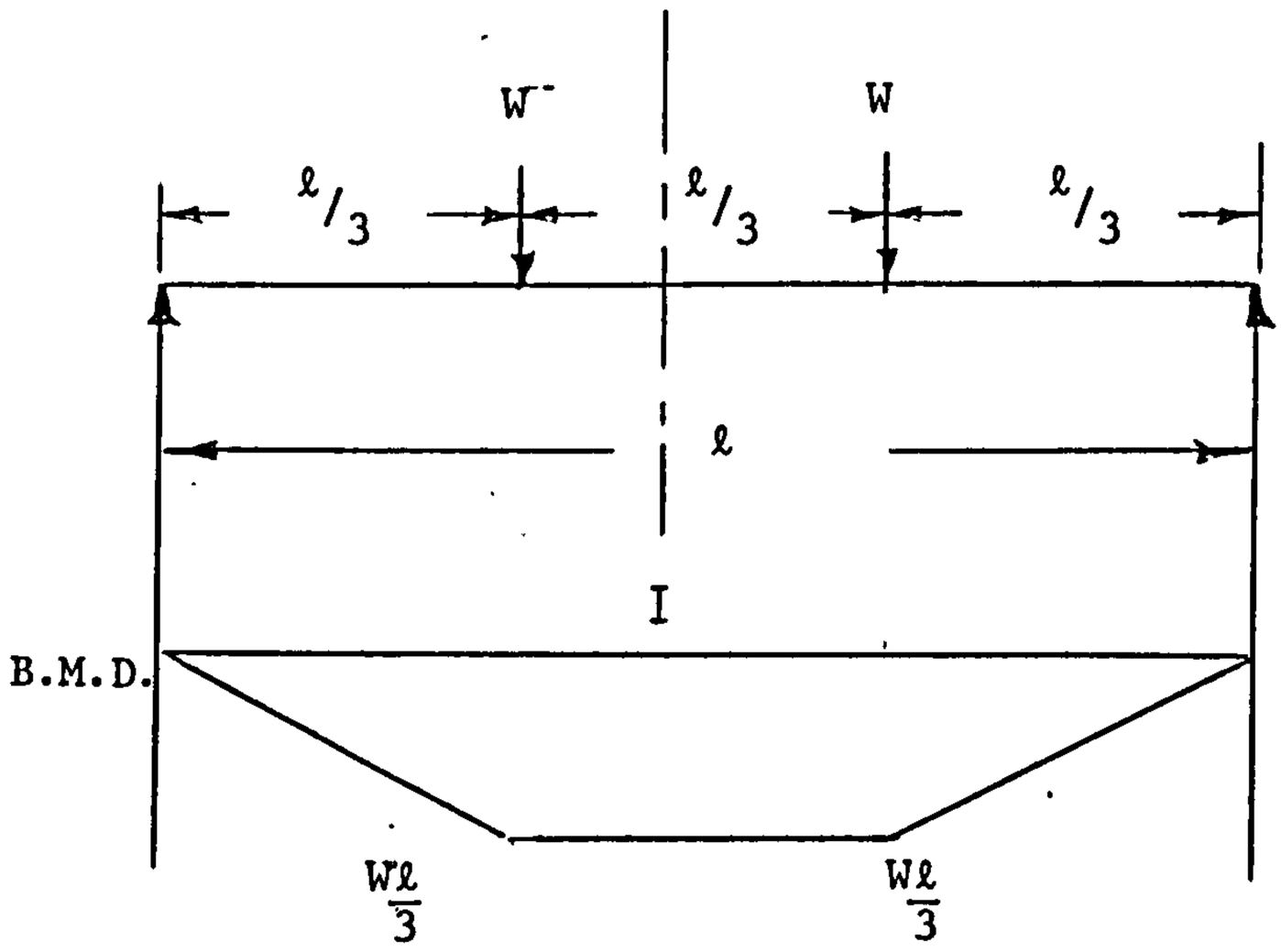

Fig. A.2 Bending moment diagram of reinforced, prestressed and composite simple beams

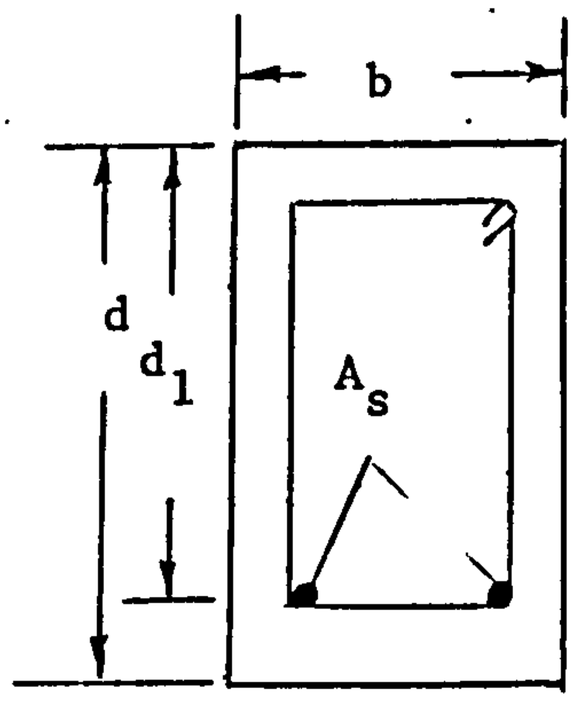

Sec. I-I

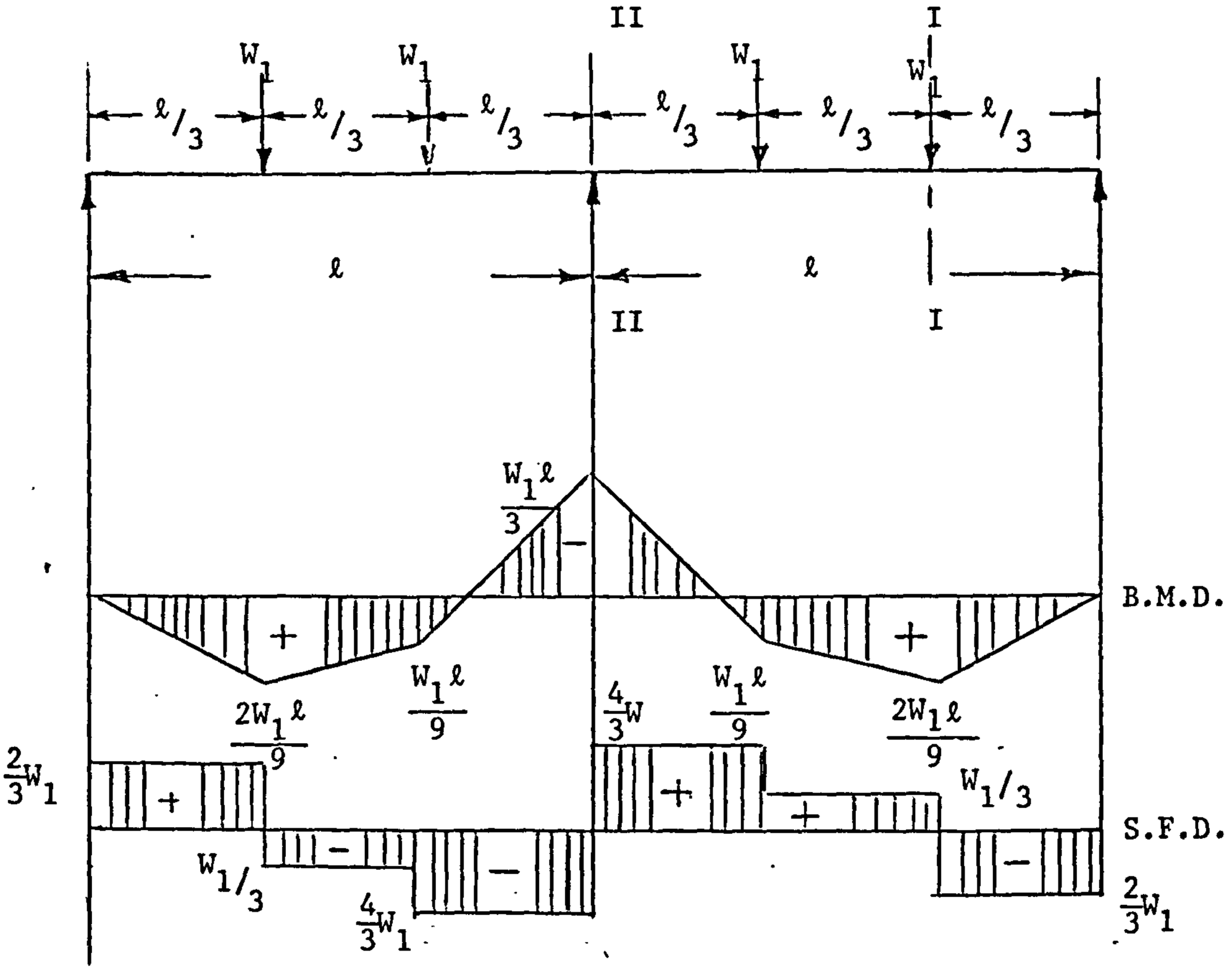

Fig. A.3 Bending moment and shearing force diagrams for a two span continuous beam

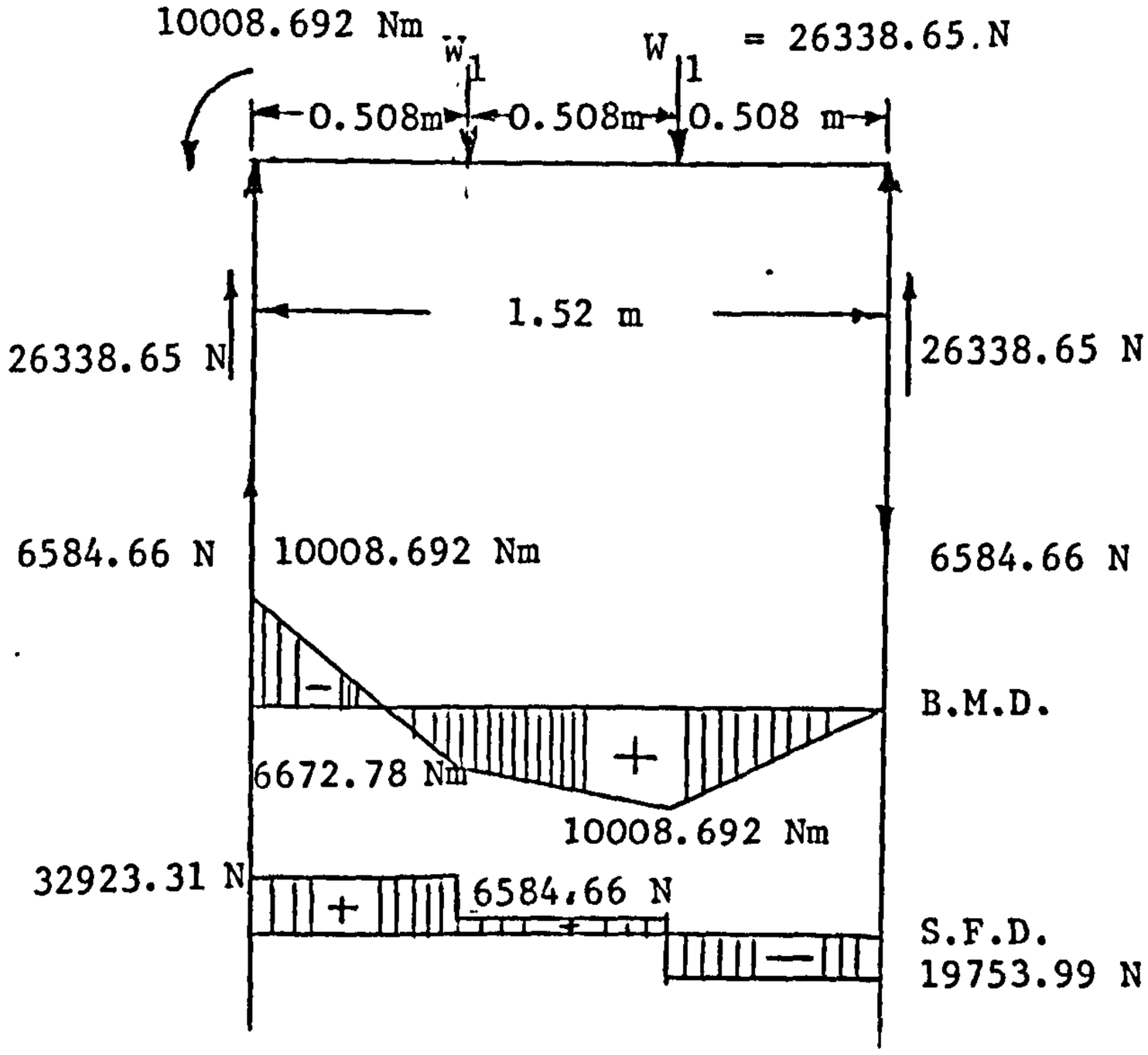

Fig. A.4 Bending moment and shearing force diagrams at ultimate failure load - R.C. continuous beam

APPENDIX B

Prediction of the deflection profile of two span continuous beam

Fig. B.1 shows the bending moment diagram M_o of two span continuous beam loaded with equal loads at the third points of each span of length L.

Calculation of deflection profile of span CB could be carried out by taking Point C as a datum and dividing the span CB to n longitudinal elements each of length ℓ as shown in Fig. B.2.

Therefore, the deflection at any point along the beam could be calculated as follows:

$$\Delta_1 = (\ell + 2d\alpha_1)\alpha_1$$

$$\Delta_2 = (\ell + 2d\alpha_1)\alpha_1 + (\ell + 2d\alpha_2)(2\alpha_1 + \alpha_2)$$

$$\Delta_3 = (\ell + 2d\alpha_1)\alpha_1 + (\ell + 2d\alpha_2)(2\alpha_1 + \alpha_2) + (\ell + 2d\alpha_3)(2\alpha_1 + 2\alpha_2 + \alpha_3)$$

$$\Delta_n = (\ell + 2d\alpha_1)\alpha_1 + (\ell + 2d\alpha_2)(2\alpha_1 + \alpha_2) + \ldots\ldots\ldots\ldots + (\ell + 2d\alpha_n)(2\alpha_1 + 2\alpha_2 + \ldots\ldots + \alpha_n)$$

if θ is the curvature/unit length.

Therefore,

$$\theta_1 \ell = 2\alpha_1$$

$$\alpha_1 = \frac{\theta_1 \ell}{2} = \frac{\theta_1 L}{2n}$$

$$\Delta_n = \left(\frac{L}{n} + \frac{2dL\theta_1}{2n}\right)\frac{\theta_1 L}{2n} + \ldots\ldots\ldots\ldots + \frac{L}{n}\left(\frac{L}{n} + \frac{2d\theta_n}{2n} L\right)$$

$$(\theta_1 + \theta_2 + \ldots\ldots\ldots \theta_n)$$

$$= \frac{L^2}{2n^2} (1 + d\theta_1)\theta_1 + (1 + d\theta_2)(2\theta_1 + \theta_2) \ldots\ldots\ldots\ldots +$$

$$(1 + d\theta_n)(2\theta_1 + 2\theta_2 + \ldots \theta_n)$$

assuming $(1 + d\theta_1),(1 + d\theta_2), ...(1 + d\theta_n) = 1$

Therefore the deflection at point n is given by

$$\Delta_n = \frac{L^2}{2n^2}\Big[\theta_1 + (2\theta_1 + \theta_2) + (2\theta_1 + 2\theta_2 + \theta_3) + (2\theta_1 + 2\theta_2 + 2\theta_3 + \theta_4) + \ldots\ldots (2\theta_1 + 2\theta_2 + \ldots\ldots \theta_n)\Big] \qquad \text{(B-1)}$$

Δ_B must be equal to zero if the whole beam is compatible where Δ_B is the deflection at point B.

If the whole beam is not compatible. Therefore, $\Delta_B = \delta$ as shown in Fig. (B-3). Compatibility and equilibrium could be achieved by calculating the deflection δ_1 at point B due to unit load applied at that point from equation (B-1) as shown in Fig. B-4.

Therefore

$$\frac{\delta}{\delta_1} = P_1$$

where P_1 is the load required to lift the end support at point B distance δ to obtain zero deflection at that point. Fig. B-5 shows the bending moment diagram M_1 due to applied load P_1 at Point B. Therefore, the actual bending moment diagram of the beam is equal to:

$$M_o \text{ diagram} + M_1 \text{ diagram}$$

Therefore a new curvature θ for each longitudinal element due to the actual bending moment ($M_o + M_1$) could be calculated.

Therefore the deflection at any point along the beam may be obtained by application of equation (B-1).

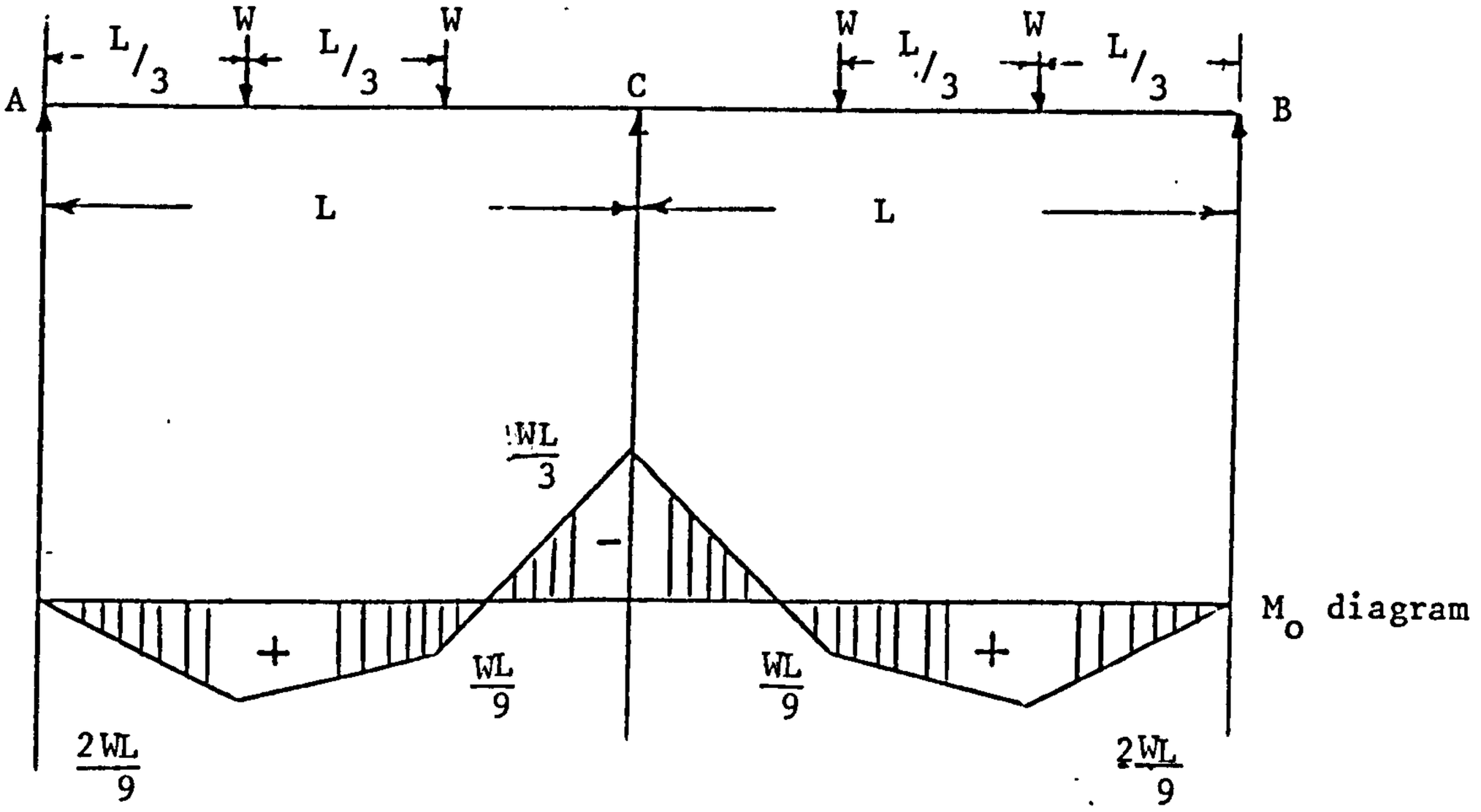

Fig. B.1 Bending Moment diagram due to applied loads

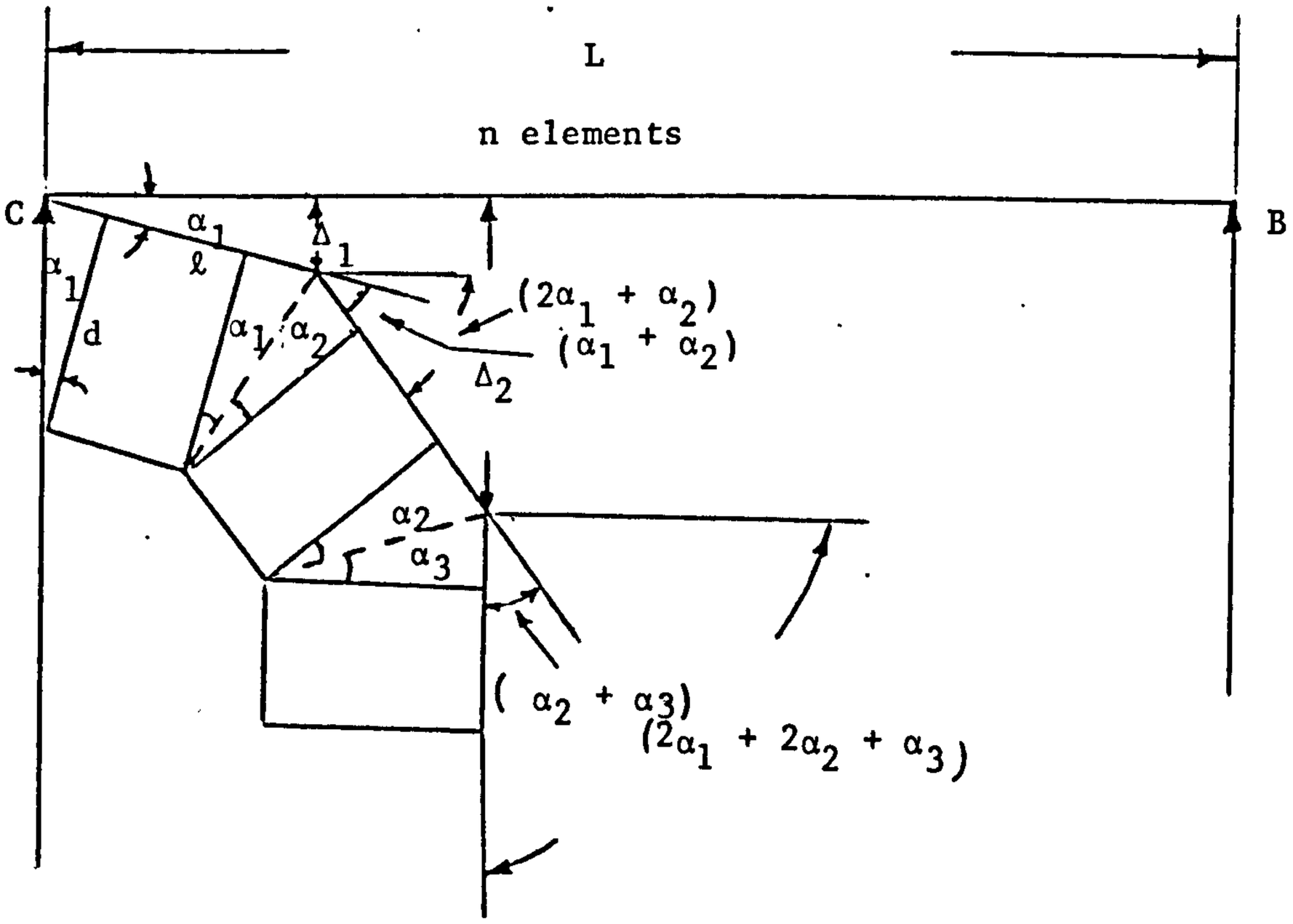

Fig. B.2 Rotations and deflection of beam elements

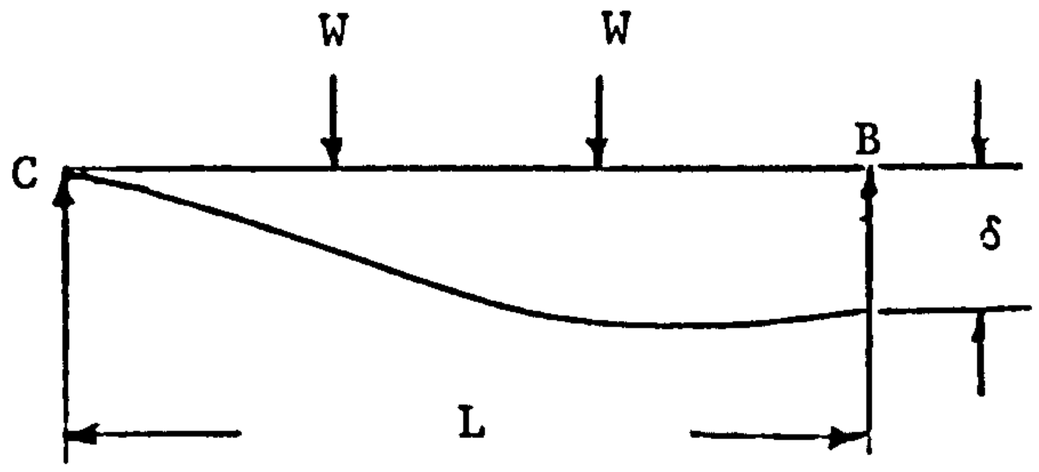

Fig. B.3 Deflection profile for half of the beam due to applied loads

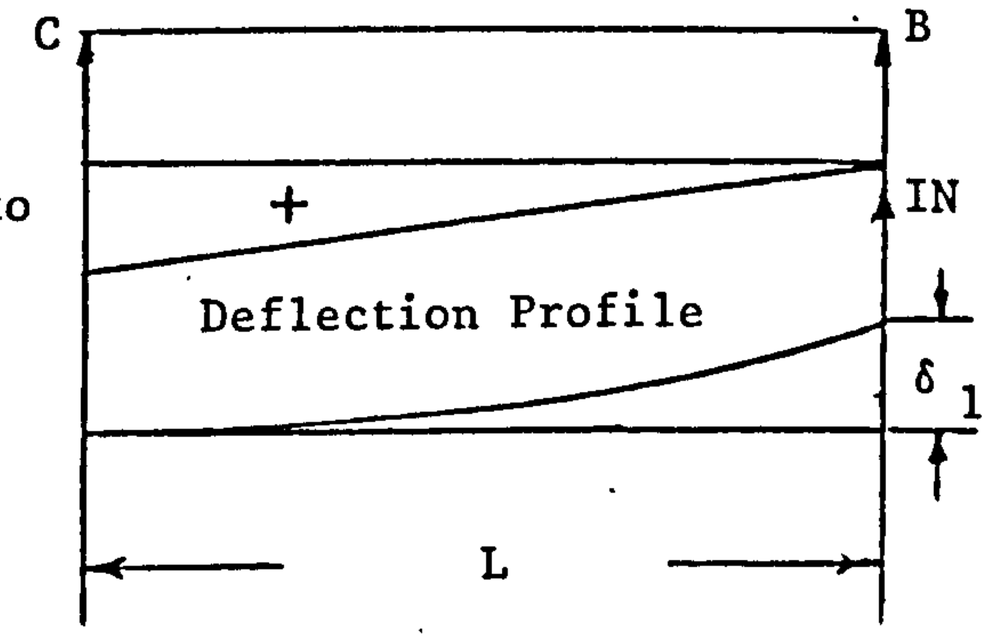

Fig. B.4 Bending moment diagram and deflection profile for half of the beam due to unit load at B

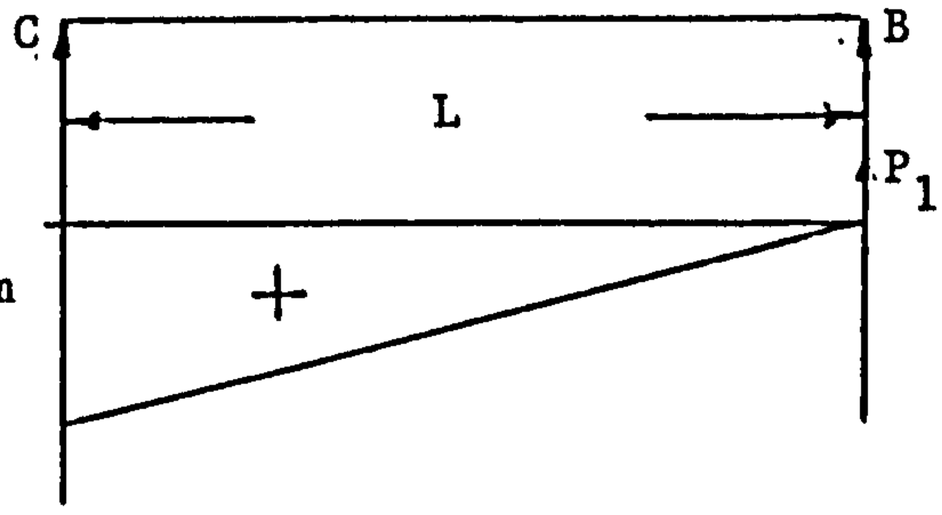

Fig. B.5 Bending moment diagram for half of the beam due to applied load P_1 at Point B

APPENDIX C

Moment-curvature relationships for Prestressed Concrete members in constant-moment zones

Moment-curvature relationships for prestressed concrete in constant-moment zones

M. J. N. Priestley*, BE(Hons), PhD, MNZIE
R. Park†, ME, PhD, CEng, MICE, MIStructE, MNZIE and
F. P. S. Lu,‡ BSc, FNZIE

UNIVERSITY OF CANTERBURY, CHRISTCHURCH, NEW ZEALAND

SYNOPSIS

The paper deals with a theoretical formulation of moment-curvature curves for prestressed concrete members subjected to constant bending moment. The theory takes into consideration the variation of curvature between cracks caused by concrete tension and makes possible the prediction of both the curvature at a crack and the average curvature along the length of the member. A report is included of tests on seven single-span pre-tensioned beams which show that the theory accurately predicts the moment-curvature relationship.

Introduction

Several theories, notably those by Baker[1], Macchi[2] and Guyon[3], have been developed to predict the ultimate load behaviour of continuous prestressed concrete structures. In general, the theories require a knowledge of the moment-curvature relationships for the sections in order that the distribution of bending moments throughout the structure at the ultimate load may be determined. Knowledge of the shape of the moment-curvature relationship also gives an indication of the ductility available from prestressed concrete members.

Moment-curvature relationships for prestressed concrete members are usually derived for the sections at which cracks form, the behaviour of the member between the cracks being ignored. However, the bond between the steel and the concrete will mean that tension is transferred from the steel to the concrete between the cracks. This build-up of concrete tension depends upon the distribution of bond stress and will only lead to new cracks between existing cracks when the tensile strength of the concrete is exceeded. Because of the tension carried by the concrete, the curvature between cracks will be less than that at the cracks. Theory will be presented in this paper for the determination of moment-curvature relationships for members with constant bending moment including the effect of concrete tension between the cracks. The theory will be compared with the results from a series of tests on single-span beams.

The results given in this paper may be seen in more detail in a thesis[4] by the first-named author.

Notation

A_s = total area of prestressing steel
b = width of section
C = compressive force in concrete
d = distance from extreme compression fibre to centroid of prestressing steel
ε_c = concrete compressive strain
ε_{ce} = concrete compressive strain at extreme compression fibre
ε_{cu} = concrete compressive strain at crushing
ε_o = concrete compressive strain at maximum stress
ε_s = steel strain above ε_{si}
ε_{si} = steel strain when concrete stress is zero
ε_{sm}, ε_{sm+1} = steel strains corresponding to steel stresses f_{sm} and f_{sm+1}, respectively
ε_t' = concrete tensile strain at modulus of rupture
f_c = concrete stress
f_{ce} = concrete compressive stress at extreme compression fibre
f_c' = 150 mm diameter × 300 mm cylinder crushing strength of concrete
f_{cu}' = 150 mm cube crushing strength of concrete
f_s = steel stress
f_{sA} = steel stress at a crack when $M = M_{cr}$

*Head of Structures Laboratory, Ministry of Works Central Laboratory, Wellington, New Zealand.
†Professor of Civil Engineering, University of Canterbury, New Zealand.
‡Now Professor of Management, University of Otago, New Zealand.

Magazine of Concrete Research : Vol. 23, No. 75-76 : June-September 1971

f_{sB} = steel stress just before cracking when $M = M_{cr}$
f_{scr} = steel stress at a crack when $M \geq M_{cr}$
f_{sn}, f_{sn+1} = steel stress at points n and $n+1$ on the steel stress-strain curve, respectively
f_{sp} = steel stress after transfer when beam is subjected to zero curvature
f_t' = modulus of rupture of concrete
k = parameter for distance from neutral axis to extreme compression fibre
k_1 = parameter for distance from neutral axis to centroid of concrete tension
l = distance from a crack
l_B = minimum distance from crack over which sufficient tension can be transferred from the steel to the concrete by bond to crack the concrete
M = moment
M_{cr} = moment at cracking
M_u = ultimate moment (when strain at extreme compression fibre of concrete reaches 0·004)
Q_c = concrete stress-strain function
Q_s = steel stress-strain function
T_c = tensile force in concrete
T_s = tensile force in steel
t = over-all depth of section
u = bond stress
u_{av} = average bond stress
u_m = maximum bond stress
x = distance from neutral axis to a fibre
γ = curvature
γ_{av} = average curvature
γ_u = curvature at ultimate moment (when strain at extreme compression fibre of concrete reaches 0·004)
$\Sigma 0$ = total surface area of prestressing steel per unit length

Development of the theory

The theory will assume that the tendons are bonded to the concrete and hence applies to the analysis of pre-tensioned and well grouted post-tensioned beams.

STRESS AND STRAIN RELATIONSHIPS

For a prestressed concrete section, zero steel strain does not correspond to zero concrete strain. Consequently the initial conditions need definition. The initial concrete strain is the strain corresponding to zero concrete stress. The initial steel strain, e_{si}, is the steel strain corresponding to the initial concrete strain.

In the general form, the steel and concrete stresses at any stage of loading are given by

$$f_s = Q_s(e_{si} + e_s) \quad \ldots\ldots(1)$$

$$f_c = Q_c(e_c) \quad \ldots\ldots(2)$$

where Q_s and Q_c denote the stress-strain functions of the steel and concrete, respectively. For concrete in tension, the variation of tensile stress with strain up to the modulus of rupture will be assumed to be linear, but the other stress-strain relationships will be assumed to be general.

STRESS CONDITIONS JUST BEFORE CRACKING

Figure 1 shows the conditions at a section when the external moment has increased to the stage of causing the modulus of rupture to be reached at the extreme tension fibre. If the usual assumption of a linear strain profile is made,

$$k = \frac{e_{cc}}{e_{cc} + e_s} = \frac{e_{cc}}{e_{cc} + e_t'} \frac{t}{d} \quad \ldots\ldots(3)$$

and

$$e_s = e_t' - (e_{cc} + e_t')(1 - d/t) \quad \ldots\ldots(4)$$

The forces acting at the section are

$$C = b \int_0^{kd} Q_c(e_c)\,dx \quad \ldots\ldots(5)$$

$$T_c = \frac{btf_t'}{2} \frac{e_t'}{e_t' + e_{cc}} \quad \ldots\ldots(6)$$

$$T_s = A_s Q_s(e_{si} + e_s) \quad \ldots\ldots(7)$$

For equilibrium, $C = T_c + T_s$ and therefore

$$b \int_0^{kd} Q_c(e_c)\,dx = \frac{btf_t'}{2} \frac{e_t'}{e_t' + e_{cc}} + A_s Q_s(e_{si} + e_s) \quad \ldots\ldots(8)$$

In equation 8, e_{cc} is the only independent variable. If the relationships Q_c and Q_s are known, it is possible to solve equation 8 to find e_{cc}. When e_{cc} has been found, T_c and T_s may be calculated and the cracking moment may be found by taking moments about the neutral axis to be

$$M_{cr} = T_c \tfrac{2}{3} \frac{e_t' t}{e_t' + e_{cc}} + T_s \left(\frac{e_t' t}{e_t' + e_{cc}} - t + d \right) + b \int_0^{kd} Q_c(e_c) x\,dx \quad \ldots\ldots(9)$$

The curvature immediately before cracking is

$$\gamma = \frac{e_{cc} + e_s}{d} = \frac{e_{cc} + e_t'}{t} \quad \ldots\ldots(10)$$

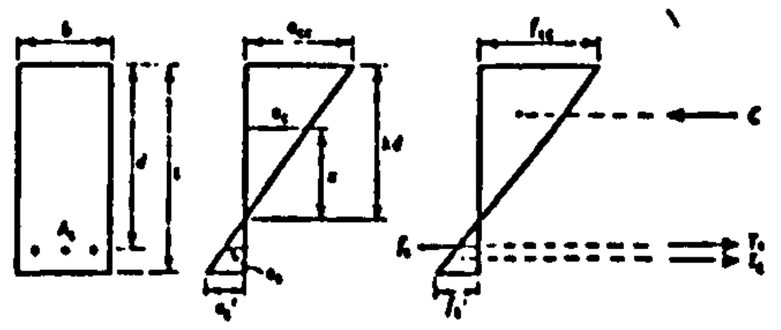

Figure 1. Conditions just before cracking begins.

STRESS CONDITIONS AFTER THE FORMATION OF CRACKS

Conditions at a crack

It is assumed that, as soon as cracking occurs, all the tension capacity of the concrete at the cracked section is effectively lost. In fact, the crack will not travel right up to the neutral axis, but the error involved is small. After cracking, the steel and concrete stresses must redistribute to balance the cracking moment without the assistance of T_c.

The normal assumption will be made that steel strains are linearly related to concrete compressive strains. Equations 3 to 10 apply, except that T_c is zero.

For equilibrium, $C = T_s$, and therefore

$$b\int_0^{kd} Q_c(e_c)\,dx = A_s Q_s(e_{si} + e_s) \quad \ldots\ldots\ldots(11)$$

Also, taking moments of these two forces about the neutral axis gives

$$M = b\int_0^{kd} Q_c(e_c)x\,dx + A_s Q_s(e_{si} + e_s)\Big)d\left(1 - \frac{e_{cc}}{e_{cc} + e_s}\right) \quad \ldots\ldots\ldots(12)$$

Equations 11 and 12 hold for any moment M equal to or greater than the cracking moment M_{cr}. If the relationships Q_c and Q_s are known, equations 11 and 12 can be solved simultaneously to yield e_{cc} and e_s, the only two unknowns involved, for a given moment M.

The curvature at the crack at all stages of loading is given by

$$\varphi = \frac{e_{cc} + e_s}{d} \quad \ldots\ldots\ldots(13)$$

Bond length

Immediately after the first crack forms in a region of constant moment ($M = M_{cr}$), a stress condition that varies between two limits exists. Let A be the section at a crack, and B be a section some distance away from the crack where the stresses have not been affected by the formation of the crack. The stresses and the stress resultants at section B are as described by equations 1 to 9.

At section B (away from the crack), the steel stress is, from equations 1 and 4

$$f_{sB} = Q_s\{e_{si} + e_t' - (e_{cc} + e_t')(1 - d/t)\} \quad \ldots\ldots(14)$$

At section A (at the crack), the steel stress is

$$f_{sA} = Q_s(e_{si} + e_s) \quad \ldots\ldots\ldots(15)$$

where e_s is found from equations 11 and 12 when $M = M_{cr}$.

At section A, all the tensile stress is carried by the steel; between sections A and B, tension is transferred from the steel to the concrete by bond. Let l_n be the minimum length between A and B over which it is possible to transfer sufficient tension to the concrete to cause the modulus of rupture to be just reached at B. Then

$$l_n = \frac{A_s(f_{sA} - f_{sB})}{u_{av}\Sigma 0} \quad \ldots\ldots\ldots(16)$$

where u_{av} is the average bond stress between the steel and the concrete and $\Sigma 0$ is the total surface area of the prestressing steel per unit length.

Crack spacing

At first cracking in a constant-moment zone, probably one crack alone will form because of the non-homogeneity of concrete. This will occur at the section with the weakest modulus of rupture. More cracks will form at sections with slightly higher moduli of rupture as the load is increased fractionally. Note that a new crack cannot form between two existing cracks unless the spacing between them is at least $2l_n$, because enough bond length is required each side of the potential crack position to build up enough tension. It is evident that, with initially random cracking, the individual crack spacings soon after the formation of the first crack will vary between two limits, l_n and $2l_n$. These cracks will constitute the final cracking pattern, apart from cracks due to causes other than flexural stresses, because at higher moments no more tension can be transferred from the steel to the concrete by bond than at first cracking, because the bond stress reaches its maximum value when cracking first occurs. Also, the area of concrete over which the tension can be distributed will increase as the neutral axis rises with increasing load. Because the crack spacing can be expected to vary between l_n and $2l_n$, the average crack spacing will be approximately equal to $1{\cdot}5l_n$.

Stress distribution at a distance l from a crack ($l \leqslant l_n$)

The assumption is made that, at a section some distance from a crack, the steel strain is still linearly related to the concrete compressive strain.

At a distance l from a crack, the steel stress will be reduced by bond and the concrete tension will build up. At this stage of the analysis, no assumption is made regarding the shape and distribution of tensile stresses and strains in the concrete across the section. The conditions at a distance from a crack are shown in Figure 2. The reduction of steel tension force over length l from the crack is given by $\int_0^l u\Sigma 0\,dl$, where u is the bond stress, and may vary with l. Therefore, the tensile stress in the steel at distance l from the crack is

$$f_s = f_{scr} - \int_0^l \frac{u\Sigma 0}{A_s}\,dl \quad \ldots\ldots\ldots(17)$$

and the steel strain is

$$e_s = Q_s^{-1}\left(f_{scr} - \int_0^l \frac{u\Sigma 0\,dl}{A_s}\right) \quad \ldots\ldots\ldots(18)$$

Magazine of Concrete Research : Vol. 23, No. 75-76 : June-September 1971

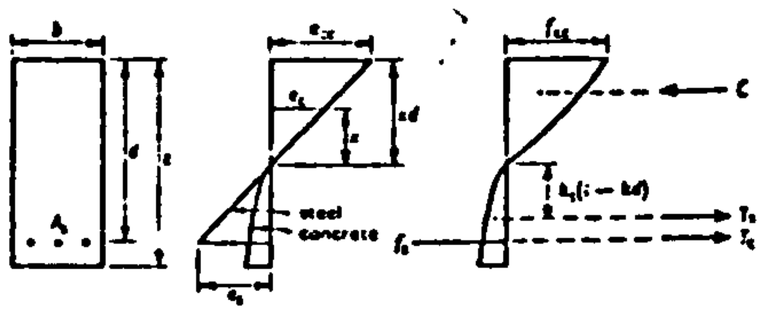

Figure 2: Conditions at a distance $l < l_0$ from a crack.

From the strain distribution in Figure 2,

$$k = \frac{e_{cc}}{e_{cc} + e_s} \quad \ldots\ldots\ldots\ldots\ldots\ldots (19)$$

For equilibrium, $C = T_c + T_s$, and therefore

$$b \int_0^{kd} Q_c(e_c)\mathrm{d}x = T_c + A_s f_s \quad \ldots\ldots\ldots\ldots (20)$$

and, if moments are taken about the neutral axis,

$$M = b \int_0^{kd} Q_c(e_c) x \mathrm{d}x + T_c k_1 \left(t - \frac{e_{cc} d}{e_{cc} + e_s}\right) + A_s f_s \frac{e_s d}{e_{cc} + e_s} \quad \ldots\ldots\ldots\ldots\ldots\ldots (21)$$

Thus, if the relationships Q_c and Q_s and the distribution of bond stress u are known, the steel stress f_{scr} at a crack for a given moment M may be found by the solution of equations 11 and 12, and the steel stress and strain at distance l from the crack may be found from equations 17 and 18. Then, if k_1 is also known, the simultaneous solution of equations 20 and 21 gives the remaining unknowns e_{cc} and T_c, and consequently the full stress and strain conditions at a distance l from a crack can be found.

The curvature at this section is then given by

$$\varphi = \frac{e_{cc} + e_s}{d} \quad \ldots\ldots\ldots\ldots\ldots\ldots (22)$$

Integration of the curvature over half the distance between the cracks gives the average curvature at moment M as

$$\varphi_{av} = \int_0^{0.75 l_0} \frac{e_{cc} + e_s}{0.75 l_0 d} \mathrm{d}l \quad \ldots\ldots\ldots\ldots (23)$$

STRESS-STRAIN AND BOND FUNCTIONS

The solution of equations 1 to 23 requires a knowledge of the steel and concrete stress-strain relationships, the variation of bond stress between cracks and the distribution of the tensile stress in the concrete at a section some distance from a crack. These are discussed in the following sections.

Steel stress-strain relationship

The actual stress-strain curve for the steel can be obtained from test results. The stress-strain curve will be represented by a number of straight lines joining specified points on the actual stress-strain curve. If a point on the curve is defined by stress f_{sn} and strain e_{sn}, the equation of the line joining point n with point $n + 1$ is

$$f_s = f_{sn} + \frac{f_{sn+1} - f_{sn}}{e_{sn+1} - e_{sn}} (e_{su} + e_s - e_{sn}) \quad \ldots\ldots (24)$$

Concrete stress-strain relationship

The widely accepted shape of the stress-strain curve proposed by Hognestad[5] for concrete in compression will be adopted. The curve consists of a second-order parabola up to the maximum stress and a linear falling branch. Hognestad assumed a maximum stress of $0{\cdot}85 f_c'$ for his curve, which was the value obtained from tests on short eccentrically loaded columns. For the present study on beams it was felt that a maximum stress equal to the cylinder strength f_c' would be more appropriate. The curve adopted is shown in Figure 3. The strains e_o and e_{cu} are the strains at maximum stress and at crushing, respectively. Typical values of $e_o = 0{\cdot}002$ and $e_{cu} = 0{\cdot}004$ will be assumed. The equation for the curve is:

for $0 \leqslant e_c \leqslant e_o$ —

$$f_c = f_c' \left\{ \frac{2e_c}{e_o} - \left(\frac{e_c}{e_o}\right)^2 \right\} \quad \ldots\ldots\ldots (25)$$

and for $e_o \leqslant e_c \leqslant e_{cu}$

$$f_c = f_c' \left(1 - 0{\cdot}15 \frac{e_c - e_o}{e_{cu} - e_o}\right) \quad \ldots\ldots (26)$$

For concrete in tension, the stress-strain curve will be assumed to be linear with a slope equal to that of the curve for compression at zero stress.

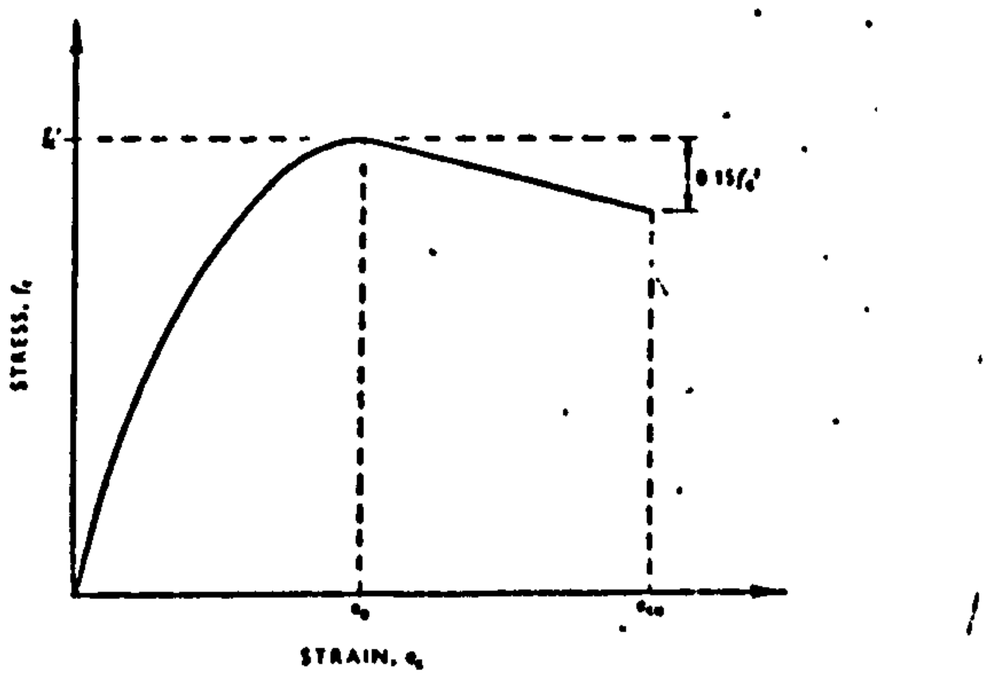

Figure 3: Stress-strain curve for concrete.

Variation of bond stress between cracks

The variation of bond stress between cracks is a problem that has not been satisfactorily resolved, although a large amount of theoretical and experimental work has been compiled on the subject. However, it is generally agreed that the bond stress is a maximum very close to the crack and decreases in some fashion further away from the crack; see Evans and Robinson[6] and Leonhardt[7], for example.

For this analysis, it will be assumed that, at first cracking, the bond stress decreases linearly from a maximum u_m at the crack to zero at a distance l_B, equal to the bond length, away from the crack. It will be further assumed that the gradient of the bond stress is independent of the distance between cracks, but is purely a function of the distance from the nearest crack.

Thus, for the average condition of two cracks spaced a distance $1{\cdot}5l_B$ apart, the bond stress distribution will be as shown in Figure 4. The bond stress distribution at $l < 0{\cdot}75l_B$ from a crack is then given by

$$u = u_m\left(1 - \frac{l}{l_B}\right) \quad \ldots\ldots\ldots\ldots\ldots\ldots(27)$$

At a distance $l \leqslant 0{\cdot}75l_B$ from a crack, the tensile steel stress is given by equations 17 and 27 as

$$f_s = f_{scr} - \int^{l} u_m\left(1 - \frac{l}{l_B}\right)\frac{\Sigma 0}{A_s}\,dl$$

$$= f_{scr} - \frac{u_m \Sigma 0}{A_s}\left(l - \frac{l^2}{2l_B}\right) \quad \ldots\ldots\ldots\ldots(28)$$

Now, from equation 16,

$$u_{av} = \frac{A_s(f_{sA} - f_{sB})}{l_B \Sigma 0}$$

and, since a linear bond distribution is assumed,

$$u_m = 2u_{av} = \frac{2A_s(f_{sA} - f_{sB})}{l_B \Sigma 0} \quad \ldots\ldots\ldots\ldots(29)$$

Substituting u_m from equation 29 into equation 28 gives the steel stress at distance $l \leqslant 0{\cdot}75l_B$ from a crack as

$$f_s = f_{scr} - 2(f_{sA} - f_{sB})\left(\frac{l}{l_B} - \frac{l^2}{2l_B^2}\right) \quad \ldots\ldots\ldots\ldots(30)$$

In equation 30, f_{scr} is the tensile steel stress at the crack given by the solution of equations 11 and 12 for the particular moment M acting, and f_{sA} and f_{sB} are the steel stresses given by equations 15 and 14 when $M = M_{cr}$. The value of f_s given by equation 30 is the value which will be used in equations 20 and 21.

Note that f_s from equation 30 is independent of the maximum bond stress u_m and thus the magnitude of the maximum bond stress does not affect the moment-curvature curves. This is to be expected because, given a certain bond stress distribution (for example, triangular, as used here), the magnitude of u_m will only alter the crack spacing. The distribution of stresses between cracks in similar beams with different values of u_m will be geometrically similar, although the crack spacing will differ.

Concrete tension distribution

The distribution of concrete tension at a section between two cracks is required in order that the parameter k_1, which gives the distance from the centroid of the concrete tensile stresses to the neutral axis, may be determined. Very little information is available as to the magnitude of k_1, but it was found that varying k_1 from $\frac{2}{3}$ to $\frac{1}{2}$ (corresponding respectively to a triangular and to a symmetrical distribution, be it rectangular or curvilinear) made a difference of less than 0·1% to the average curvature. The analysis is evidently insensitive to this variable, and a constant value of $\frac{1}{2}$ was chosen.

SEQUENCE OF CALCULATIONS

The equations obtained by the substitution of the stress-strain and bond stress relationships assumed in the previous section into the appropriate equations of 1 to 23 were programmed for solution by a digital computer[11]. The calculation of the moment-curvature curves for the constant-moment zone of a given prestressed concrete member with increasing moment using the derived equations may be carried out as follows.

(1) The value of e_{cc} which satisfies equation 8 is found by trial and error, and the cracking moment and the corresponding curvature are found from equations 9 and 10 respectively.

(2) The moment-curvature relationship for a cracked section is obtained by substituting gradually increasing values for e_{cc} up to e_{cu} into equation 11 to find e_{st} and then into equations 12 and 13 to find the corresponding moments and curvatures respectively.

(3) The moment-curvature relationships for sections between cracks are found by substituting various values of l/l_B and gradually increasing values of e_{cc} into equation 20 to find T_c, and then into equations 21 and 22 to find the moments and corresponding curvatures, respectively, at the various sections. A comparison of

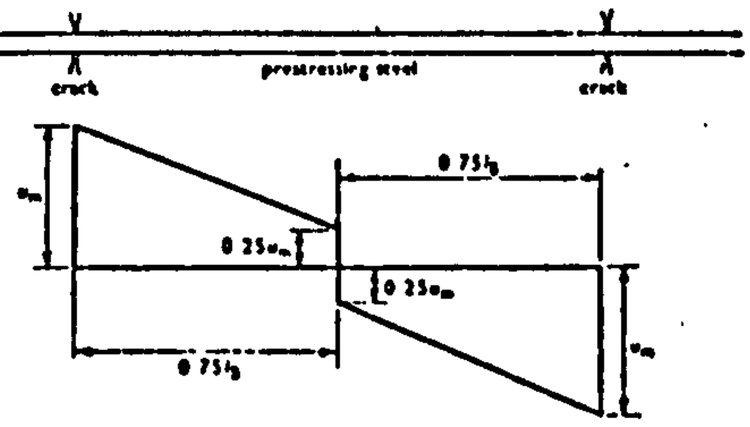

Figure 4: Bond stress distribution between adjacent cracks.

Magazine of Concrete Research : Vol. 23, No. 75-76 : June-September 1971

the average curvature along the zone given by equation 23 with the curvature at a crack given by equation 13 at each increment of moment is of interest.

Tests on single-span beams

TEST BEAMS

Seven single-span beams were tested in an experimental programme to check the theory developed above. All had a rectangular section 203 mm deep × 102 mm wide and were tested over a simply supported span of 4267 mm. The load was applied through a centrally mounted screw-jack device operating through a spreader beam as shown in Figure 5 to give a central constant-moment zone 1829 mm long.

Strains were measured on both sides of the beams throughout the constant-moment zone by means of Demec strain gauges with a 50·8 mm gauge length. Four gauge lengths above mid-depth at each section enabled the local curvature to be calculated from the gradient of the compressive strain distribution. Interpolation between these readings allowed the curvature at a crack to be calculated. The average curvature of the constant-moment zone was found by averaging the local curvatures.

Four of the beams had straight wires in one row at the centroid of the concrete section. The wires of the remaining three beams, again in one row, were harped at the load-points to increase the eccentricity.

Two-legged 6·35 mm diameter mild-steel stirrups were included at 51 mm spacing in the shear spans of each beam, but only one beam (beam 4) had any stirrups in the constant-moment zone. This beam had two-legged 6·35 mm diameter stirrups at 102 mm spacing in that zone.

Details of the beams are given in Table 1. The stress-strain curves for the prestressing steel are shown in Figure 6. The concrete was made from graded aggregate with a 10 mm maximum size and ordinary Portland cement. The mix proportions by weight were water : cement : aggregate :: 0·5 : 1·0 : 6·0. Prestress was transferred to the concrete at 7 days, and a measure of the elastic, creep and shrinkage losses was obtained from strain measurements on the concrete from before transfer until testing. The beams were tested at 28 days.

FAILURE

One of the reasons for loading by screw jack rather than by hydraulic jack was that this method would allow observation of any tendency for the load to reach a maximum value and then fall off as the deflection was increased. In other words, any falling-branch behaviour of the moment-curvature curve could be examined.

Falling-branch behaviour has been observed by La Grange[8]. However, in none of the beams tested in this programme was falling-branch behaviour detected. Failure was always sudden, even though the loading system would allow the load to drop off at constant deflection.

The reason for this is that, when the moment capacity of the beam at the failure section begins to decrease, there will be an elastic recovery of deformation over the remainder of the beam which results in an increase in deformation at the region of failure, even though the deflection at the load-points is being held constant. This increase in plastic deformation will cause a further reduction in the moment capacity of the critical section which will lead to a sudden failure of the beam if the slope of the falling branch of the moment-curvature curve for the region of failure is too steep to enable that region to absorb the energy released by the elastic recovery of the remainder of the beam. Thus the slope of the falling branch of the moment-curvature relationship of the test beams was too steep to be detected in these tests. A test arrangement with less elastic recovery was evidently necessary to trace falling-branch behaviour.

The presence of closed stirrups at close spacing, or the use of helices of small pitch in the compression zone, to increase the strain capacity of the compressed

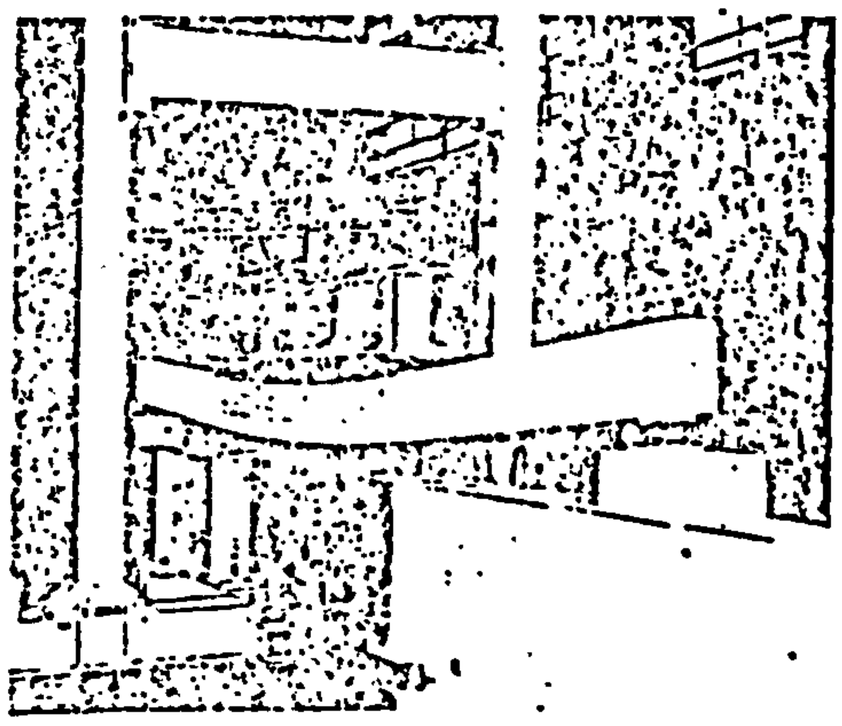

Figure 5: Test set-up.

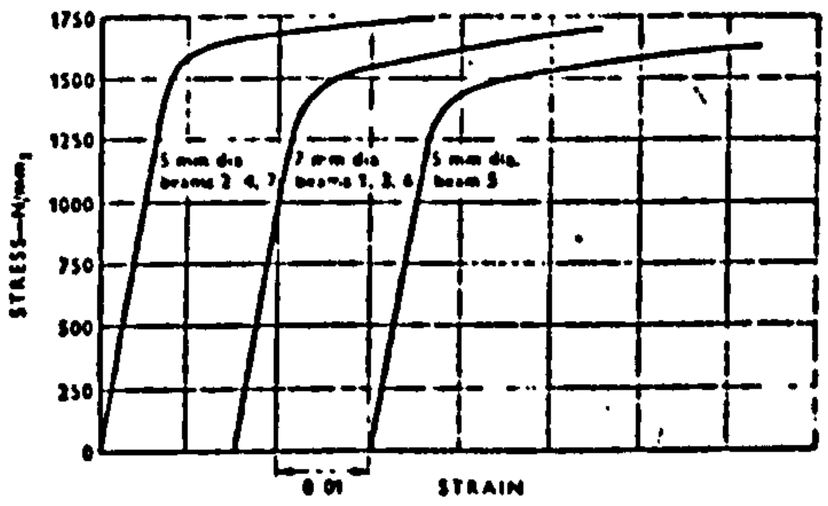

Figure 6. Stress-strain curves for steel.

concrete by confinement, would appear to be necessary if ductile behaviour is required after crushing of the concrete has begun.

The ultimate moments, shown in Table 1, agreed closely with the values predicted by the theory developed above. Apart from beams 3 and 6, the discrepancy between theory and experiment was between 1 and 4%. Beams 3 and 6 suffered bond failures under one of the load-points. The bond failures extended far enough into the shear span and constant-moment span to enable a portion of the beams on both sides of the load-point to act as unbonded or partially bonded beams. This resulted in higher curvatures and lower failure loads for these two beams. As the prestressing wire used for both of these beams was new and shiny, beam 4, a duplicate to beam 3 but having more pitted wire, was cast and tested. This beam behaved satisfactorily.

MEASURED CURVATURES

Curvature distributions along the constant-moment zone determined from the measured strains along the beam are shown for two of the beams tested in Figures 7 and 8. The comparative uniformity of the peak curvatures, even at very high moments, should be noted. Some previous investigators, for example La Grange[8], have stated that, even in a constant-moment zone, only one or two cracks will widen more than the other cracks and the plastic hinging will effectively occur over only part of the zone. As may be seen from Figures 7 and 8, this behaviour was not observed in this test programme. In most cases, it was impossible to tell from observations of the cracks where failure would occur, even at the penultimate increment of load, although examination of the curvature distributions in general shows that the concrete above the failure crack was subjected to higher compressive strains than the concrete above other cracks. This is to be expected, as failure will occur above the crack at the section which has the lowest compressive strength.

Figure 9 shows the failure section of one of the beams.

MOMENT-CURVATURVES: COMPARISON WITH THEORY

Figures 10 to 13 show the theoretical and experimental moment-curvature curves for four of the beams tested in this study. For each beam, the theoretical maximum curvature (i.e. the curvature at a crack) is compared with the experimental maximum curvature obtained from the average of the experimental curvature peaks measured at cracks, and the theoretical average curvature along the constant-moment zone is compared with the average experimental curvature measured along that zone. The theoretical curves were calculated from the theory above, a compressive crushing strain of 0·004 being assumed. Because the variation in the actual crushing strain from beam to beam was from 0·0035 to 0·0043, the experimental maximum curvatures measured at the cracks differ somewhat from the theoretical maximum values. The values of ultimate compressive strain found from each beam individually would give better agreement between theory and experiment, but it was desired to use as little empirical data as possible in the theoretical analysis and the constant value of 0·004 was chosen. To normalize the curves, all values of moment have been divided by the theoretical ultimate moment and the curvatures have been divided by the theoretical ultimate curvature at a crack.

Relationship between moment and average curvature

The agreement between theory and experiment for the moment versus average curvature curves is the most important part of these graphs, as it gives a measure of the accuracy of the method of analysis. The agreement is good, even near failure where the variation between the theoretical and experimental curves increases owing to the slight difference between the theoretical and actual ultimate moments.

TABLE 1: Properties of beams tested.

Beam No.	Number of wires	Diameter of wire (mm)	Steel area A_s (mm²)	Steel stress* f_{sp} (N/mm²)	Steel eccentricity (mm)	Cube strength† f_{cu}' (N/mm²)	Modulus of rupture f_t' (N/mm²)	Theoretical ultimate moment $M_{u\,theor}$ (kN m)	Experimental ultimate moment $M_{u\,exp}$ (kN m)	$\frac{M_{u\,exp}}{M_{u\,theor}}$	Average crack spacing (mm)	Concrete compressive strain at failure
1	2	7	77·2	831	0	52·8	4·31	10·16	10·50	1·03	302	0·0038
2	4	5	81·1	786	0	54·9	3·58	11·32	11·57	1·02	180	0·0036
3	2	7	77·2	655	41	52·3	3·64	15·19	13·67	0·90	140	—
4	2	7	77·2	656	41	44·9	4·56	14·60	14·73	1·01	122	0·0043
5	4	5	81·1	619	42	48·7	4·26	16·81	17·52	1·04	140	0·0041
6	4	7	154·3	827	0	52·4	4·15	15·68	14·25	0·91	124	—
7	4	5	81·1	940	0	54·9	4·65	11·31	11·61	1·03	155	0·0035

* steel stress after transfer when beam is subjected to zero curvature.

† $f_c' = 0{\cdot}87 f_{cu}'$ was found from tests on companion cylinders.

Magazine of Concrete Research : Vol. 23, No. 75-76 . June-September 1971

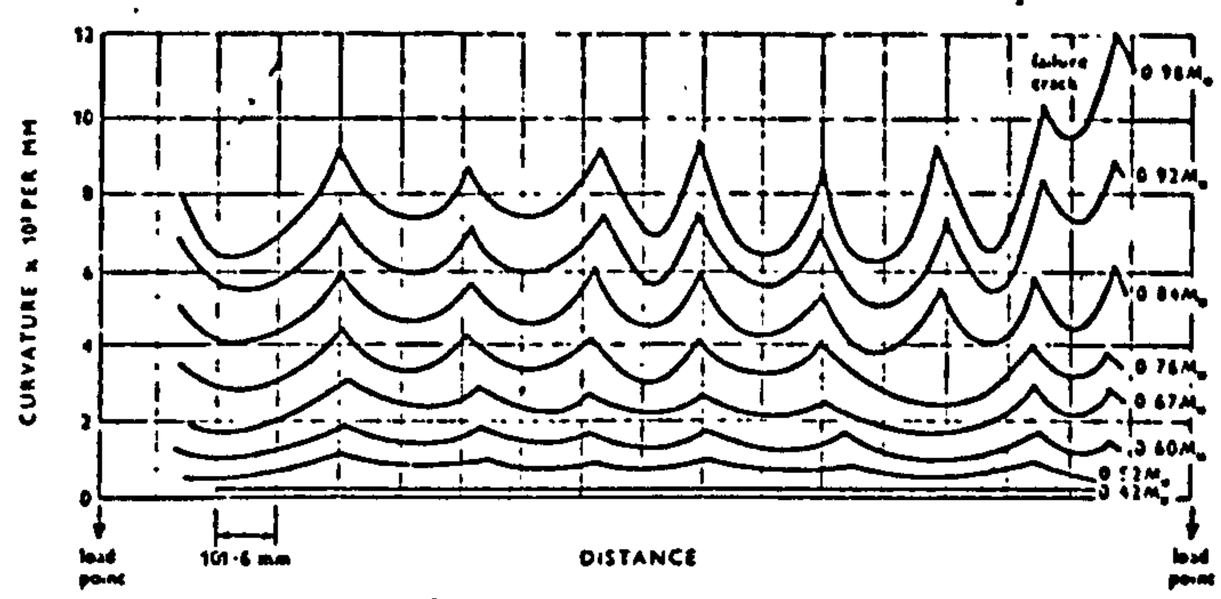

Figure 7: Curvature distribution along constant-moment zone of beam 2.

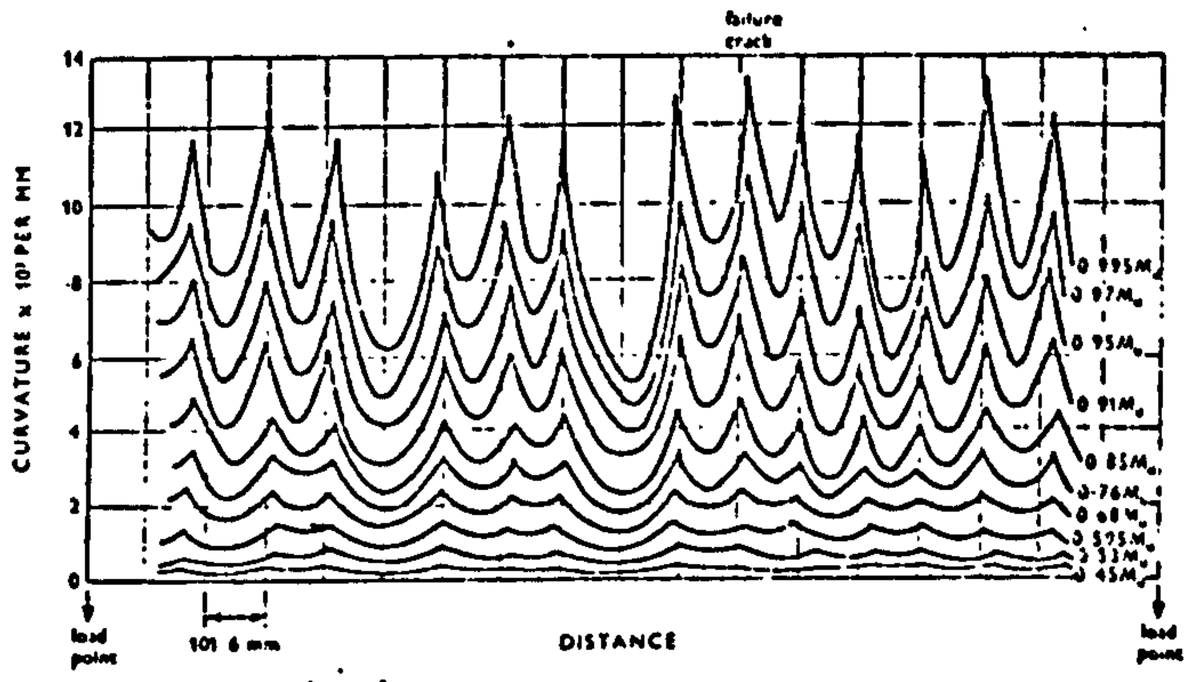

Figure 8: Curvature distribution along constant-moment zone of beam 5

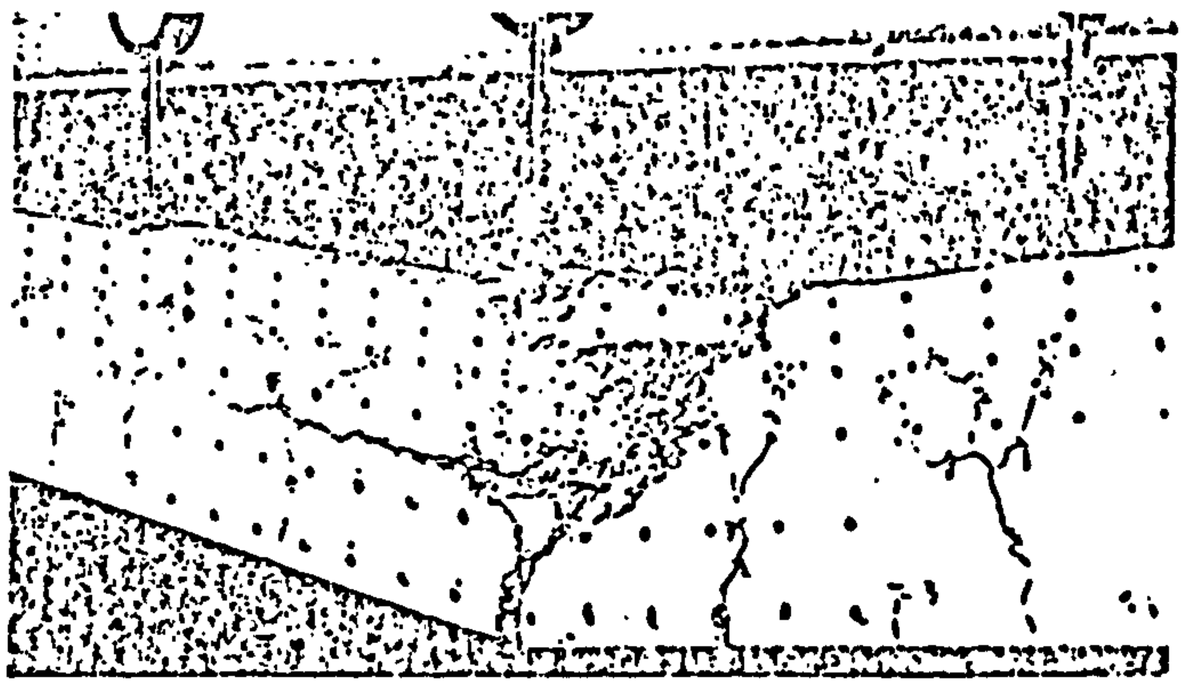

Figure 9: Typical failure zone of beam.

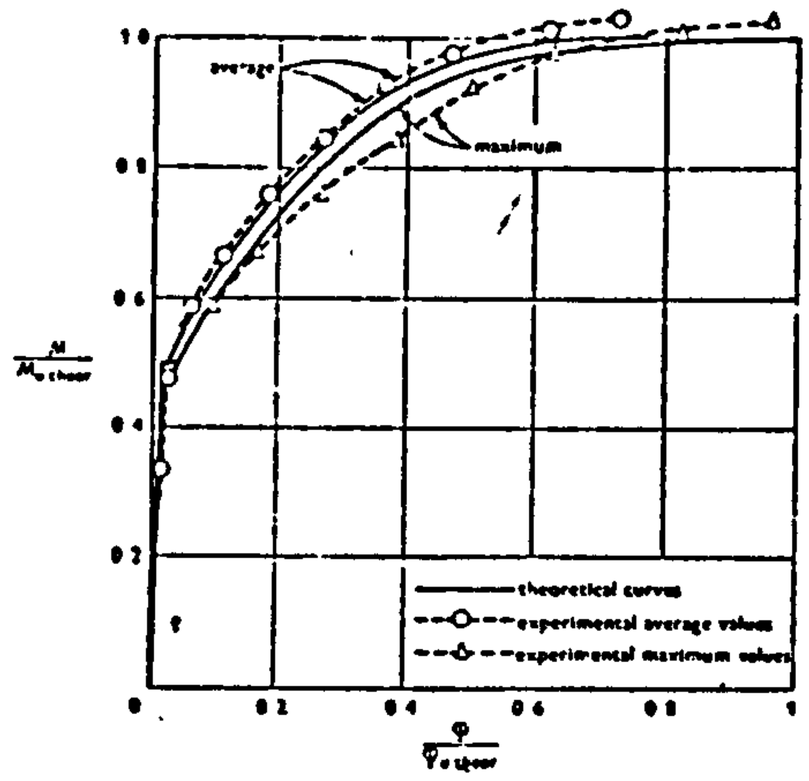

Figure 10: Moment-curvature relationships for beam 1.

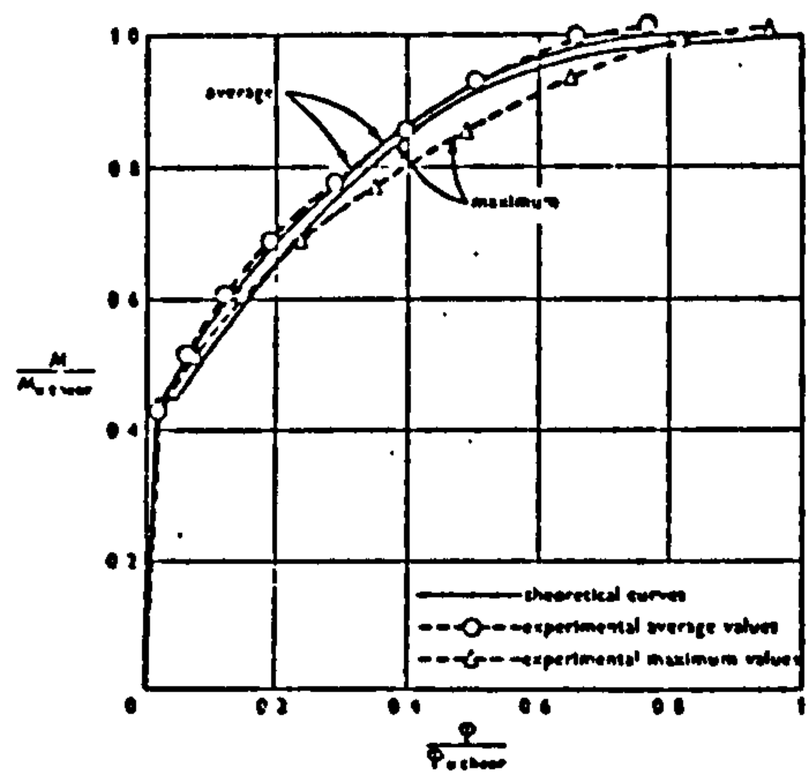

Figure 11: Moment-curvature relationships for beam 2.

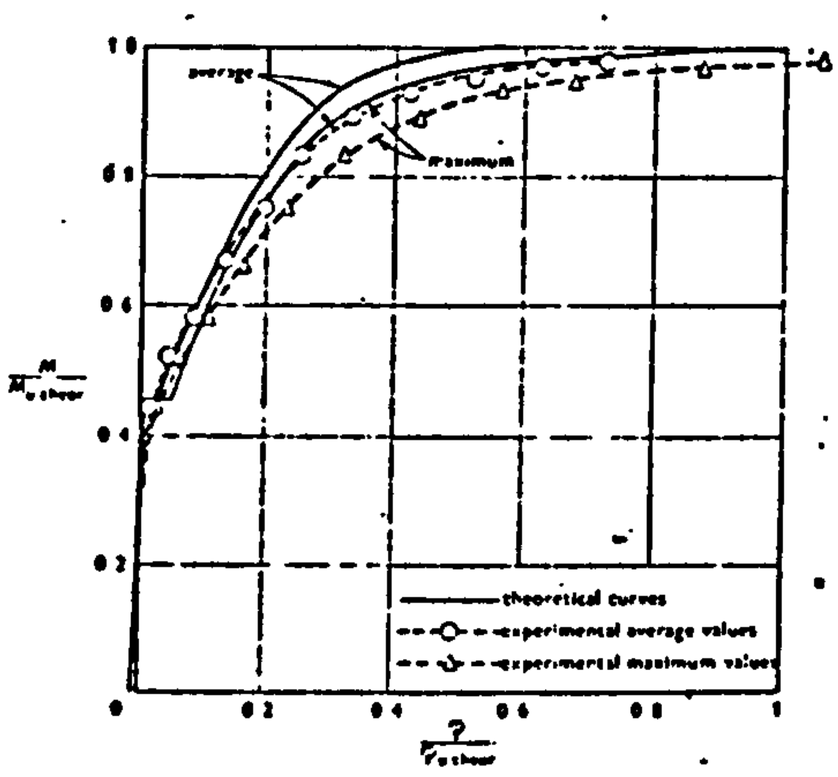

Figure 12: Moment-curvature relationships for beam 4.

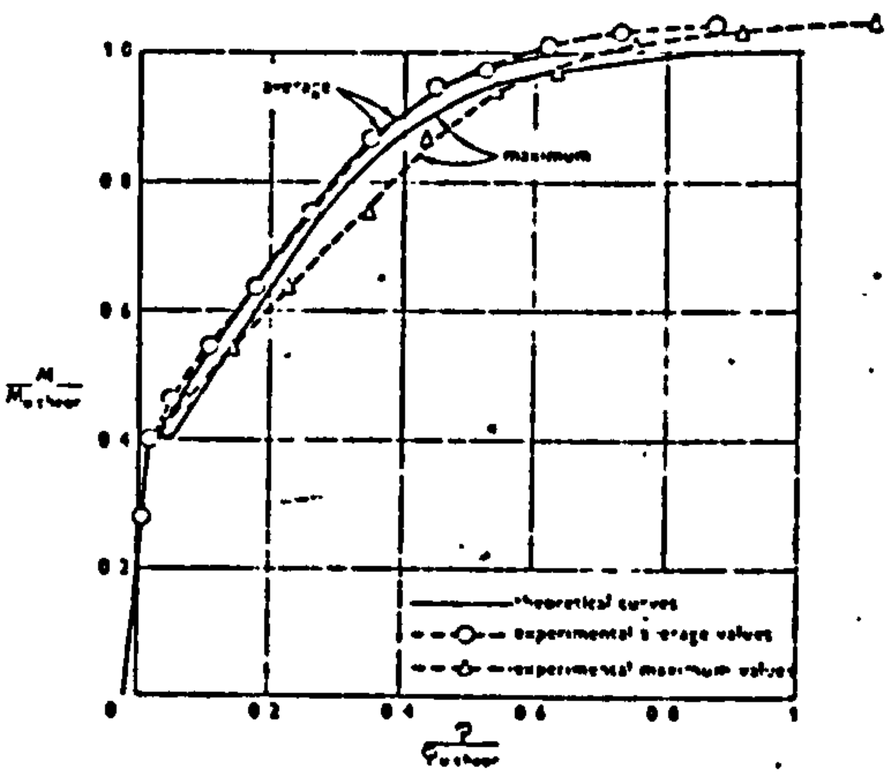

Figure 13: Moment-curvature relationships for beam 5.

Relationship between moment and maximum curvature

It is noticeable in Figures 10 to 13 that the agreement between theory and experiment is very much better for the average curvature than for the maximum curvature. This will largely be due to errors in estimating the experimental maximum curvatures. The experimental values for the maximum curvature were found by extrapolating curvatures measured at 50·8 mm intervals to obtain the values at the cracks, and then averaging the curvatures at the cracks throughout the constant-moment zone. If, as is quite probable, there is some loss of bond near the cracks, then the curvature at the crack will not peak sharply, as is shown in Figures 7 and 8, but will have a small saddle. Even a small amount of this behaviour would be sufficient to explain the comparatively small, but consistent, variation between the theoretical and experimental maximum curvature curves.

CRACKING AND CONCRETE TENSION BETWEEN CRACKS

Although there was no shear in the constant-moment zone of each beam, the initially vertical flexural cracks split into two inclined cracks at about the mid-height of the beam. This behaviour is caused by vertical tensile stresses set up at cracks by the difference between the curvature on the compression and on the tension faces of the beam. A full analysis of this behaviour has been given by Fenwick[9].

Magazine of Concrete Research: Vol. 23, No. 75-76: June-September 1971

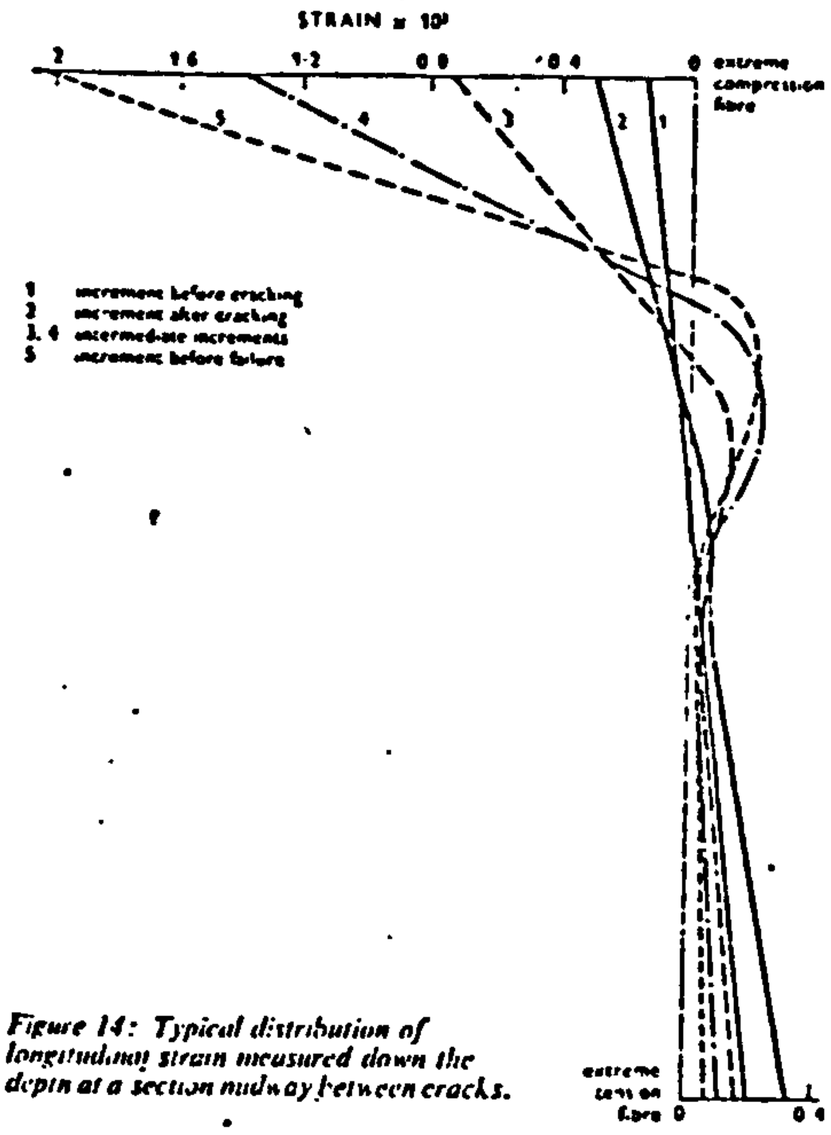

Figure 14: Typical distribution of longitudinal strain measured down the depth at a section midway between cracks.

The use of a large number of gauge lengths, as described above, enabled the concrete tensile strains between cracks to be investigated. A typical situation midway between cracks is shown in Figure 14. Before cracking, the vertical distribution of tensile strains is linear. As the load is increased after cracking, the tensile strain decreases at the extreme fibre and increases higher up the beam. Eventually a bulge forms above the level of the steel. Finally the strain at the tensile surface of the beam decreases to a value considerably less than at cracking and in some cases actually changes sign to become a small compressive strain.

Conclusions

The theory presented in this paper for the moment-curvature relationships of prestressed concrete members including the effect of concrete tension between cracks is developed by a purely analytical approach. The only empirical data included is used to define the stress-strain relationships for concrete and for steel and the bond stress distribution between cracks.

It is shown that the difference between the average curvature along a constant-moment zone and the maximum curvature at a crack may be quite significant. For example, for the beams of Figures 10 to 13 at the cracking moment, the average curvature may be as little as one-half of the maximum curvature; also, for these beams at $0{\cdot}6M_u$ and $0{\cdot}95M_u$, the average cervature may be as low as 77% and 79% of the maximum curvatures respectively, and at M_u the difference may be even larger. Hence the use of the more accurate values of average curvature may be justified when determining the deformation of members in spite of the rather long analysis, particularly since the agreement between the test results and theory is good. The theory applies to regions of constant bending moment but, in the general case of a moment diagram with varying ordinates, the member could be divided into small elements of length and the moment at the centre of each element regarded as being constant over the length of the element. The method is too complex for hand analysis but it is well suited for solution by a computer.

ACKNOWLEDGEMENTS

Grateful acknowledgement is made by the authors to the N.Z. Portland Cement Association, the N.Z. Ministry of Works and the N.Z. University Grants Committee for financial assistance. The work described in this paper formed part of that executed in the Civil Engineering Department of the University of Canterbury, New Zealand, by the first-named author during studies for the degree of Doctor of Philosophy supervised by the second- and third-named author.

REFERENCES

1. BAKER, A. L. L. *The ultimate load theory applied to the design of reinforced and prestressed concrete frames.* London, Concrete Publications, 1956. pp. 91.
2. MACCHI, G. Moment redistribution beyond elastic limit and at failure in prestressed concrete beams. *Journal of the Prestressed Concrete Institute.* Vol. 2, No. 2. September 1957. pp. 8–26.
3. GUYON, Y. *Prestressed concrete.* Vol. 2. London, Contractors Record, 1960. pp. xx, 741.
4. PRIESTLEY, M. J. N. *Moment redistribution in prestressed concrete continuous beams.* Thesis submitted to the University of Canterbury, Christchurch, New Zealand for the degree of PhD. 1966. pp. 189 & 162 appendixes.
5. HOGNESTAD, E. *A study of combined bending and axial load in reinforced concrete members.* Urbana, University of Illinois, 1951. pp. 128. Engineering Experiment Station Bulletin Series No. 399. pp. 128.
6. EVANS, R. H. and ROBINSON, G. W. Bond stresses in prestressed concrete from X-ray photographs. *Proceedings of the Institution of Civil Engineers.* Vol. 4, Part 1. 1955. pp. 212-235.
7. LEONHARDT, F. *On the need to consider the influence of lateral stresses on bond.* Paper presented to the Rilem Symposium on Bond and Crack Formation in Reinforced Concrete. Stockholm, Tekniska Hogskolans Rotoprinttryckeri, 1957. pp. 29–33.
8. LA GRANGE, L. E. *Moment redistribution in prestressed concrete beams and frames.* Thesis submitted to the University of Cambridge for the degree of PhD. 1961. pp. 153.
9. FENWICK, R. C. *Shear strength of reinforced concrete beams.* Thesis submitted to the University of Canterbury, Christchurch, New Zealand, for the degree of PhD. 1966. pp. 335.

Contributions discussing the above paper should be in the hands of the Editor not later than 31 December 1971.

REFERENCES

REFERENCES

1. NEVILLE, A.M.,"Properties of concrete", Pitman Publishing book 1973.

2. TROXELL, G. E., RAPHAEL, J. M. and DAVIS, R. E., "Long-time creep and shrinkage tests on plain and reinforced concrete", Proceedings A.S.T.M., Vol.58, 1958, pp 1101-1120.

3. PHILLEO, R., "Some Physical Properties of concrete at high temperatures", JACI, V.54, 1957, pp 857-864.

4. SAEMANN, J. C., and WASHA, G. W., "Variation of mortar and concrete properties with temperature", JACI, V.54, 1957, pp 385-395.

5. THEUER, A. U., "Effect of temperature on the stress-deformation of concrete", Journal of Research, National Bureau of Standards, V.18, Feb. 1937, pp 195-204.

6. ENGLAND, G. L., "A study of the time-dependent strains in concrete maintained at elevated temperatures and their effects in reinforced concrete", Ph.D. Thesis, University of London, 1961.

7. SERAFIM, J. L. and GUERRIRO, M. Q., "Influence of temperature on the creep of mass concrete", RILEM Bulletin No. 6, March 1960, pp 23-32.

8. GLUCKLICH, J. and ISHAI, O., "The effect of temperature on the deformation of hardened cement paste", RILEM Symposium on Concrete and Reinforced Concrete in hot countries, Haifa, July, 1960.

9. NASSER, K. W. and NEVILLE, A. M., "Creep of concrete at elevated temperatures", J. Amer. Concr. Inst., 62, pp 1567-79, Dec. 1965.

10. MARECHAL, J. C., "Variations in the Modulus of Elasticity and Poissons ratio with temperature", JACI Seminar on Concrete for Nuclear Reactors, West Berlin, Oct. 1970, pp 5

11. NEVILLE, A. M., "The relation between creep of concrete and the stress-strength ratio", ibid, pp 285-92.

12. NEVILLE, A. M., STAUNTON, M. M. and BONN, G. M., "A study of the relation between creep and gain of strength of concrete", Symp. on Structure of Portland Cement Paste and Concrete, Special Report No. 90, pp 186-203 highw. Res. Bd., Washington D.C., 1966.

13. BENNETT, E. W. and LOAT, D. R., "Shrinkage and creep of concrete as affected by the fineness of Portland Cement", Mag.Concr.Res., 22, No. 71, pp 69-78 June 1970.

14. HOPE, B. B., NEVILLE, A. M. and GURUSWAMI, A., "Influence of admixtures on creep of concrete containing normal weight aggregate", R.I.L.E. Int. Symp. on Admixtures for Mortar and Concrete, pp 17-32, Brussels, Sept. 1967.

15. JESSOP, E. L., WARD, M. A. and NEVILLE, A. M., "Influence of water reducing and set retarding admixtures on creep of light weight aggregate concrete", R.I.L.E.M. Int. Symp. on Admixtures for Mortar and Concrete, pp 35-46, Brussels, Sept. 1967.

16. KELLEY, J. W., "Some time-temperature effects in mass concrete", JACI, Vol. 34, 1938, pp 573-586.

17. LEE, C. R., "Creep and shrinkage in restrained concrete", Fourth Congress on Large Dams, 1951, Vol. 3, Questions 15, R.46.

18. PRIESTLEY, M. J., PARK, R. and LU, F. P. S., "Moment curvature relationship for prestressed concrete in constant-moment zones", Magazine of Concrete Research, Vol. 23, No. 75-76, June-Sept. 1971, pp 69-78.

19. ROSS, A. D., ENGLAND, G. L. and SUAN, R. H., "Prestressed concrete beams under sustained temperature crossfall", Magazine of Concrete Research Vol. 17, No. 52, Sept. 1965, pp 117-126.

20. SUAN, R. H., "The long-term behaviour of simply supported and continuous concrete beams subjected to a thermal gradient", Thesis submitted to the University of London for the degree of Ph.D. 1964.

21. ENGLAND, G. L., and ROSS, A. D., "Reinforced concrete under thermal gradients", Magazine of Concrete Research, Vol. 14, No. 40, March 1962, pp 5-12.

22. ARTHANARI, S. and YU, C. W., "An analysis of the creep and shrinkage effects upon prestressed concrete members under temperature gradient and its application", Magazine of Concrete Research, Vol. 19, No. 60, Sept. 1967, pp 157-164.

23. MARECHAL, J. C., "Le fluage du Beton en fonction de la temperature", Materials and Structures, 2, No. 8, pp 111-15, Paris, March - April 1969.

24. JOHANSEN, R. and BEST, C. H., "Creep of concrete with and without ice in the system", R.I.L.E.M. Bul. No. 16, pp 47-57, Paris, Sept. 1962.

25. SAEMANN, J. C., WARREN, C., and WASHA, G. W., "Effect of curing on the properties affecting shrinkage cracking of concrete block", JACI, Vol. 51, 1955, pp 833-852.

26. U.S. Bureau of Reclamation, Concrete Manual, 7th Ed., Denver, Colorado, 1966.

27. MEYERS, S. L., "How temperature and moisture changes may affect the durability of concrete", Rock Products, pp 153-57, Chicago, Aug. 1951.

28. WALKER, S., BLOEM, D. L., and MULLEN, W. G., "Effects of temperature changes on concrete as influenced by aggregates", J. Amer. Concr. Inst., 48, pp 661-79, April 1952.

29. ENGLAND, G. L., "Long-term thermal stresses in prestressed concrete structures", Proceedings of Conference on prestressed concrete pressure vessels, 13-17 March 1967, The Institution of Civil Engineers, London 1968.

30. WHITNEY, C. S., "Plastic theory in reinforced concrete design", Transactions ASCE, Vol. 107, 1942, pp 251-326.

31. MEYERS, S. L., "Thermal expansion characteristics of hardened cement paste and of concrete", Highway Research Board, Proc. V. 30, 1950, pp 193-203.

32. BONNELL, D. C. R. and HARPER, F. C., "The thermal expansion of concrete", D.S.I.R. Building Research Station Technical Paper No. 7, 1951.

33. MEYERS, S. L., "Thermal coefficient of expansion of Portland cement", Industrial and Engineering Chemistry, 1940, Vol. 32, pp 1107-1112.

34. DHONDY, S. S., "An investigation of some problems in the creep of concrete", M.Sc.(Eng.) 1957, King's College, London.

35. HAJNAL-KONYI, K., "Tests on beams with sustained loading", Magazine of Concrete Research, Vol. 15, No. 43, March 1963, pp 3-14.

36. WASHA, G. W. and FLUCK, P. G., "Effect of compressive reinforcement on the plastic flow of reinforced concrete beams", JACI, Vol. 49, 1952, pp 89-108.

37. GLANVILLE, W. H., and THOMAS, F. G., "Further investigation on the creep or flow of concrete under load", Building Research Technical Paper No. 21, D.S.I.R., London, 1939.

38. BERWANGER, C., and SARKAR, A. F., "Thermal Expansion of concrete and reinforced concrete", JACI, Proceedings V.73, Nov. 1976 pp 618-621.

39. WASHA, G. W. and FLUCK, P. G., "Plastic flow (creep) of reinforced concrete continuous beams", JACI, Proceedings V. 52, No. 5, Jan. 1956, pp 549-561.

40. NEVILLE, A. M. and DILGER, W., "Creep of Concrete, plain, reinforced and prestressed", North Holland, Amsterdam, Netherlands, 1970, pp 622.

41. CEB-FIP REPORT, "International Recommendations for the calculation and execution of concrete structures", PRAUGE, June 1970, Cement and Concrete Association, London, 80, pp.

42. ACI Committee 209, Subcommittee 2, "Prediction of creep, shrinkage and temperature effects in concrete structures", American Concrete Institute Publication, SP-27, 1971, pp 51-93.

43. BRANSON, D. E. and CHRISTIASON, M. L., "Time dependent concrete properties related to design-strength and elastic properties, creep and shrinkage", ACI Publication, SP-27, 1971, pp 257-277.

44. McHENRY, D., "A new aspect of creep in concrete and its application to design", Proceedings of the American Society for testing Materials, Vol. 43, 1943, pp 1069-1086.

45. DAVIES, R. D., "Some experiments on the applicability of the principle of super position to the strains of concrete subjected to stress, with particular reference to prestressed concrete", Magazine of Concrete Research, Vol. 9, No. 27, Nov. 1957, pp 161-172.

46. ROSS, A. D.. "Creep of concrete under variable stress", Journal A.C.I., Vol. 54, No. 3, March 1958, pp 739-758.

47. ENGLAND, G. L. and ILLSTON, J. M., "Methods of computing stress in concrete from a history of measured strain", Civil Engineering and Public Works Review, London, Vol. 60, April 1965, pp 513-517, May 1965, pp 692-694, and June 1965, pp 846-847.

48. GAMBLE, B. R., "A constitutive relationship for maturing concrete", International Association for Bridge and Structural Engineering, Symposium on Design of Concrete Structures for Creep, Shrinkage and Temperature Changes, Madrid, 1970, pp 90-98.

49. KOUNTOURIS, C. L., "Time-dependent forces induced by settlement of supports in continuous prestressed concrete structures", M.Sc. Thesis, Civil Engineering Department, University of Calgary 1976, 103 pp.

50. EVANS, R. H. and ROBINSON, G. W., "Bond stresses in prestressed concrete from X-ray photographs", Proceedings of the Institution of Civil Engineers, Vol. 4, Part 1, 1955, pp 212-235.

51. LEONHARDT, F. "On the need to consider the influence of lateral stresses on bond", Paper presented to the R.I.L.E.M. Symposium on Bond and Crack Formation in Reinforced Concrete, Stockholm, Tekniska Hogskolans Rotoprinttryckeri, 1957, pp 29-33.

52. ACI COMMITTEE 435, "Deflections of prestressed concrete members", JACI, Vol. 60, 1963, pp 1697-1728.

53. CORLEY, W. G., SOZEN, M. A., and SIESS, C. P., "Time dependent deflections of prestressed concrete beams" Highway Research Board Bulletin 307, 1961.

54. BRANSON, D. E. and OZELL, A. M., "Camber in prestressed concrete beams", JACI Vol. 57, 1961, pp 1549-1574.

55. BRANSON, D. E., MEYERS, B. L. and KRIPANARAYANAN, K. M., "Time dependent deformations of non-composite and composite prestressed concrete structures", Symposium on Concrete Deformation, Highway Research Record, No. 324, 1970, pp 15-43.

56. DELARUE, J., "Fluage et Beton precontraint", RILEM, Paris, Nov. 1958.

57. COTTINGHAM, W. S., FLUCK, P. G. and WASHA, G. W., "Creep of prestressed concrete beams", JACI, Proc. Vol. 57, Feb. 1961, pp 929-36.

58. CERNICA, J. N. and CHARIGNON, M. J., "Plastic strain in prestressed concrete beams under sustained loads", JACI, Vol. 58, 1961, pp 215-222.

59. EVANS, R. H. and PARKER, A. S., "Behaviour of prestressed concrete composite beams", JACI, Vol. 51, May 1955, pp 861-878.

60. OZELL, A. M., "Behaviour of simple-span and continuous composite prestressed concrete beams", JPCI, Vol. 2, No. 1, June 1957, pp 18-74.

61. BRYSON, J. O., SKODA, L. F. and WATSTEIN, D., "Flexural behaviour of prestressed split-beam composite concrete sections", JPCI, Vol. 10, No. 3, June 1965, pp 77-91.

62. MATTOCK, A. H., "Precast-prestressed concrete bridges - creep and shrinkage studies", Journal of the PCA Research and Development Laboratories, Vol. 3, No. 2, May 1961, pp 32-66.

63. BRANSON, D. E. and OZELL, A. M., "A report on differential shrinkage in composite prestressed concrete beams", JPCI, Vol. 4, No. 3, Dec. 1959, pp 61-78.

64. EVANS, R. H. and CHUNG, H. W., "Shrinkage and deflection of composite prestressed concrete beams", Concrete and Constructional Engineering, Vol. 61, No. 4, April 1966, pp 135-143.

65. DILGER, W. and NEVILLE, A. M., "Effect of creep and shrinkage in composite members", Proceedings of the second Australian Conference on Mechanics of Structures and Materials, Adelaide, 1969, pp 20.

66. RAO, V. J. and DILGER, W. H., "Analysis of composite prestressed concrete beams", Journal of the Structural Division, Proceedings of the American Society of Civil Engineers, Vol. 100, No.ST10, Oct. 1974, pp 2109-2121.

67. TADROS, M. K., GHALI, A., and DILGER, W. H., "Time dependent analysis of composite frames", Journal of the Structural Division, Proceedings American Society of Civil Engineers, Vol. 103, No. ST4, April 1977, pp 871-884.

68. DAVIS, H. S. "Thermal considerations in the design of concrete shields", Proc. A.S.C.E., ST.5, Sept. 1958, Paper 1755.

69. FISCHER, P., "Differential temperature moments in rigid frames", JACI, Vol. 59, 1962, pp 815-841.

70. BONSALL, W., "Stress in reinforced concrete shields for nuclear reactors", Proc. I.C.E., Vol. 16, 1960, pp 259-270.

71. DAVIDSON, I., "Some contributions from nuclear power to engineering practice", Proc. I.C.E., Vol. 17, 1960, pp 121-136.

72. HASSID, S., "Temperature stresses in continuous frames", JACI, Vol. 54, 1957, pp 415-420.

73. HANNAH, I. W., "Thermal stresses in concrete", Nuclear Engineering, Feb. 1961, pp 69-74.

74. HANNANT, D. J., "Thermal stresses in reinforced concrete", Ph.D. Thesis, University of Nottingham, 1961.

75. HANNAH, I. W., Discussion on "Some contribution from nuclear power to engineering practice", Proc. I.C.E., Vol. 20, Sept. 1961, p 191.

76. YU, W. W., and WINTER, G., "Instantaneous and long-term deflections of reinforced concrete beams under working loads", ACI Journal, Proc. Vol. 57, July 1960.

77. BRANSON, D. E., "Instantaneous and time-dependent deflections of simple and continuous reinforced concrete beams", Report 7, Alabama Highway Research Board, Bureau of Public Roads, August 1963.

78. British Standards Institution, Code of Practice for the structural use of concrete (CP 110), British Standards Institution, London 1972.

79. CEB recommendations for an International Code of Practice for reinforced concrete, American Concrete Institute and Cement and Concrete Association, London, 1964.

80. BEEBY, A. W., "Short-term deformations of reinforced concrete members", Technical Report TRA 408, Cement and Concrete Association, March 1968.

81. Draft Unified Code for the structural use of Concrete, issued for comment, British Standards Institution, 1969.

82. ACI Committee 435, "Deflections of reinforced concrete flexural members", ACI Journal, Proc. Vol. 63, June 1966.

83. MOHAMEDBHAI, G. T. G., "A study of the deflections of reinforced concrete flexural members", Ph.D. thesis, University of Manchester, 1971.

84. HOGNESTAD, E., HANSON, H. W., and McHENRY, D., "Concrete stress distribution in ultimate strength design", ACI Journal, Proc. Vol. 52, December 1955 pp 455-479.

85. Tentative recommendations for prestressed concrete, "ACI Journal, Proc. Vol. 54, January 1958, pp 545-578.

86. B.S. Code of Practice, CP.114 "The structural use of reinforced concrete in buildings", British Standards Institution, London, 1957.

87. England, G. L., "Numerical creep analyses applied to concrete structures", ACI Journal, Proc. Vol. 64, June 1967, pp 301-311.

88. Stevens, R. F., "Deflections of reinforced concrete beams", Proc. of the Institution of Civil Engineers, Part 2, Research and Theory, Vol. 53, September 1972, pp 207-224.

89. Illston, J. M. and Stevens, R. F., "Long-term cracking in reinforced concrete beams", Proc. of the Institution of Civil Engineers Part 2, Research and Theory, December 1972, pp 445-459.

90. Clark, L. A. and Speirs, D. M., "Tension stiffening in reinforced concrete beams and slabs under short-term load, "Technical report 42.521, Cement and Concrete Association, July 1978.

91. Srinivasa Rao, P. and Subrahmanyam, B. V., "Trisegmental moment-curvature relations for reinforced concrete members", ACI Journal, Proc. Vol 70, May 1973, pp 346-351.